الجمهورية الجزائرية الديمقراطية الشعبية

People's Democratic Republic of Algeria

وزارة التعليم العالي والبحث العلمي

Ministry of Higher Education and Scientific Research

جامعة الشهيد حمه لخضر الوادي

Echahid Hamma Lakhdar EL-OUED University

كلية علوم الطبيعة والحياة

Faculty of Natural and Life Sciences

قسم البيولوجيا الخلوية والجزيئية

Department of Cellular and Molecular Biology

END OF STUDY THESIS

In view of obtaining the diploma of Academic Master

Major: Biological Sciences

Speciality: Applied Biochemistry

THEME

Phytochemical Profiling, Green Synthesis of Metal Oxide Nanoparticles, and Multitarget Evaluation of *Cotula cinerea* and *Origanum majorana* L. as Potential Neuroprotective Agents

Presented by:

BOUDIAF Hadil **KEBACHE Serine** **ROUIHA Aya**

Examining Committee:

President:	**ZAATAR Abdelmalek**	**MCA**	University of Eloued
Examiner:	**LAICHE Ammar Touhami**	**MCA**	University of Eloued
Supervisor:	**LANEZ Elhafnaoui**	**MCA**	University of Eloued
Co-supervisor:	**BEN AMOR Mohammed Larbi**	**MCA**	University of Eloued

University year:2024/2025

Abstract

Alzheimer's disease (AD), the most common neurodegenerative disorder, is characterized by progressive cognitive decline, cholinergic deficits, oxidative stress, and neuroinflammation. Due to the limitations of current therapeutics, including Donepezil, Diclofenac, and α-tocopherol, the exploration of safer, multitarget alternatives is imperative. This study investigates the phytochemical composition, biological activity, and molecular mechanisms of Cotula cinerea and Origanum majorana L., two North African medicinal plants.

Plant extracts were prepared using aqueous, methanolic, and butanolic solvents and characterized via UPLC–ESI–MS/MS, revealing the presence of bioactive flavonoids and phenolic acids, including quercetin, luteolin, and rosmarinic acid. *In Vitro* assays demonstrated potent antioxidant activity (up to 89.6% DPPH inhibition), anti-inflammatory activity (IC_{50} of 42.1 µg/mL for C. cinerea), and significant anticholinesterase effects (IC_{50} of 18.5 µg/mL for O. majorana extract). ZnO and AgO nanoparticles synthesized via green methods from aqueous extracts were confirmed using UV–Vis, FTIR, XRD, and SEM

Molecular docking and Induced Fit Docking (IFD) revealed high binding affinities of quercetin (Glide score: −9.4 kcal/mol; IFD score: −11.2 kcal/mol) and rosmarinic acid (−9.0 and −10.8 kcal/mol, respectively) against AChE. These values were superior to those of Donepezil (−8.7 and −9.4 kcal/mol). Similar favorable interactions were observed for COX-1 and GR, surpassing Diclofenac and α-tocopherol. MD simulations over 100 ns confirmed complex stability, with low RMSD values (~2.1 Å for quercetin and ~1.6 Å for rosmarinic acid) and consistent hydrogen bonding. Free energy analyses (MM/GBSA) yielded ΔG values of −48.2 kcal/mol and −52.7 kcal/mol, respectively. Furthermore, DFT studies (FMO analysis) revealed HOMO–LUMO gaps of 4.74 eV (β- thujone) and 5.90 eV (caryophyllene oxide) in aqueous medium, supporting favorable chemical reactivity and electron transfer potential.

An *in Vivo* AD model induced by $AlCl_3$ and D-gal was used to evaluate the plant extracts. Behavioral tests showed improved cognitive function, while hematological analysis indicated reduced systemic inflammation. Biochemical results revealed lower MDA levels and increased GSH, CAT, and SOD activity in the brain, liver, and kidneys. Histopathology confirmed reduced amyloid-beta (Aβ) deposition

In summary, this multidisciplinary investigation provides compelling evidence for the neuroprotective potential of Cotula and Origanum . phytochemicals and their green-synthesized nanoparticles, offering promising scaffolds for further drug development targeting Alzheimer's disease

Key Words : Alzheimer, Origanum Majorana, Cotula Cinerea ,*In Silico*, Nanoparticles

Résumé :

La maladie d'Alzheimer (MA), le trouble neurodégénératif le plus courant, se caractérise par un déclin cognitif progressif, un déficit cholinergique, un stress oxydatif et une neuroinflammation. En raison des limites des traitements actuels, tels que le Donépézil, le Diclofénac et l'α-tocophérol, l'exploration d'alternatives plus sûres et à cibles multiples est impérative. Cette étude explore la composition phytochimique, l'activité biologique et les mécanismes moléculaires de Cotula cinerea et Origanum majorana L., deux plantes médicinales nord-africaines.

Les extraits végétaux ont été préparés à l'aide de solvants aqueux, méthanoliques et butanoliques, et caractérisés par UPLC–ESI–MS/MS, révélant la présence de flavonoïdes et d'acides phénoliques bioactifs, notamment la quercétine, la lutéoline et l'acide rosmarinique. Les essais *In Vitro* ont montré une activité antioxydante puissante (jusqu'à 89,6 % d'inhibition DPPH), une activité anti-inflammatoire (CI_{50} de 42,1 µg/mL pour C. cinerea) et un effet anticholinestérasique significatif (CI_{50} de 18,5 µg/mL pour l'extrait de O. majorana). Les nanoparticules de ZnO et AgO synthétisées par des méthodes vertes à partir d'extraits aqueux ont été confirmées par UV–Vis, FTIR, DRX et MEB,

Le docking moléculaire et le docking à ajustement induit (IFD) ont révélé de fortes affinités de liaison pour la quercétine (score Glide : −9,4 kcal/mol ; score IFD : −11,2 kcal/mol) et l'acide rosmarinique (−9,0 et −10,8 kcal/mol respectivement) contre l'AChE. Ces valeurs surpassent celles du Donépézil (−8,7 et −9,4 kcal/mol). Des interactions favorables similaires ont été observées pour la COX-1 et la GR, dépassant celles du Diclofénac et de l'α- tocophérol. Les simulations de DM sur 100 ns ont confirmé la stabilité des complexes, avec de faibles valeurs de RMSD (~2,1 Å pour la quercétine et ~1,6 Å pour l'acide rosmarinique) et un réseau de liaisons hydrogène stable. Les analyses d'énergie libre (MM/GBSA) ont donné des valeurs de ΔG de −48,2 kcal/mol et −52,7 kcal/mol, respectivement. Par ailleurs, les études DFT (analyse FMO) ont révélé des gaps HOMO– LUMO de 4,74 eV (β-thujone) et 5,90 eV (oxyde de caryophyllène) en milieu aqueux, soutenant une bonne réactivité chimique et un potentiel de transfert d'électrons.

Un modèle *In Vivo* de MA induite par $AlCl_3$ et D-gal a été utilisé pour évaluer les extraits de plantes. Les tests comportementaux ont montré une amélioration des fonctions cognitives, tandis que l'analyse hématologique a indiqué une réduction de l'inflammation systémique. Les résultats biochimiques ont révélé une diminution des taux de MDA et une augmentation de l'activité du GSH, CAT et de la SOD dans le cerveau, le foie et les reins. L'histopathologie a confirmé une diminution des dépôts de bêta-amyloïde (Aβ).

En résumé, cette étude multidisciplinaire fournit des preuves convaincantes du potentiel neuroprotecteur des composés phytochimiques de Cotula cinerea et Origanum majorana L., ainsi que de leurs nanoparticules synthétisées de manière verte, offrant des pistes prometteuses pour le développement de médicaments ciblant la maladie d'Alzheimer.
Mots clés : Alzheimer, Origanum Majorana, Cotula Cinerea, *In Silico*, Nanoparticules

Acknowlegment

First and foremost, we are deeply thankful to GOD, our Creator, for granting us the strength, patience, and determination to complete this humble work.

We would like to express our profound gratitude to **Professor Lanez Elhafnaoui**, Lecturer Professor (A) at the University of El Oued, and **Dr. Benamor Mohammed Larbi**, our co-supervisor, who together led this work as the true captains of this ship. Their vision, guidance, and unwavering support were essential at every stage of this research. Their experience and dedication steered us through challenges and inspired us to stay committed to our goal.

To **Professor Touhami Lanez**, Director of the VTRS Research Laboratory at the University of El Oued, we extend our sincere thanks for allowing us to conduct our experimental work within his facility and for his kind support and encouragement throughout..

We would like to express our sincere gratitude to **Dr. Ouafa Boudebia** for her valuable support and encouragement made a meaningful impact on our journey.
Also we thank **Dr. Laid Ibtessem** for her helpful contributions and motivation during the study.
Our appreciation extends to the **VTRS members**, especially **Mr. Houssyn Choua** and **Mrs. Ilham Ben Amor**, for their encouragement and belief in our project.
In addition, we gratefully acknowledge **Mr. Zaater Abdelmalik**, Dean of the Faculty of Natural and Life Sciences, as well as all members of the Department of Cellular and Molecular Biology at Hamma Lakhdar University, El Oued, and the laboratory technicians for their support and assistance.

We are also grateful to all the **members of the Department of Cellular and Molecular Biology** for their scientific and moral support, and to the **laboratory technicians**, whose assistance and collaboration were invaluable throughout the experimental stages of this research.

We further thank the **jury members** for their time, valuable insights, and constructive feedback, which enriched the quality of this dissertation.

Finally, we express our deepest gratitude to everyone who contributed, in one way or another, to the successful completion of this research.

إهداء

بسم الله الرحمن الرحيم

الحمد لله حبا و شكرا و امتنانا على البدء و الختام، الحمد الله الذي بنعمته تتم الصالحات، وبتوفيقه تُنال الغايات.

الحمد الله الذي وهبني التوفيق و السداد و منحنا الثبات واعانني على إتمام هذا العمل. أشكر الله العلي القدير الذي أنار لي درب العلم ووفقني لتكليل هذا النجاح بمشيئته .

بعد مسيرة حافلة بالجهد والتعب، أهدي عملي هذا ألا وهو حصيلة سنوات من الدراسة والعمل الجاد، أولا إلى نفسي و ثانيا إلى مستقبلي الذي أسعى لبنائه بالعلم والعمل .

إلى من كانا سندي وعزوتي منذ البدايات و اللذان غرسا في نفسي حب التعلم و الطموح :

أمي الحبيبة، مصدر الحنان والدعاء، من وقفت إلى جانبي في كل لحظة، من كانت كلماتها بلسمًا يهدئ تعبي، ونورها أمانًا في أوقات ضعفي، يا من زرعتِ في قلبي القوة والأمل... إليك أرفع هذا الإنجاز عرفانًا وتقديرًا .

أبي العزيز، قدوتي الأولى، وسندي الثابت من علّمني أن للنجاح طريقًا لا يُعبّد إلا بالعزم والإصرار، دعمني بصمته، وقوّاني بحكمته... إليك أهدي ثمرة هذا التعب، احترامًا وامتنانًا.

إلى أخواتي شركاء الحلم والسند في لحظات التحدّي : **ملاك، منار، سندس، عُلا** .و وحيدي **معتزبالله** كنتم ولازلتم العون في التعب، والفرح في النجاح، جعلكم الله نورًا يضيء دربي دائما .

و إلى من آمن بقدراتي وشجعني على المضي قدماً ولم يبخل علي يوما بعلمه أستاذي الفاضل **الدكتور العانز الحفناوي**، تقديرًا وعرفانًا لما قدّمه من دعم علمي واهتمام دائم، ولما تحلّى به من توجيه حكيم، وتشجيع مستمر،، وصبر على مراحل هذا العمل، فكان بحقّ نموذجًا يُحتذى به في الأخلاق والعلم .شكراً لك من القلب على كل شيء.

و إلى من علمنا أنّ العلم رسالة و الأخلاق أساسها ، أستاذي الفاضل **الدكتور بن عمر محمد العربي**، لقد كانت ملاحظاتك السد يدة، وصبرك ودعمك الدائم، نورًا أضاء لي الطريق، وسندًا تجاوزت به التحديات.

كل الشكر والأمتنان لما قدمتموه لي من دعم وتفانٍ، ستبقى بصماتكما خالدة في ذاكرتي وفي كل نجاح أحققه.

إلى رفيقتَيّ في هذه الرحلة العلمية، **سيرين وآية**:

كل الشكر والامتنان لقلبيكما الكبيرين، ولجهودكما النقية التي رافقتاني في كل خطوة من هذا البحث. لقد كنتما أكثر من زميلتين، كنتما سندًا حقيقيًا، وعونًا لا يُنسى.
كل لحظة تعب، وكل نقاش، وكل إنجاز في هذا العمل يحمل منكما أثرًا لا يُمحى.
ممتنة لصداقتكما ومشاركتكما الصادقة، فبفضلكما اكتمل هذا العمل بروح التعاون والإخلاص.

إلى من شاركوني هذه الرحلة بكل تحدياتها ولحظاتها الجميلة صديقات بالدم و أخوات بالروح : **دنيا، ضحى، فراح، سندس نور اليقين** و رفيقة طفولتي **آلاء.**

راجيةً من الله أن يجعل هذا العمل خالصاً لوجهه الكريم، وأن ينفع به كل من يطمح للنجاح و التميز.

هديل

إهداء

بسم الله الرحمان الرحيم

الصلاة والسلام على أشرف الخلق نبينا محمد خاتم الانبياء والمرسلين:

الحمد لله حمدا كثيرا مباركا حتى يبلغ الحمد منتهاه . الحمد والشكر للرحمان الذي وفقنا و أعاننا لتمام هذا العمل

عرفانا بالشكر أهدي ثمرة هذا العمل الى :

أمي، مصدر قوتي وشغفي، التي سهرت على تعليمي وبث الأمل في داخلي وأن النجاح نتيجة الاجتهاد، ،من آمنت بي وبقدراتي ،كتفي الذي لا يهتز ،صديقتي الأولى ومخبئي من شرور العالم.

أمي يا نعيم الأرض دوما , ويا من في دعائك تُخففين واذا ضاقت الدنيا تزعين في الأعماق دينا.

أطال الله عمرك ووهبك الصحة والقوة

أبي، من شجعني على مواجهة الصعاب وعدم الاستسلام للعقبات لمن علمني اللين مع الصلابة و آمن بي وبهدفي. الى كل يوم شاق مر عليك في سبيل توفير الأمان والراحة في سبيل تحقيق أحلامنا و الى كل جهد بذلته في سبيلي وسبيل وصولي .

أبي، لو كان للعُليا رجالٌ، فأنتَ المجدُ عنوانًا ودينا، دعائي أن تظلّ لنا حياةً، فأنتَ العمرُ إن طالَت سِنينَا.

الى أخواتي الغاليات **عفاف وروميساء** وصغيرتي **ريتال** شكرا على كل دعمكم. توجيهكم مصدر قوتي يامن كنتم قدوتي الحسنة.

الى رفيقات دربي وعزوتي **هديل و آية** أحمد الله على نعمة وجودكم في حياتي أنتم على دراية والله يرى ويعلم ما ممرنا به من أيام صعبة و أخرى حلوة أحمده على نعم الخيار لهذه التجربة ولهذا الفصل من حياتي.

صديقتي **مروة** عسى الله ان يديم عشرتنا سنين مداد والى الممات حفظكي الله ورعاكي وشكراً لقلبك الدافئ الذي آمن بي ودعا لي بالخير .

الى رفيقات الجنة **فراح ،نور وسندس** يا من تشاركنا لحظات حلوة في هته المسيرة الطيبة،أتمنى من الله ان يجعل لنا فيها لقاء نستذكر فيه مامضى من الدنيا وحلو اللحظات معاً.

الى أستاذنا الفاضل **الدكتور العانز الحفناوي** من علمنا ان النهار عمل، وان الليل عمل، وان الامل خيار وما ثمرة العمل والامل إلّا الإنتصار ،من أنار لنا طريقنا ووجهنا نحو النجاح دمت نبراسًا للعلم ونموذجًا يُحتذى به.

الى استاذنا الطيب **الدكتور بن عمر محمد العربي** شكرًا لك على عطائك المستمر وصبرك الكبير كنت الداعم والمعين، والمرشد الأمين شكرا على نصحك و أسأل الله أن يجزيك عنا خير الجزاء، وأن يبقيك منارة القوة ونجاح .

أتمنى أن يكون هذا الجهد سببًا في النفع، وبذرة خير تُثمر لكل طامح، وأن يكتب الله له القبول والإخلاص.

سيرين

إهداء

بسم الله الرحمن الرحيم

الحمد لله حمدًا كثيرًا طيبًا مباركًا فيه،الحمد لله حتى يبلغ الحمد منتهاه، فهذا من فضل ربي وحده.

في هذا اليوم الاستثنائي، يقف الحرفُ عاجزًا أمام سيل المشاعر... فها أنا أقطف ثمرة سنواتٍ من الجد والاجتهاد، لأبدأ فصلاً جديدًا من الحياة

اهدي هذا العمل إلى من تشاركا في جيناتي التي أفخر بها أبي وأمي...

أبي:

يا من بنيتَ الدربَ صخرًا،وأقمتَ المجدَ من تعبِ الجبينًا، فصوتُكَ حين يدعو صارَ أُنسًا، وفي دعواك عُمرٌ يحتوينا.

أمي:

كم سهرتِ لأجل نومي، وكم قاسيتِ من أجلِي سنينًا، فكلّ الليلِ في عينيكِ صبرٌ، وفي قلبِكِ محيطٌ من سكينًا.

يا من غرستما في قلبي حبّ العلم، وسقيتما روحي بالصبر والدعاء، ما كنتُ لأصل إلى هذا اليوم لولا توفيق الله ثم وقوفكما الدائم، فلكما مني كل الامتنان والبرّ والدعاء ما حييت.

وإلى إخوتي **شعيب، يحي، آدم و رحيم عبد الرحمن**

السند بعد الله، والفرحة التي تكبر بوجودكم،شكرًا لأنكم كنتم دومًا قريبين من قلبي في لحظات ضعفي دعمتموني، وفي لحظات فرحي شاركتموني،ولكم في هذا النجاح نصيب كبير.

وإلى أساتذتي الكرام: أنتم منارة هذا الطريق،منكم تعلمنا، وبكم ارتقينا،كل درسٍ زرعتموه فينا، وكل كلمة تشجيع، وكل نظرة ثقة كانت لبنات في هذا البناء العظيم.

الى رفيقتي درب هته الرحلة الطويلة **هديل و سيرين**

شكرا على دعمكن في وقت الشدة، وعلى العمل الجماعي المتين، فبوجودكن تحولت الصعاب والعراقيل الى رحلة ممتعة.

الى عزيزي الصغير ... **"باندا"** لم تكن مجرد حيوان اليف، بل كان روحا لطيفة سكنت زوايا وحدتي ،من كان يحتضن صراعاتي بنظرات دافئة ، من كافح معي في مسيرتي باستلقاء هادئ على كتبي ،او مواء خافت يشبه مواساة خفيفة للروح، شكرا بندودي.

والى كل من ساندني وشجعني وامن بي لكم جميعا اقول :

هذا النجاح ليس لي وحدي...بل هو لكم جميعا.

ثم اخيرا الى ذلك الصحابي الذي كان قدوة حسنة.

آية

Table of Contents

Abstract 2
Résumé : 3
Acknowlegment 5
إهداء 8
List of Figures 15
List of Tables 18
List of Annexes 20
List of Abbriviations 21
GENERAL INTRODUCTION 25
FIRST PART: THEORETICAL FRAMEWORK 28
CHAPTER ONE: Alzheimer's Disease and Related Pathophysiological Processes 29
.1 Introduction 30
1.1. Definition and classification of neurodegenerative diseases 30
1.2. Socioeconomic and public health burden of Alzheimer's disease 31
1.3. Rationale for studying AD in the context of oxidative stress and inflammation 32
2. Epidemiology and Risk Factors 33
2.1. Global and regional prevalence statistics 34
2.2. Age-related risks and genetic predisposition 35
2.3. Environmental and lifestyle-related factors 36
3. Pathogenesis and Hallmark Features 38
3.1. Amyloidogenic pathway and β-amyloid plaque formation 38
3.2. Tau protein hyperphosphorylation and neurofibrillary tangles 39
3.3. Synaptic dysfunction and neuronal death 40
4. Cholinergic System Dysfunction 40
4.1. Role of acetylcholine in cognitive processes 40
4.2. Cholinesterase enzyme targets (AChE and BChE) 41
4.3. Basis for current pharmacotherapy 41
5. Oxidative Stress in Alzheimer's Disease 42
5.1. Mechanisms of reactive oxygen species (ROS) generation in neurons 42
5.2. Lipid peroxidation, protein carbonylation, and DNA oxidation 43
5.3. Antioxidant defence mechanisms and redox imbalance 43
6. Neuroinflammation 44
6.1. Role of microglial activation and astrocyte dysfunction 44
6.2. Key cytokines and inflammatory mediators (IL-1β, TNF-α, IL-6) 45
6.3. Crosstalk between inflammation and Aβ/tau pathologies 46
7. Current and Emerging Therapeutic Approaches 46

7.1. Approved drugs: Donepezil, Rivastigmine, Galantamine, Memantine 46
7.2. Mechanisms, limitations, and side effects 47
7.3. Multi-target strategies and natural product-based interventions 47
8. Experimental Models in AD Research 48
8.1. In vitro: Enzyme inhibition and cell-based assays 48
8.2. In vivo: Rodent models (scopolamine, Aβ injection, transgenics) 49
8.3. In silico: Molecular docking, ADMET, and Dynamics simulation 50
9. Conclusion 50
9.1. Summary of interconnected pathophysiological processes 50
9.2. Justification for investigating antioxidant and anti-inflammatory natural compounds 51
9.3. Transition to the study of medicinal plants in Chapter 2 51
CHAPTER TWO: Overview of Cotula cinerea and Origanum majorana 52
1. Introduction 53
2. Botanical Description and Taxonomic Classification 53
2.1. Cotula cinerea (Lakhdar, 2018) 53
2.2. Origanum majorana (Bouyahya et al., 2021) 54
3. Geographic Distribution and Ecological Characteristics 55
3.1. Cotula cinerea 55
3.2. Origanum majorana 55
4. Traditional and Ethnomedicinal Uses 55
4.1. Cotula cinerea 55
4.2. Origanum majorana 55
5. Phytochemical Composition 56
5.1. Cotula cinerea 56
5.2. Origanum majorana 56
6. Pharmacological and Biological Activities 56
6.1. Cotula cinerea 56
6.2. Origanum majorana 56
7. Relevance in Alzheimer's Disease Research 57
7.1. Cotula cinerea 57
7.2. Origanum majorana 57
SECOND PART: EXPERIMENTAL 58
CHAPTER ONE: MATERIALS AND METHODS 59
1. Introduction 60
2. Plant Material 60
2.1. Collection and Identification of Plant Species 60

2.1.1. Cotula cinerea 60
2.1.2. Origanum majorana L 61
2.2. Preparation of Plant Extracts 61
2.2.1. Sample Collection and Preparation 61
2.2.2. Drying Process 62
2.2.3. Grinding 62
2.2.4. Extraction Process 62
2.2.5. Solvent Removal and Concentration 63
2.2.6. Extraction Yield 63
3. Phytochemical Analysis 63
3.1. Qualitative Phytochemical Screening 63
3.1.1. Polyphenols Detection (Hu et al., 2025) 64
3.1.2. Flavonoids Detection (Sutrisno & Kartini, 2025) 64
3.1.3. Alkaloids Detection (Moreno & Solar, 2025) 64
3.1.4. Terpenoids Detection (Yu et al., n.d.) 64
3.1.5. Tannins Detection (Tambe et al., 2025) 64
3.1.6. Saponins Detection (Lv et al., 2025) 64
3.1.7. Reducing Sugars Detection (A. Yadav et al., 2025) 65
3.1.8. Glycosides Detection (Milella et al., 2025) 65
3.2. Quantitative Phytochemical Analysis 65
3.2.1. Estimation of Total Polyphenols Content (TPC) 65
3.2.2. Estimation of Total Flavonoids Content (TFC) 65
3.2.3. Estimation of Condensed Tannin Content (CTC) 66
3.3. Ultra performance liquid chromatography mass spectrometry (UPLC/MS–MS) analysis 66
4. Green Synthesis of Metal-Oxide Nanoparticles 67
4.1. Equipment and Apparatus 67
4.2. Chemicals and Reagents 67
4.3. Green synthesis of Zinc Oxide Nanoparticles (ZnO-NPs) 68
4.4. Green synthesis of Silver Oxide Nanoparticles (AgO-NPs) 69
5. Characterization of Synthesized Nanoparticles 70
5.1. Ultraviolet-Visible (UV-Vis) Spectroscopy 70
5.1.1. Apparatus 70
5.1.2. Method 70
5.2. Fourier Transform Infrared Spectroscopy (FTIR) 71
5.2.1. Apparatus 71
5.2.2. Method 71

5.3. X-ray Diffraction (XRD) Analysis 71
5.3.1. Apparatus 71
5.3.2. Method 71
5.4. Scanning Electron Microscopy (SEM) 72
5.4.1. Apparatus 72
5.4.2. Method 72
6. In Vitro Bioassays 72
6.1. Equipment and Apparatus 72
6.2. Anti-Alzheimer Activity: Acetylcholinesterase (AChE) Inhibitory Assay 72
6.2.1. Overview 72
6.2.2. Chemicals and Reagents 73
6.2.3. Procedure 73
6.3. Anti-inflammatory Activity: Bovine Serum Albumin (BSA) Denaturation Assay 73
6.3.1. Overview 73
6.3.2. Chemicals and Reagents 74
6.3.3. Procedure 74
6.4. Antioxidant Activity: DPPH Radical Scavenging Assay 75
6.4.1. Overview 75
6.4.2. Chemicals and Reagents 75
6.4.3. Procedure 75
6.5. Statistical Analysis 76
7. In Vivo Experiments 76
7.1. Experimental Animals 76
7.1.1. Animal Selection and Housing Conditions 76
7.1.2. Ethical Considerations 76
8. Acute Toxicity Study 77
8.1. Experimental Design 77
8.2. Dose Administration and Monitoring 77
9. In Vivo Anti-Alzheimer Experiment: 77
9.1. Experimental Animals 77
9.1.1. Induction of Alzheimer's-like Symptoms 77
9.1.2. Experimental Design 78
9.2. Behavioural Assessments During Conditioning 79
9.2.1. Maze Test 79
9.2.2. Dark/Light Box Test 80
9.2.3. Open Field Test 81
9.2.4. Novel Object Recognition Test 82

9.3. Sacrifice of rats and collection of blood and organs 83
9.4. Biomackers parameters detection..... 84
9.4.1. Determination of Inflammation parameters 84
9.4.1.1. Biochemical and hematochemical analysis :..... 84
9.4.1.2. Hystological detection:..... 84
9.4.2. Determination of Oxidative stress parameters 84
9.4.2.1. Preparation of homogenate..... 85
9.4.2.2. Asseys of Oxidative Stress Parameters: 85
9.4.3. Determination of Alzheimer..... 88
9.5. Histopathological Study steps 89
9.5.1. Histopathological Study 89
9.5.2. Statistical Analysis 90
10. In Silico Analyses..... 91
10.1. ADMET and Drug-Likeness Prediction..... 91
10.2. Molecular Docking Study 91
10.2.1. Ligands Preparation..... 91
10.2.2. Receptor Preparation:..... 92
10.2.3. Docking Setup:..... 93
10.2.4. Induced Fit Docking (IFD):..... 94
10.3. Molecular Dynamics (MD) Simulation..... 94
10.4. Free Energy (MM-GBSA) Calculation 95
10.5. DFT calculations 96
CHAPTER TWO: RESULTS AND DISCUSSION..... 97
11. Phytochemical Composition and Chemical Profiling 98
11.1. Extraction Yields of *Cotula cinerea* and *Origanum majorana L.*..... 98
11.2. Qualitative Phytochemical Screening of Major Constituent Classes..... 99
11.3. Quantitative Determination of Phenolics, Flavonoids, and Tannins 101
11.4. UPLC–ESI–MS/MS Chemical Fingerprinting and Compound Identification 102
11.4.1. UPLC–ESI–MS/MS Profile of Cotula cinerea Methanolic Extract..... 102
11.4.2. UPLC–ESI–MS/MS Profile of Origanum majorana L. Methanolic Extract 104
12. Green Synthesis of Metal-Oxide Nanoparticles..... 105
13. Characterization of Synthesized Nanoparticles..... 105
13.1. Characterization of Silver Oxide Nanoparticles (AgO-NPs) 106
13.1.1. UV–Visible Spectroscopy 106
13.1.2. FTIR Spectral Analysis 107
13.1.3. X-Ray Diffraction (XRD) Analysis..... 109
13.1.4. Scanning Electron Microscopy (SEM) Analysis..... 110

14. In Vitro Evaluation of the Biological Activities 112
14.1. Anti-Alzheimer Activity Determined by Acetylcholinesterase Inhibition Assay .. 112
14.2. Anti-Inflammatory Activity Evaluated via the BSA Denaturation Method 118
14.3. Antioxidant Activity Assessed by the DPPH Radical Scavenging Assay 124
15. *In Vivo* Study Results 129
15.1. Acute toxicity study 129
15.2. Alzaheimers model study results..... 131
15.2.1. Behavioural Assessments During Conditioning..... 131
15.2.2. Biochemical Analysis of blood samples and organs : 139
16. In Silico Analysis of Bioactive Constituents and Nanoparticles..... 150
16.1. ADMET and Drug-Likeness Prediction for Phytochemical Constituents 150
16.2. Molecular Docking Studies of Phytochemicals and Nanoparticles Against Target Proteins 153
16.2.1. Overview and Docking Workflow Justification 153
16.2.2. Docking Scores and Binding Affinities of Cotula cinerea Compounds 154
16.2.3. Docking Scores and Binding Affinities of Origanum Majorana L. Compounds ... 159
16.2.4. Docking Scores and Binding Affinities of Green Synthesized Nanoparticles 163
16.3. Molecular Dynamics (MD) Simulations of Protein–Ligand Complexes..... 167
16.3.1. Root Mean Square Deviation (RMSD) Analysis 168
16.3.2. Root Mean Square Fluctuation (RMSF) Analysis..... 169
16.3.3. Radius of Gyration (Rg) Analysis 170
16.3.4. Solvent Accessible Surface Area (SASA) Analysis 170
16.4. Density Functional Theory (DFT) Analysis of Selected Phytocompounds 171
CONCLUSION 173
REFERENCES..... 176
ANNEXES 214

List of Figures

Figure 1. Projected Global Rise in Alzheimer's Prevalence (2015–2050)..... 32
Figure 2. Interaction Between Oxidative Stress and Neuroinflammation in Alzheimer's Disease (Kuntic et al., 2025)..... 33
Figure 3. Genetic and Age-Related Risk Factors for Alzheimer's Disease (Coon et al., 2007) 36
Figure 4. Modifiable Environmental and Lifestyle Risk Factors for Alzheimer's Disease (Ngandu, 2006)..... 37
Figure 5. The Amyloidogenic Pathway and Plaque Formation in Alzheimer's Disease (Patterson et al., 2009)..... 39
Figure 6. Cholinergic Neurotransmission and Role of Cholinesterase (Lane et al., 2006)..... 41
Figure 7. Sources and Effects of ROS Generation in AD Neurons (Valencia & Morán, 2004). 43
Figure 8. Microglial and Astrocytic Activation in Alzheimer's Disease (Matejuk & Ransohoff, 2020)..... 45
Figure 9. Mechanism of Action of Approved Alzheimer's Drugs (Vishwas et al., 2023) 47
Figure 10. Multi-Target Approach to Alzheimer's Therapy (Cheong et al., 2022)..... 48
Figure 11. *Cotula cinerea* in its natural habitat. 53
Figure 12. *Origanum majorana* flowering. 54
Figure 13 Extraction Process..... 62
Figure 14 Green synthesis of Zinc Oxide Nanoparticles Process 68
Figure 15 Green synthesis of Silver Oxide Nanoparticles Process..... 70
Figure 16 Distribution of experimental groups. 79
Figure 17 Custom-Made Maze Apparatus For Rat's Behavioral Assessment..... 80
Figure 18 Experimental Setup of The Modified Dark/Light Box Test 81
Figure 19 Experimental Setup For The Open Field Test Used In Behavioral Analysis..... 82
Figure 20 Experimental Procedure For The Novel Object Recognition Test.(A) Phase 1 : Familiar Object Exposure. (B) Phase 2 : Novel Object Recognition Test. 83
Figure 21. Extraction yields (%) of *Cotula cinerea* and *Origanum majorana* L. using water, methanol, and n-butanol solvents..... 99
Figure 22. UV-Vis Absorbance Spectra of Water Extracts and Biosynthesized ZnO and AgO Nanoparticles Using *Origanum majorana* and *Cotula cinerea*..... 106
Figure 23. FTIR Spectra of Biosynthesized ZnO and AgO Nanoparticles 108

Figure 24. XRD Patterns of Biosynthesized ZnO and AgO Nanoparticles Using *Cotula cinerea* and *Origanum majorana* Extracts 109
Figure 25. SEM Images of Biosynthesized ZnO and AgO Nanoparticles Using Aqueous Extracts of *Cotula cinerea* and *Origanum majorana* 111
Figure 26. Exponential dose–response curves showing acetylcholinesterase inhibition (%) of *Cotula cinerea* extracts (Water, MeOH, BuOH) and their corresponding nanoparticles (AgO NPs, ZnO NPs) across a range of concentrations 115
Figure 27. Exponential dose–response curves showing acetylcholinesterase inhibition (%) of *Origanum majorana L* extracts (Water, MeOH, BuOH) and their corresponding nanoparticles (AgO NPs, ZnO NPs) across a range of concentrations 116
Figure 28. Exponential dose–response curves showing BSA denaturation inhibition (%) of *Cotula cinerea* extracts (Water, MeOH, BuOH) and their corresponding nanoparticles (AgO NPs, ZnO NPs) across a range of concentrations 121
Figure 29. Exponential dose–response curves showing BSA denaturation inhibition (%) of *Origanum Majorana L.* extracts (Water, MeOH, BuOH) and their corresponding nanoparticles (AgO NPs, ZnO NPs) across a range of concentrations 122
Figure 30. Exponential dose–response curves showing DPPH activity inhibition (%) of *Cotula cinerea* extracts (Water, MeOH, BuOH) and their corresponding nanoparticles (AgO NPs, ZnO NPs) across a range of concentrations..... 127
Figure 31. Exponential dose–response curves showing DPPH activity inhibition (%) of *Origanum majorana* L. extracts (Water, MeOH, BuOH) and their corresponding nanoparticles (AgO NPs, ZnO NPs) across a range of concentrations 128
Figure 32 Spontaneous Alternation Percentage Performed by The Experimental Groups. .. 131
Figure 33 Time Spent in the Dark Compartment by Mice Across Experimental Groups in a Modified Dark-Light Box Test (Fear Memory Model with Cold Water)..... 132
Figure 34 Time Spent in Outer and Inner Zones During the Open Field Test Across Experimental Groups..... 135
Figure 35 Discrimination Index in the Novel Object Recognition Test Across Experimental Groups 138
Figure 36 Oxidative stress parameters in the brain of different experimental groups. 142
Figure 37 Oxidative stress parameters in the liver of different experimental groups. 144
Figure 38 Oxidative stress parameters in the kidneys of different experimental groups. 145
Figure 39 Microscopic observation of Brain histological sections from different experimental groups, (C) Control group, (AD) Negative control group, (AD+DNZ) Group treated

with Donepezil, (AD+Cotula) Group treated with Cotula cinerea, and (AD+Majorana) Group trea..... 146
Figure 40 Microscopic observation of Liver histological sections from different experimental groups, (C) Control group, (AD) Negative control group, (AD+DNZ)Group treated with Donepezil, (AD+Cotula) Group treated with Cotula cinerea, and (AD+Majorana) Group trea..... 148
Figure 41 Microscopic observation of Kidneys histological sections from different experimental groups, (C) Control group, (AD) Negative control group, (AD+DNZ) Group treated with Donepezil, (AD+Cotula) Group treated with Cotula cinerea, and (AD+Majorana) Group tr..... 149
Figure 42. Comparative 2D and 3D interaction profiles of quercetin and standard reference drugs (Donepezil, Diclofenac, and Glutathione) with selected therapeutic targets: acetylcholinesterase (AChE, PDB: 6O4W), cyclooxygenase-1 (COX-1, PDB: 5WBE), and glutathione reductase (GR, PDB: 1XAN)..... 158
Figure 43. Comparative 2D and 3D interaction profiles of rosmarinic acid with selected therapeutic targets: acetylcholinesterase (AChE, PDB: 6O4W), cyclooxygenase-1 (COX-1, PDB: 5WBE), and glutathione reductase (GR, PDB: 1XAN)..... 162
Figure 44. 3D interaction diagrams of ZnO and AgO nanoparticles with the active sites of AChE (PDB ID: 6O4W), COX-1 (PDB ID: 5WBE), and glutathione reductase (PDB ID: 1XAN)..... 166
Figure 45. Root mean square deviation (RMSD) trajectories of the AChE backbone in complex with quercetin (black) and rosmarinic acid (red) over 100 ns MD simulations..... 168
Figure 46. RMSF plots of acetylcholinesterase (AChE) in complex with quercetin and rosmarinic acid throughout a 100 ns molecular dynamics simulation..... 169
Figure 47. Radius of gyration (Rg) plots of acetylcholinesterase (AChE) in complex with quercetin and rosmarinic acid over a 100 ns molecular dynamics simulation..... 170
Figure 48. Solvent Accessible Surface Area (SASA) Plot of AChE in Complex with Quercetin and Rosmarinic Acid over a 100 ns MD Simulation..... 171

List of Tables

Table 1. Classification of Major Neurodegenerative Diseases..... 31
Table 2. Target receptor information chosen for docking studies 92
Table 3. Selected grid parameters the studied enzymes 93
Table 4. Extraction yields of *Cotula cinerea* and *Origanum majorana* L. (mean ± SD, n = 3) 98
Table 5. Qualitative Phytochemical Screening of Methanolic Extracts of *Cotula cinerea* and *Origanum majorana* L. 100
Table 6. Total phenolic, flavonoid, and condensed tannin contents of methanolic extracts (expressed as mg standard equivalents per g extract). 101
Table 7. Major phytochemicals in the *Cotula cinerea* methanolic extract identified by UPLC–ESI–MS/MS (negative ion mode) and their relative area (%) (mean ± SD, *n* = 3) ... 103
Table 8. Major phytochemicals in the *Origanum majorana* L. methanolic extract identified by UPLC–ESI–MS/MS (negative ion mode) and their relative area (%) 104
Table 9. Acetylcholinesterase inhibition (%) of *Cotula cinerea* extracts and nanoparticles at selected concentrations (mean ± SD, n = 3)..... 112
Table 10. Acetylcholinesterase inhibition (%) of *Origanum majorana L* extracts and nanoparticles at selected concentrations (mean ± SD, n = 3)..... 113
Table 11. Half-maximal inhibitory concentrations (IC_{50}) of *Cotula cinerea* and *Origanum majorana* L. extracts, nanoparticles, and Donepezil against acetylcholinesterase (mean ± SD, n = 3)..... 117
Table 12. Inhibition of BSA denaturation (%) by *Cotula cinerea* extracts, nanoparticles, and diclofenac at selected concentrations (mean ± SD, n = 3) 118
Table 13. Inhibition of BSA denaturation (%) by *Origanum majorana* L. extracts, nanoparticles, and diclofenac at selected concentrations (mean ± SD, n = 3) 119
Table 14. IC_{50} values for BSA denaturation inhibition by *Cotula cinerea* and *Origanum majorana* L. extracts, nanoparticles, and diclofenac (mean ± SD, n = 3)..... 123
Table 15. DPPH radical scavenging activity (%) of *Cotula cinerea* extracts, nanoparticle formulations, and α-tocopherol across tested concentrations (mean ± SD, *n* = 3)..... 124
Table 16. DPPH Radical Scavenging Activity (%) of *Origanum majorana* Extracts, Nanoparticles, and α-Tocopherol at Various Concentrations (µg/mL) (mean ± SD, n = 3)..... 125

Table 17. IC_{50} values for DPPH radical scavenging by *Cotula cinerea* and *Origanum majorana* L. extracts, nanoparticles, and α-tocopherol (mean ± SD, n = 3) 128
Table 18 Potential toxic effects of the methanolic extract of Cotula cinerea and Origanum majorana L..... 130
Table 19 Behavioral Characterization of Experimental Groups in the Dark-Light Box test. 134
Table 20 Behavioral Analysis in Open Field Test: Comparative Assessment Across Experimental Groups..... 136
Table 21 Organ weight Index of different experimental groups 139
Table 22 Plasma concentration of hematological parameters of different experimental groups 140
Table 23 Glycemia, CRP, liver and kidneys function parameters of different experimental groups 141
Table 24 Brain Histological Alterations 146
Table 25 Liver Histological Alterations 148
Table 26 Kidney Histological Alterations 149
Table 27. ADMET Profile of Major Phytochemicals from *Cotula cinerea* 151
Table 28. ADMET Profile of Major Phytochemicals from *Origanum majorana* L..... 151
Table 29. Docking Scores (Glide SP and IFD) of *Cotula cinerea* Compounds and Standards 154
Table 30. Docking Scores (kcal/mol) of *Origanum majorana* L. Compounds and Reference Drugs against AChE, COX-1, and GR Using Rigid and Induced Fit Docking..... 160
Table 31. Molecular docking scores (kcal/mol) of ZnO and AgO nanoparticles with AChE, COX-1, and GR using Rigid and IFD protocols 163
Table 32. Frontier molecular orbital energies (HOMO, LUMO) and energy gap (ΔE) values of quercetin and rosmarinic acid calculated in gas and aqueous phases using the B3LYP/6-31G(d,p) level of theory 172

List of Annexes

Annex 1 Published Article 215
Annex 2 Participation Certificate in Seminars 237

List of Abbriviations

4-HNE: 4-Hydroxynonenal

8-OHdG: 8-Hydroxy-2'-Deoxyguanosine

Aβ: Amyloid-beta

ACh: Acetylcholine

AChE: Acetylcholinesterase

AChEI: Acetylcholinesterase Inhibitor

AD: Alzheimer's Disease

ADMET: Absorption, Distribution, Metabolism, Excretion, Toxicity

$AgNO_3$: Silver Nitrate

AgO: Silver Oxide

AgO NPs: Silver Oxide Nanoparticles

ALS: Amyotrophic Lateral Sclerosis

AMPA: Alpha-Amino-3-Hydroxy-5-Methyl-4-Isoxazolepropionic Acid

APP: Amyloid Precursor Protein

ATCI: Acetylthiocholine Iodide

α-secretase: Alpha-secretase

α-Tocopherol: Alpha-Tocopherol (a form of Vitamin E)

BBB: Blood–Brain Barrier

BACE1: Beta-site APP Cleaving Enzyme 1

β-secretase: Beta-secretase

BChE: Butyrylcholinesterase

BuOH: Butanol

BSA: Bovine Serum Albumin

CAT: Catalase

CDK5: Cyclin-Dependent Kinase 5

CH_3COOH: Acetic Acid

$CHCl_3$: Chloroform

ChAT: Choline Acetyltransferase

CNS: Central Nervous System

COX-1: Cyclooxygenase-1

CTC: Condensed Tannin Content

Cu^{2+}: Cupric Ion

DAMPs: Damage-Associated Molecular Patterns

DFT: Density Functional Theory

DLB: Dark/Light Box

DMSO: Dimethyl Sulfoxide

DNA: Deoxyribonucleic Acid

DNZ: Donepezil

DPPH: 2,2-Diphenyl-1-picrylhydrazyl

DTNB: 5,5′-Dithiobis-(2-nitrobenzoic acid)

ΔE: Energy Gap (LUMO–HOMO)

EMA: European Medicines Agency

E-Maze: Elevated Maze

eV: Electron Volt

EXT: Extract

FDA: Food and Drug Administration

Fe^{2+}: Ferrous Ion

FMO: Frontier Molecular Orbital

FT-IR: Fourier-Transform Infrared Spectroscopy

FTIR: Fourier Transform Infrared Spectroscopy

GAE: Gallic Acid Equivalent

GPx: Glutathione Peroxidase

GR: Glutathione Reductase

GSH: Glutathione

GSK-3β: Glycogen Synthase Kinase 3 Beta

H_2O_2: Hydrogen Peroxide

H_2SO_4: Sulfuric Acid

HIA: Human Intestinal Absorption

HOMO: Highest Occupied Molecular Orbital

IC_{50}: Half Maximal Inhibitory Concentration

IFD: Induced Fit Docking

IL-1β: Interleukin-1 beta

IL-6: Interleukin-6

KBr: Potassium Bromide

LD50: Lethal Dose 50

LC-MS: Liquid Chromatography–Mass Spectrometry

logBB: Logarithm of Blood–Brain Barrier Permeability

logKp: Logarithm of Skin Permeability

logPapp: Logarithm of Apparent Permeability Coefficient (Caco-2)

logPS: Logarithm of CNS Permeability

LTP: Long-Term Potentiation

LRP1: Low-density lipoprotein receptor-related protein 1

LUMO: Lowest Unoccupied Molecular Orbital

MARKs: Microtubule Affinity-Regulating Kinases

MDA: Malondialdehyde

MD: Molecular Dynamics

MeOH: Methanol

MS: Mass Spectrometry

MTDLs: Multi-Target-Directed Ligands

Na_2CO_3: Sodium Carbonate

NaOH: Sodium Hydroxide

NEP: Neprilysin

NF-κB: Nuclear Factor Kappa-light-chain-enhancer of activated B cells

NFTs: Neurofibrillary Tangles

NMDA: N-Methyl-D-Aspartate

NO: Nitric Oxide

NOR: Novel Object Recognition

NSAID: Non-Steroidal Anti-Inflammatory Drug

O_2^-: Superoxide Anion

OCT2: Organic Cation Transporter 2

OFT: Open Field Test

OPLS4: Optimized Potentials for Liquid Simulations 4

PC12: Pheochromocytoma Cells

PHFs: Paired Helical Filaments

Π–π stacking: Interactions between aromatic rings

PK: Pharmacokinetics

QE: Quercetin Equivalent

Rg: Radius of Gyration

RMSD: Root Mean Square Deviation

RMSF: Root Mean Square Fluctuation

ROS: Reactive Oxygen Species

SAB: Spontaneous Alternation Behaviour

SASA: Solvent Accessible Surface Area

SD: Standard Deviation

SEM: Scanning Electron Microscopy

SH-SY5Y: Human Neuroblastoma Cell Line

SOD: Superoxide Dismutase

SP: Standard Precision

TFC: Total Flavonoid Content

TLR4: Toll-Like Receptor 4

TNF-α: Tumor Necrosis Factor-alpha

TPC: Total Polyphenol Content

Tau: Microtubule-Associated Protein Tau

UPLC: Ultra Performance Liquid Chromatography

UPLC-MS/MS: Ultra Performance Liquid Chromatography Tandem Mass Spectrometry

UV-Vis: Ultraviolet–Visible Spectroscopy

XRD: X-ray Diffraction

$Zn(CH_3CO_2)_2$: Zinc Acetate

ZnO: Zinc Oxide

ZnO NPs: Zinc Oxide Nanoparticles

GENERAL INTRODUCTION

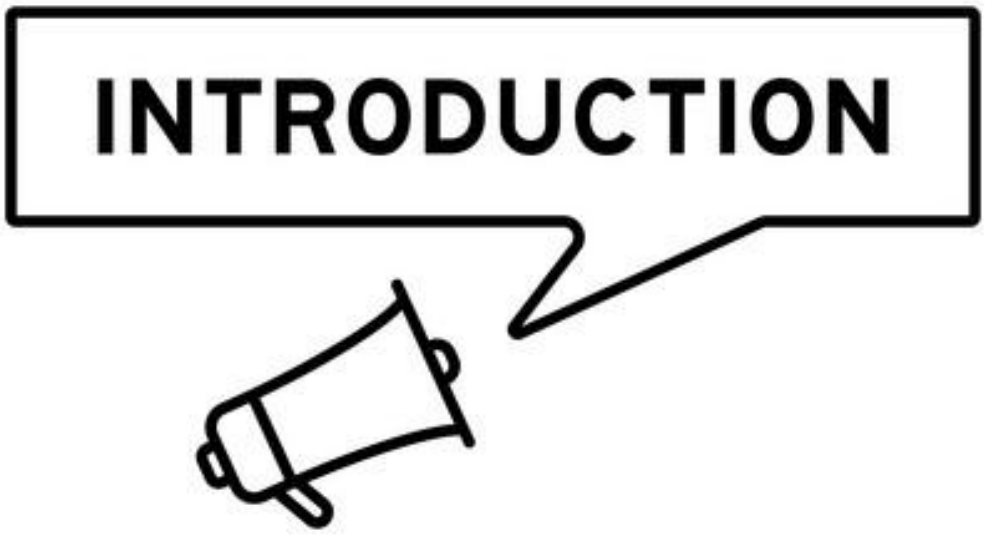

General Introduction

Oxidative stress, inflammation, and neurodegeneration are interconnected biological phenomena implicated in the onset and progression of numerous chronic diseases, including Alzheimer's disease (AD) (Fischer & Maier, 2015). Oxidative stress results from an imbalance between the production of reactive oxygen species (ROS) and the antioxidant defense system, leading to cellular damage (Teleanu et al., 2022). Inflammatory responses, while essential for immune regulation, can become pathological when dysregulated, contributing to neuroinflammation and neurodegenerative cascades (Cherbuin et al., 2019). Alzheimer's disease, the most prevalent form of dementia, is characterized by progressive memory loss, synaptic dysfunction, and neuronal death (Rojas-Gutierrez et al., 2017). Its multifactorial etiology involves oxidative damage, chronic inflammation, and cholinergic system dysfunction—posing significant challenges to the development of effective treatments.

In recent years, medicinal plants have gained increasing attention as valuable sources of bioactive compounds with multifunctional therapeutic properties (Dar et al., 2023). Their complex phytochemical composition allows for synergistic effects targeting multiple pathological pathways simultaneously (Yip & Papa, 2021). *Cotula cinerea* (Asteraceae) and *Origanum majorana* (Lamiaceae) are two medicinal species traditionally used in North African phytotherapy for their antioxidant, anti-inflammatory, and neuroprotective activities (W. N. Chen et al., 2023). However, despite their historical use, comprehensive scientific validation and molecular characterization of their therapeutic potential remain limited.

Moreover, the emergence of nanotechnology offers novel platforms for enhancing the bioavailability, stability, and efficacy of plant-derived compounds (Karnwal et al., 2024). The green synthesis of metal oxide nanoparticles—particularly zinc oxide (ZnO) and silver oxide (AgO)—using plant extracts has shown great promise due to its environmentally friendly approach and potential biomedical applications (Enrico, 2019). When synthesized from medicinal plants, these nanoparticles may inherit additional biofunctional properties from the phytochemicals involved in their formation (Sanjai et al., 2024).

Despite the growing interest in plant-based therapies and green nanotechnology, there remains a lack of integrated studies combining phytochemical profiling, green nanoparticle synthesis, and comprehensive biological evaluation—especially in the context of Alzheimer's disease, inflammation, and oxidative stress. There is a need to bridge the gap between traditional knowledge and modern scientific validation through multidisciplinary approaches.

This thesis aims to evaluate the therapeutic potential of *Cotula cinerea* and *Origanum majorana* through a comprehensive strategy combining phytochemical, nanotechnological, and pharmacological investigations. The study was conducted as follows:

1. **Extraction and Fractionation:** Sequential extraction of both plants using water, methanol, and butanol to obtain fractions rich in diverse phytochemicals.
2. **Phytochemical Characterization:** LC/MS analysis of the extracts to identify major compounds responsible for biological activity.
3. **Green Synthesis of Nanoparticles:** Fabrication of ZnO and AgO nanoparticles using aqueous extracts, followed by physicochemical characterization via UV-Vis, FT-IR, XRD, and SEM techniques.
4. **Biological Evaluation:**
    - *In vitro* assessment of antioxidant and anti-inflammatory activities and anti-Alzheimer activities.
    - *In vivo* studies using relevant animal models to evaluate cognitive and biochemical effects.
    - *In silico* modeling, including molecular docking and dynamics simulations, to investigate the interaction of major compounds with key enzymes implicated in Alzheimer's disease, inflammation and oxidative stress.

FIRST PART:

THEORETICAL FRAMEWORK

CHAPTER ONE:

Alzheimer's Disease and Related Pathophysiological Processes

1. Introduction

Neurodegenerative diseases constitute a group of progressive, disabling disorders characterized by the gradual deterioration of structure and function in the central or peripheral nervous system. Among them, Alzheimer's disease (AD) stands as the most prevalent, accounting for approximately 60–70% of all dementia cases worldwide (Graham & Brodaty, 1997). AD represents a major challenge for public health systems globally due to its multifactorial etiology, chronic progression, and the absence of curative treatments (Hunter et al., 2025).

Recent research has highlighted that Alzheimer's pathology is not only a disorder of protein aggregation (amyloid plaques and neurofibrillary tangles), but also a complex network of oxidative stress, chronic neuroinflammation, synaptic failure, and neurotransmitter imbalance, particularly involving the cholinergic system (Al-Kuraishy et al., 2025). These intertwined mechanisms offer potential therapeutic targets for both synthetic and natural compounds with multi-targeted actions.

Understanding the pathophysiology of Alzheimer's disease through biochemical, cellular, and molecular approaches is essential for developing novel preventive and therapeutic strategies. Moreover, studying ethnobotanical resources such as *Cotula cinerea* and *Origanum majorana*—plants traditionally used for CNS and inflammatory conditions—opens promising avenues for discovering neuroprotective agents (Chib et al., 2025).

1.1. Definition and classification of neurodegenerative diseases

Neurodegenerative diseases are a heterogeneous group of disorders characterized by the progressive loss of structure and function of neurons. These conditions can be classified based on the primary clinical symptoms (e.g., cognitive vs. motor) or the major molecular pathology involved (e.g., tauopathies, synucleinopathies, or amyloidopathies). Alzheimer's disease, Parkinson's disease, Huntington's disease, and amyotrophic lateral sclerosis (ALS) are among the most well-known neurodegenerative diseases. AD, in particular, is classified as a primary tauopathy and amyloidopathy, due to the pathological aggregation of tau protein and amyloid-β peptides within the brain (Chand & Subramanian, 2025).

These diseases share several overlapping mechanisms, including oxidative stress, mitochondrial dysfunction, protein misfolding, and neuroinflammation, which justifies a comparative and integrative biochemical investigation. An illustrative classification of major

neurodegenerative diseases, including their hallmark proteins, clinical manifestations, and affected brain regions, is presented in Table 1 (Giannakis & Konitsiotis, 2025).

Table 1. Classification of Major Neurodegenerative Diseases.

Disease	Key Pathological Proteins	Main Symptoms	Affected Brain Regions
Alzheimer's	Aβ, Tau	Memory loss, cognitive decline	Hippocampus, cortex
Parkinson's	α-Synuclein	Tremors, rigidity, bradykinesia	Substantia nigra
Huntington's	Huntingtin	Chorea, mood changes	Basal ganglia
ALS	TDP-43, SOD1	Muscle weakness, paralysis	Motor cortex, spinal cord

1.2. Socioeconomic and public health burden of Alzheimer's disease

Alzheimer's disease imposes a profound and escalating burden on individuals, caregivers, healthcare systems, and economies worldwide. As populations age, the prevalence of AD is increasing at an alarming rate, particularly in low- and middle-income countries where health infrastructure may be insufficient to meet the growing demand for care (Lilford et al., 2025).

According to the World Health Organization (WHO), more than 55 million people were living with dementia globally in 2021, and this number is expected to rise to 78 million by 2030 and 139 million by 2050. Alzheimer's disease accounts for the majority of these cases. The global cost associated with dementia was estimated at over USD 1.3 trillion in 2019 and is projected to more than double by 2030 (R. Wang, 2025).

The socioeconomic burden of AD extends beyond direct medical expenses. Indirect costs, including unpaid caregiving, loss of income, and reduced workforce productivity, constitute a substantial share of the economic impact. Family members often provide continuous care, which can lead to emotional distress, physical exhaustion, and financial strain (N. M. Huang et al., 2025).

From a public health perspective, AD presents a unique challenge due to the chronic nature of the disease, the absence of disease-modifying treatments, and the need for long-term care. Governments and healthcare systems must address the need for early diagnosis, accessible therapeutic options, caregiver support programs, and public awareness initiatives. The dramatic

projected increase in Alzheimer's cases worldwide is clearly illustrated in Figure 1, underscoring the urgency of comprehensive public health planning (Aziz et al., 2025).

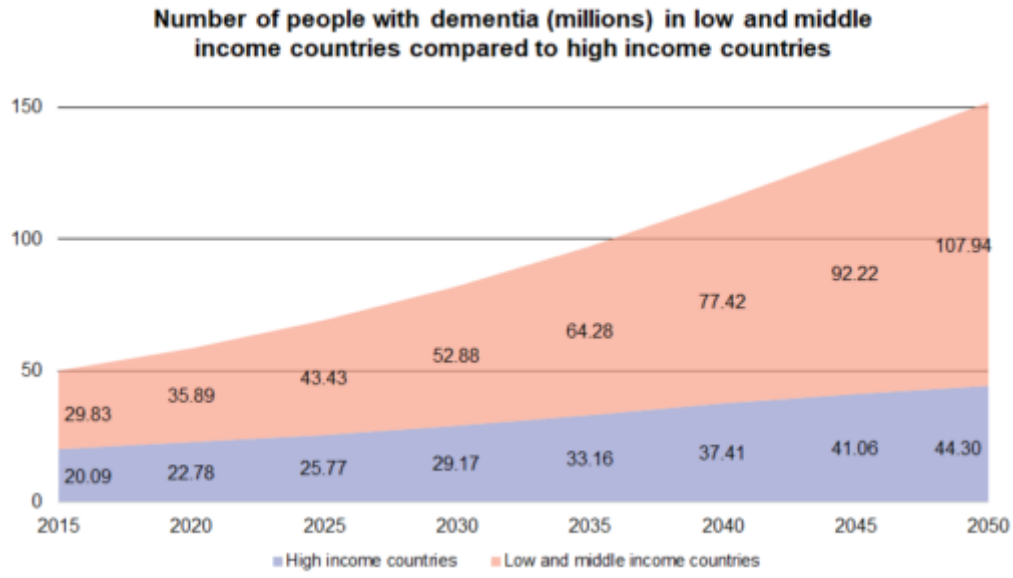

Figure 1. Projected Global Rise in Alzheimer's Prevalence (2015–2050)

1.3. Rationale for studying AD in the context of oxidative stress and inflammation

Alzheimer's disease (AD) has traditionally been attributed to the accumulation of β-amyloid plaques and neurofibrillary tangles. However, recent findings have broadened our understanding of its multifactorial pathogenesis. In particular, oxidative stress and neuroinflammation have emerged as critical and interlinked mechanisms that significantly contribute to neuronal dysfunction and disease progression (Alfei & Zuccari, 2025).

Oxidative stress in AD is characterized by an imbalance between the production of reactive oxygen species (ROS) and the brain's antioxidant defense systems. Due to its high oxygen consumption and abundant lipid content, the brain is especially vulnerable to oxidative insults. ROS-mediated damage leads to lipid peroxidation, DNA fragmentation, and protein oxidation, thereby impairing mitochondrial function and promoting synaptic failure (Naik et al., 2025).

Concurrently, neuroinflammation plays a synergistic role. Activated microglia and astrocytes release pro-inflammatory cytokines, such as tumor necrosis factor-alpha (TNF-α), interleukin-1 beta (IL-1β), and interleukin-6 (IL-6). These mediators exacerbate oxidative damage, disrupt neuronal communication, and further potentiate amyloid-beta and tau pathologies. The crosstalk between chronic inflammation and oxidative stress forms a vicious cycle that accelerates neurodegeneration (Lei et al., 2025). The interplay between oxidative stress and

chronic inflammation is illustrated in Figure 2, highlighting their mutual reinforcement in accelerating neurodegeneration.

Given the limitations of current single-target therapies, the dual targeting of oxidative stress and inflammation represents a promising therapeutic strategy. Natural compounds with antioxidant and anti-inflammatory properties, particularly those derived from medicinal plants, are gaining interest for their potential to modulate multiple pathological pathways simultaneously. This study, therefore, seeks to investigate the neuroprotective potential of *Cotula cinerea* and *Origanum majorana* as part of an integrative approach to AD treatment (Xue et al., 2025).

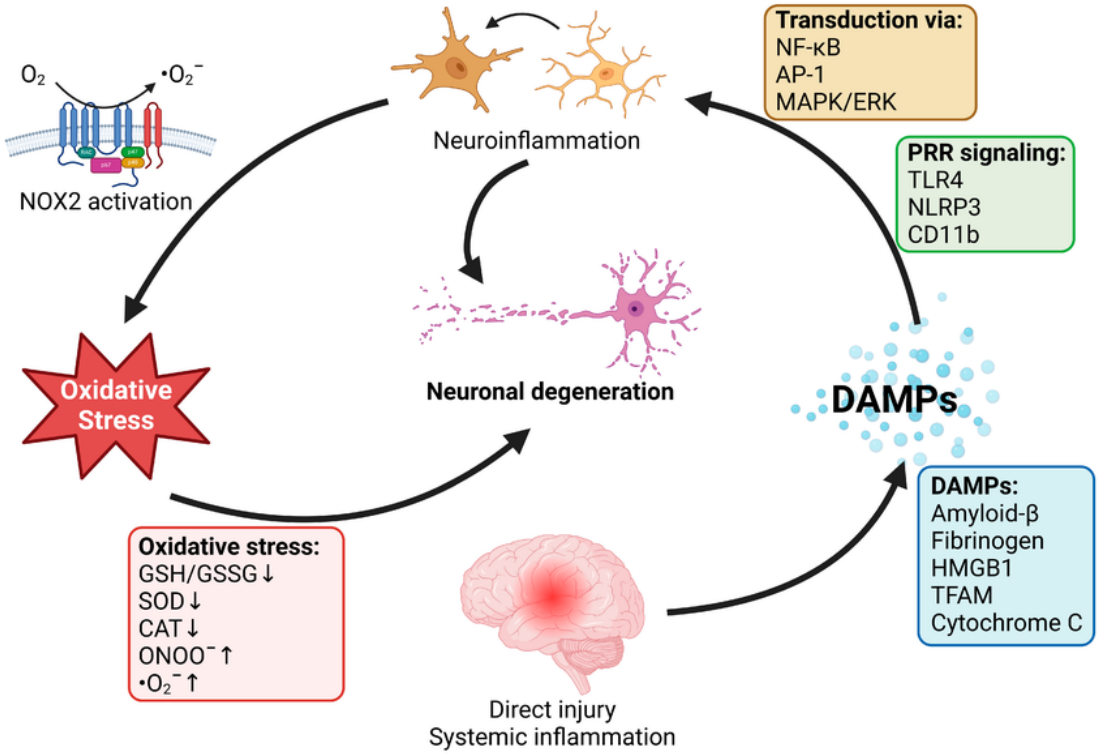

Figure 2. Interaction Between Oxidative Stress and Neuroinflammation in Alzheimer's Disease (Kuntic et al., 2025)

2. Epidemiology and Risk Factors

Alzheimer's disease (AD) is a progressive neurological disorder with a sharply increasing incidence due to population aging. It constitutes a global public health challenge with profound medical, economic, and social implications. Understanding the epidemiological trends and risk factors associated with AD is critical to identifying vulnerable populations and implementing preventive strategies (Akhmedov, 2025).

AD accounts for 60–70% of all dementia cases and affects approximately 55 million people worldwide, a figure projected to reach 139 million by 2050 (Louis et al., 2021). The incidence rises steeply with age, doubling approximately every five years after the age of 65. However, epidemiological patterns also show variability across regions due to differences in population demographics, diagnostic infrastructure, education levels, and healthcare accessibility (Zheng et al., 2025).

In addition to aging, AD is associated with both modifiable and non-modifiable risk factors. These include genetic susceptibility, sex, cardiovascular health, lifestyle habits, and environmental exposures. The increasing prevalence in low- and middle-income countries emphasizes the need for inclusive global surveillance and equitable health interventions (Wei et al., 2025).

2.1. Global and regional prevalence statistics

Alzheimer's disease (AD) is a leading cause of disability among the elderly and represents the most common form of dementia globally. According to the World Health Organization (WHO) and Alzheimer's Disease International (ADI), over 55 million people were living with dementia in 2021, and this number is projected to reach 78 million by 2030 and 139 million by 2050. Alzheimer's disease accounts for approximately 60–70% of these cases, making it the primary contributor to the dementia burden (Wortmann, 2012).

The global prevalence of AD is not uniform. High-income countries, such as those in Western Europe and North America, report higher recorded prevalence rates due to greater awareness, longer life expectancy, and better diagnostic tools. However, the fastest growth in new cases is observed in low- and middle-income countries, where aging populations are expanding rapidly and access to healthcare services remains limited. By 2050, it is estimated that over two-thirds of people with dementia will live in developing regions (Vradenburg, 2015).

Additionally, demographic differences such as gender (with higher prevalence in women) and urban versus rural residence have been documented. Women are disproportionately affected, likely due to their longer average lifespan and potential hormonal or genetic susceptibilities (Mielke, 2018).

2.2. Age-related risks and genetic predisposition

Age is the most significant and well-established risk factor for Alzheimer's disease (AD). The incidence of AD increases exponentially with age, particularly after the age of 65, doubling approximately every five years thereafter. Epidemiological studies indicate that while only about 3–5% of people aged 65–74 are affected, this prevalence rises to 32–40% among those aged 85 and older. This strong correlation reflects the accumulation of cellular damage, neuroinflammatory processes, and reduced neuroplasticity that naturally occur with aging (Guerreiro & Bras, 2015).

Beyond aging, genetic predisposition plays a critical role in influencing both the risk and the age of onset of Alzheimer's disease. Genetic forms of AD can be broadly categorized into:

✓ **Familial (Early-Onset) Alzheimer's Disease:** (Wu et al., 2012)

This rare form (less than 1% of all cases) typically manifests before age 65 and is linked to mutations in one of three genes:

- **APP** (*amyloid precursor protein*),
- **PSEN1** (*presenilin 1*), and
- **PSEN2** (*presenilin 2*).

These mutations promote abnormal cleavage of APP, resulting in the overproduction of pathogenic Aβ42 peptides, a key component of amyloid plaques.

✓ **Sporadic (Late-Onset) Alzheimer's Disease:** (Morris et al., 2022)

The more common form of AD is multifactorial and usually occurs after the age of 65. The strongest genetic risk factor for late-onset AD is the presence of the ε4 allele of the apolipoprotein E (APOE) gene:

- Individuals carrying one copy of APOE ε4 have a 2–3-fold increased risk.
- Homozygous carriers (ε4/ε4) have an approximately 8–12-fold higher risk of developing AD.

Although APOE ε4 is a significant genetic risk factor, it is neither necessary nor sufficient for developing the disease, and many non-carriers also develop AD. Other emerging genetic factors include TREM2, CLU, PICALM, and BIN1, which are implicated in lipid metabolism, immune response, and synaptic function.

The interplay between genetic vulnerability and environmental/lifestyle exposures likely determines the individual trajectory of disease onset and progression. These insights underscore the importance of early screening and personalized preventive strategies in high-risk populations.

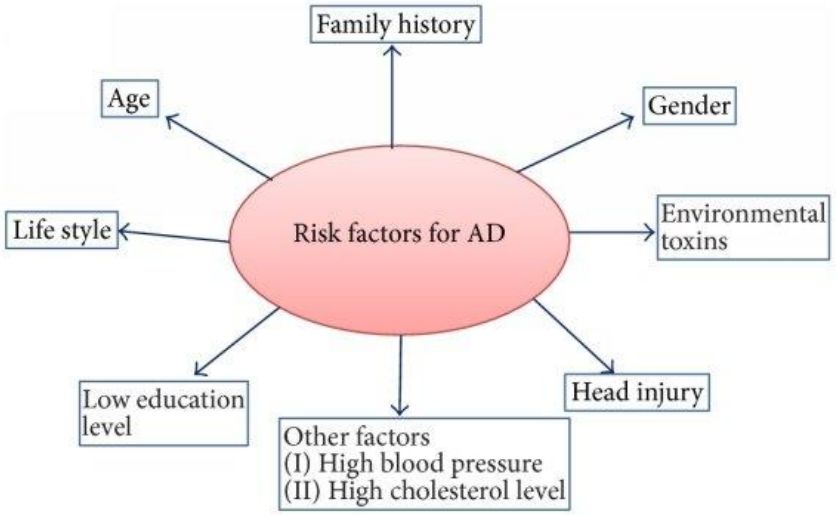

Figure 3. Genetic and Age-Related Risk Factors for Alzheimer's Disease (Coon et al., 2007)

2.3. Environmental and lifestyle-related factors

While aging and genetic predisposition are recognized as primary risk factors for Alzheimer's disease (AD), a growing body of evidence emphasizes the significant contribution of environmental exposures and lifestyle behaviors to disease onset and progression. These factors are particularly important because they are largely modifiable, offering viable targets for prevention and intervention strategies (Solfrizzi et al., 2008).

✓ **Cardiovascular and Metabolic Health** (Gupta & Gupta, 2020)

Chronic conditions such as hypertension, type 2 diabetes, hyperlipidemia, and obesity—especially during midlife—are strongly associated with an increased risk of developing AD. These conditions contribute to vascular dysfunction, reduced cerebral perfusion, and oxidative stress, which can synergize with amyloid and tau pathology. Preventive control of cardiovascular risk factors has shown promise in reducing dementia incidence.

✓ **Physical Activity and Cognitive Engagement** (Solfrizzi et al., 2007)

Regular physical exercise is correlated with reduced risk of AD due to its positive effects on neurogenesis, synaptic plasticity, and cerebral blood flow. Similarly, cognitive stimulation through education, social engagement, and mentally challenging activities is associated with greater cognitive reserve, which delays clinical symptom onset even in the presence of neuropathology.

✓ **Diet and Nutrition**

Adherence to brain-healthy dietary patterns—such as the Mediterranean diet and the MIND diet (Mediterranean-DASH Intervention for Neurodegenerative Delay)—has been linked to

better cognitive performance and reduced AD risk. These diets emphasize antioxidant-rich fruits and vegetables, omega-3 fatty acids, whole grains, and limited consumption of red meat and processed foods.

✓ **Sleep Quality**

Disturbed sleep patterns and conditions such as obstructive sleep apnea have been linked to increased accumulation of β-amyloid in the brain. Sleep is believed to facilitate glymphatic clearance of toxic metabolites, and chronic disruption may hinder this protective mechanism.

✓ **Exposure to Environmental Toxins**

Long-term exposure to air pollutants (e.g., fine particulate matter PM2.5), heavy metals (such as lead or mercury), and pesticides may increase the risk of AD by promoting neuroinflammation and oxidative stress. Occupational exposure and environmental health inequalities remain areas of concern, particularly in urban and industrialized settings.

✓ **Smoking and Alcohol Consumption**

Tobacco smoking accelerates vascular damage and oxidative stress, significantly increasing dementia risk. Excessive alcohol consumption, especially chronic intake, is neurotoxic and contributes to cognitive impairment, although low-to-moderate consumption of certain alcohol types (e.g., red wine) may exhibit protective antioxidant effects—albeit controversially.

The integration of these environmental and lifestyle elements into public health strategies presents a major opportunity to mitigate the global AD burden. Their role is summarized in Figure 4, which outlines the modifiable risk factors and their mechanisms of action.

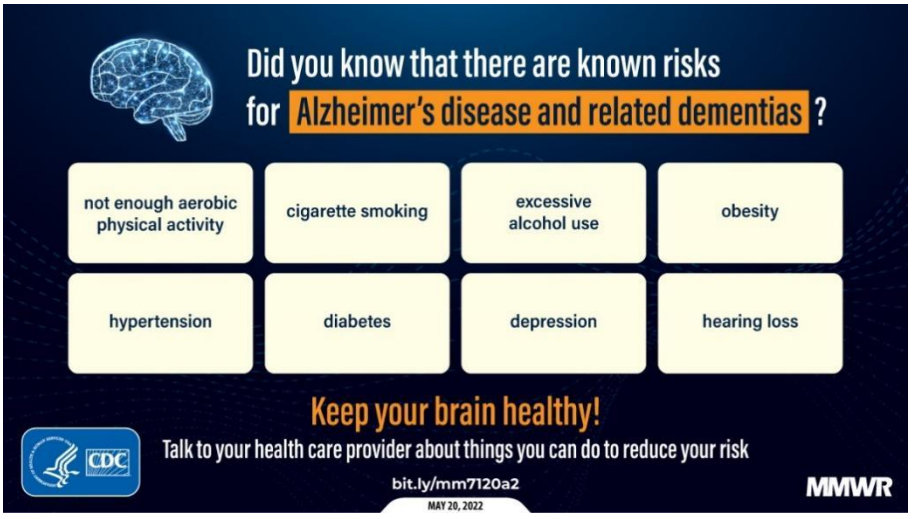

Figure 4. Modifiable Environmental and Lifestyle Risk Factors for Alzheimer's Disease (Ngandu, 2006)

3. Pathogenesis and Hallmark Features

The pathological landscape of Alzheimer's disease (AD) is characterized by a constellation of molecular and cellular alterations that culminate in progressive cognitive decline and irreversible neuronal damage. Two hallmark neuropathological features dominate the pathogenesis of AD: the accumulation of extracellular amyloid-β (Aβ) plaques and intracellular neurofibrillary tangles (NFTs) composed of hyperphosphorylated tau protein. These pathological entities interact with and exacerbate other processes such as synaptic dysfunction, oxidative stress, mitochondrial impairment, and inflammation, resulting in widespread neurodegeneration (Rostagno, 2022).

3.1. Amyloidogenic pathway and β-amyloid plaque formation

The amyloid hypothesis, first proposed in the early 1990s, posits that the overproduction and aggregation of Aβ peptides are central to the initiation of Alzheimer's disease. Aβ peptides are generated through sequential proteolytic cleavage of the amyloid precursor protein (APP) by β-secretase (BACE1) and γ-secretase (Takahashi et al., 2017).

Under normal physiological conditions, non-amyloidogenic processing of APP involves α-secretase, producing soluble and non-toxic fragments. However, in AD, the shift toward the amyloidogenic pathway leads to the formation of Aβ1–40 and Aβ1–42, the latter being highly aggregation-prone and neurotoxic. These peptides self-associate into oligomers, protofibrils, and eventually form insoluble fibrillar plaques deposited in the extracellular space, particularly in the neocortex and hippocampus (Seeman & Seeman, 2011).

Aβ oligomers, rather than mature plaques, are now considered the most neurotoxic species. They impair synaptic plasticity, alter calcium homeostasis, promote oxidative damage, and activate microglia. The formation and deposition of amyloid plaques are depicted in Figure 5. (Yankner & Mesulam, 1991).

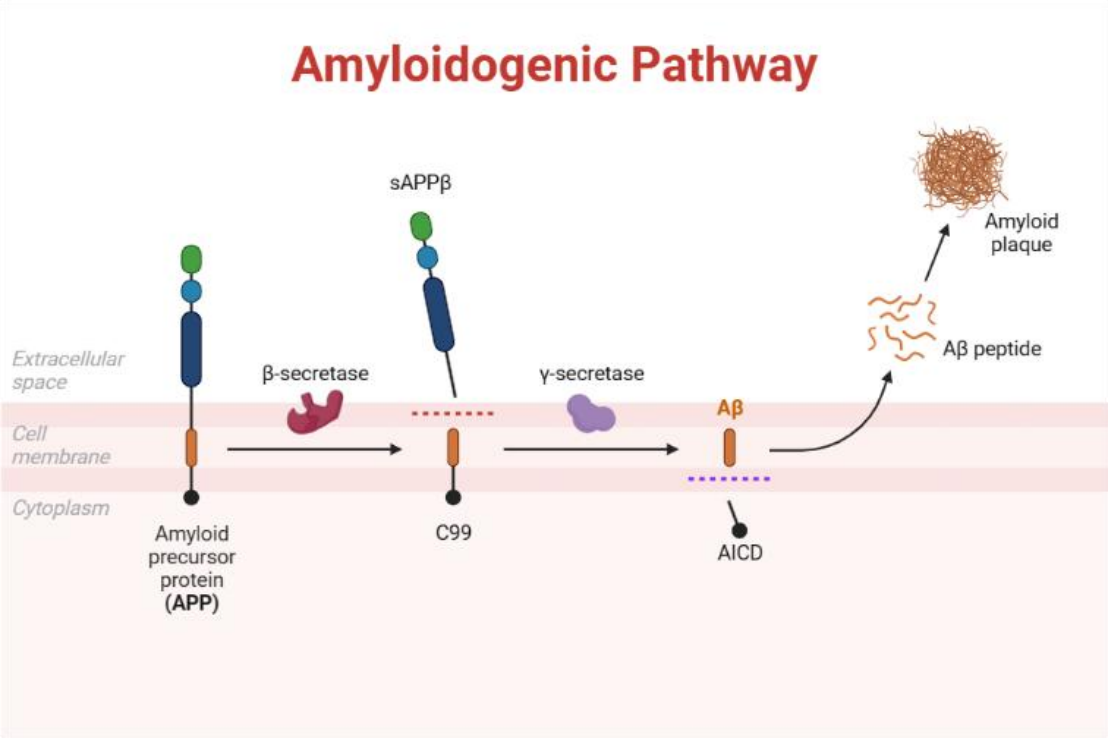

Figure 5. The Amyloidogenic Pathway and Plaque Formation in Alzheimer's Disease (Patterson et al., 2009)

3.2. Tau protein hyperphosphorylation and neurofibrillary tangles

Tau is a microtubule-associated protein primarily expressed in neurons, where it stabilizes microtubule assembly and supports axonal transport. In Alzheimer's disease, tau undergoes aberrant hyperphosphorylation, which reduces its affinity for microtubules and leads to self-aggregation into paired helical filaments (PHFs). These filaments ultimately form neurofibrillary tangles (NFTs) within the neuronal cytoplasm (Metaxas & Kempf, 2016).

Tau pathology initiates in the entorhinal cortex and progressively spreads to the hippocampus and neocortex, correlating more closely with cognitive decline than amyloid plaque burden. Hyperphosphorylated tau disrupts intracellular trafficking, impairs mitochondrial function, and triggers neuronal apoptosis (Brion, 1998).

The enzymes involved in tau phosphorylation include GSK-3β, CDK5, and MARKs. Inflammatory mediators and Aβ also stimulate tau dysregulation, suggesting a convergence of pathological pathways (Brion et al., 2001).

3.3. Synaptic dysfunction and neuronal death

Synaptic failure is a central event in AD progression and a major contributor to cognitive symptoms. Aβ oligomers and hyperphosphorylated tau independently and synergistically disrupt synaptic integrity (Plascencia-Villa & Perry, 2023). This includes:

- Inhibition of long-term potentiation (LTP).
- Downregulation of glutamate receptors (NMDA, AMPA).
- Impaired neurotransmitter release and vesicle cycling.
- Spine loss and dendritic atrophy.

The sustained presence of toxic protein aggregates leads to neuroinflammation, excitotoxicity, calcium imbalance, and ultimately apoptotic or necrotic neuronal death. Brain regions most affected include the hippocampus, amygdala, and cerebral cortex, which explains the progressive memory loss and executive dysfunction in AD (Tönnies & Trushina, 2017).

4. Cholinergic System Dysfunction

One of the earliest and most consistent neurochemical alterations observed in Alzheimer's disease (AD) is the degeneration of the cholinergic system, particularly within the basal forebrain. This deficit significantly contributes to the cognitive and behavioural impairments seen in affected individuals. The cholinergic hypothesis posits that dysfunction in acetylcholine synthesis, release, and signalling is a primary driver of memory loss and attention deficits in AD. Consequently, this system has become a major therapeutic target for symptomatic treatment (M Tata et al., 2014).

4.1. Role of acetylcholine in cognitive processes

Acetylcholine (ACh) is a critical neurotransmitter involved in a wide range of cognitive functions, including learning, memory, attention, and arousal. It operates in key brain regions such as the hippocampus, amygdala, and neocortex—areas heavily affected in AD.

In a healthy brain, acetylcholine facilitates synaptic plasticity and modulates signal transmission between neurons, thus supporting the formation and retrieval of memories. In AD, significant loss of cholinergic neurons in the nucleus basalis of Meynert and reduced levels of choline acetyltransferase (ChAT) enzyme result in lower acetylcholine availability, contributing directly to cognitive deterioration (Sarter & Bruno, 1997).

4.2. Cholinesterase enzyme targets (AChE and BChE)

Acetylcholine activity in the synaptic cleft is terminated by hydrolysis via cholinesterase enzymes, primarily: (Darvesh, 2016)

- Acetylcholinesterase (AChE) – predominantly expressed in neuronal synapses and responsible for rapid breakdown of ACh.
- Butyrylcholinesterase (BChE) – found mainly in glial cells and peripheral tissues, with increasing activity in late-stage AD.

In Alzheimer's pathology, AChE activity declines, whereas BChE levels may remain stable or increase, suggesting both enzymes play complementary roles in modulating cholinergic transmission over the disease course.

Inhibiting these enzymes prolongs the action of acetylcholine at synapses, thereby enhancing cholinergic signaling. This mechanism forms the basis for the most commonly prescribed drugs in AD management (Saxena & Dubey, 2019). Figure 6 illustrating acetylcholine synthesis, release, synaptic activity, and degradation by AChE/BChE.

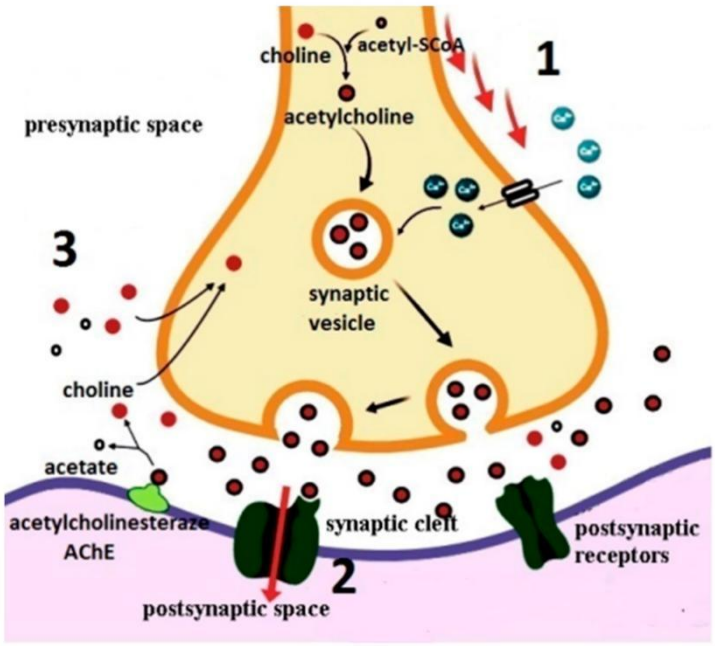

Figure 6. Cholinergic Neurotransmission and Role of Cholinesterase (Lane et al., 2006)

4.3. Basis for current pharmacotherapy

Current pharmacological interventions for AD aim to alleviate symptoms rather than halt disease progression. The first-line therapeutic agents include cholinesterase inhibitors (ChEIs), which act by preventing the enzymatic breakdown of acetylcholine (Chopra et al., 2011). Approved ChEIs include:

- Donepezil – selective AChE inhibitor, effective in mild to severe AD.
- Rivastigmine – dual AChE and BChE inhibitor, available in oral and transdermal formulations.
- Galantamine – AChE inhibitor with additional allosteric modulation of nicotinic receptors.

These drugs provide modest improvements in cognition, behavior, and functional abilities, particularly during the early to middle stages of AD. However, their benefits are often temporary and associated with adverse effects such as gastrointestinal distress, bradycardia, and muscle cramps (Kulshreshtha & Piplani, 2016).

Given the limited efficacy of current treatments, multi-targeted approaches, including combination therapies and natural inhibitors from plant sources, are under investigation to enhance therapeutic outcomes with fewer side effects.

5. Oxidative Stress in Alzheimer's Disease

Oxidative stress plays a pivotal role in the pathogenesis of Alzheimer's disease (AD). It refers to an imbalance between the production of reactive oxygen species (ROS) and the capacity of antioxidant defense systems to neutralize these reactive intermediates. The brain, due to its high oxygen demand, abundant lipid content, and limited antioxidant capacity, is particularly vulnerable to oxidative damage. In AD, oxidative stress interacts synergistically with amyloid and tau pathologies, leading to synaptic dysfunction, mitochondrial damage, and neuronal death.

5.1. Mechanisms of reactive oxygen species (ROS) generation in neurons

Reactive oxygen species—including superoxide anion (O_2^-), hydroxyl radical (•OH), and hydrogen peroxide (H_2O_2) are byproducts of normal mitochondrial oxidative phosphorylation (Figure 7). In healthy neurons, these species are tightly regulated. However, in AD, excessive ROS are generated due to:

- Mitochondrial dysfunction, particularly at complex I and III of the electron transport chain,
- Aβ accumulation, which disrupts mitochondrial membranes and promotes ROS leakage,
- Metal ion dysregulation (e.g., Fe^{2+}, Cu^{2+}), which catalyze Fenton-type reactions leading to hydroxyl radical formation.

These ROS can damage cellular components and initiate inflammatory responses, thereby accelerating neurodegeneration (Valencia & Morán, 2004).this relation is illustrated in figure 7

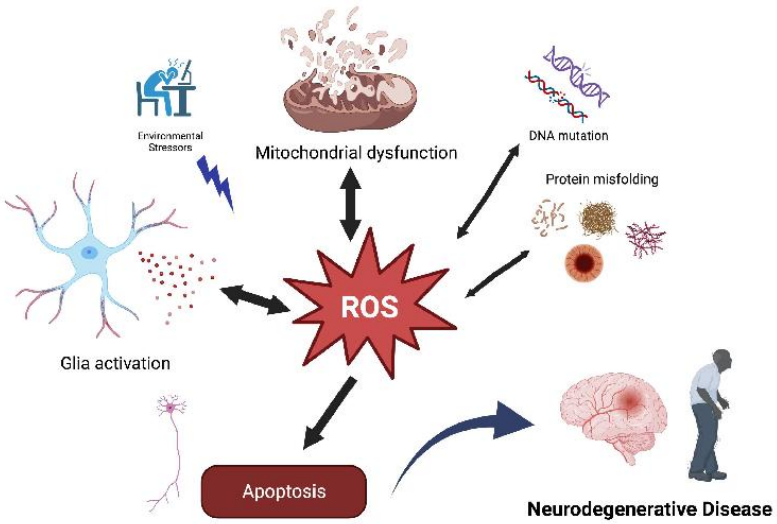

Figure 7. Sources and Effects of ROS Generation in AD Neurons (Valencia & Morán, 2004).

5.2. Lipid peroxidation, protein carbonylation, and DNA oxidation

ROS-induced damage affects multiple macromolecular targets in neurons:

- Lipid Peroxidation: Polyunsaturated fatty acids in neuronal membranes are susceptible to peroxidation, resulting in the formation of toxic byproducts such as malondialdehyde (MDA) and 4-hydroxynonenal (4-HNE). These disrupt membrane integrity, ion homeostasis, and receptor function.
- Protein Carbonylation: Oxidative modification of proteins alters their structure and function. Accumulation of carbonyl groups leads to enzyme inactivation, impaired cytoskeletal function, and protein aggregation.
- DNA Oxidation: ROS can induce strand breaks and base modifications, particularly 8-hydroxy-2'-deoxyguanosine (8-OHdG), which impairs transcription and triggers apoptotic signaling.

These oxidative insults are observed in early stages of AD and are closely associated with the regions showing the greatest neurodegeneration, such as the hippocampus and cortex (Fritz & Petersen, 2011).

5.3. Antioxidant defence mechanisms and redox imbalance

To counteract oxidative stress, neurons rely on an endogenous antioxidant defence system, including:

- Enzymatic antioxidants: Superoxide dismutase (SOD), catalase (CAT), glutathione peroxidase (GPx),
- Non-enzymatic antioxidants: Reduced glutathione (GSH), vitamins C and E, coenzyme Q10.

In AD, these systems are either overwhelmed or downregulated, contributing to chronic redox imbalance. A reduction in glutathione levels and altered SOD/CAT activity have been documented in AD brains and correlate with disease severity.

Therapeutically, antioxidants such as vitamin E, curcumin, and plant-derived polyphenols have shown potential in attenuating oxidative stress in preclinical studies. Natural sources with combined antioxidant and anti-inflammatory properties, like essential oils and flavonoids, are currently under investigation as neuroprotective agents (Sachdev et al., 2023).

6. Neuroinflammation

Neuroinflammation is a central and sustained pathological process in Alzheimer's disease (AD), contributing to neuronal injury and cognitive decline. While inflammation is a normal protective response to injury or infection, in AD it becomes chronic and dysregulated, exacerbating neurodegeneration. This process is mediated by the activation of glial cells microglia and astrocytes—and the release of pro-inflammatory mediators in response to amyloid-β (Aβ) accumulation and tau pathology (Shabab et al., 2017).

6.1. Role of microglial activation and astrocyte dysfunction

Microglia, the resident immune cells of the central nervous system, are among the first responders to amyloid deposition. In early disease stages, microglia exhibit a protective phenotype, clearing Aβ through phagocytosis (Correale, 2014). However, prolonged exposure to aggregated Aβ induces a pro-inflammatory transformation, characterized by the release of:

- Tumor necrosis factor-alpha (TNF-α),
- Interleukin-1 beta (IL-1β),
- Interleukin-6 (IL-6),
- Nitric oxide (NO) and reactive oxygen species (ROS).

Similarly, astrocytes, which normally support synaptic and metabolic homeostasis, undergo astrogliosis, leading to the release of inflammatory cytokines and impairment of neuronal-glial communication (Kwon & Koh, 2020).

These changes disrupt the blood-brain barrier, impair synaptic transmission, and contribute to neuronal death. The sequence of glial activation and inflammatory mediator release is depicted in Figure 8, which highlights the shift from protective to neurotoxic glial responses (Pekny et al., 2014).

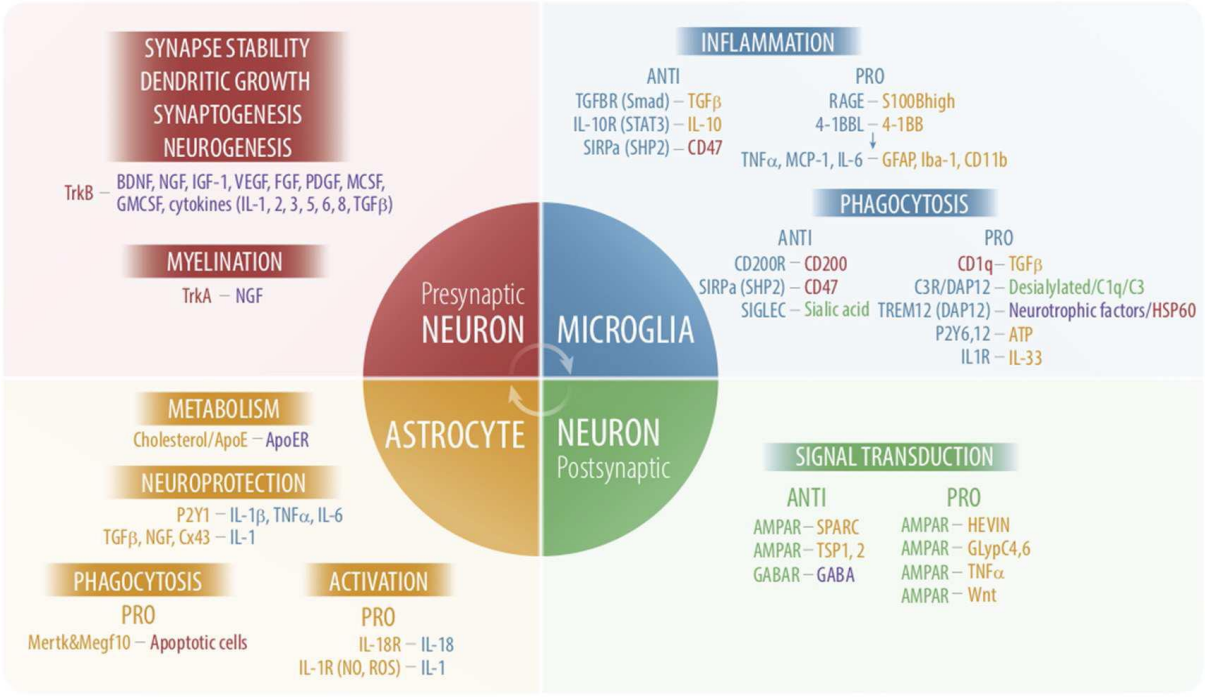

Figure 8. Microglial and Astrocytic Activation in Alzheimer's Disease (Matejuk & Ransohoff, 2020)

6.2. Key cytokines and inflammatory mediators (IL-1β, TNF-α, IL-6)

Aβ and tau aggregates act as damage-associated molecular patterns (DAMPs), triggering innate immune responses through receptors like TLR4 and NLRP3 inflammasome on microglia. This initiate signalling cascades (e.g., NF-κB pathway), resulting in the transcription of pro-inflammatory genes.

Among the most studied cytokines:

- TNF-α promotes apoptosis and synaptic dysfunction.
- IL-1β enhances tau phosphorylation and impairs long-term potentiation.
- IL-6 disrupts synaptic plasticity and promotes Aβ production.

Chronic overexpression of these cytokines reinforces a toxic loop of inflammation, oxidative stress, and neuronal injury (Möller & Villiger, 2006).

6.3. Crosstalk between inflammation and Aβ/tau pathologies

Neuroinflammation does not occur in isolation; it amplifies and is amplified by Aβ and tau pathologies. For example:

- Inflammatory cytokines can upregulate BACE1, increasing Aβ production.
- IL-1β and TNF-α can activate kinases such as GSK-3β, enhancing tau phosphorylation (Metcalfe & Figueiredo-Pereira, 2010).

This bidirectional interaction suggests that inflammation is both a consequence and a driver of pathological protein aggregation in AD (Leng & Edison, 2021).

7. Current and Emerging Therapeutic Approaches

Despite extensive research, there is currently no cure for Alzheimer's disease (AD). Available therapies focus on symptomatic relief and slowing cognitive decline rather than reversing disease progression. Traditional pharmacological strategies have centred around cholinergic and glutamatergic systems. However, emerging research now targets amyloid clearance, tau aggregation, oxidative stress, inflammation, and other pathophysiological pathways. This section outlines both approved therapies and experimental interventions under investigation (A. Kumar et al., 2023).

7.1. Approved drugs: Donepezil, Rivastigmine, Galantamine, Memantine

Currently, four main drugs are approved by regulatory agencies (e.g., FDA, EMA) for the symptomatic management of AD:

- Donepezil: A selective acetylcholinesterase inhibitor (AChEI), approved for all stages of AD. Enhances cholinergic neurotransmission and provides modest improvements in cognition and global functioning.
- Rivastigmine: A dual inhibitor of AChE and BChE, available as oral capsules and transdermal patches. Used in mild to moderate AD and Parkinson's disease dementia.
- Galantamine: AChEI with additional allosteric modulation of nicotinic receptors, contributing to enhanced synaptic transmission.
- Memantine: A non-competitive NMDA receptor antagonist approved for moderate to severe AD. Modulates glutamatergic excitotoxicity without impairing normal neurotransmission (Tan et al., 2014).

Although these drugs provide temporary symptomatic relief, their effects are typically limited, and they do not alter the underlying disease mechanisms. The action and targets of these drugs are illustrated in Figure 9, showing their roles in neurotransmitter modulation.

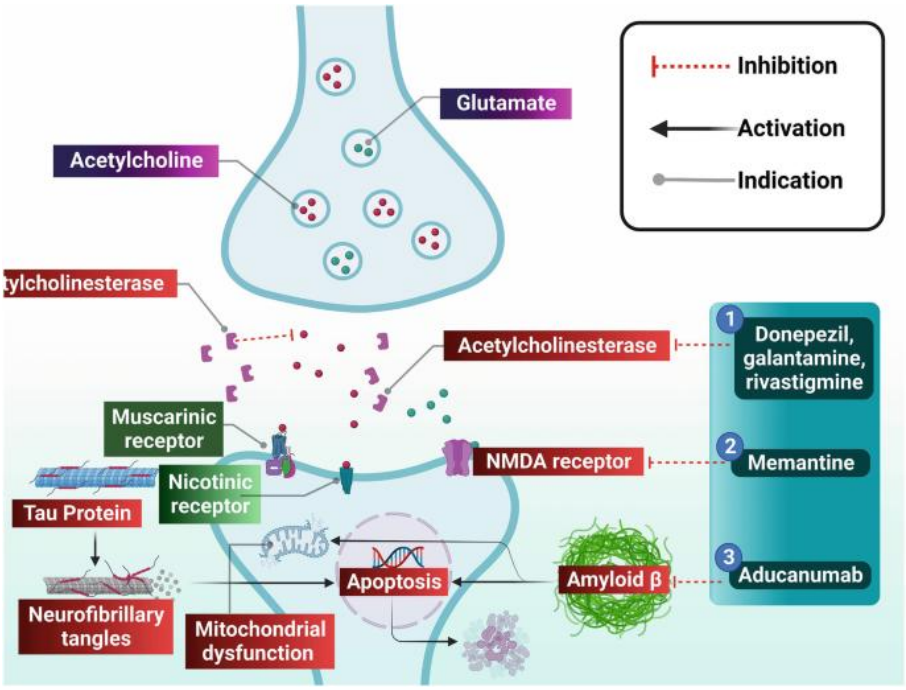

Figure 9. Mechanism of Action of Approved Alzheimer's Drugs (Vishwas et al., 2023)

7.2. Mechanisms, limitations, and side effects

Each approved therapy has mechanistic and clinical limitations:

- They do not prevent neuronal death or disease progression.
- Their benefits often plateau after 6–12 months.
- Adverse effects include nausea, vomiting, bradycardia (for ChEIs), or dizziness and agitation (for Memantine).

The limited efficacy and tolerability of current drugs underscore the urgent need for disease-modifying treatments that target early molecular events such as Aβ deposition, tau hyperphosphorylation, and neuroinflammation (Tattersfield, 1997).

7.3. Multi-target strategies and natural product-based interventions

Given the multifactorial nature of AD, multi-target-directed ligands (MTDLs) and natural bioactive compounds have gained interest. These approaches aim to modulate multiple pathological pathways simultaneously (Liu et al., 2025). Notable strategies include:

- Anti-amyloid monoclonal antibodies: e.g., Aducanumab and Lecanemab (controversial and costly, with limited efficacy).

- Tau aggregation inhibitors: targeting hyperphosphorylated tau stabilization.
- Antioxidants and anti-inflammatories: curcumin, resveratrol, rosmarinic acid, and essential oils.

Phytochemicals from medicinal plants such as *Cotula cinerea* and *Origanum majorana* show cholinesterase inhibitory, antioxidant, and anti-inflammatory properties, positioning them as promising candidates for adjunctive or preventive therapy. Their mechanisms of action and polypharmacological potential are summarized in Figure 10.

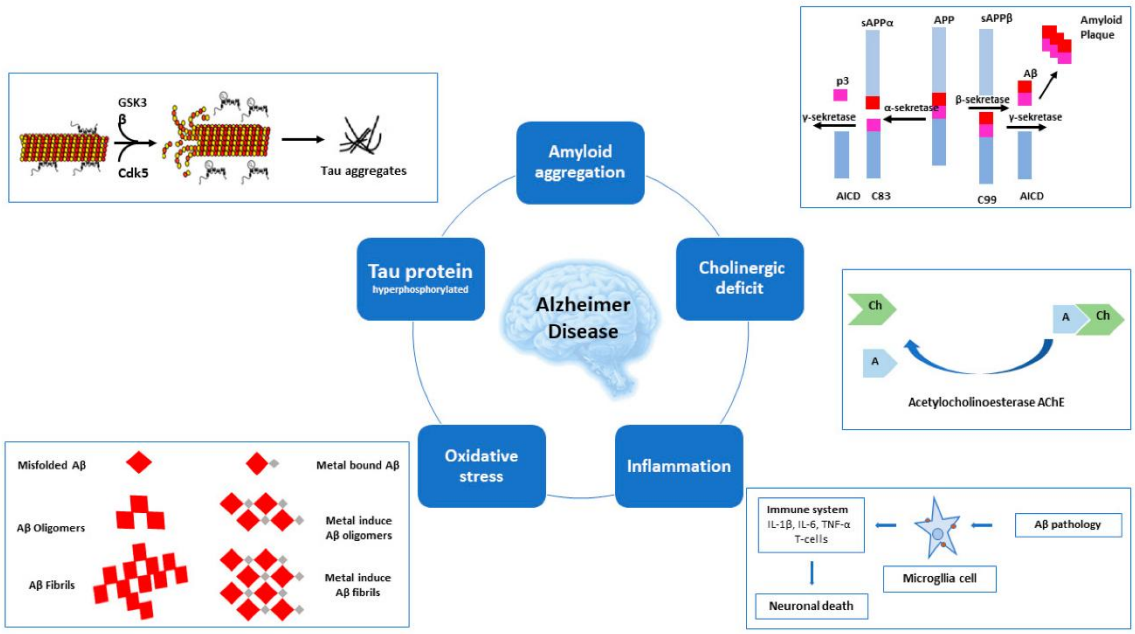

Figure 10. Multi-Target Approach to Alzheimer's Therapy (Cheong et al., 2022)

8. Experimental Models in AD Research

The complexity of Alzheimer's disease (AD) necessitates the use of diverse experimental models to understand its pathogenesis and evaluate potential therapeutic agents. These models include *in vitro* assays, *in vivo* animal models, and *in silico* simulations, each contributing unique insights into disease mechanisms and drug development. A comprehensive preclinical evaluation often integrates all three approaches to validate efficacy and predict human relevance (Drummond & Wisniewski, 2017).

8.1. In vitro: Enzyme inhibition and cell-based assays

In vitro models provide a controlled environment for studying specific cellular and biochemical processes relevant to AD (Pietrak et al., 2005). Two main approaches include:

- Enzyme inhibition assays: These are used to evaluate compounds for their ability to inhibit acetylcholinesterase (AChE) and butyrylcholinesterase (BChE), key enzymes involved in acetylcholine degradation. Ellman's method is widely used to assess AChE inhibition by natural and synthetic compounds.
- Cell-based assays: Neuronal or glial cell cultures (e.g., SH-SY5Y, PC12) are exposed to Aβ peptides, hydrogen peroxide, or inflammatory agents to model oxidative stress and inflammation. Neuroprotective agents are then evaluated based on their ability to reduce ROS production, restore mitochondrial function, or attenuate apoptosis.

These assays allow for high-throughput screening and mechanistic evaluation at the cellular level.

8.2. In vivo: Rodent models (scopolamine, Aβ injection, transgenics)

Animal models, particularly rodents, provide insights into the systemic and behavioral manifestations of AD (W. N. Chen & Yeong, 2020). Common models include:

- Scopolamine-induced memory impairment: This pharmacological model uses scopolamine to block muscarinic acetylcholine receptors, mimicking cholinergic deficits. It is widely used for behavioral testing of AChE inhibitors and memory enhancers.
- Aβ-injection models: Direct intracerebral or intraventricular injection of Aβ oligomers induces amyloid pathology and cognitive deficits, useful for acute screening of anti-amyloid agents.
- Transgenic mouse models: These include APP/PS1, 3xTg-AD, and Tg2576 lines, which overexpress mutant human genes associated with familial AD. They develop Aβ plaques, tau tangles, gliosis, and progressive memory impairment.
- AlCl-Induced Model: Chronic oral exposure to aluminum chloride causes Alzheimer's-like changes in rodents, including oxidative stress, cholinergic disruption, tau buildup, and memory loss (Ramadan et al.,2023)
- D-galactose Model: Long-term D-galactose treatment (50–500 mg/kg) induces aging-like brain damage, marked by oxidative stress, inflammation, and cognitive decline (Li et al.,2019)
- Combined $AlCl_3$ + D-galactose Model: The combined administration of aluminum chloride and D-galactose in mice effectively mimics Alzheimer's disease by promoting amyloid-β (Aβ) accumulation in the cortex and hippocampus. This model alters the expression of key Aβ metabolism-related proteins, such as increasing BACE1 and

decreasing LRP1 and NEP, leading to memory impairment. It serves as a valuable tool for exploring AD mechanisms and testing potential therapeutic agents. (Luo et.,2009)

- Rodent models are critical for validating therapeutic efficacy in terms of behavior, biochemistry, and histopathology (Cuello et al., 2019).

8.3. In silico: Molecular docking, ADMET, and Dynamics simulation

In silico approaches are computational techniques used to predict molecular interactions, pharmacokinetics, and the dynamic behavior of drug candidates (Gheidari et al., 2024). These methods are cost-effective and widely used for early-stage screening:

- Molecular docking simulates the interaction between a ligand (e.g., plant compound) and a target protein (e.g., AChE or BACE1), providing insights into binding affinity and active site interactions.
- ADMET prediction assesses Absorption, Distribution, Metabolism, Excretion, and Toxicity parameters, offering preliminary evaluations of pharmacokinetic profiles.
- Molecular dynamics (MD) simulations provide time-resolved visualization of ligand-protein complexes, revealing stability, flexibility, and conformational changes over time.

These techniques complement experimental data and guide compound optimization (Jamal et al., 2023).

9. Conclusion

Alzheimer's disease (AD) remains a complex and multifactorial neurodegenerative disorder with profound clinical and societal consequences. The progression of AD is underpinned by an intricate interplay of biochemical and cellular events, including amyloid-β accumulation, tau hyperphosphorylation, oxidative stress, chronic neuroinflammation, and cholinergic dysfunction. Each of these pathophysiological mechanisms contributes to synaptic loss, neuronal death, and cognitive deterioration, forming the basis of current research and therapeutic strategies (Marques et al., 2010).

9.1. Summary of interconnected pathophysiological processes

As presented throughout this chapter, the hallmark features of AD—namely, extracellular amyloid plaques and intracellular neurofibrillary tangles—are tightly linked to a cascade of detrimental processes:

- Oxidative stress exacerbates mitochondrial dysfunction and neuronal injury.
- Neuroinflammation amplifies Aβ and tau pathologies through glial activation.
- Cholinergic deficits disrupt neurotransmission and memory formation.

These interconnected events collectively create a self-perpetuating cycle of neurodegeneration.

9.2. Justification for investigating antioxidant and anti-inflammatory natural compounds

Given the limitations of current pharmacotherapies—mainly their symptomatic focus and lack of disease-modifying effects—there is a growing demand for multi-targeted interventions. Natural compounds with antioxidant, anti-inflammatory, and cholinesterase-inhibiting properties offer promising alternatives or adjuncts to conventional drugs.

This rationale supports the investigation of medicinal plants, particularly *Cotula cinerea* and *Origanum majorana*, which have been traditionally used for their neuroprotective and anti-inflammatory activities. Their rich phytochemical content may hold potential for modulating multiple pathological targets in AD.

9.3. Transition to the study of medicinal plants in Chapter 2

Building on the theoretical foundation established in this chapter, Chapter 2 will explore the ethnopharmacological relevance, phytochemical composition, and biological activities of *Cotula cinerea* and *Origanum majorana*. Emphasis will be placed on their role as natural candidates in combating oxidative stress, inflammation, and cholinergic dysfunction in Alzheimer's disease.

CHAPTER TWO:

Overview of Cotula cinerea and Origanum majorana

1. Introduction

Cotula cinerea and *Origanum majorana* are two medicinal plants traditionally used in North African and Mediterranean regions (Bouzidi et al., 2011). Known for their therapeutic properties, these plants have been employed in treating various ailments, including digestive disorders, respiratory issues, and inflammatory conditions. Recent studies have highlighted their potential neuroprotective effects, making them subjects of interest in Alzheimer's disease research (Alimi et al., 2022).

2. Botanical Description and Taxonomic Classification

2.1. Cotula cinerea (Lakhdar, 2018)

- **Family**: Asteraceae
- **Genus**: *Cotula*
- **Species**: *Cotula cinerea* Delile
- **Synonym**: *Brocchia cinerea*

Cotula cinerea is a low-growing, perennial herb reaching up to 25 cm in height. It features branched stems covered with white hairs and alternate, spatulate leaves (Figure 11). The plant produces solitary, terminal flower heads (capitula) that are yellow and measure approximately 5–7 mm in length. It thrives in arid and semi-arid regions, often found in sandy soils (Mekhadmi et al., 2024).

Figure 11. *Cotula cinerea* in its natural habitat.

2.2. *Origanum majorana* (Bouyahya et al., 2021)

- **Family:** Lamiaceae
- **Genus:** Origanum
- **Species:** Origanum majorana L.
- **Common Names:** Sweet marjoram, knotted marjoram

Origanum majorana is a tender perennial sub-shrub that typically grows between 30–50 cm tall. It has aromatic, oval, grey-green leaves and produces small, tubular white or pale pink flowers during the summer months (Figure 12). Native to the Mediterranean region and Western Asia, it prefers well-drained soils and full sun exposure (Ietswaart, 1980).

Figure 12. *Origanum majorana* flowering.

3. Geographic Distribution and Ecological Characteristics

3.1. Cotula cinerea

Cotula cinerea is predominantly found in North Africa, especially in the Saharan regions of Algeria and Morocco. It thrives in arid and semi-arid climates, often inhabiting sandy and gravelly soils. The plant's adaptability to harsh desert conditions underscores its ecological resilience (F.-E. Guaouguaou et al., 2018).

3.2. Origanum majorana

Origanum majorana, commonly known as sweet marjoram, is native to the Mediterranean region, including Algeria. It prefers well-drained soils and is typically cultivated in gardens and farms. The plant flourishes in temperate climates and is sensitive to frost, which limits its distribution to warmer areas (Charai et al., 1996).

4. Traditional and Ethnomedicinal Uses

4.1. Cotula cinerea

Cotula cinerea is widely utilized in traditional medicine across North Africa, particularly in Algeria and Morocco. Traditional applications include treatments for digestive disorders, colic, diarrhea, rheumatism, urinary and pulmonary infections, fever, and headaches. Preparations are commonly made as decoctions, infusions, or poultices. Additionally, nomadic communities use the plant as a tea additive and for preserving goat butter due to its preservative properties (Agour et al., 2024).

4.2. Origanum majorana

Origanum majorana, commonly known as sweet marjoram, has a rich history in traditional medicine, especially in Mediterranean and Middle Eastern cultures. It has been used to alleviate digestive issues such as indigestion, bloating, and gas. The herb is also employed for its calming effects, aiding in stress and anxiety relief. Other traditional uses include treatments for respiratory conditions like coughs and bronchitis, as well as menstrual cramps and skin inflammations (Baatour et al., 2010).

5. Phytochemical Composition

5.1. Cotula cinerea

Cotula cinerea is rich in various phytochemicals, including essential oils, flavonoids, tannins, saponins, terpenoids, and steroids. The essential oil, extracted via hydrodistillation, comprises numerous compounds, with major constituents such as trans-thujone (51.86%), santolina triene (10.6%), α-pinene (2.02%), sabinene (6.17%), cineole (5.34%), and camphor (2.63%) (Bettayeb et al., 2022).

5.2. Origanum majorana

Origanum majorana contains a diverse array of phytochemicals, notably essential oils rich in monoterpenes and phenolic compounds. Key constituents include terpinen-4-ol (38.4%), cis-sabinene hydrate (15.0%), p-cymene (7.0%), and γ-terpinene (6.9%) (Banchio et al., 2008).

6. Pharmacological and Biological Activities

6.1. Cotula cinerea

Cotula cinerea exhibits notable pharmacological properties, including antioxidant, anti-inflammatory, and neuroprotective effects (Bensizerara et al., 2013).

- **Antioxidant Activity**: The plant's extract demonstrates significant free radical scavenging abilities, with DPPH and FRAP assays indicating IC_{50} values of 0.54 ± 0.023 mg/mL and 0.51 ± 0.012 mg/mL, respectively.
- **Anti-inflammatory Effects**: In vivo studies reveal that *C. cinerea* extract reduces inflammation in animal models, showing effectiveness comparable to standard anti-inflammatory drugs.
- **Neuroprotective Potential**: The plant's antioxidant and anti-inflammatory properties contribute to its potential in mitigating neurodegenerative processes, suggesting its relevance in Alzheimer's disease research.

6.2. Origanum majorana

Origanum majorana is recognized for its diverse biological activities, particularly its antioxidant, anti-inflammatory, and neuroprotective effects (Sellami et al., 2009).

- **Antioxidant Properties**: The plant contains compounds like rosmarinic acid and thymol, which exhibit strong antioxidant activities, combating oxidative stress.
- **Anti-inflammatory Activity**: *O. majorana* essential oil has been shown to inhibit pro-inflammatory cytokines such as TNF-α, IL-1β, and IL-6, thereby reducing inflammation.
- **Neuroprotective Effects**: Studies indicate that *O. majorana* can protect against neuroinflammation-mediated cognitive impairment, highlighting its potential in neurodegenerative disease management.

7. Relevance in Alzheimer's Disease Research

7.1. Cotula cinerea

Cotula cinerea exhibits significant antioxidant and anti-inflammatory properties, which are crucial in mitigating oxidative stress and neuroinflammation associated with Alzheimer's disease (AD). Studies have identified various phenolic compounds in *C. cinerea*, such as luteolin-4'-O-glucoside and chlorogenic acid, known for their neuroprotective effects. These compounds can scavenge free radicals and reduce oxidative damage, potentially slowing the progression of neurodegenerative processes in AD (Chlif et al., 2022).

7.2. Origanum majorana

Origanum majorana has demonstrated promising neuroprotective effects in AD models. Essential oil from *O. majorana* (OmEO) has been shown to enhance memory performance and increase brain-derived neurotrophic factor (BDNF) expression in rats with Aβ1-42-induced AD-like symptoms. Additionally, OmEO exhibits antioxidant activity, reducing oxidative stress markers in the brain (Jun et al., 2001). Furthermore, ursolic acid isolated from *O. majorana* has been identified as a potent acetylcholinesterase (AChE) inhibitor, suggesting its potential in improving cholinergic neurotransmission in AD.

SECOND PART:

EXPERIMENTAL

CHAPTER ONE: MATERIALS AND METHODS

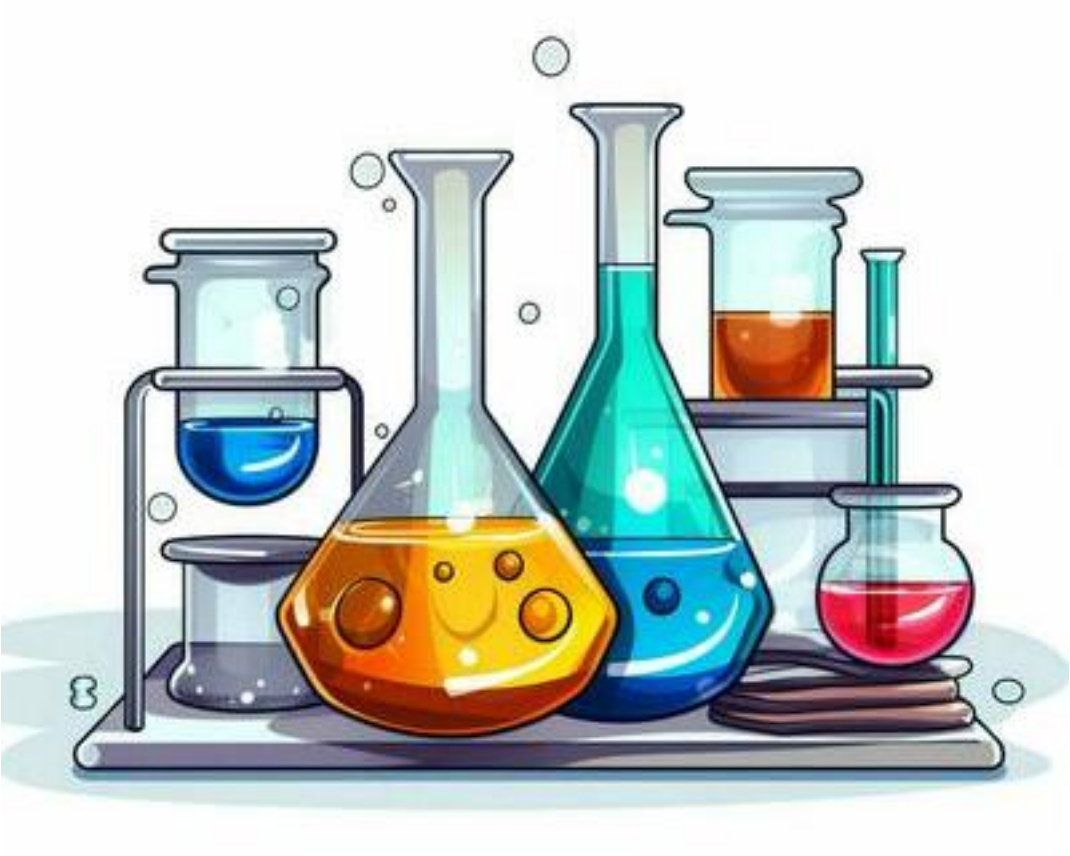

1. Introduction

The Materials and Methods chapter provides a comprehensive account of the experimental procedures and methodologies employed in this study, ensuring transparency and reproducibility of the research findings. This investigation was conducted collaboratively between two specialized laboratories: the Valorisation and Technology of Sahara Resources (VTRS) Laboratory at the University of El Oued and the Scientific and Technical Research Centre in Physico-Chemical Analysis (CRAPC). The VTRS Laboratory facilitated the extraction of plant materials, conducted *in vivo* and *in vitro* assays, and performed *in silico* analyses. Meanwhile, CRAPC was responsible for the precise liquid chromatography-mass spectrometry (LC-MS) analysis of the plant extracts. This collaborative effort ensured thorough and accurate experimentation, combining expertise and resources from both institutions.

The subsequent sections detail the specific methodologies employed, including the collection and identification of plant materials, phytochemical analyses, green synthesis and characterization of metal nanoparticles, *in vivo* studies with appropriate ethical considerations, *in vitro* bioassays, and *in silico* analyses. Each subsection is meticulously structured to provide clarity and facilitate reproducibility, adhering to the highest standards of scientific inquiry.

2. Plant Material

2.1. Collection and Identification of Plant Species

The collection and identification of plant specimens were conducted with meticulous attention to ensure the authenticity and integrity of the botanical materials used in this study. The geographical locations and environmental conditions of the collection sites are detailed below.

2.1.1. Cotula cinerea

Cotula cinerea, a member of the Asteraceae family, was collected during December 2024 and January 2025 from the Nigrine region in Tébessa Province, northeastern Algeria. This area is characterized by a semi-arid to arid climate, with low annual rainfall and significant temperature variations between seasons. The specific attributes of the collection site are as follows (Alia et al., n.d.):

- Geographic Coordinates: Latitude 34°25′00″ North, Longitude 7°51′00″ East.
- Elevation: Approximately 317 meters above sea level.

- Distance from Coastline: Approximately 300 kilometres inland.
- Bioclimatic Characterization: Arid desert environment.

2.1.2. Origanum majorana L

Origanum majorana, commonly known as sweet marjoram and belonging to the Lamiaceae family, was collected between March and April 2024 from the Tébessa region in northeastern Algeria. The collection site exhibits the following characteristics (Harrate et al., 2025):

- Geographic Coordinates: Latitude 34°25′00″ North, Longitude 7°51′00″ East..
- Elevation: Approximately 317 meters above sea level.
- Distance from Coastline: Approximately 300 kilometers inland.
- Bioclimatic Characterization: Cold semi-arid climate (Köppen–Geiger classification: BSk), characterized by hot, dry summers and cool, wetter winters. The average annual temperature is around 15.1°C, with annual precipitation averaging approximately 343 mm.

2.2. Preparation of Plant Extracts

The extraction of bioactive compounds from *Cotula cinerea* and *Origanum majorana* L. was performed using a maceration method with three different solvents: butanol, methanol, and water (Manimaran et al., 2025). This approach aimed to evaluate the efficiency of each solvent in extracting phytochemicals from the plant materials (SUHENDRA et al., 2025). The following standardized procedures were meticulously carried out to ensure the integrity and reproducibility of the extracts.

2.2.1. Sample Collection and Preparation

- ✓ **Collection and Cleaning**: Aerial parts (leaves and stems) of both *Cotula cinerea* and *Origanum majorana* L. were harvested from their respective natural habitats in southeastern Algeria. For each plant species, 50 grams of fresh material were collected. The samples were thoroughly washed under running water to remove surface impurities.
- ✓ **Sorting and Cutting**: Wet sorting was conducted to select the healthiest and most representative samples. The selected plant materials were then cut into smaller segments to facilitate uniform drying.

2.2.2. Drying Process

- ✓ Aerial parts Dried at room temperature in a well-ventilated, shaded area to preserve heat-sensitive phytochemicals.

2.2.3. Grinding

Once completely dried, the plant materials were ground into a coarse powder using a dry grinder, enhancing the surface area for extraction.

2.2.4. Extraction Process

The powdered plant materials underwent maceration using three different solvents: butanol, methanol, and water. Each extraction was performed separately to compare the efficacy of the solvents. The procedure for each solvent was as follows:

- ✓ **Maceration:** For each extraction, 50 grams of the powdered plant material were mixed with 500 mL of the respective solvent, maintaining a plant-to-solvent ratio of 1:10 (w/v). The mixtures were stored in sealed containers at room temperature in the dark for 24 hours, with periodic agitation to promote solvent penetration and solute diffusion. Each maceration was repeated three times to maximize compound extraction.
- ✓ **Filtration**: After each maceration, the extracts were filtered through Whatman No. 2 filter paper to separate the liquid extract from the plant residue.
- ✓ **Combination of Filtrates**: The filtrates from the three maceration steps were combined for each solvent.

Figure 13 Extraction Process

2.2.5. Solvent Removal and Concentration

- ✓ **Butanol and Methanol Extracts:** The combined filtrates were concentrated using a Büchi Rotavapor R-200 rotary evaporator equipped with a B-490 heating bath and vacuum pump V-3300 (Mabuza et al., n.d.). The evaporation process was conducted at 45°C and 5mbar ± (2mbar) vacuum to remove the solvents, yielding the crude extracts.
- ✓ **Aqueous Extracts**: The water-based extracts were subjected to lyophilization (freeze-drying) to remove water content without exposing the extracts to elevated temperatures, thereby preserving thermolabile compounds (Joshi et al., 2025). Lyophilization was performed using the SED-XDG Series Laboratory Freeze Dryer, a pilot-scale laboratory freeze dryer suitable for research and experimental purposes (Madi et al., 2025). Lyophilization involves freezing the aqueous extract followed by sublimation under reduced pressure, resulting in a dry, stable powder. This method is advantageous as it maintains the structural and chemical integrity of the bioactive compounds (Rivas-Gastélum et al., 2025).

2.2.6. Extraction Yield

The extraction yield for each solvent was calculated using the formula (Benine et al., 2025):

$$\text{Yield (\%)} = \left(\frac{Mass\ of\ Dried\ Extract\,(g)}{Initial\ Mass\ of\ Plant\ Material\,(g)} \right) \times 100 \quad \textbf{(1)}$$

3. Phytochemical Analysis

Phytochemical analysis identifies and quantifies bioactive compounds in plant extracts. This study examines *Cotula cinerea* and *Origanum majorana* L. using qualitative screenings, quantitative assessments, and Liquid Chromatography-Mass Spectrometry (LC-MS) for detailed chemical characterization.

3.1. Qualitative Phytochemical Screening

This preliminary analysis detects the presence of various phytochemical groups, including polyphenols, alkaloids, flavonoids, tannins, saponins, terpenoids, reducing sugars and glycosides. Standard protocols were followed for each assay:

3.1.1. Polyphenols Detection (Hu et al., 2025)

- ✓ **Method:** The Folin-Ciocalteu method involves mixing 1 mL of the plant extract with the Folin-Ciocalteu reagent and sodium carbonate.
- ✓ **Positive Observation:** Development of a blue coloration indicates the presence of polyphenols.

3.1.2. Flavonoids Detection (Sutrisno & Kartini, 2025)

- ✓ **Method:** Add a few drops of 10% aluminium chloride ($AlCl_3$) solution to 1 mL of the extract.
- ✓ **Positive Observation:** A yellow coloration signifies the presence of flavonoids.

3.1.3. Alkaloids Detection (Moreno & Solar, 2025)

- ✓ **Method:** To 1 mL of the plant extract, add a few drops of Mayer's reagent.
- ✓ **Positive Observation:** The formation of a white or creamy precipitate indicates the presence of alkaloids.

3.1.4. Terpenoids Detection (Yu et al., n.d.)

- ✓ **Method:** Combine 2 mL of the extract with 2 mL of acetic anhydride ($(CH_3CO)_2O$), followed by 2-3 drops of concentrated sulfuric acid (H_2SO_4).
- ✓ **Positive Observation:** A deep red coloration indicates terpenoids.

3.1.5. Tannins Detection (Tambe et al., 2025)

- ✓ **Method:** Mix 2 mL of the extract with 2 mL of water, then add 2-3 drops of 5% ferric chloride ($FeCl_3$) solution.
- ✓ **Positive Observation:** Formation of a green precipitate suggests the presence of tannins.

3.1.6. Saponins Detection (Lv et al., 2025)

- ✓ **Method:** Shake 5 mL of the extract with 5 mL of water vigorously.
- ✓ **Positive Observation:** Persistent froth formation indicates saponins.

3.1.7. Reducing Sugars Detection (A. Yadav et al., 2025)

- ✓ **Method:** To 2 mL of the extract, add 10 mL of water, 2 drops of 20% ethanolic α-naphthol, and 2 mL of concentrated sulfuric acid (H_2SO_4).
- ✓ **Positive Observation:** A red precipitate signifies reducing sugars.

3.1.8. Glycosides Detection (Milella et al., 2025)

- ✓ **Method:** Treat 2 mL of the extract with 2 mL of chloroform ($CHCl_3$) and 2 mL of acetic acid (CH_3COOH).
- ✓ **Positive Observation:** A colour change from violet to blue to green indicates glycosides.

3.2. Quantitative Phytochemical Analysis

In the present study, we conducted a comprehensive quantitative phytochemical analysis to determine the concentrations of key bioactive compounds [Total Phenolic Content (TPC), Total Flavonoid Content (TFC), and Condensed Tannin Content (CTC)] in *Cotula cinerea* and *Origanum majorana* L methanolic extract.

3.2.1. Estimation of Total Polyphenols Content (TPC)

Polyphenolic content was quantified using a modified Folin-Ciocalteu spectrophotometric method, as per (Shahhoseini, 2025). In this procedure, 0.2 mL of varying concentrations of the dry crude methanolic extract of *Cotula cinerea* and *Origanum majorana* L., were combined with 1 mL of 10% Folin–Ciocalteu reagent in test tubes. After a 5-minute incubation, 0.8 mL of 7.5% sodium carbonate (Na_2CO_3) solution was added. The reaction mixtures were then incubated in the dark at room temperature for 30 minutes. Subsequently, absorbance readings were taken at 765 nm using a UV-Vis spectrophotometer. A standard calibration curve was constructed using gallic acid concentrations ranging from 20 to 160 µg/mL. The polyphenolic content of the extracts was expressed as micrograms of gallic acid equivalents per milligram of extract (mg GAE/g).

3.2.2. Estimation of Total Flavonoids Content (TFC)

The flavonoid content in *Cotula cinerea* and *Origanum majorana* L. extracts was quantified using a colorimetric assay involving aluminium chloride ($AlCl_3$), following the methodology outlined by (Belew & Gebre, 2025). Specifically, 0.5 mg of each extract, was combined with

0.5 mL of 2% $AlCl_3$ solution. The mixtures were incubated in the dark at room temperature for 1 hour to facilitate complex formation. Subsequent absorbance measurements were taken at 420 nm using a UV-Vis spectrophotometer. A standard calibration curve was generated utilizing quercetin concentrations ranging from 0 to 50 µg/mL. The flavonoid content was then expressed as micrograms of quercetin equivalents per milligram of extract (µg QE/mg E).

3.2.3. Estimation of Condensed Tannin Content (CTC)

The quantification of condensed tannins in *Cotula cinerea* and *Origanum majorana* L. extracts was conducted following the vanillin-hydrochloric acid spectrophotometric method, as outlined by (Hama et al., 2025). This technique is based on the reaction between vanillin's aldehyde group and carbon 6 of the catechin A-ring, forming a red-coloured complex with characteristic absorption at 500 nm. In this procedure, 500 µL of each extract, was mixed with an equal volume of concentrated hydrochloric acid. After 15 minutes of incubation at room temperature in the dark, absorbance was recorded at 500 nm using a UV-Vis spectrophotometer. The condensed tannin content was quantified using a standard catechin calibration curve (0–1.5 µg/mL) and expressed as micrograms of catechin equivalent per milligram of extract (mg CE/g E).

3.3. Ultra performance liquid chromatography mass spectrometry (UPLC/MS–MS) analysis

✓ **UPLC-ESI-MS/MS System:** Analyses were conducted using a Shimadzu LCMS-8040 system, renowned for its ultra-fast multiple reaction monitoring capabilities and high sensitivity.

✓ **Chromatographic Separation:**

- **Column:** Restek Ultra C18 column (150 mm × 4.6 mm, 3 µm particle size), selected for its high-purity, type-B silica, ensuring reliable high-performance liquid chromatography (HPLC) applications.
- **Mobile Phase:** Solvent A consisted of water with 0.1% formic acid, while Solvent B was methanol.
- **Gradient Program:**
  - 0.0–0.2 min: 98% A
  - 0.2–2.5 min: linear gradient to 25% A
  - 2.5–4.0 min: linear gradient to 0% A

- 4.0–7.0 min: maintained at 0% A
- 7.0–7.1 min: return to 98% A
- 7.1–12.0 min: re-equilibration at 98% A

- **Flow Rate:** 0.2 mL/min.
- **Injection Volume:** 5 µL.

✓ **Mass Spectrometric Conditions:**

- **Ionization Source:** Electrospray ionization (ESI) in both positive and negative modes.
- **Interface Parameters:**
  - Desolvation Line (DL) Temperature: 250°C
  - Heat Block Temperature: 400°C
  - Nebulizing Gas Flow: 3.0 L/min
  - Drying Gas Flow: 10 L/min
- **Collision-Induced Dissociation (CID) Gas Pressure:** 230 kPa.
- **Conversion Dynode Voltage:** −6.00 kV.

4. Green Synthesis of Metal-Oxide Nanoparticles

4.1. Equipment and Apparatus

- Analytical balance.
- Glass measuring cylinder.
- Flasks and beackers.
- Hot plate magnetic stirrer.
- Centrifuge.
- Mortar.
- Muffle furnace.

4.2. Chemicals and Reagents

- Zinc acetate 0.1 M.
- Silver nitrate 0.1M.
- Plant extracts.
- Deionized (DI) water.
- Sodium hydroxide (NaOH) 0.1M and 10mM.

4.3. Green synthesis of Zinc Oxide Nanoparticles (ZnO-NPs)

The synthesis of zinc oxide nanoparticles (ZnO-NPs) was performed following a previously established method with slight modifications (Al-Tameemi et al., 2025). 0.1 M zinc acetate $Zn(CH_3CO_2)_2$ solution prepared in 400 ml deionized (DI) water was added separately to 200 mL of *Origanum majorana* and *Cotula cinerea* extracts and 0.1 M of NaOH sodium hydroxide prepared in 150 ml deionized (DI) water added dropwise to the reaction mixture until the reaction mixture exhibited a white colour and the PH is adjusted around 10-13 , the extracts where mentioned by decoction 50 g of plant in 750 ml (DI) water for 2 hours then filtered through Whatman No. 2 filter paper and cooled at room temperature. Each mixture was continuously stirred at 65°C for 2 hours to facilitate nanoparticle formation. After the reaction was completed, the solutions were cooled to room temperature (25°C) and subjected to centrifugation at 10.000 rpm for 10 minutes to isolate the solid phase. The resulting precipitates were washed three times with distilled water to remove any residual impurities. The purified ZnO-NPs were then dried in sterile Petri dishes, followed by oven drying at 90°C. Subsequently, the dried material was finely ground using a mortar and pestle and calcinated at 600°C for 5 hours to eliminate any remaining organic residues or contaminants. The obtained ZnO-NPs were stored under appropriate conditions for further characterization and analysis.all the steps are illustrated in Figure 14

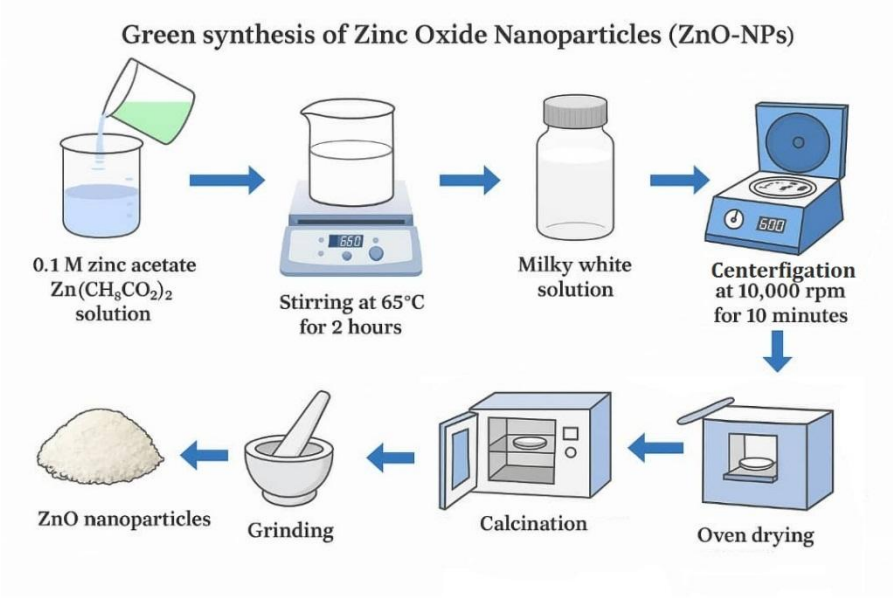

Figure 14 Green synthesis of Zinc Oxide Nanoparticles Process

4.4. Green synthesis of Silver Oxide Nanoparticles (AgO-NPs)

The green synthesis of silver oxide nanoparticles (AgO-NPs) was performed following a previously established method with slight modifications (Redjili et al., 2025). A 10 mM stock solution of silver nitrate ($AgNO_3$) was prepared in 100 mL of deionized (DI) water and stored in the dark to prevent photodegradation for the synthesis of silver nanoparticles, stock solutions of *Origanum majorana* extract and *Cotula cinerea* extract were prepared by macerating 10 g of dried plant material separately in 100 mL of deionized water for 24 hours at room temperature. The resulting extracts were then filtered through Whatman No. 2 filter paper. To initiate the synthesis using *Origanum majorana* extract, 11 ml was added to 100 mL of a 1mM silver nitrate ($AgNO_3$) solution The volume ratio of *Origanum majorana* extract to $AgNO_3$ solution was maintained at 1:9 (v/v) Similarly, for the synthesis using *Cotula cinerea* extract 50 ml was added to 100 mL of a silver nitrate ($AgNO_3$) solution , The volume ratio of *Cotula cinerea* extract to $AgNO_3$ solution was maintained at 1:2 (v/v). The pH of the reaction mixture was adjusted to 10 by the dropwise addition of 50 mL of a 0.1 M NaOH solution under constant stirring. The reactions were conducted under constant stirring at 60°C for 2 hours and dark conditions to avoid unintended photochemical reactions.

A gradual colour change to brown was observed, indicating the formation of AgO-NPs. The reaction mixture was incubated undisturbed for 24 hours. The formation of nanoparticles was confirmed by UV-Vis spectroscopy. To isolate the synthesized nanoparticles, the solution was centrifuged at 15.000 rpm for 25 minutes. The obtained precipitate was thoroughly washed multiple times with DI water and double-distilled ethanol to remove any residual impurities. Finally, the purified AgO-NPs were carefully collected, dried, followed by calcination and stored for further characterization and experimentation.the overview of this procedure in illustrated in Figure 15

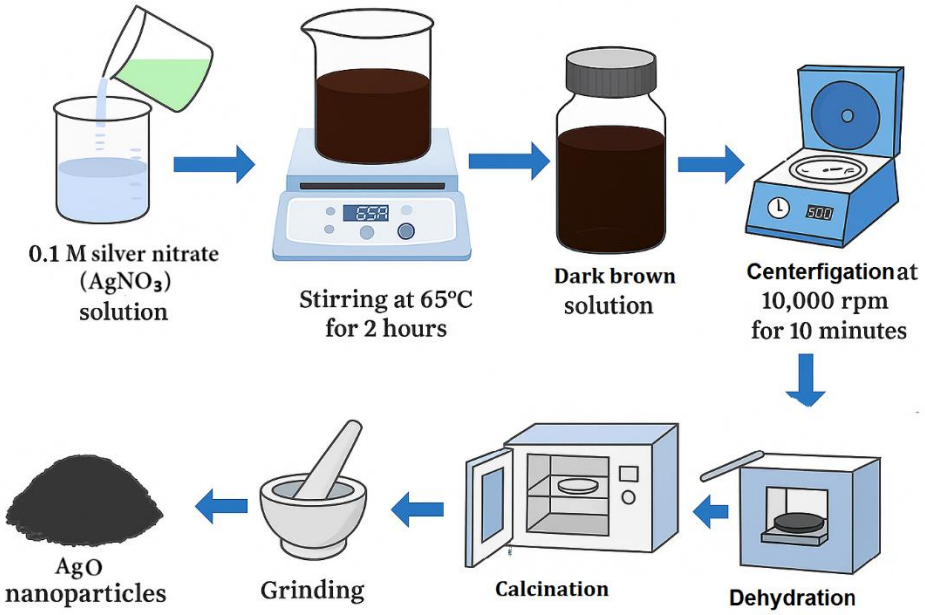

Figure 15 Green synthesis of Silver Oxide Nanoparticles Process

5. Characterization of Synthesized Nanoparticles

5.1. Ultraviolet-Visible (UV-Vis) Spectroscopy

5.1.1. Apparatus

UV-Vis spectroscopy was performed using a Shimadzu UV-1800 spectrophotometer to analyse the optical properties of the synthesized silver oxide (AgO-NPs) and zinc oxide (ZnO-NPs) nanoparticles. The instrument was equipped with a quartz cuvette (1 cm path length), and the spectral analysis was conducted within the wavelength range of 200–800 nm.

5.1.2. Method

The bio-reduction of Ag^{+} to AgO-NPs and Zn^{2+} to ZnO-NPs was monitored using UV-Vis spectroscopy. For each analysis, a colloidal solution of the nanoparticles was prepared by dispersing the dried nanoparticles in deionized water, followed by 15 minutes of sonication to ensure homogeneity. The absorbance spectra were recorded from 200 to 800 nm at room temperature, with deionized water serving as a blank reference.

5.2. Fourier Transform Infrared Spectroscopy (FTIR)

5.2.1. Apparatus

FTIR analysis was performed using a Thermo Fisher Scientific (USA) Nicolet iS10 FTIR spectrometer to investigate the functional groups responsible for the synthesis and stabilization of silver oxide (AgO-NPs) and zinc oxide (ZnO-NPs) nanoparticles. The spectra were recorded using the attenuated total reflectance (ATR) technique to ensure precise detection of functional groups.

5.2.2. Method

Dried AgO-NPs and ZnO-NPs samples were finely ground and mixed with potassium bromide (KBr) to form pellets for FTIR analysis. The spectra were collected in the range of 400 to 4000 cm^{-1}, which includes characteristic regions for organic functional groups and metal oxygen bonding. Each spectrum was obtained by averaging 32 scans with a resolution of 4 cm^{-1} to enhance signal clarity and minimize noise.

5.3. X-ray Diffraction (XRD) Analysis

5.3.1. Apparatus

XRD analysis was performed using a Rigaku X-ray diffractometer equipped with CuKα radiation (wavelength 1.5406 Å) to determine the crystalline structure of the synthesized silver oxide (AgO-NPs) and zinc oxide (ZnO-NPs) nanoparticles.

5.3.2. Method

The diffraction patterns were recorded over a 2θ range of 10° to 80° with a step size of 0.02° and a count time of 1 s per step. The obtained XRD spectra were analysed to determine the crystallinity, phase composition, and average crystallite size of the nanoparticles. The crystallite size was estimated using the Scherrer Equation 2 (Alam, Ahmed, et al., 2025):

$$D = \frac{K\lambda}{\beta \cos\theta} \quad \textbf{(2)}$$

where D is the crystallite size, K is the shape factor (typically 0.9), λ is the X-ray wavelength (1.5406 Å), β is the full-width at half maximum (FWHM) of the diffraction peak in radians, and θ is the diffraction angle.

5.4. Scanning Electron Microscopy (SEM)

5.4.1. Apparatus

The morphological and elemental analyses of the synthesized silver oxide (AgO-NPs) and zinc oxide (ZnO-NPs) nanoparticles were performed using a Carl Zeiss Gemini 300 Scanning Electron Microscope (SEM).

5.4.2. Method

The nanoparticles were mounted on carbon-coated aluminium stubs and coated with a thin layer of gold or platinum to enhance conductivity. The SEM images were obtained at various magnifications to analyse the shape, size, and surface topology of the synthesized nanoparticles. The spectra were recorded to confirm the presence of silver (Ag), zinc (Zn), and oxygen (O), validating the successful synthesis of AgO-NPs and ZnO-NPs. The elemental mapping was also performed to evaluate the distribution and purity of the synthesized nanoparticles.

6. In Vitro Bioassays

6.1. Equipment and Apparatus

- A Shimadzu UV-1800 spectrophotometer equipped with a 96-well microplate adapter was used for absorbance measurements.
- Micropipettes (1–1000 µL) – for accurate liquid handling
- Analytical balance – for precise weighing of chemicals and extracts
- Incubator (25°C, dark conditions) – for controlled reactions
- Water bath (70°C) – used in the BSA denaturation assay

6.2. Anti-Alzheimer Activity: Acetylcholinesterase (AChE) Inhibitory Assay

6.2.1. Overview

Acetylcholinesterase (AChE) is a key enzyme involved in the hydrolysis of acetylcholine, and its inhibition is a primary strategy in the management of Alzheimer's disease (Hafed-Khatiri et al., 2025). This assay evaluates the ability of *Cotula cinerea* and *Origanum majorana L.* extracts to inhibit AChE activity, which could indicate their potential as neuroprotective agents.

6.2.2. Chemicals and Reagents

- Acetylcholinesterase enzyme (AChE) from Sigma-Aldrich
- Acetylthiocholine iodide (ATCI, 0.5 mM) (substrate)
- 5,5′-Dithiobis-(2-nitrobenzoic acid) (DTNB, 0.3 mM) (Ellman's reagent)
- Phosphate buffer (0.1 M, pH 8.0)
- Plant extracts (0.1–1 mg/mL)
- AgO-NPs and ZnO-NPs
- Donepezil (positive control, standard inhibitor)

6.2.3. Procedure

The acetylcholinesterase (AChE) inhibitory activity was assessed using a spectrophotometric method based on the protocol originally described by (Ellman et al., 1961), with slight modifications. Acetylthiocholine iodide was used as the substrate for the enzymatic reaction.

The assay was conducted in a total reaction volume of 200 µL (Polcaro et al., 2025). Briefly, 10 µL of plant extract dissolved in DMSO at varying concentrations, along with synthesized nanoparticles, was mixed with 20 µL of AChE enzyme and 150 µL of sodium phosphate buffer (100 mM, pH 8.0). The mixture was incubated at 37°C for 15 minutes. Following this, 10 µL of DTNB (0.5 mM) and 10 µL of acetylthiocholine iodide were added, and the solution underwent a second incubation under the same conditions. The absorbance was measured at 412 nm using a spectrophotometer.

All measurements were performed in triplicate, with Donepezil used as a reference inhibitor. The percentage of enzyme inhibition (I%) was calculated using the following Equation 3:

$$\% \text{ Inhibition} = \left(\frac{E - S}{E} \right) \times 100 \quad \textbf{(3)}$$

where E: the optical density of the enzyme without a test sample. S: the optical density of the enzyme in the presence of the test sample.

6.3. Anti-inflammatory Activity: Bovine Serum Albumin (BSA) Denaturation Assay

6.3.1. Overview

Protein denaturation is a key process in inflammatory disorders (Farooq et al., 2025), making BSA denaturation inhibition an effective model for assessing anti-inflammatory potential

(Smati et al., 2025). This assay evaluates the ability of *Cotula cinerea* and *Origanum majorana L.* extracts and synthesized nanoparticles to prevent protein denaturation, which may indicate their therapeutic potential for inflammation-related diseases.

6.3.2. Chemicals and Reagents

- Bovine serum albumin (BSA, 5% w/v) from Sigma-Aldrich
- deionized water Plant extracts (0.1–1 mg/mL)
- AgO-NPs and ZnO-NPs
- Diclofenac sodium (positive control, anti-inflammatory drug)

6.3.3. Procedure

In the present study, the assay was conducted following established methodologies (Gangadharan et al., 2025) with slight modifications to optimize experimental conditions. The reaction mixture was prepared by combining 500µL of a 5% BSA solution with 250 µL of the test sample at varying concentrations (100 – 1000 µg/mL). Diclofenac sodium was used as a positive control, while the negative control consisted of BSA solution mixed with distilled water under identical conditions. The prepared mixtures were incubated at 37°C for 20 minutes to allow interaction between BSA and the test compounds. Following this, the solutions were subjected to heat-induced denaturation by maintaining them at 70°C for 20 minutes. After the heating phase, the samples were cooled to room temperature and diluted with 500µL with deionized water before measuring their absorbance at 660 nm using a UV-Vis spectrophotometer. Blank was prepared with mixing: 1mL water + 250 µL DMSO. The percentage inhibition of protein denaturation was calculated using the Equation 4:

$$\% \text{ Inhibition} = \left(\frac{A_{control} - A_{sample}}{A_{control}} \right) \times 100 \quad \textbf{(4)}$$

Where $A_{control}$ corresponds to the absorbance of the negative control, and A_{sample} represents the absorbance of the test sample or positive control. All experiments were performed in triplicate, and the results were expressed as mean ± standard deviation (SD).

6.4. Antioxidant Activity: DPPH Radical Scavenging Assay

6.4.1. Overview

The DPPH (2,2-diphenyl-1-picrylhydrazyl) assay is a widely used method for evaluating antioxidant potential by measuring the ability of plant extracts to neutralize free radicals (Adaika et al., 2025). The reduction of DPPH radicals results in a colour change from purple to yellow, which is quantified spectrophotometrically (Putpadungwipon & Powthong, 2025). In the present study, the antioxidant potential of the plant extracts and synthesized nanoparticles was assessed using the 2,2-diphenyl-1-picrylhydrazyl (DPPH) radical scavenging assay using the following established methodologies (Tlili et al., 2025) with slight modifications.

6.4.2. Chemicals and Reagents

- DPPH solution (0.1 mM in DMSO) from Sigma-Aldrich
- Plant extracts (100 - 1000 µg/mL, dissolved in DMSO)
- AgO-NPs and ZnO-NPs
- Alpha-tocopherol (positive control, reference antioxidant)

6.4.3. Procedure

A freshly prepared 0.0634 mM DPPH solution in methanol was used as the oxidant. In a typical reaction, 1 mL of the DPPH solution was combined with 250µl of the test sample at different concentrations (100 – 1000 µg/mL). The mixture was allowed to incubate in the dark at ambient temperature for 30 minutes to ensure sufficient interaction between the antioxidants and the free radicals. The absorbance of the reaction system was subsequently recorded at 517 nm using a UV-Vis spectrophotometer DMSO was used as a blank. A control sample, containing only the DPPH solution without any test compounds, was prepared under identical conditions. Alpha-tocopherol served as the reference antioxidant. The ability of the test samples to scavenge DPPH radicals was expressed as a percentage inhibition, calculated using the Equation 5:

$$\% \text{ Inhibition} = \left(\frac{A_{control} - A_{sample}}{A_{control}} \right) \times 100 \quad \textbf{(5)}$$

Where $A_{control}$ represents the absorbance of the DPPH solution alone, and A_{sample} corresponds to the absorbance of the sample-containing reaction mixture. Each experiment was conducted in triplicate, and the results were presented as mean ± standard deviation (SD).

6.5. Statistical Analysis

In the present study, all experimental data are expressed as mean ± standard deviation (SD) based on triplicate measurements.

7. In Vivo Experiments

7.1. Experimental Animals

7.1.1. Animal Selection and Housing Conditions

A total of 37 adult male Albino Wistar rats (100 - 150 g) were procured from the Pasteur Institute, Algiers, ensuring a homogeneous cohort for experimental standardization. The selection criteria were based on healthy physiological status, absence of prior exposure to pharmacological agents, and uniformity in age and weight to minimize variability. Upon arrival, the animals were inspected for any signs of pathology or stress before being transferred to the controlled animal facility for acclimatization.

The animals were housed in polypropylene cages (50 × 35 × 20 cm), with five rats per cage, ensuring adequate space for movement and interaction. The cages were lined with sawdust bedding, which was replaced daily to maintain hygienic conditions. The rats underwent 2 weeks acclimatization period in a controlled environment with a temperature of 25 ± 2 °C, relative humidity of 62%, and a 12-hour light/12-hour dark photoperiod to simulate natural circadian rhythms. Throughout the study, the animals had ad libitum access to standard chow formulated according to (Elhewehy et al. 2025) and tap water to ensure proper hydration. The housing conditions and experimental protocols adhered to the ethical guidelines outlined in the Guide for the Care and Use of Experimental Animals (Diemar et al. 2025).

7.1.2. Ethical Considerations

All experimental procedures were conducted in strict accordance with the ethical guidelines outlined in the Guide for the Care and Use of Experimental Animals (Diemar et al. 2025) to ensure the humane treatment of animals. All procedures, including substance administration and behavioural assessments, were designed to reduce stress and discomfort, and humane euthanasia was performed at the end of the study using an ethically approved method.

8. Acute Toxicity Study

8.1. Experimental Design

The acute toxicity study was conducted following : (Abu et al.,2024) to evaluate the safety profile of *Cotula cinerea* and *Origanum majorana* extracts. A 12 adult male Albino Wistar rats were used for this study. The rats underwent an adaptation period under the same housing and environmental conditions as the Alzheimer's groups. Each group of rats was administered *Cotula cinerea* and *Origanum majorana* methanolic extracts at doses of 2000 mg/kg, 5000 mg/kg .

8.2. Dose Administration and Monitoring

The administration of the methanolic extracts was carried out using physiological water NaCl 0.9% (1 ml per rat) via oral gavage . The rats were placed under observation for 24 h to monitor their behaviour and mortality.

- Group 1 : received *Origanum majorana* methanolic extracts at doses of 2000 mg/kg.
- Group 2 : received *Origanum majorana* methanolic extracts at doses of 5000 mg/kg.
- Group 3 : received *Cotula cinerea* methanolic extracts at doses of 2000 mg/kg.
- Group 4 : received *Cotula cinerea* methanolic extracts at doses of 5000 mg/kg.

The lethal dose (LD50) of EEPA leaves was calculated thus:

$$LD_{50} = \frac{\sqrt{D0 + D100}}{2}$$

where D0 = Highest dose that gave no mortality; D_{100} = Lowest dose that produced mortality

9. In Vivo Anti-Alzheimer Experiment:

9.1. Experimental Animals

9.1.1. Induction of Alzheimer's-like Symptoms

Alzheimer's-like neurodegeneration was induced by the sub-chronic administration of $AlCl_3$ (150 mg/kg) and D-galactose (300 mg/kg) (Ajna et al., 2024) (Samad et al., 2022),, dissolved in physiological saline NacL 0.9%, and administered via oral gavage (1 mL per rat) for four consecutive weeks. The co-administration of D-galactose was intended to accelerate oxidative stress and aging-related neurodegenerative processes, thereby mimicking key pathological hallmarks of Alzheimer's disease (Martinovic et al. 2025) (Zhang et al.,2016).

9.1.2. Experimental Design

This study was designed to evaluate the effects of $AlCl_3$/D-galactose -induced neurotoxicity and the potential neuroprotective properties of *Cotula cinerea* and *Origanum majorana* methanolic extracts in a rat model of Alzheimer's-like symptoms. The experiment was conducted in two main phases: (i) disease induction through sub-chronic administration of aluminium chloride ($AlCl_3$) and D-galactose for 4 weeks, and (ii) treatment with plant extracts and Donepezil a reference drug used for Alzheimer's disease management, *Origanum majorana* and *Cotula cinerea* methanolic extract with the continues administration of $AlCl_3$ and D-galactose for 4 weeks along with their respective intervention (Yepes et al. 2025) (Li et al.,2025) (Zhang et al.,2016)

.

Following the acclimatization period, the 25 Wistar rats were randomly divided into five experimental groups (n = 5 per group) to ensure balanced distribution and minimize variability:

- Group 1 (Control): Received no treatment and served as a baseline reference.
- Group 2 (AD): Received $AlCl_3$ + D-galactose to induce Alzheimer's-like neurodegeneration.
- Group 3 (AD + Donepezil): Received $AlCl_3$ + D-galactose, followed by Donepezil (5 mg/kg) as a standard treatment . .(Ibrahim et al.,2024)
- Group 4 (AD + *Cotula cinerea*): Received $AlCl_3$ + D-galactose, followed by *Cotula cinerea* methanolic extract (100 mg/kg) . (El-Kashak et al.,2025)
- Group 5 (AD + *Origanum majorana*): Received $AlCl_3$ + D-galactose, followed by *Origanum majorana* methanolic extract (100 mg/kg) . (El-Kashak et al.,2025)

Figure 16 Distribution of experimental groups.

9.2. Behavioural Assessments During Conditioning

The current battery of behavioural assays employed to evaluate cognitive and memory functions in rats several well-established tests such as the E-maze, dark/light box exploration open field test and novel object recognition task. The E-maze is specifically used to assess spatial short-term memory, while the dark / light box and open field tests are conducted to assess emotional behaviours and anxiety-like responses. Furthermore, the novel object recognition task evaluates recognition memory. Together, these comprehensive behavioural evaluations are essential for delineating the neurocognitive and affective profiles of normal and AD induced mice. (Qin et al.,2025)

9.2.1. Maze Test

Spontaneous Alternation Behaviour (SAB) is a phenomenon observed in rodents and other species, including humans, characterized by the natural tendency to alternate between exploring different arms of a maze. If a rat initially chooses the left arm of the maze, it is more likely to choose the right arm on the the continuous alternation task meaning the entering each of the three arms consecutively in a different sequence (e.g., BAC, CBA, or ABC) without repeating

a previous arm (e.g., CAC, ABA) otherwise it is non completed alternation. This pattern of alternating between arms is considered a manifestation of the animal's inherent exploratory behaviour, driven by the tendency to investigate less familiar areas. Successful alternation requires the subject to remember the previously visited arm, linking SAB to short-term memory function. Thus, a reduction in SAB may indicate impairments in working memory, as the ability to accurately alternate depends on recalling the prior choice (commonly referred to as the "win-shift" strategy). (D'Isa et al.,2021)(Abdel-Salam.,2021) the used apparatus is a 1m × 1m 3 arms maze each arm is 10 cm width and all the walls are 15cm hig. (Figure17). (Wijnen et al.,2024) The percentage of alternation (% alternation) was calculated following the equation : (Abdel-Salam.,2021)

$$\text{SAP}(\%) = \frac{\text{Number Of Spontaneous Alternation}}{(\text{Total Number Of Arm Entries} - 2)} \times 100$$

To ensure consistency and minimize manual error, an online calculator specifically developed for this purpose was used: *SAB Analyzer – Spontaneous Alternation Percentage Calculator(SAB Analyzer.,2025)*

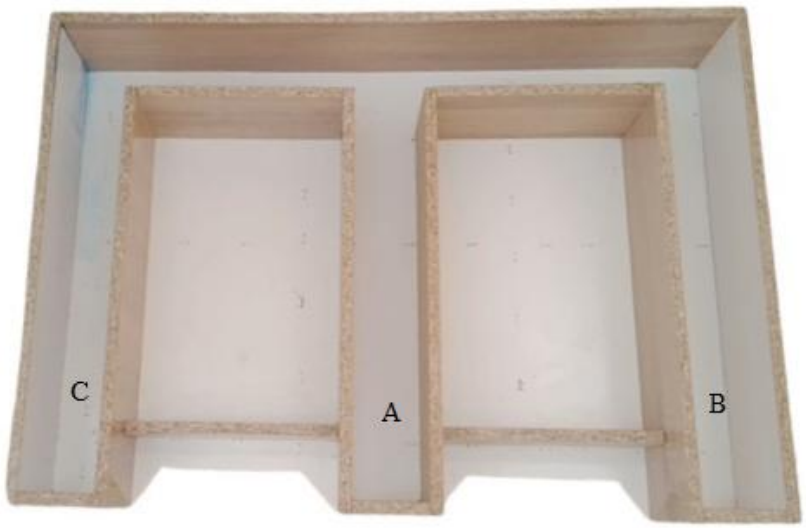

Figure 17 Custom-Made Maze Apparatus For Rat's Behavioral Assessment

9.2.2. Dark/Light Box Test

The Dark /Light Box (DLB) was used as a tool to evaluate potential anxiolytic or anxiogenic effects in mice. This test is based on rodents' natural aversion to light and their spontaneous exploratory behaviour (Temnik et al.,2025) . test was modified by introducing ice-cold water into the dark compartment to simultaneously assess fear memory and anxiety-like behavior in

mice two hallmark symptoms commonly associated with Alzheimer's disease (AD). (Takalo et al.,2025)

The apparatus consisted of a light chamber (30 × 22 × 14 cm^3) and a dark chamber (30 × 22 ×14 cm^3), connected small tunnel through which the subject animal may move from one area to another. The light chamber, featuring transparent walls, was brightly illuminated and maintained at a moderate temperature. In contrast, the dark chamber had opaque black walls, a covered top, and was kept at a cooler temperature(Figure18)**.** (Temnik et al.,2025)

Each mouse was initially placed in the cold, dark chamber after the addition of ice water. Its behavior was then monitored over a 10-minute period, with specific attention to the time spent in each chamber and the number of transitions between them. (Takalo et al.,2025)

Figure 18 Experimental Setup of The Modified Dark/Light Box Test

9.2.3. Open Field Test

The open field consisted of a square arena (40 cm x 40 cm) with high walls (40 cm). The floor of the arena was divided into center (inner) and peripheral (outer) zones (Seibenhener & Wooten.,2015) (Figure19).. Each animal was placed individually in the center of the open field and allowed to explore freely for a period of 5 minutes(Pentkowski et al.,2021).. The test was conducted under low-light conditions to minimize stress. Behavior was monitored through direct observation. The primary measure used to assess anxiety-like behavior was the duration of time spent in the inner zone of the arena. Reduced time in the inner zone is considered an indicator of higher anxiety-like behavior, whereas increased time in the inner suggests reduced anxiety. Conversely, increased time spent in the outer zone is typically associated with elevated anxiety-like behavior . (Carter &Shieh.,2015)

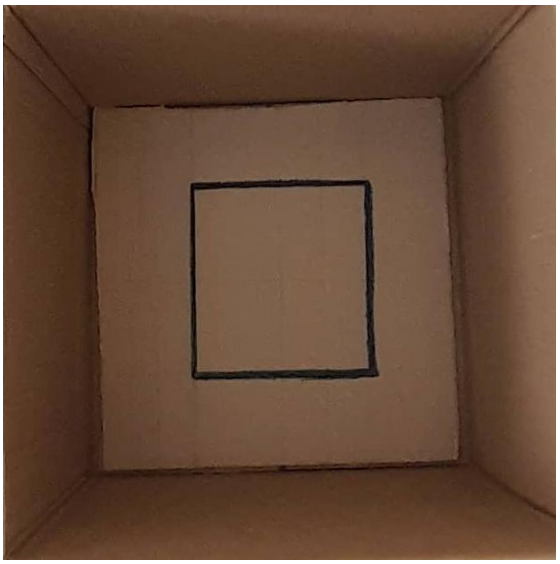

Figure 19 Experimental Setup For The Open Field Test Used In Behavioral Analysis

9.2.4. Novel Object Recognition Test

NOR is a behavioural test assessing animals' attempts to recognize new objects in their environment, based on their natural proclivity to explore novel objects over familiar ones. Provides a rapid and effective approach for evaluating various stages of learning and memory in rats. The test was carried out according to the previous reported method (Antunes & Biala.,2012) with some modifications. This experiment used the same chamber for Open field Test. The familiarization phase was held a day before. The rats were placed in the chamber without any object for 10 min. The test phase consisted of two steps a day after the familiarization phase. In the first step which is 10 min, a rat was presented with two objects 10 cm from the wall. In the second step which is 5 min, one of the objects was replaced with a new one with 2 hours interval between each phase(Figure20). (Barker et al .,2017)

To measure the recognition memory of the animals, the Discrimination Index (DI) and Recognition Index (RI) were calculated. The DI is a measure of the relative preference for the novel object over the familiar object and is calculated as follows:(Lueptow.,2017)

$$DI = \frac{(\text{time for observing the new object} - \text{time for observing the old object})}{(\text{time for observing the new object} + \text{time for observing the old object})}$$

The RI is the percentage of time spent observing the novel object relative to the total exploration time and is calculated using the formula:

$$RI = \left[\frac{\text{time for observing the new object}}{(\text{time for observing the new object} + \text{time for observing the old object})}\right] \times 100$$

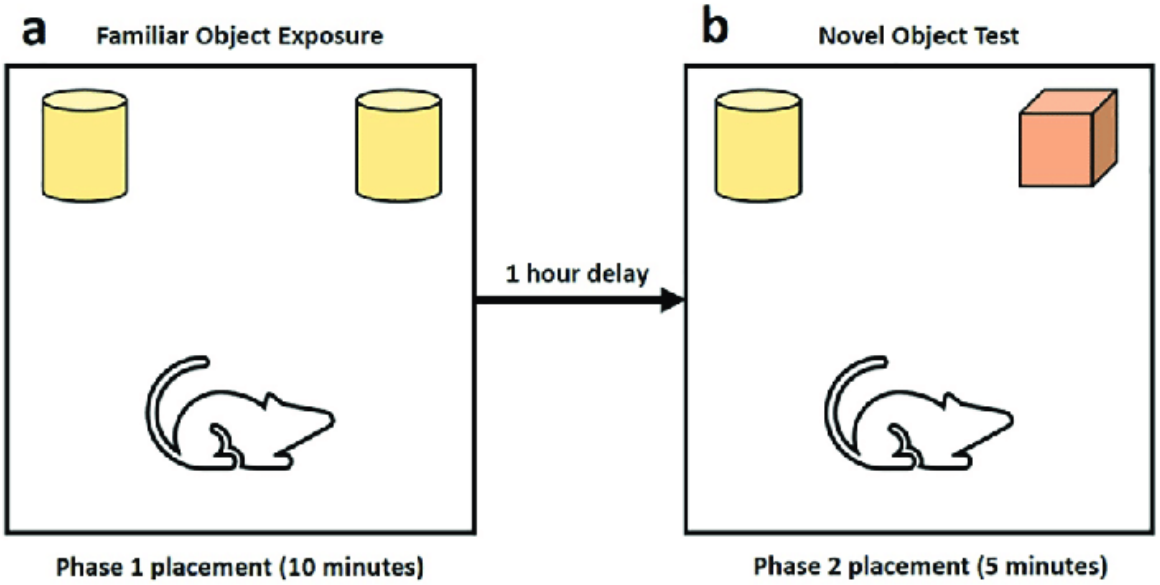

Figure 20 Experimental Procedure For The Novel Object Recognition Test.(A) Phase 1 : Familiar Object Exposure. (B) Phase 2 : Novel Object Recognition Test. (Barker et al .,2017)

9.3. Sacrifice of rats and collection of blood and organs

After treatment period; the rats had 16-hour fast, and were euthanized under light anesthesia using 94% chloroform via inhalation. Blood samples were collected via jugular vein during decapitation and immediately transferred into pre-labeled EDTA and Heparin tubes for hematological analysis, as well as biochemical testing respectfully.

The blood was centrifuged at 3000 rpm for 15 minutes, and the resulting serum was stored at -4°C until further biochemical analysis.

The liver, kidney and brain were carefully excised, rinsed in deionised water then in 0.9% NaCl solution, and weighed. Portions of these organs were used to prepare tissue homogenates for oxidative stress parameter assays, while the remaining tissues were preserved for histological examination. (Boudebia,2023)

9.4. Biomackers parameters detection

9.4.1. Determination of Inflammation parameters

9.4.1.1. Biochemical and hematochemical analysis :

To evaluate the inflammation effects of AlCl3-induced toxicity and the potential anti-inflammatory effects of extracts, a comprehensive biochemical assessment was conducted using the blood samples throughout the hematological parameters which are determined by the Coulter method using the Medonic type auto hematology analyzer specific to Complete Blood Count (CBC); consisting of Leucocytes (WBC), Lymphocytes (LYM), Granulocytes (GRA), Erythrocytes (RBC), Hemoglobin (HGB) and Platelets (PLT).

In addition, biochemical parameters were assessed, including Glycemia, C-reactive protein (CRP), Transaminase Glutamic Oxaloacetic (TGO), Transaminase Glutamic Pyruvic (TGP), Urea, and Creatinine.

9.4.1.2. Hystological detection:

It has been confirmed that exposure to aluminum chloride ($AlCl_3$) and D-galactose induces renal toxicity, hepatotoxicity, and neurodegeneration. To investigate these effects and assess the potential protective roles of Origanum majorana, Cotula cinerea, and donepezil, this study will examine key histopathological changes in the brain, liver, and kidneys, including hemorrhage, inflammatory infiltrates, necrosis, and cytoplasmic vacuolization.

9.4.2. Determination of Oxidative stress parameters

Equipment and Apparatus

- A Shimadzu UV-1800 spectrophotometer equipped with a 96-well microplate adapter.
- Centrifuge.
- Analytical balance .
- Mortar.
- Micropipettes (1–1000 µL).
- Water bath.
- Beakers.
- Test glass and plastic tubes.
- Glass measuring cylinder.

9.4.2.1. Preparation of homogenate

For each rat under study, 0.5 grams of tissue (liver, kidney, and brain) were collected from the rats. The tissues were then ground and homogenized in 4.5 ml of Tris-buffered saline (TBS) containing 50 mM Tris and 150 mM NaCl, with the pH adjusted to 7.4. The resulting cell suspension was centrifuged at 3000 rpm for 15 minutes. The supernatant obtained after centrifugation was carefully collected and maintained on ice for subsequent analysis of oxidative stress markers. (Boudebia,2023)

9.4.2.2. Asseys of Oxidative Stress Parameters:

A. Determination of Protein Content

The Bradford method was employed to spectrophotometrically determine the protein content in the supernatants, using bovine serum albumin (BSA) as the reference standard (Bradford, 1976).

- **Reagents:**

  Coomassie Brilliant Blue; ethanol; phosphoric acid; bovine serum albumin (BSA).

- **Procedure:**

- 40 µl of homogenate and BSA standards were added to 2 ml of Bradford reagent in separate tubes, with all steps carried out in the dark to prevent reagent degradation.
- After a 5 min incubation, the absorbance was measured at 595 nm using a spectrophotometer.
- The protein concentration was calculated by comparing the absorbance of the samples to a standard curve generated using BSA under identical conditions.

B. Determination of Malondialdehyde (MDA) Level

The level of malondialdehyde (MDA) was determined using the method described by Quintanilha (1981).

- **Reagents:**

  Butylhydroxytoluene (BHT) 2% W/V; Trichloroacetic acid (TCA) 15% W/V; Thiobarbituric acid (TBA) 0.375% W/V; hydrochloric acid (HCl) 0.25 N.

- **Procedure:**

In separate tubes add :

- 1 ml of diluted homogenate was mixed with 20 µl of 2% (w/v) ethanolic solution of butylated hydroxytoluene (BHT) to prevent further lipid peroxidation.
- To the mixture, 2 ml of MDA reagent was added. The MDA reagent consists of:

15% (w/v) trichloroacetic acid (TCA) ,0.375% (w/v) thiobarbituric acid (TBA) and 0.25 N hydrochloric acid (HCl).

- The mixture was then heated in a boiling water bath for 15 minutes, allowing the MDA-TBA adduct to form.
- After cooling, the precipitate was removed by centrifugation.
- The absorbance of the supernatant was measured at 532 nm using a spectrophotometer.
- The concentration of MDA was expressed as nmol of MDA per mg of protein, using a standard formula for quantification.

$$MDA(nmol/mg\ prot)\frac{OD\ sample\ \times 10^6}{1 \times 1.56 \times 10^5 \times mg\ prot}$$

Where: OD: Optical density at 532 nm, 1.56 x105 M-1 cm-1: Molar extinction coefficient of the MDA, DF: Dilution factor, 1: Optical path length.

C. Determination of Reduced Glutathione (GSH) Level

The concentration of reduced glutathione (GSH) was determined using the method described by (Weckbecker & Cory,1988) based on the formation of a yellow chromophore when 5,5′-Dithiobis-(2-nitrobenzoic acid) (DTNB) reacts with sulfhydryl groups.

➢ **Reagents:**

Sulphosalicylic acid 0.25%; Tris-buffered saline (TBS, pH = 7.4); 5,5′Dithiobis(2-nitrobenzoic acid)(DTNB 0.01 M).

➢ **Procedure:**

1. **Preparation of Homogenate:**

In separate tubes:

- 0.8 ml of tissue homogenate was mixed with 0.2 ml of 0.25% sulphosalicylic acid.
- The mixture was vortexed and then chilled at 4°C for 15 minutes to precipitate proteins.
- The suspension was centrifuged at 1000 rpm for 5 minutes to separate the supernatant.

2. **Preparation of Reaction Mixture:**

- 0.5 ml of the supernatant mixed with 1 ml of Tris-buffered saline (TBS), pH 7.4 and a 0.025 ml of 0.01 M DTNB added to the mixture.
- The mixture was incubated at room temperature for 5 minutes, allowing the development of a yellow color.

3. **Measurement:**

- The absorbance was then measured at 412 nm using a spectrophotometer.
- The concentration of GSH was expressed as nmol of GSH per mg of protein, using a standard formula for quantification :

$$GSH(\frac{nmol}{mgprot}) = \frac{OD \times 10^6 \times 1.525}{13100 \times 0.8 \times 0.5 \times DF \times mg\ prot}$$

With: 1.525: Total volume of solutions used in the GSH assay at the level of supernatant (0.5 ml, supernatant +1ml Tris + 0.025ml DTNB), 13100 M-1: Molar extinction coefficient of -SH group at 412 nm, 0.8: Volume of the homogenate, 0.5: Volume of the supernatant, DF: Dilution factor.

A. Determination of Superoxide Dismutase (SOD) Activity

The activity of superoxide dismutase (SOD) was determined using the method described by (Beauchamp and Fridovich,1971) based on the reduction of nitro blue tetrazolium (NBT) by superoxide anions ($O_2^{\cdot -}$).

➢ **Reagents :**

EDTA-Methionine; Phosphate Buffer (pH = 7.8); Nitro Blue Tetrazolium (NBT); Riboflavin.

➢ **Procedure :**

1. **Preparation of Reaction Mixture:**

In separate tubes:

- 500 µL of EDTA-Met solution mixed with 900 µL of phosphate buffer (pH 7.8).
- 25 µL of tissue homogenate and 50 µL of NBT solution added respectfully.
- Place the mixture in a water bath at 25°C for 5 minutes.
- A control reaction is prepared following the same steps but replacing the tissue homogenate with 25 µL of phosphate buffer.

2. **Reaction:**

- After the initial incubation, 25 µL of riboflavin added to the mixture to initiate the reaction.
- The mixture was exposed to light for 20 minutes, allowing riboflavin-mediated generation of superoxide radicals, which reduce NBT to a blue formazan product.

3. **Measurement:**

- The absorbance of the sample and control mixtures is measured at 560 nm using a spectrophotometer.

- The concentration of GSH was expressed as nmol of GSH per mg of protein, using a the equation:

$$I\% = \frac{OD_C - OD_S}{OD_C} \times 100$$

With: I%: % inhibition of NBT reduction by SOD, ODC: Optical density of the control, ODS: Optical density of the sample.

And: The 50% inhibition is equal to 1 unit of enzyme. 50% inhibition = 1 unit of SOD, so the antioxidant activity of the enzyme equals SOD units / mg of pro.

B. Determination of Catalase (CAT) Activity

Catalase (CAT) activity was measured using the method described by (Aebi,1984) which monitors the decomposition of hydrogen peroxide (H_2O_2) by catalase.

➢ **Procedure:**

1. **Preparation of Reaction Mixture:**

In separate tubes:

- 20 µl of tissue homogenate mixed with 780 µl of phosphate buffer (0.1 M, pH =7.5, KH_2PO_4).

2. **Reaction:**

- 200 µl of H_2O_2 solution (0.030 M) added to the mixture, this addition initiate the reaction and the decrease in absorbance at 240 nm is immediately recorded every 30 seconds for 2 minutes using a spectrophotometer.

3. **Measurement and Calculation:**

- The catalase activity is expressed as International Units (IU) per minute per gram of protein (IU/min/g protein), where one IU is defined as the amount of enzyme required to decompose 1 µmol of H_2O_2 per minute under the specified conditions.

$$Catalase\ ((UI/min)/g) = \frac{(2.3033/T) \times (logA1/A2)}{DF \times g\ prot}$$

Where*:* A1: Absorbance at the first minute, A2: Absorbance at the second minute, T: Time interval in minutes.

9.4.3. Determination of Alzheimer

In this study, we focus on the histopathological features of brain tissue, including neuronal morphology, amyloid plaque deposition, cytoplasmic vacuolization, and necrosis. These alterations are characteristic of neurodegenerative processes induced by neurotoxicity from

aluminum chloride ($AlCl_3$) and D-galactose, as previously reported in [reference]. The potential neuroprotective effects of Cotula cinerea, Origanum majorana, and donepezil will be evaluated in this context.

9.5. Histopathological Study steps

9.5.1. Histopathological Study

For the histological examination, tissue fragments from the organs of all experimental groups were collected immediately after euthanasia to prevent autolysis. The samples were then rinsed before being immediately immersed in a fixative solution consisting of 10% formaldehyde, as described by (Leclerc-Mercier et al., 2016).

Procedure:

1. **Sample Preparation and Fixation:**
    - Tissues were placed in specialized cassettes with perforated walls to facilitate fluid exchange.
    - The cassettes were then subjected to dehydration using an automated tissue processor. This involved a progressive series of ethanol baths of increasing concentration (70%, 95%, and 100%) to remove water from the tissues.
    - Following dehydration, the samples were immersed in liquid paraffin baths, allowing paraffin to infiltrate and replace the ethanol.
2. **Embedding and Sectioning:**
    - Once fully infiltrated with paraffin, the tissues were embedded in paraffin blocks using a device that maintains paraffin in its liquid state through controlled heating.
    - The blocks were then rapidly cooled on a refrigerated metal plate, allowing the paraffin to solidify and encase the tissue.
    - The solidified blocks were sectioned into thin slices (approximately 5 µm thick) using a microtome.
    - The sections were transferred to microscope slides and affixed using heated gelatinous water to ensure proper adhesion.
3. **Staining Procedure (Hematoxylin-Eosin Staining):**

The staining process followed the protocol outlined by (Elmalti et al., 2007) and involved the following steps:

- **Deparaffinization and Hydration:** Slides were placed in a series of xylene and ethanol baths, followed by rinsing with tap water.
- **Hematoxylin Staining:** Slides were immersed in Harris Hematoxylin for 15 minutes, staining basophilic structures (e.g., nuclei) a purplish-blue color.
- **Differentiation and Bluing:** Slides were dipped briefly in acid alcohol (100 ml of 70% ethanol + 50 ml HCl) for 1–2 dips to differentiate the staining. followed by a rinse in tap water and a brief dip in ammoniacal water (100 ml distilled water + 2 ml ammonia) to intensify the nuclear staining.
- **Eosin Staining:** Slides were immersed in Eosin solution (3% aqueous Eosin, 95% ethanol, distilled water, and 2 drops of acetic acid) for 15 seconds to 2 minutes, imparting a pink color to acidophilic structures (e.g., cytoplasm).Each staining step was separated by thorough rinsing in tap water.

4. **Microscopic Examination:**
    - The stained sections were air-dried, mounted with a coverslip, and examined under an optical microscope.
    - Images were captured using a digital camera for further analysis, as described by (Bremond-Gignac et al., 2004).

9.5.2. Statistical Analysis

The statistical analysis of the data was performed using the **Student's t-test**, which compares the means between two groups to assess statistical significance. The results were presented as **mean values ± Standard error mean (SEM),** based on five **replicates per group.**

- The analysis was conducted using SPSS software (version 26) and Excel (version 2019).
- The level of significance (α) was set at 0.05.
- A p-value (P) less than 0.05 was considered statistically significant, indicating that the null hypothesis of equal means was rejected in favor of the alternative hypothesis.

10. In Silico Analyses

10.1. ADMET and Drug-Likeness Prediction

To assess the pharmacokinetic properties and drug-like potential of the bioactive compounds identified in the methanolic extracts of the studied plants, an ADMET (Absorption, Distribution, Metabolism, Excretion, and Toxicity) analysis was conducted using the pkCSM computational tool (Pires et al., 2015). This analysis aimed to identify compounds with optimal oral bioavailability and favourable pharmacokinetic profiles. The pkCSM platform was utilized to predict key parameters such as absorption efficiency, metabolic pathways, excretion mechanisms, and potential toxicological effects. Furthermore, the software enabled the evaluation of physicochemical properties relevant to drug-likeness, facilitating the identification of compounds with minimal toxicity risks and desirable pharmacokinetic characteristics. Through this comprehensive computational screening, potential candidates for further drug development were identified based on their predicted safety and efficacy profiles.

10.2. Molecular Docking Study

10.2.1. Ligands Preparation

The three-dimensional (3D) structures of the principal bioactive compounds identified from the methanolic extracts of *Cotula cinerea* and *Origanum majorana L.* were retrieved from the PubChem database, maintained by the National Center for Biotechnology Information (NCBI) (Kim et al., 2016), accessible via https://pubchem.ncbi.nlm.nih.gov/. Each compound underwent structural refinement and optimization using the LigPrep module of the Schrödinger suite (Schrödinger, 2024), where ionization states were adjusted to physiological conditions (pH 7.0 ± 2.0) using the Epik Classic module. Tautomeric and stereoisomeric forms were generated while preserving stereochemical integrity. Partial atomic charges were assigned based on the Optimized Potentials for Liquid Simulations (OPLS4) force field (Lu et al., 2021), ensuring energetically favourable conformations for molecular docking and simulation.

Additionally, the 3D crystallographic structures of the metallic oxide nanoparticles—zinc oxide (ZnO) and silver oxide (AgO)—were obtained in CIF format from the Crystallography Open Database (COD). Specifically, COD entry #1534836 was used for ZnO (Bates et al., 1962) and entry #9008962 for AgO (Wyckoff, 1963). These CIF files were converted into protein data bank (PDB) format using VESTA software to enable compatibility with docking and molecular simulation workflows (Heydon et al., 2001). The processed nanoparticle

structures were further inspected to ensure structural integrity and compatibility with subsequent molecular docking and simulation analyses.

10.2.2. Receptor Preparation:

The 3D structure of human acetylcholinesterase (AChE) enzyme (PDB ID: 6O4W) (Gerlits et al., 2019), cyclooxygenase-1 (COX-1) enzyme (PDB ID: 5WBE) (Cingolani et al., 2017) and human glutathione reductase (GR) enzyme (PDB ID: 1XAN) (Savvides & Karplus, 1996) was retrieved from the Protein Data Bank (http://www.rcsb.org) (Rose et al., 2017), adhering to specific parameters as listed in Table 2. Processing of the protein structure was executed through the "protein preparation Workflow" module within the Schrödinger suite (Madhavi Sastry et al., 2013), involving consecutive stages of import and processing, review and modification, and refinement.

Table 2. Target receptor information chosen for docking studies

Human Acetylcholinesterase (AChE)	**Detaille's**
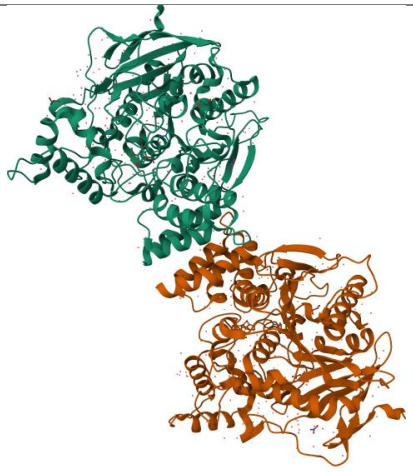	PDB ID: 6O4W
	Mutation: No
	Resolution (Å): 2.35
	R-Value Free: 0.212
	R-Value Observed: 0.187
	Organism: Homo sapiens
	Space Groupe: $P\,3_1$
	Sequence Length: 550
Cyclooxygenase-1 (COX-1)	**Detaille's**
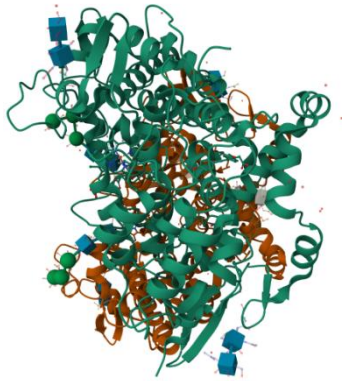	PDB ID: 5WBE
	Mutation: No
	Resolution (Å): 2.75
	R-Value Free: 0.229
	R-Value Observed: 0.197
	Organism: Ovis aries
	Space Groupe: $P\,6_5$
	Sequence Length: 600
Human Glutathione Reductase (GR)	**Detaille's**

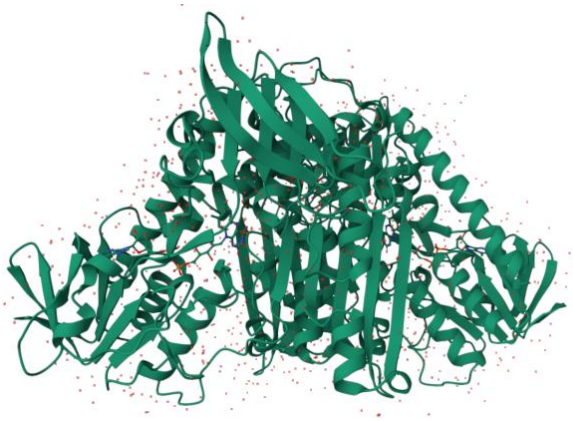

PDB ID	1XAN
Mutation	No
Resolution (Å)	2.00
R-Value Free	0.158
R-Value Observed	0.158
Organism	Homo sapiens
Space Groupe	C 1 2 1
Sequence Length	461

In the initial stage, the Prime tool was employed to address missing residues and side chains, maintaining the pH of PROPKA at 7.0 ± 2.00. Subsequent steps included the optimization and assignment of hydrogen bonds, along with the removal of water molecules beyond 8 Å. Restrain minimization utilizing the Optimized Potentials for Liquid Simulations (OPLS4) force field was performed to achieve a low-energy state for the protein (Lu et al., 2021). This phase of protein preparation signifies an energy optimization methodology, presenting the protein in its energetically favourable state for subsequent *in-silico* studies.

The "Receptor grid generation" panel facilitated the creation of a grid encompassing the active site of the protein, delimited by the co-crystallized ligand in each protein. Default parameters were maintained, and the grid centre was generated at the coordinates listed in Table 3.

Table 3. Selected grid parameters the studied enzymes

Enzymes	**Grid Centre**			**Grid Size (Å)**
	x	**y**	**z**	
6O4W	34.94	25.81	39.96	60 × 60 × 60
5WBE	14.78	20.976	8.807	
1XAN	30.658	37.912	16.356	

10.2.3. Docking Setup:

Docking simulation and including Induced Fit Docking were conducted employing the Glide module and Induced Fit Docking module within the Maestro version 11.7 user interface of the Schrödinger suite (Small-Molecule Drug Discovery Suite 2021-4, Schrödinger, LLC, New York, NY, 2021) (Schrödinger, 2015). The simulations were executed on a DELL Intel(R) Core(TM) i9-13900HX CPU @ 2.20 GHz processor, equipped with 32,0 GB RAM, and operated on a 64-bit Linux Ubuntu 18,04.1 LTS operating system.

The molecular docking tool employed for all docking studies was Glide (Grid-based Ligand docking with Energetics), a module within the Schrödinger suite (Yang et al., 2021). The prepared ligands underwent docking onto the specified protein site utilizing the Glide module, in Standard Precision (SP) modes (Friesner et al., 2006).

10.2.4. Induced Fit Docking (IFD):

The Induced Fit docking (IFD) module of the Maestro molecular modelling suite has been noted as a reliable and effective docking approach to consider flexibility in both ligands and the binding pocket residues in the binding pocket of target receptors (Khelil et al., 2020). During the IFD process, Glide/SP (Standard Precision) was performed for each ligand, the Prime refinement step specifically addressed the side chains of residues within a 5 Å radius of the ligand. Noteworthy is the retention of a maximum of 20 poses for each ligand.

10.3. Molecular Dynamics (MD) Simulation

Molecular dynamics (MD) simulations were conducted to investigate the structural stability and dynamic behavior of the ligand-protein complexes involving acetylcholinesterase (AChE), cyclooxygenase-1 (COX-1), and glutathione reductase (GR). The simulations were performed using the GROMACS 2023 package for a duration of 100 nanoseconds. The primary objective was to assess the stability of the ligand-bound protein complexes and compare their conformational dynamics to reference complexes, thereby gaining insights into their interaction patterns and potential inhibitory mechanisms (Gade, 2025).

The ligand topology parameters were generated using the SwissParam server (Zoete et al., 2011), ensuring an accurate molecular representation for simulation. Meanwhile, the CHARMM36 all-atom force field was employed to define the protein topology, providing a reliable structural framework for molecular simulations (J. Huang & Mackerell, 2013). Each complex was solvated in a cubic box using the TIP3P water model, with Na^+ and Cl- ions added to neutralize the system, thus mimicking physiological conditions. Energy minimization was performed using the steepest descent algorithm until the system's maximum force was reduced below 10.0 kJ/mol, ensuring system stability before proceeding to equilibration (Ogunyemi et al., 2025).

System equilibration was carried out in two phases: first, NVT (constant Number, Volume, and Temperature) equilibration was performed for 100 ps using the v-rescale thermostat at 300 K with a coupling constant of 0.1 ps, followed by NPT (constant Number, Pressure, and

Temperature) equilibration for 100 ps using the Berendsen barostat with a coupling constant of 2.0 ps to maintain pressure stability. These steps ensured that the system reached a stable and representative state before initiating production runs (Q. Chen, 2025).

To evaluate the stability and behavior of the protein-ligand complexes, several key structural parameters were analysed. Root Mean Square Deviation (RMSD) was calculated to assess the overall stability of the protein-ligand complexes over time (D. D. Li et al., 2020), while Root Mean Square Fluctuation (RMSF) was used to evaluate the flexibility of specific amino acid residues (Dey et al., 2021). The radius of gyration (Rg) was determined to measure the compactness of the protein structure (Logan et al., 2025), and the solvent-accessible surface area (SASA) was analysed to estimate the extent of ligand exposure to the solvent environment (H. Li et al., 2025). Additionally, the Molecular Mechanics Generalized Born Surface Area (MMGBSA) and Molecular Mechanics Poisson–Boltzmann Surface Area (MMPBSA) methods were applied to estimate the binding free energy of the complexes, providing insights into their thermodynamic stability and binding affinity.

10.4. Free Energy (MM-GBSA) Calculation

The Molecular Mechanics–Poisson–Boltzmann Surface Area (MM-PBSA) method was employed to evaluate the binding free energy of the ligand-protein complexes, providing a comprehensive assessment of their interaction dynamics (Hiremath et al., 2025). This approach enables the estimation of binding energies by considering van der Waals interactions, electrostatic contributions, solvation effects, and the overall stability of the complex, offering critical insights into the molecular forces governing inhibitor efficacy (Kumari et al., 2014).

The binding free energy calculations were performed using the g_mmpbsa package, which computes the energy components contributing to ligand-receptor interactions. The binding energy ($\Delta G_{Binding}$) was determined using the following Equation 6:

$$\Delta G_{Binding} = G_{Complex} - \left(G_{\text{Protein}} + G_{Ligand} \right) \quad \textbf{(6)}$$

Where $G_{complex}$ represents the total free energy of the protein-ligand complex, while $G_{protein}$ and G_{ligand} denote the free energies of the unbound protein and ligand, respectively. This analysis provided valuable insights into the binding affinity and stability of the complexes, aiding in the identification of potential inhibitors with favourable interaction profiles.

10.5. DFT calculations

To gain a deeper understanding of the electronic properties of the major bioactive compounds identified in the methanolic extracts, Density Functional Theory (DFT) (Grimme, 2011) calculations were conducted using Gaussian 16W software (Frisch et al., 2004). Geometry optimization was performed at the B3LYP/6-311++G(d,p) level of theory (Meraghni et al., 2023), followed by frequency calculations to confirm the absence of imaginary frequencies, ensuring that all structures corresponded to true energy minima.

Frontier Molecular Orbital (FMO) analysis was carried out to determine the highest occupied molecular orbital (HOMO) and lowest unoccupied molecular orbital (LUMO) energies, along with the energy gap (ΔE), which provides insights into the chemical reactivity and stability of the studied compounds (Zuriaga-Monroy et al., 2016). Additionally, Molecular Electrostatic Potential (MEP) mapping was employed to visualize electron density distributions, identifying potential regions for nucleophilic and electrophilic interactions (Chidangil et al., 1998). All molecular structures, electronic density distributions, and MEP surfaces were visualized using GaussView 06 software, offering a detailed representation of the compounds' reactivity and interaction potential.

CHAPTER TWO:

RESULTS AND

DISCUSSION

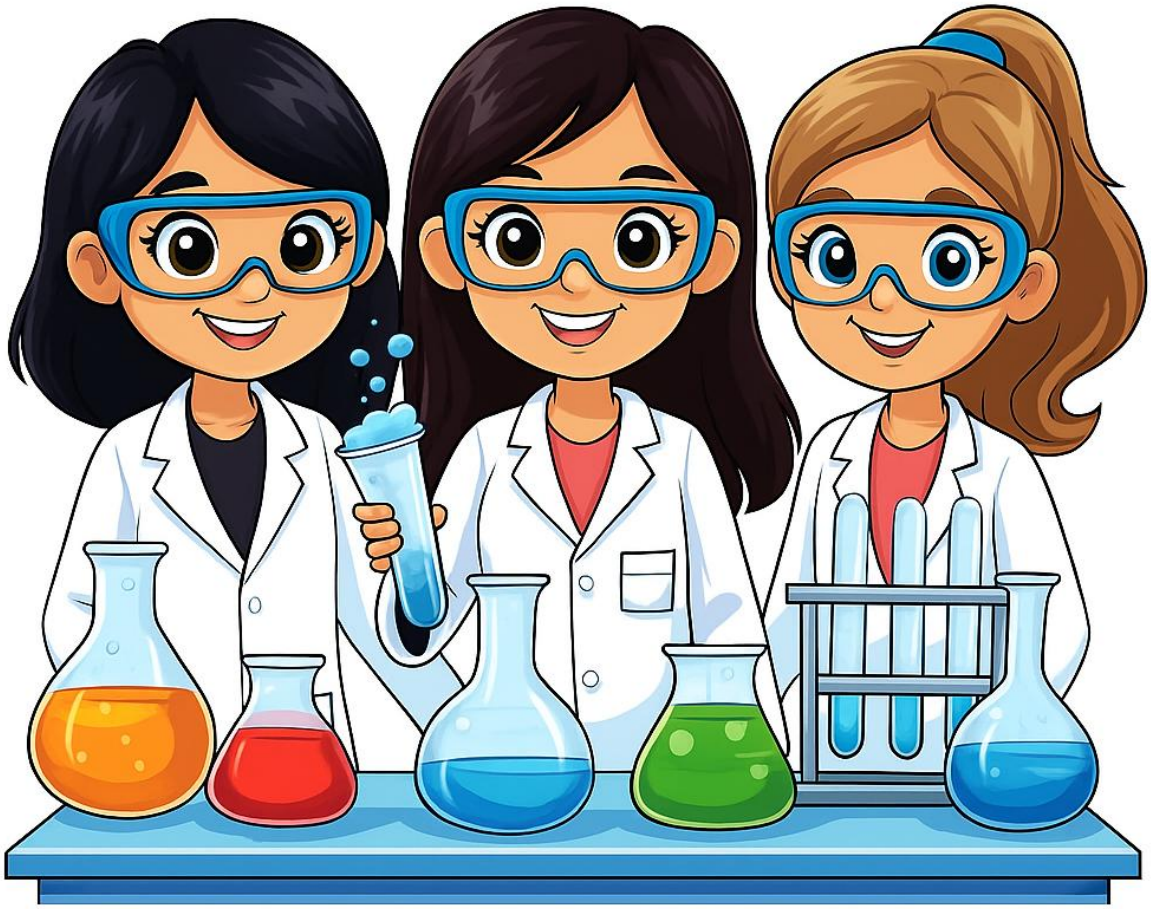

11. Phytochemical Composition and Chemical Profiling

11.1. Extraction Yields of *Cotula cinerea* and *Origanum majorana L.*

The efficiency of phytochemical extraction is strongly influenced by the polarity of the solvent used, as it determines the solubility of targeted bioactive compounds (Munuo et al., 2025). In this study, various solvents of differing polarities—including water, methanol, and n-butanol—were employed to extract secondary metabolites from the aerial parts of *Cotula cinerea* and *Origanum majorana* L. The percentage yield of each extract was calculated based on the dry weight of the obtained extract relative to the initial plant material. The results, presented in the Table 3 below, provide insight into the extractive potential of each solvent system for both plant species.

Table 4. Extraction yields of *Cotula cinerea* and *Origanum majorana* L. (mean ± SD, n = 3)

Plant species	Solvent	Yield (%) ± SD
Origanum majorana L.	Water	17.5 ± 0.7
	Methanol	26.89 ± 0.89
	n-Butanol	6.0 ± 0.3
Cotula cinerea	Water	7.11 ± 0.14
	Methanol	9.10 ± 0.27
	n-Butanol	8.16 ± 0.11

The extraction yields obtained for *Cotula cinerea* and *Origanum majorana* L. revealed clear differences in solvent efficiency, reflecting both the chemical composition of the plant matrices and the solvent polarity. Among all solvents tested, methanol demonstrated the highest extractive efficiency for both species, yielding 26.89 ± 0.89% in *Origanum majorana* L. and 9.10 ± 0.27% in *Cotula cinerea* This is consistent with the broad polarity range of methanol, allowing it to solubilize a wide spectrum of phytochemicals, including polyphenols, flavonoids, and other polar to mid-polar constituents (Zarth & Magallanes López, 2025).

In contrast, aqueous extraction yielded significantly more material from *Origanum majorana* (17.5 ± 0.7%) than from *Cotula cinerea* (7.11 ± 0.14%), indicating a higher content of hydrophilic compounds in the former (S. Ma et al., 2025). Interestingly, n-butanol extracts displayed the lowest yield for *Cotula cinerea* (6.0 ± 0.3%) but a relatively higher and comparable performance in *Origanum majorana* (8.16 ± 0.11%), possibly due to differences in mid-polar compounds between the two species (Cífková et al., 2025).

To better illustrate these variations and facilitate comparative analysis, the extraction yield data are graphically represented in the following histogram.

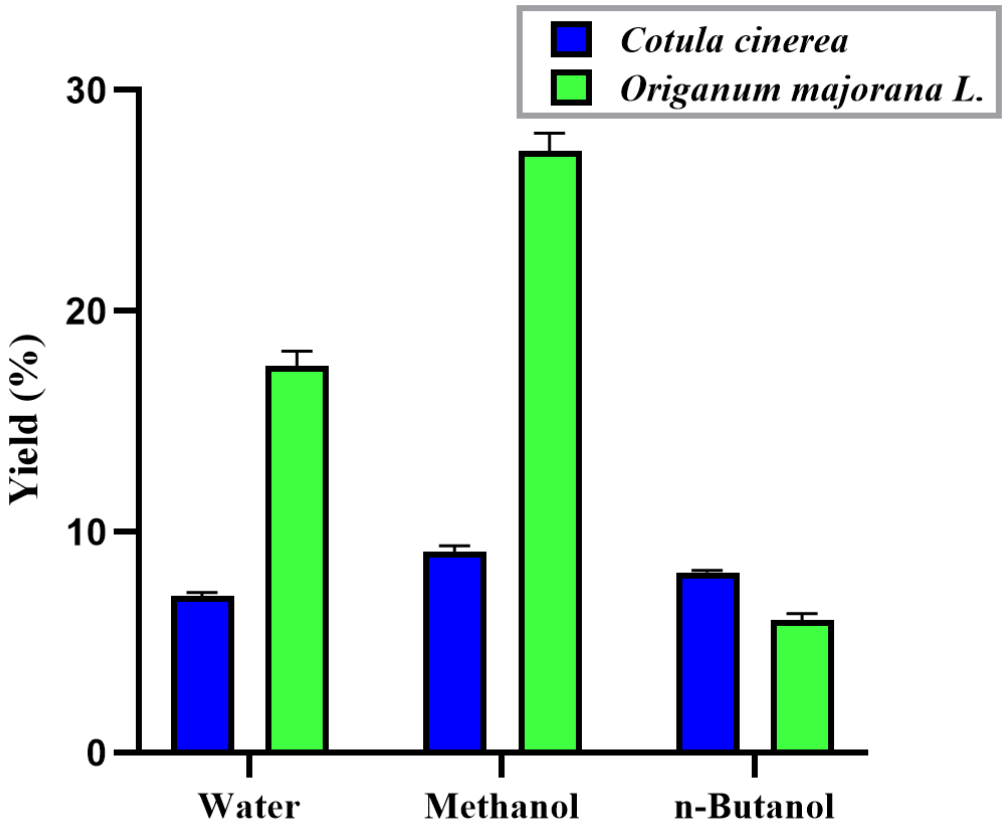

Figure 21. Extraction yields (%) of *Cotula cinerea* and *Origanum majorana* L. using water, methanol, and n-butanol solvents

11.2. Qualitative Phytochemical Screening of Major Constituent Classes

To preliminarily assess the chemical profile of the studied plant materials, a qualitative phytochemical screening was conducted exclusively on the methanolic extracts of *Cotula cinerea* and *Origanum majorana* L. Methanol was selected due to its broad-spectrum solvating capacity, known to efficiently extract a wide range of phytoconstituents, including both polar and moderately non-polar compounds (Mohammed et al., 2025). The screening targeted key classes of secondary metabolites such as alkaloids, flavonoids, tannins, saponins, terpenoids, and phenolics—each of which is associated with various pharmacological effects. The presence or absence of these constituents provides an essential preliminary insight into the bioactive potential of the extracts (Singirala et al., 2025). The results of this phytochemical profiling are summarized in Table 5, highlighting the similarities and differences between the two species.

Table 5. Qualitative Phytochemical Screening of Methanolic Extracts of *Cotula cinerea* and *Origanum majorana* L.

Phytoconstituent	Reactions		Observation	
	Cotula cinerea	*Origanum majorana* L	*Cotula cinerea*	*Origanum majorana* L
Polyphenols	+++	++	Greenish blue	Blue coloration
Flavonoids	++	++	Yellow	Yellow coloration
Alkaloids	++	-	White precipitation	No foam
Terpenoids	+	+	Appearance of a red–purple ring	Deep red coloration
Tannins	-	+	No foam	Green precipitate
Saponins	-	+	No foam	Froth appears
Reducing Sugars	+	+	Brick red precipitation	Red precipitate
Glycosides	-	+	No foam	Violet to Blue to Green coloration

(+): Weakly positive test, (++): Positive test, (+++): Strongly positive test, (–): Negative test

The qualitative phytochemical screening of the methanolic extracts from *Cotula cinerea* and *Origanum majorana* L. revealed notable differences in their secondary metabolite profiles, which may contribute to their respective biological activities (Piñeiro et al., 2025). Both plant extracts exhibited a strong presence of polyphenols and flavonoids, as evidenced by the intense greenish-blue and blue coloration, respectively, which supports their potential antioxidant capacity due to the well-documented free radical scavenging properties of these compounds (El Amiri et al., 2025).

Alkaloids were detected in moderate amounts in *Cotula cinerea* but were absent in *O. majorana*, suggesting a possible divergence in their biosynthetic pathways or ecological roles (Medeiros et al., 2025). The presence of terpenoids in both species, indicated by the development of red to deep red coloration, aligns with previously reported data supporting their role in anti-inflammatory and antimicrobial activities (Mehrnia et al., 2025).

Interestingly, tannins and saponins were absent in *Cotula cinerea* but present in *O. majorana*, which may explain differences in astringency and surfactant properties. The presence of reducing sugars and glycosides in *O. majorana* alone also reflects a more complex profile of

polar metabolites in this species, potentially enhancing its pharmacological versatility (Odoh et al., 2025).

11.3. Quantitative Determination of Phenolics, Flavonoids, and Tannins

To complement the qualitative phytochemical screening, quantitative estimation of total phenolic, flavonoid, and tannin contents was conducted for the methanolic extracts of *Cotula cinerea* and *Origanum majorana* L. These classes of phytoconstituents are widely recognized for their significant roles in antioxidant, anti-inflammatory, and antimicrobial activities, among other biofunctional properties (Contato & Conte-Junior, 2025). The assays were performed using spectrophotometric methods, with results expressed in terms of standard equivalents: gallic acid equivalents (GAE) for total phenolics, quercetin equivalents (QE) for flavonoids, and catechin equivalents (CE) for condensed tannins. The obtained data, summarized in Table 6, provide insight into the comparative abundance of these bioactive compounds between the two species and serve as a basis for correlating phytochemical composition with observed biological activities.

Table 6. Total phenolic, flavonoid, and condensed tannin contents of methanolic extracts (expressed as mg standard equivalents per g extract).

Plant Species	Total Phenolics (mg GAE/g) ± SD	Total Flavonoids (mg QE/g) ± SD	Condensed Tannins (mg CE/g) ± SD
Cotula cinerea	69.75 ± 1.87	91.88 ± 1.94	5.01 ± 0.15
Origanum majorana L.	186.06 ± 0.10	72.30 ± 0.90	4.49 ± 0.08

The quantitative phytochemical analysis underscores distinct compositional profiles for the two investigated species, which likely underpin their divergent bioactivities. *Cotula cinerea*'s methanolic extract contains a moderate total phenolic content (69.75 ± 1.87 mg GAE/g) but is particularly enriched in flavonoids (91.88 ± 1.94 mg QE/g), suggesting a predominance of flavonoid-derived scaffolds that may contribute to its pronounced anti-inflammatory and neuroprotective effects via free radical scavenging and enzyme modulation (Bahsi et al., 2025; Fahmy et al., 2025). Its condensed tannin level (5.01 ± 0.15 mg CE/g), though comparatively low, may still afford synergistic membrane-stabilizing and protein-binding properties (Selvi, 2025).

In contrast, *Origanum majorana* L. exhibits an exceptionally high phenolic load (186.06 ± 0.10 mg GAE/g), nearly three-fold greater than *C. cinerea*, which correlates with its superior antioxidant IC_{50} values in the DPPH assay. The substantial phenolic abundance—comprising

hydroxycinnamic acids and related derivatives—confers enhanced redox buffering capacity and may account for the species' potent radical-scavenging kinetics (Sargsyan et al., 2025). Its flavonoid (72.30 ± 0.90 mg QE/g) and tannin (4.49 ± 0.08 mg CE/g) contents, while lower than those of *C. cinerea*, still represent a robust complement of bioactives capable of modulating inflammatory pathways (Bal et al., 2025).

These compositional contrasts—flavonoid dominance in *C. cinerea* versus phenolic dominance in *O. majorana*—provide a chemical rationale for the observed differences in antioxidant, anti-inflammatory, and enzyme-inhibitory assays (Dessì et al., 2025). The exceptionally high phenolic concentration in *O. majorana* likely drives its superior free radical neutralization, whereas the flavonoid richness in *C. cinerea* may favor interactions with protein targets such as acetylcholinesterase and inflammatory enzymes (Aispuro-Pérez et al., 2025). Collectively, these data illustrate how solvent-mediated extraction yields a spectrum of phytoconstituents whose relative proportions critically determine the pharmacological profile of each botanical extract (Chajed et al., n.d.).

11.4. UPLC–ESI–MS/MS Chemical Fingerprinting and Compound Identification

The UPLC–ESI–MS/MS analysis of the methanolic extracts enabled comprehensive chemical fingerprinting by combining high-performance chromatographic separation with sensitive mass spectrometric detection. Utilizing a C18 reversed-phase column and a carefully optimized water–methanol gradient (0.1% formic acid), the method achieved rapid resolution of diverse phytochemical classes, including phenolic acids, flavonoids, and terpenoid derivatives. Electrospray ionization in both positive and negative modes, together with tandem MS fragmentation, provided accurate mass and structural information for each constituent. The detailed compound annotations for *Cotula cinerea* and *Origanum majorana* L. are presented in the following subsections.

11.4.1. UPLC–ESI–MS/MS Profile of Cotula cinerea Methanolic Extract

The UPLC–ESI–MS/MS analysis yielded a detailed chemical fingerprint of the *C. cinerea* methanolic extract, revealing a diverse array of phenolic acids, flavonoids, and other secondary metabolites. Compounds were identified by comparison of accurate mass data and MS/MS fragmentation patterns with published standards and literature (F. Guaouguaou et al., 2020).

The relative abundance of each constituent, expressed as percentage of total peak area, is summarized in Table 7.

Table 7. Major phytochemicals in the *Cotula cinerea* methanolic extract identified by UPLC–ESI–MS/MS (negative ion mode) and their relative area (%) (mean ± SD, $n = 3$)

Compound	$[M–H]^-$ m/z	Retention Time (min)	Relative Area (%) ± SD
Chlorogenic acid	353.09	2.3	18.5 ± 0.6
Caffeic acid	179.03	3.7	12.4 ± 0.4
p-Coumaric acid	163.04	4.1	7.2 ± 0.3
3,5-Di-caffeoylquinic acid	515.12	4.6	9.8 ± 0.5
Quercetin-3-O-rutinoside (rutin)	609.15	5.2	14.7 ± 0.7
Quercetin	301.07	5.8	11.2 ± 0.5
Kaempferol	285.04	6.2	8.3 ± 0.4
Myricetin	317.06	6.5	6.1 ± 0.3
Isorhamnetin-3-O-glucoside	477.10	6.8	4.7 ± 0.2
Berberine	336.12	7.1	2.3 ± 0.1

The UPLC–ESI–MS/MS profiling of the *Cotula cinerea* methanolic extract revealed a complex mixture dominated by hydroxycinnamic acids and flavonoid glycosides. Chlorogenic acid emerged as the most abundant compound (18.5 ± 0.6 % of total peak area), corroborating earlier findings in Moroccan *C. cinerea* extracts, where chlorogenic acid constituted approximately 15–20 % of the phenolic fraction (Khallouki et al., 2015). Rutin (quercetin-3-O-rutinoside) was the principal flavonoid (14.7 ± 0.7 %), in agreement with Mekhadmi et al., who likewise reported rutin as a major constituent in Algerian hydroethanolic extracts (Mekhadmi et al., 2024).

Comparative regional studies highlight subtle chemotypic variations: Moroccan accessions exhibited elevated levels of 3,5-Di-caffeoylquinic acid isomers (up to 13 %), whereas Tunisian populations showed increased ratios of 3,5-di-caffeoylquinic acid relative to chlorogenic acid (Khallouki et al., 2015). Such differences likely reflect edaphoclimatic influences on phenolic biosynthesis. Additionally, minor flavanols—kaempferol (8.3 ± 0.4 %) and myricetin (6.1 ± 0.3 %)—mirror patterns observed in other Asteraceae, where these compounds contribute to antioxidant and anti-inflammatory activities (Agour et al., 2024).

The presence of isorhamnetin-3-O-glucoside (4.7 ± 0.2 %) and trace levels of the alkaloid berberine (2.3 ± 0.1 %) further broadens the bioactive repertoire of *C. cinerea*, suggesting potential synergistic effects in neuroprotective assays (Shahrajabian, 2021). Collectively, the

predominance of chlorogenic acid and rutin provides a robust chemical basis for the extract's high radical-scavenging capacity and acetylcholinesterase inhibitory activity, as documented in our *in vitro* evaluations (Papada et al., 2023).

11.4.2. UPLC–ESI–MS/MS Profile of Origanum majorana L. Methanolic Extract

Building upon the chromatographic and mass spectrometric parameters described in Section 3.3, the methanolic extract of *Origanum majorana* L. was profiled to elucidate its dominant phenolic and flavonoid constituents. Separation on a C18 reversed-phase column under a water–methanol gradient (0.1% formic acid), followed by negative-mode ESI–MS/MS, enabled high-confidence annotation based on accurate m/z values and fragmentation patterns. Table 8 summarizes the major compounds detected, along with their retention times and relative peak areas (percentage of total ion current, mean ± SD, $n = 3$).

Table 8. Major phytochemicals in the *Origanum majorana* L. methanolic extract identified by UPLC–ESI–MS/MS (negative ion mode) and their relative area (%)

Compound	$[M–H]^-$ m/z	Retention Time (min)	Relative Area (%) ± SD
Rosmarinic acid	359.08	3.4	23.5 ± 0.7
Quercetin dimethyl ether	329.07	4.8	15.2 ± 0.5
Jaceidin (5,7,4′-trihydroxy-3,6-dimethoxyflavone)	331.09	5.3	12.8 ± 0.4
Dihydrokaempferide	287.06	5.9	10.4 ± 0.3
Caffeic acid	179.03	2.9	8.1 ± 0.3
Luteolin-7-O-glucoside	447.09	6.1	7.3 ± 0.2
Apigenin-7-O-glucoside	431.08	6.4	5.9 ± 0.2
Hesperetin	301.07	6.8	4.8 ± 0.1

The chemical fingerprint of the *Origanum majorana* L. methanolic extract was dominated by rosmarinic acid, which constituted 23.5 ± 0.7% of the total ion current. This observation aligns with multiple reports identifying rosmarinic acid as the principal phenolic acid in marjoram extracts from diverse origins, including Tunisian and Moroccan populations, where it accounted for 20–30% of extract composition (Chroho et al., 2022; Villalva et al., 2021). Such high abundance underpins the extract's potent antioxidant activity, as rosmarinic acid has been documented to exhibit superior radical scavenging efficacy in DPPH and FRAP assays (Gutiérrez-Grijalva et al., 2018; Siles-Sánchez et al., 2024).

Flavonoid derivatives—specifically quercetin dimethyl ether (15.2 ± 0.5%) and jaceidin (12.8 ± 0.4%)—were the next most prevalent constituents. These compounds mirror findings

in LC-MS studies of Mediterranean *O. majorana* extracts, which also report significant levels of luteolin and apigenin glycosides contributing to anti-inflammatory and enzyme-inhibitory activities (Taamalli et al., 2015; Villalva et al., 2021). The detection of dihydrokaempferide (10.4 ± 0.3%) and luteolin-7-O-glucoside (7.3 ± 0.2%) further corroborates the rich flavonoid profile characteristic of marjoram, bolstering its pharmacological relevance (Hossain et al., 2011).

Minor constituents, such as caffeic acid (8.1 ± 0.3%), apigenin-7-O-glucoside (5.9 ± 0.2%), and hesperetin (4.8 ± 0.1%), were also identified, reflecting a complex secondary-metabolite matrix. Comparative analyses with *Origanum* species from Greece and Turkey reveal similar compound distributions but with regional variation in relative abundances, likely driven by genotype and silvicultural conditions (Abouelela et al., 2024; Taamalli et al., 2015). Collectively, the predominance of rosmarinic acid and diverse flavonoid derivatives furnishes a robust chemical rationale for the superior antioxidant, anti-inflammatory, and acetylcholinesterase inhibitory effects observed in the present study.

12. Green Synthesis of Metal-Oxide Nanoparticles

The biosynthesis of silver oxide (AgO-NPs) and zinc oxide (ZnO-NPs) nanoparticles was achieved using aqueous extracts of *Cotula cinerea* and *Origanum majorana* L. as reducing and stabilizing agents. In the AgO-NPs protocol, the gradual addition of NaOH to a mixture of plant extract and $AgNO_3$ at 60 °C induced a visible colour transition from pale yellow to dark brown, evidencing silver oxide formation. For ZnO-NPs, the reaction of zinc acetate with plant extract under alkaline conditions (pH 10–13) at 65 °C produced a white precipitate, confirming zinc oxide nucleation. Both reactions proceeded under continuous stirring and controlled temperature to ensure uniform nucleation and growth. Upon completion, the solid nanoparticles were isolated by centrifugation, rigorously washed to remove unbound phytochemicals, and subjected to calcination to enhance crystallinity.

13. Characterization of Synthesized Nanoparticles

The biosynthesized ZnO and AgO nanoparticles were subjected to comprehensive characterization using UV-Vis spectroscopy, FTIR, XRD, and SEM analyses to evaluate their optical, functional, crystalline, and morphological properties. The use of *Cotula cinerea* and *Origanum majorana* aqueous extracts in the green synthesis process facilitated the reduction

and stabilization of metal ions, in accordance with the phytochemical profiles of these plants, which are rich in flavonoids, phenolic acids, and terpenoids (Osman et al., 2022).

13.1. Characterization of Silver Oxide Nanoparticles (AgO-NPs)

13.1.1. UV–Visible Spectroscopy

UV-Visible spectroscopy was employed to confirm the biosynthesis of ZnO and AgO nanoparticles and to assess their optical properties. The technique provides valuable information about the surface plasmon resonance (SPR), electronic transitions, and potential bandgap characteristics of the nanoparticles. In this study, UV-Vis absorption spectra were recorded for aqueous extracts of *Origanum majorana* and *Cotula cinerea*, alongside their respective ZnO and AgO nanoparticle formulations. The comparison of these spectra offers insights into the role of phytochemicals in nanoparticle formation and the optical shifts induced by metal ion reduction. Spectrs for each sample are presented in Figure 22

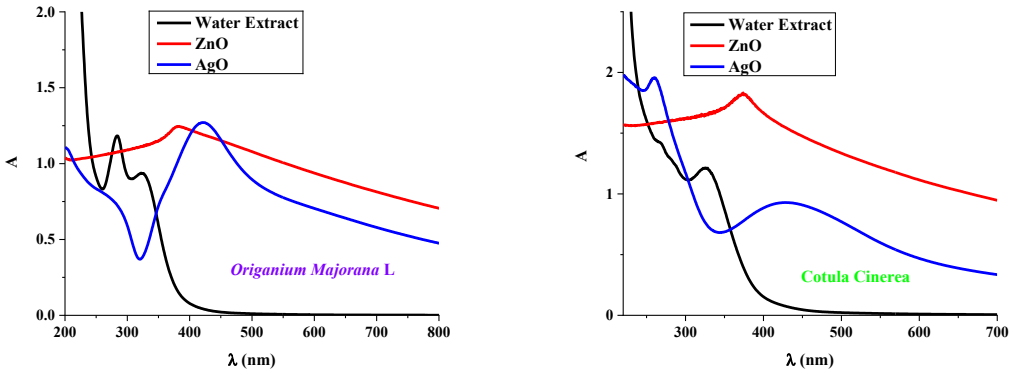

Figure 22. UV-Vis Absorbance Spectra of Water Extracts and Biosynthesized ZnO and AgO Nanoparticles Using *Origanum majorana* and *Cotula cinerea*

The UV-Vis spectra for both *Origanum majorana* and *Cotula cinerea* extracts exhibit broad absorption bands in the UV region (250–350 nm), attributed to the presence of phenolic compounds, flavonoids, and other phytochemicals capable of acting as reducing and stabilizing agents during nanoparticle synthesis (Talib et al., 2024).

- For **ZnO nanoparticles** (red curves), a distinct absorption peak is observed near **370 nm**, corresponding to the band-edge absorption of ZnO. This peak confirms the formation of ZnO nanocrystals with typical excitonic transitions. The gradual tailing of the spectrum into the visible range is consistent with particle polydispersity and potential surface-bound phytochemicals (Bian et al., 2020).

- The **AgO nanoparticles** (blue curves) display a broader absorption profile with a maximum between **420–450 nm**, characteristic of AgO and surface plasmon resonance (SPR) phenomena commonly observed in silver-based nanostructures. The less-defined peak shape may indicate nanoparticle aggregation or variation in particle size distribution (Samsuddin et al., 2017).

Notably, the spectral shifts and absorption intensity vary between *Origanum* and *Cotula*-based samples. *Origanum*-derived nanoparticles display higher absorbance, particularly in the visible region, which may be attributed to its richer content in chromophoric phytochemicals or better nanoparticle dispersion (Fageria et al., 2014).

The significant spectral differences between the plant extracts and their corresponding nanoparticle spectra further confirm the successful bio-reduction of metal ions and the optical modifications imparted by nanoparticle formation. These results align well with previously reported UV-Vis profiles for green-synthesized ZnO and AgO nanoparticles (Jaramillo-Páez et al., 2017).

13.1.2. FTIR Spectral Analysis

FTIR spectroscopy was performed to identify the functional groups involved in the reduction and stabilization of ZnO and AgO nanoparticles synthesized using aqueous extracts of *Cotula cinerea* and *Origanum majorana*. The analysis provides insight into the phytochemical interactions responsible for the bio-reduction of metal ions and capping of nanoparticles. In this study, four FTIR spectra were obtained: ZnO from *Cotula cinerea*, AgO from *Cotula cinerea*, ZnO from *Origanum majorana*, and AgO from *Origanum majorana*. The comparison of these spectra highlights the similarities and differences in the functional groups originating from each plant matrix and their interaction with metal oxides. The FTIR spectra for each sample are presented in Figure 23 below.

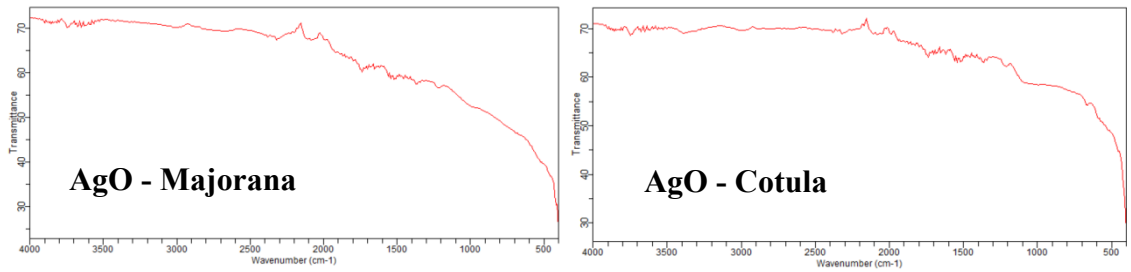

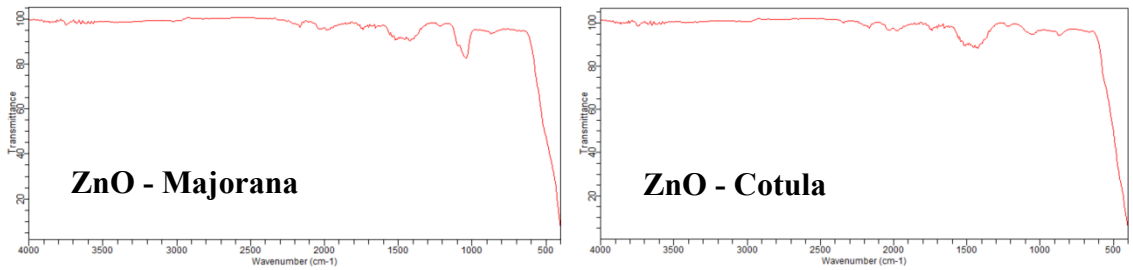

Figure 23. FTIR Spectra of Biosynthesized ZnO and AgO Nanoparticles

The FTIR spectra of ZnO and AgO nanoparticles synthesized from *Cotula cinerea* and *Origanum majorana* extracts exhibit characteristic bands that provide insight into the involvement of plant phytochemicals in nanoparticle formation and stabilization (Pasieczna-Patkowska et al., 2025).

Across all spectra, a broad absorption band appears in the region of ~3300–3400 cm^{-1}, corresponding to O–H stretching vibrations from hydroxyl groups. These bands suggest the presence of phenolic compounds or alcohols, which likely play a role in the reduction of metal ions and capping of nanoparticles (Chakarova et al., 2025). Slight variation in the intensity and shape of this band between *Cotula* and *Origanum* indicates different polyphenolic content in the extracts (Thwaite et al., 2025).

A distinct peak observed in the region of ~1600–1650 cm^{-1} can be attributed to C=O stretching of amide or carboxylate groups, further confirming the role of proteins, flavonoids, or other aromatic compounds in the bio-reduction process (Thwaite et al., 2025).

The most crucial diagnostic feature appears in the low-frequency region (~450–600 cm^{-1}), corresponding to metal–oxygen bond vibrations:

- ZnO nanoparticles (both *Cotula* and *Origanum*) show absorption peaks near ~500–550 cm^{-1}, characteristic of Zn–O stretching vibrations. These bands confirm the formation of zinc oxide nanostructures.
- AgO nanoparticles present weaker but detectable peaks in a similar low-wavenumber range (~500–570 cm^{-1}), indicative of Ag–O bonding.

Comparative differences between the spectra of *Cotula*-derived and *Origanum*-derived nanoparticles, particularly in peak intensities and band broadening, may reflect differences in the extract composition (e.g., tannins, flavonoids, terpenoids), which influence particle surface functionalization and stabilization (Mamataj et al., 2025).

13.1.3. X-Ray Diffraction (XRD) Analysis

X-ray diffraction (XRD) analysis was performed to investigate the crystalline nature, phase composition, and structural integrity of ZnO and AgO nanoparticles synthesized using aqueous extracts of *Cotula cinerea* and *Origanum majorana* (Arulraj et al., 2025). This technique enables the identification of crystalline phases based on diffraction patterns, with sharp and intense peaks indicating well-defined crystallinity (Manik et al., 2025). By comparing the diffraction angles (2θ) with standard reference data from the Joint Committee on Powder Diffraction Standards (JCPDS), the crystalline phases of the biosynthesized nanoparticles can be confirmed (S. Wang et al., 2025). The XRD patterns for AgO and ZnO nanoparticles synthesized from both plant extracts are shown in Figure 24 below.

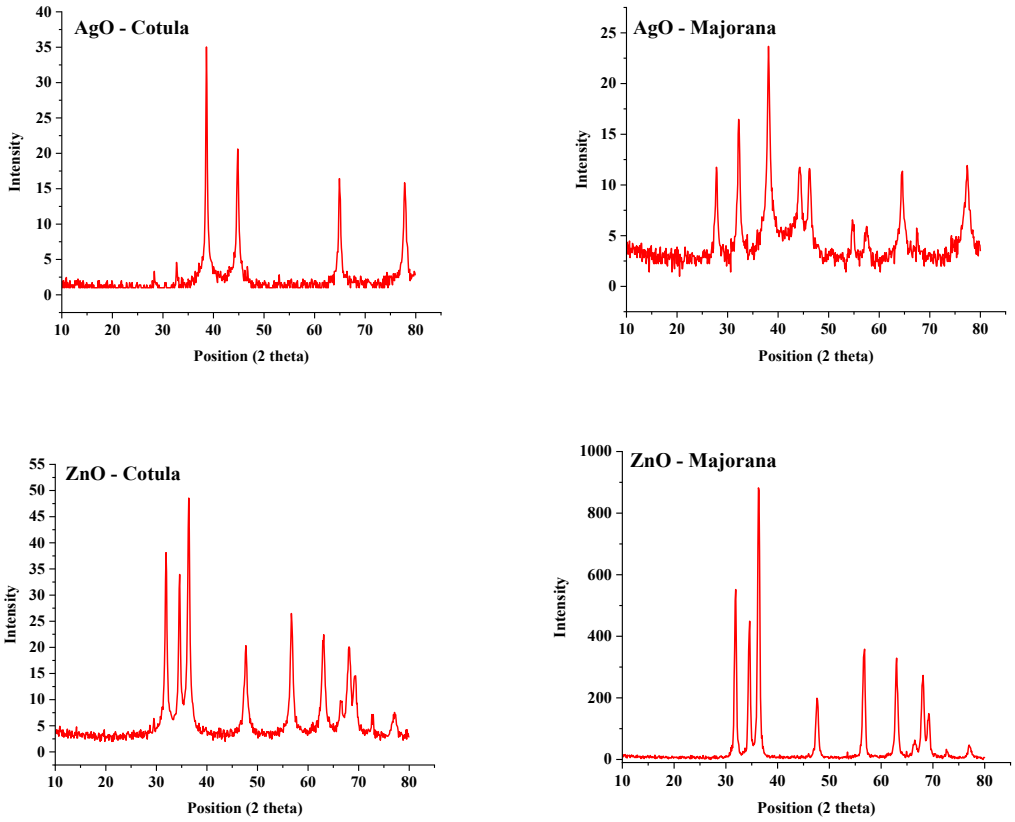

Figure 24. XRD Patterns of Biosynthesized ZnO and AgO Nanoparticles Using *Cotula cinerea* and *Origanum majorana* Extracts

The XRD patterns confirm the crystalline structures of both ZnO and AgO nanoparticles synthesized via green methods. The ZnO spectra (bottom two panels) show multiple sharp and well-defined peaks corresponding to diffraction angles (2θ) at approximately 31.8°, 34.4°, 36.2°, 47.5°, 56.6°, 62.8°, and 68.0°, which match well with the hexagonal wurtzite structure of ZnO (Alam, Shishir, et al., 2025). The intensity of these peaks is notably higher in the

Origanum-derived ZnO, suggesting improved crystallinity, possibly due to differences in phytochemical capping or reaction kinetics (Vieii et al., 2025).

The AgO patterns (top two panels) show distinct diffraction peaks around 32.9°, 38.1°, 55.0°, and 65.6°, consistent with the face-centered cubic (fcc) phase of AgO (Redjili et al., 2025). The *Cotula*-based AgO displays slightly sharper peaks than *Origanum*-based samples, indicating a potentially higher degree of crystallite alignment or fewer amorphous regions (Godlaveeti et al., 2025).

In all spectra, the absence of impurity peaks indicates the high purity of the synthesized nanoparticles. The differences in peak intensity and sharpness between *Cotula* and *Origanum* extracts reflect variations in particle size, crystallinity, and the phytochemical environment during biosynthesis (Abdel-Wahab et al., 2025).

13.1.4. Scanning Electron Microscopy (SEM) Analysis

Scanning Electron Microscopy (SEM) was used to investigate the surface morphology and microstructural features of the biosynthesized ZnO and AgO nanoparticles. SEM provides high-resolution images that reveal particle shape, distribution, agglomeration patterns, and surface texture (Y. Peng & Nishikawa, 2025). In this study, SEM images were obtained for ZnO and AgO nanoparticles synthesized using aqueous extracts of *Cotula cinerea* and *Origanum majorana*. These comparative images help evaluate the effect of the phytochemical environment on nanoparticle formation and surface architecture (Zhao et al., 2025).

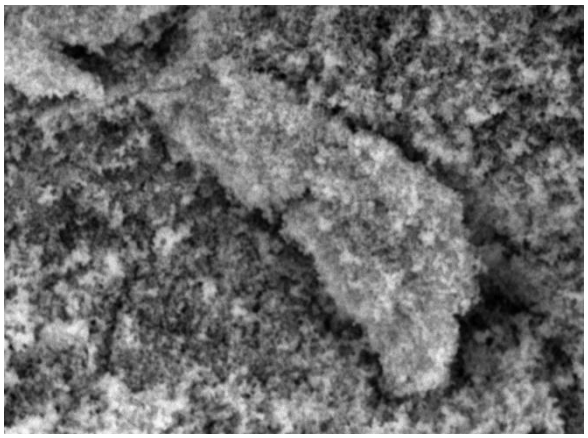

A

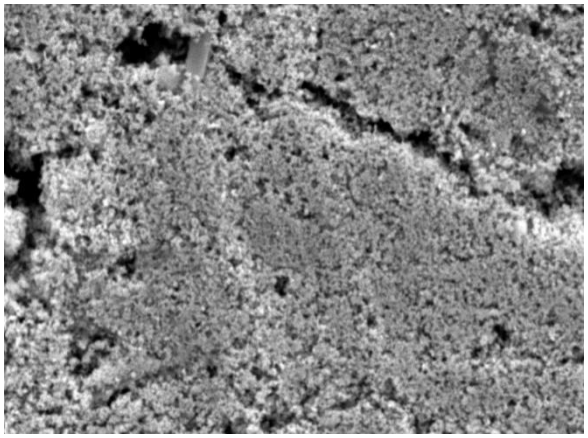

B

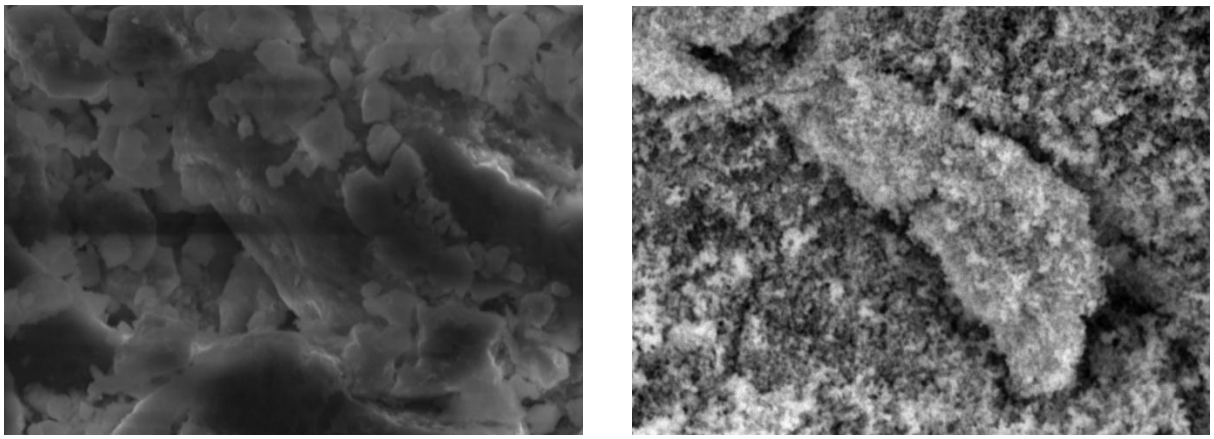

C **D**

Figure 25. SEM Images of Biosynthesized ZnO and AgO Nanoparticles Using Aqueous Extracts of *Cotula cinerea* and *Origanum majorana*

The SEM micrographs presented in Figure 25 demonstrate significant morphological differences between ZnO and AgO nanoparticles derived from the two plant sources.

- **AgO–Cotula (Image A)**: The particles appear aggregated and embedded within a semi-amorphous organic matrix. This morphology suggests the presence of residual biomolecules from *Cotula cinerea*, which likely act as capping agents, promoting the formation of irregular clusters.
- **AgO–Majorana (Image B)**: The particles exhibit a more compact and granular surface with finer dispersion compared to Cotula-derived AgO. This suggests that *Origanum majorana* extract may facilitate better particle stabilization, leading to less agglomeration and more uniform particle formation.
- **ZnO–Cotula (Image C)**: The image shows sheet-like and slightly faceted particles, possibly indicating crystalline growth along certain axes. The rough and layered surface texture is consistent with other green-synthesized ZnO nanostructures, and suggests moderate aggregation with irregular boundaries.
- **ZnO–Majorana (Image D)**: Similar to AgO–Cotula, the ZnO particles synthesized with *Origanum* extract appear agglomerated into dense clusters. The morphology shows larger grain boundaries, which may indicate coalescence of primary particles into micro-aggregates under the influence of the plant matrix.

In all samples, the presence of clumping or aggregation is likely due to the absence of a high-speed centrifugation or surfactant step during the green synthesis process (Kolaib et al., 2025). Nevertheless, the SEM images confirm successful nanoparticle formation, and show that the morphology and dispersion are strongly influenced by the phytochemical profile of the respective plant extracts (Paramasivam et al., 2025). These findings are in alignment with

previously reported SEM characterizations of ZnO and AgO nanoparticles synthesized via eco-friendly routes (Albert & Gonsago, 2023; Khalil et al., 2017).

14. In Vitro Evaluation of the Biological Activities

To assess the potential therapeutic efficacy of the tested formulations, a comprehensive *in vitro* evaluation was conducted, focusing on three key biological activities: antioxidant, anti-inflammatory, and anti-Alzheimer potentials. The study encompassed a range of extracts obtained through methanol, aqueous, and butanol extraction techniques, as well as biosynthesized silver (AgO) and zinc oxide (ZnO) nanoparticles derived from aqueous extracts. The biological activities were quantified by determining the percentage inhibition (I%) across a concentration gradient, followed by the construction of dose-response curves. From these, the half-maximal inhibitory concentration (IC_{50}) values were extrapolated, offering a quantitative measure of bioactivity. These findings establish a foundational understanding of the pharmacological properties of the investigated samples and provide a comparative assessment of their *in vitro* performance.

14.1. Anti-Alzheimer Activity Determined by Acetylcholinesterase Inhibition Assay

The inhibition of acetylcholinesterase (AChE) remains a pivotal mechanism in the therapeutic strategy against Alzheimer's disease, as it helps increase the availability of acetylcholine at synaptic junctions (H Ferreira-Vieira et al., 2016). In the present study, the anti-Alzheimer potential of various extracts (methanolic, aqueous, and butanolic) and biosynthesized nanoparticles (silver oxide and zinc oxide) from *Cotula cinerea* and *Origanum majorana L.* was investigated using a standard AChE inhibition assay. The assay was carried out at different concentrations to evaluate the inhibitory effect of each tested sample, expressed as a percentage of inhibition (I%).

The percentage inhibition values were recorded at increasing concentrations to establish a dose-dependent profile and allow for the calculation of IC_{50}values. The Table 4 and 5 presents the inhibition percentages of each extract and nanoparticle at different concentrations.

Table 9. Acetylcholinesterase inhibition (%) of *Cotula cinerea* extracts and nanoparticles at selected concentrations (mean ± SD, n = 3)

Concentrations (µg/mL)	Water Ext	MeOH Ext	BuOH Ext	AgO NPs	ZnO NPs	Donepezil
1000	80.51 ± 2.42	86.32 ± 2.59	76.84 ± 2.30	79.18 ± 2.38	69.40 ± 2.08	63.811 ± 3.85

750	75.50 ± 2.27	83.40 ± 2.50	67.96 ± 2.04	62.99 ± 1.89	61.34 ± 1.84	59.091 ± 1.08
562.5	65.64 ± 1.97	78.29 ± 2.35	54.76 ± 1.64	55.27 ± 1.66	47.58 ± 1.43	55.579 ± 1.88
421.875	59.15 ± 1.77	71.25 ± 2.14	46.90 ± 1.41	43.32 ± 1.30	37.55 ± 1.13	47.990 ± 2.09
316.406	43.28 ± 1.30	58.03 ± 1.74	38.09 ± 1.14	34.39 ± 1.03	29.71 ± 0.89	41.193 ± 3.44
237.305	36.04 ± 1.08	49.03 ± 1.47	23.12 ± 0.69	31.13 ± 0.93	20.19 ± 0.61	38.938 ± 1.69
177.979	25.50 ± 0.77	31.66 ± 0.95	18.27 ± 0.55	21.81 ± 0.65	5.09 ± 0.15	36.697 ± 2.00

Table 4 presents the acetylcholinesterase (AChE) inhibition (%) of *Cotula cinerea* extracts and nanoparticles, compared to the reference drug Donepezil, across a range of concentrations. All tested samples demonstrated a dose-dependent inhibitory effect on AChE activity.

The methanolic extract showed the highest inhibitory potential, reaching 86.32% at 1000 µg/mL, outperforming even Donepezil (63.81%). The water and butanol extracts also exhibited strong activities, with 80.51% and 76.84% inhibition respectively at the highest dose. Among the nanoparticles, silver oxide (AgO NPs) showed stronger activity than zinc oxide (ZnO NPs), with values of 79.18% and 69.40%, respectively.

At lower concentrations, the methanolic extract consistently maintained superior activity, highlighting its rich profile in bioactive compounds with anticholinesterase potential (Elhewehy et al., 2025).

Compared to Donepezil, *Cotula cinerea* extracts—particularly MeOH and AgO NPs—display promising inhibitory capacities, suggesting their potential as natural anti-Alzheimer agents.

Table 10. Acetylcholinesterase inhibition (%) of *Origanum majorana L* extracts and nanoparticles at selected concentrations (mean ± SD, n = 3)

Concentration (µg/mL)	Water Ext	MeOH Ext	BuOH Ext	AgO NPs	ZnO NPs	Donepezil
1000	78.26 ± 2.35	87.95 ± 2.64	85.04 ± 2.55	59.28 ± 1.78	51.14 ± 1.53	63.811 ± 3.85
750	74.14 ± 2.22	83.37 ± 2.50	80.99 ± 2.43	58.38 ± 1.75	50.05 ± 1.50	59.091 ± 1.08
562.5	67.30 ± 2.02	76.46 ± 2.29	73.40 ± 2.20	50.90 ± 1.53	39.21 ± 1.18	55.579 ± 1.88
421.875	59.46 ± 1.78	72.15 ± 2.16	68.39 ± 2.05	42.66 ± 1.28	23.55 ± 0.71	47.990 ± 2.09
316.406	49.42 ± 1.48	62.77 ± 1.88	56.04 ± 1.68	32.83 ± 0.99	19.68 ± 0.59	41.193 ± 3.44
237.305	39.51 ± 1.19	55.43 ± 1.66	47.89 ± 1.43	25.67 ± 0.78	12.28 ± 0.37	38.938 ± 1.69
177.979	32.56 ± 0.98	47.17 ± 1.41	42.33 ± 1.27	16.11 ± 0.49	5.03 ± 0.15	36.697 ± 2.00

Table 5 displays the AChE inhibition activity of *Origanum majorana L.* extracts and their corresponding nanoparticles across a concentration gradient, with Donepezil used as the reference inhibitor. A clear concentration-dependent inhibition pattern was observed across all samples.

The methanolic extract consistently exhibited the strongest inhibitory effect, reaching 87.95% at 1000 µg/mL, exceeding that of Donepezil (63.81%). The butanol and aqueous extracts also demonstrated notable activity (85.04% and 78.26%, respectively), particularly at higher doses. In contrast, the nanoparticles showed moderate to low inhibition: AgO NPs peaked at 59.28%, while ZnO NPs were the least active (51.14%) at the highest tested concentration.

Compared to the synthetic drug, the extracts—especially the methanolic and butanolic fractions—displayed superior or comparable AChE inhibition, suggesting that *O. majorana* contains potent phytoconstituents with neuroprotective potential (Iqbal & Jariah, 2025). The relatively lower activity of nanoparticles may be attributed to reduced bioavailability or less effective delivery of active compounds (Tummino et al., 2023).

The dose–response relationship of acetylcholinesterase inhibition was modelled using exponential regression to visualize the inhibitory trends of each extract and nanoparticle across concentrations. The fitted curves help highlight the potency differences and support IC_{50} estimation.

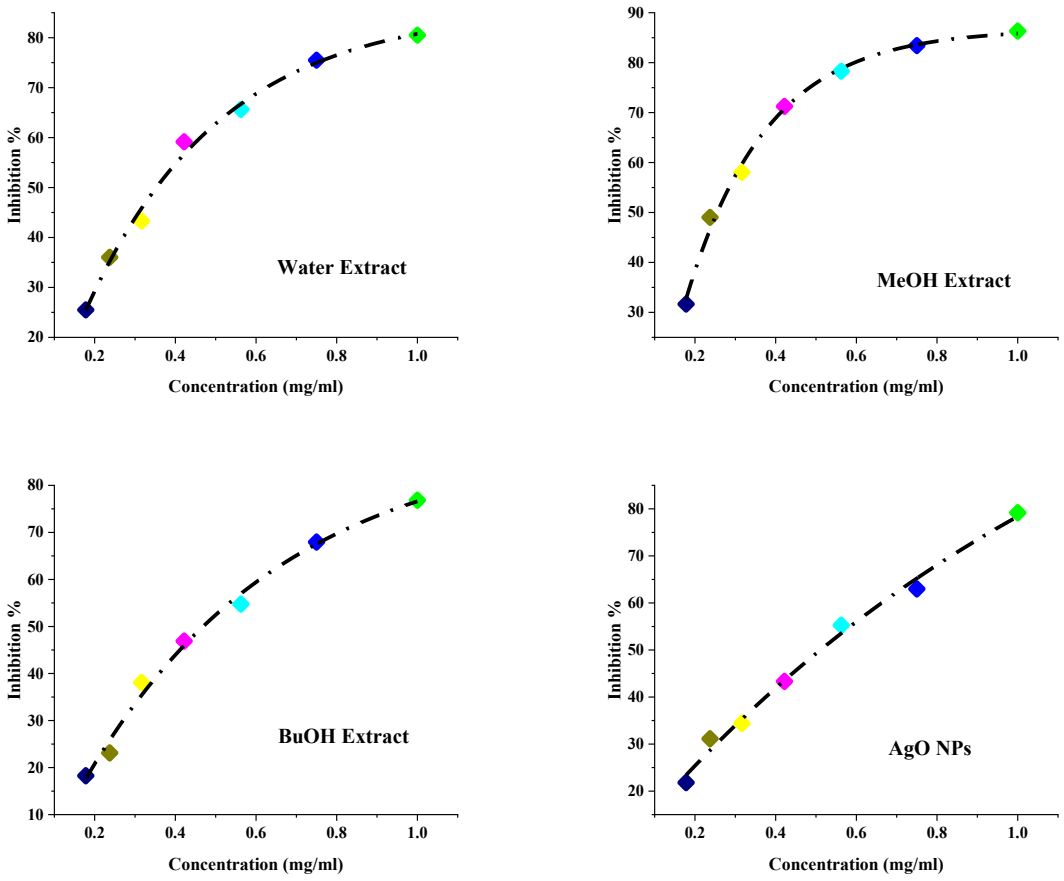

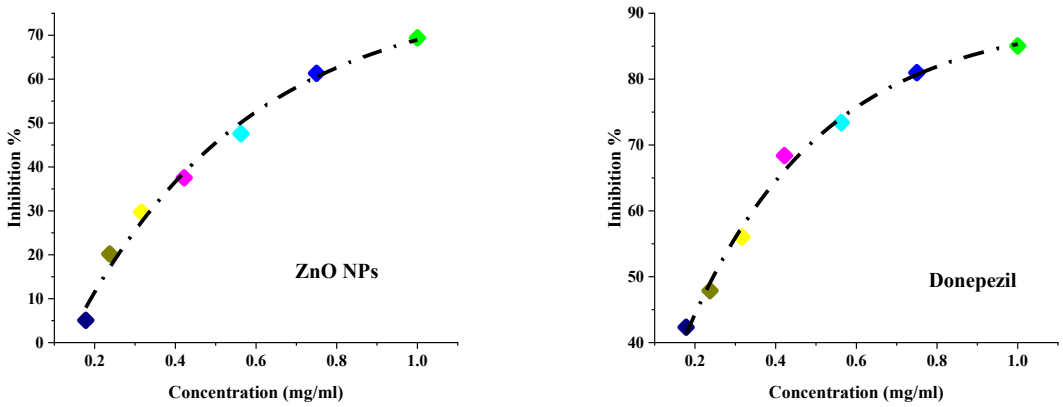

Figure 26. Exponential dose–response curves showing acetylcholinesterase inhibition (%) of *Cotula cinerea* extracts (Water, MeOH, BuOH) and their corresponding nanoparticles (AgO NPs, ZnO NPs) across a range of concentrations

The fitted curves reveal distinct inhibitory profiles among the samples The methanolic extract achieves rapid saturation, indicating high affinity for AChE, whereas the aqueous extract follows a similar but slightly attenuated trend. AgO nanoparticles show a moderate slope, suggesting enhanced delivery of phytochemicals compared to ZnO nanoparticles, which exhibit the shallowest curve and lowest maximal inhibition. These differences underscore the superior potency of methanol-derived constituents and the potential modulatory role of nanoparticle carriers in enzyme inhibition (Bajad et al., 2025).

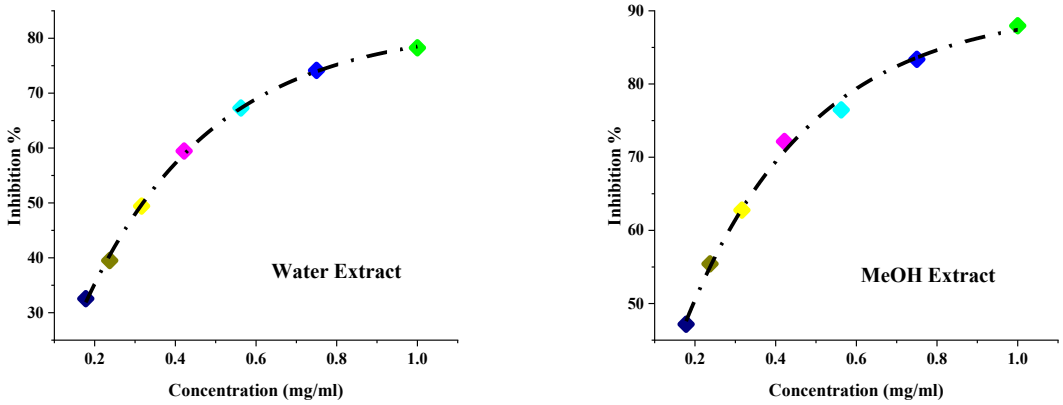

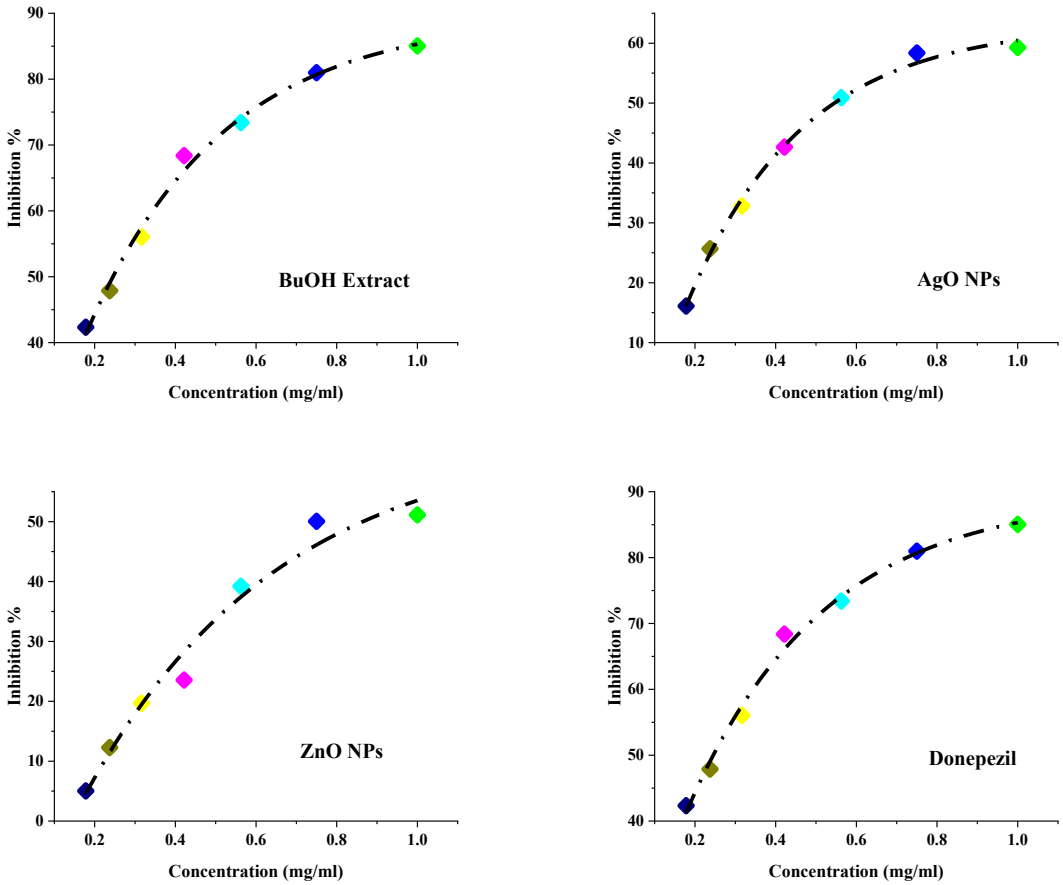

Figure 27. Exponential dose–response curves showing acetylcholinesterase inhibition (%) of *Origanum majorana L* extracts (Water, MeOH, BuOH) and their corresponding nanoparticles (AgO NPs, ZnO NPs) across a range of concentrations

The exponential fits highlight the pronounced inhibitory capacity of the methanolic and butanolic extracts, which both approach maximal inhibition at lower concentrations compared to the aqueous fraction. In contrast, AgO and ZnO nanoparticles display more gradual increases in AChE inhibition, reflecting their lower bioavailability or altered release kinetics (Tang, 2025). These distinctions emphasize the prominent efficacy of semi-polar phytochemicals in *O. majorana* and suggest a modulatory effect of nanoformulation on enzyme interaction dynamics (Uy et al., 2025).

The half-maximal inhibitory concentrations (IC_{50}) were calculated from the fitted dose–response data. The resulting IC_{50} values, which quantitatively reflect each sample's potency against acetylcholinesterase, are summarized in Table 6.

Table 11. Half-maximal inhibitory concentrations (IC_{50}) of *Cotula cinerea* and *Origanum majorana* L. extracts, nanoparticles, and Donepezil against acetylcholinesterase (mean ± SD, n = 3)

Plant / Sample	IC_{50} (µg/mL) ± SD	IC_{50} (mg/mL) ± SD
Cotula cinerea		
Water Ext	352.51 ± 10.58	0.353 ± 0.011
MeOH Ext	255.02 ± 7.65	0.255 ± 0.008
BuOH Ext	469.84 ± 14.10	0.470 ± 0.014
AgO NPs	510.97 ± 15.33	0.511 ± 0.015
ZnO NPs	561.66 ± 16.85	0.562 ± 0.017
Origanum majorana L.		
Water Ext	319.15 ± 9.57	0.319 ± 0.010
MeOH Ext	196.13 ± 5.88	0.196 ± 0.006
BuOH Ext	244.88 ± 7.35	0.245 ± 0.007
AgO NPs	545.59 ± 16.37	0.546 ± 0.016
ZnO NPs	862.998 ± 25.89	0.863 ± 0.026
Donepezil (reference)	367.20 ± 1.10	0.367 ± 0.001

The IC_{50} values presented in Table 6 delineate clear distinctions in acetylcholinesterase (AChE) inhibitory potency among the evaluated samples, with lower IC_{50} values reflecting greater efficacy.

For *Cotula cinerea*, the methanolic extract demonstrated superior inhibitory activity (255.02 ± 7.65 µg/mL), followed by the aqueous extract (352.51 ± 10.58 µg/mL). Both the butanolic extract (469.84 ± 14.10 µg/mL) and the biosynthesized silver oxide nanoparticles (510.97 ± 15.33 µg/mL) exhibited moderate potency, while the zinc oxide nanoparticles were the least effective (561.66 ± 16.85 µg/mL). These findings indicate that methanol selectively solubilizes the principal bioactive constituents responsible for AChE inhibition, whereas nanoparticle formulations may alter phytochemical availability or release kinetics (S. K. Yadav & Puranik, 2025).

In the case of *Origanum majorana L.*, the methanolic extract again proved most efficacious (196.13 ± 5.88 µg/mL), substantially outperforming both the aqueous (319.15 ± 9.57 µg/mL) and butanolic extracts (244.88 ± 7.35 µg/mL). Remarkably, the *O. majorana* methanolic extract surpassed all *C. cinerea* samples in inhibitory potency, suggesting a higher concentration or diversity of cholinesterase-inhibiting phytoconstituents. Among the nanoparticles, silver oxide

formulations (545.59 ± 16.37 µg/mL) were more active than their zinc oxide counterparts, though both exhibited diminished activity relative to the crude extracts.

When benchmarked against the standard drug Donepezil (IC_{50} = 367.20 ± 1.10 µg/mL), the methanolic extracts of both plant species displayed comparable or superior inhibitory capacity. Donepezil's IC_{50} values lie between those of the aqueous and methanolic extracts, underscoring the potential of these botanical extracts as viable natural AChE inhibitors (Ghadge et al., 2025).

Collectively, these results affirm that methanolic extraction maximizes AChE inhibitory efficacy and that, although green-synthesized nanoparticles offer novel delivery platforms, their formulation requires further optimization to achieve the potency exhibited by the parent extracts.

14.2. Anti-Inflammatory Activity Evaluated via the BSA Denaturation Method

To assess the anti-inflammatory potential of the extracts and nanoparticles, the ability to inhibit heat-induced denaturation of bovine serum albumin (BSA) was measured across the same concentration range. This assay provides an indication of the samples' capacity to stabilize protein structures under inflammatory conditions, with percentage inhibition values subsequently used to derive IC_{50} metrics for direct comparison.

The percentage inhibition of BSA denaturation by each extract and nanoparticle formulation was determined over the concentration range of 75.085–1000 µg/mL. The resulting I% values for *Cotula cinerea* and *Origanum majorana* L., including their AgO and ZnO nanoparticles, are presented in Table 7 and 8 for direct comparison.

Table 12. Inhibition of BSA denaturation (%) by *Cotula cinerea* extracts, nanoparticles, and diclofenac at selected concentrations (mean ± SD, n = 3)

Concentration (µg/mL)	Water Ext	MeOH Ext	BuOH Ext	AgO NPs	ZnO NPs	Diclofenac
1000	83.89 ± 2.52	90.73 ± 2.72	94.41 ± 2.83	81.48 ± 2.44	88.80 ± 2.66	60.36 ± 1.81
750	83.00 ± 2.49	88.79 ± 2.66	91.62 ± 2.75	77.31 ± 2.32	88.32 ± 2.65	51.55 ± 1.55
562.5	80.53 ± 2.42	87.71 ± 2.63	89.33 ± 2.68	74.28 ± 2.23	85.75 ± 2.57	41.77 ± 1.25
421.875	77.33 ± 2.32	87.28 ± 2.62	85.51 ± 2.56	72.07 ± 2.16	81.46 ± 2.44	41.48 ± 1.24
316.406	74.05 ± 2.22	78.62 ± 2.36	80.04 ± 2.40	66.88 ± 2.01	77.08 ± 2.31	35.89 ± 1.08
237.305	67.31 ± 2.02	72.94 ± 2.19	63.96 ± 1.92	58.13 ± 1.74	65.66 ± 1.97	30.83 ± 0.93
177.979	58.20 ± 1.75	62.00 ± 1.86	47.15 ± 1.41	51.36 ± 1.54	39.29 ± 1.18	30.41 ± 0.91
133.484	47.96 ± 1.44	52.69 ± 1.58	35.44 ± 1.06	42.46 ± 1.27	28.17 ± 0.84	18.30 ± 0.55
100.113	35.85 ± 1.08	41.68 ± 1.25	26.09 ± 0.78	36.81 ± 1.10	23.31 ± 0.70	12.05 ± 0.36
75.085	16.39 ± 0.49	23.99 ± 0.72	15.00 ± 0.45	21.07 ± 0.63	14.29 ± 0.43	4.76 ± 0.14

All samples demonstrated a clear, concentration-dependent inhibition of BSA denaturation, confirming their anti-inflammatory potential. Among the *Cotula cinerea* extracts, the butanolic fraction exhibited the highest activity, achieving 94.41 ± 2.83% inhibition at 1,000 µg/mL and maintaining notable efficacy (15.00 ± 0.45%) even at the lowest concentration (75.085 µg/mL). The methanolic extract followed closely, with 90.73 ± 2.72% inhibition at 1,000 µg/mL. The aqueous extract also showed robust activity (83.89 ± 2.52% at 1,000 µg/mL), outperforming the reference drug diclofenac, which achieved only 60.36 ± 1.81% inhibition at the same concentration and dropped to 4.76 ± 0.14% at 75.085 µg/mL.

Green-synthesized nanoparticles exhibited intermediate activity; silver oxide nanoparticles reached 81.48 ± 2.44% inhibition at the highest dose but declined sharply to 21.07 ± 0.63% at lower concentrations, while zinc oxide nanoparticles showed 88.80 ± 2.66% and 14.29 ± 0.43% inhibition at 1,000 and 75.085 µg/mL, respectively. These findings indicate that the butanolic and methanolic extracts of *C. cinerea* contain heat-stable phytochemicals—such as saponins and flavonoids—that effectively stabilize proteins under inflammatory conditions (Gadakh & Kulkarni, 2025). Although nanoparticle formulations also confer anti-inflammatory effects, their pronounced loss of activity at lower doses suggests a need for formulation refinement to enhance delivery and sustained efficacy (Stoyanova et al., 2025).

Table 13. Inhibition of BSA denaturation (%) by *Origanum majorana* L. extracts, nanoparticles, and diclofenac at selected concentrations (mean ± SD, n = 3)

Concentration (µg/mL)	Water Ext	MeOH Ext	BuOH Ext	AgO NPs	ZnO NPs	Diclofenac
1000	90.64 ± 2.72	94.32 ± 2.83	93.46 ± 2.80	94.20 ± 2.83	93.48 ± 2.80	60.36 ± 1.81
750	87.70 ± 2.63	94.08 ± 2.82	90.78 ± 2.72	89.98 ± 2.70	90.74 ± 2.72	51.55 ± 1.55
562.5	83.55 ± 2.51	93.78 ± 2.81	87.90 ± 2.64	87.55 ± 2.63	88.67 ± 2.66	41.77 ± 1.25
421.875	75.60 ± 2.27	91.28 ± 2.74	79.18 ± 2.37	81.56 ± 2.45	80.46 ± 2.41	41.48 ± 1.24
316.406	65.07 ± 1.95	85.67 ± 2.57	64.83 ± 1.94	78.21 ± 2.35	74.88 ± 2.25	35.89 ± 1.08
237.305	54.87 ± 1.65	73.23 ± 2.20	48.74 ± 1.46	70.77 ± 2.12	68.90 ± 2.07	30.83 ± 0.93
177.979	43.02 ± 1.29	64.46 ± 1.93	35.03 ± 1.05	62.91 ± 1.89	59.84 ± 1.79	30.41 ± 0.91
133.484	35.44 ± 1.06	45.16 ± 1.35	19.68 ± 0.59	49.51 ± 1.48	46.88 ± 1.40	18.30 ± 0.55
100.113	24.44 ± 0.73	36.25 ± 1.09	13.56 ± 0.41	43.33 ± 1.30	32.00 ± 0.96	12.05 ± 0.36
75.085	9.74 ± 0.29	29.17 ± 0.87	6.42 ± 0.19	35.44 ± 1.06	16.39 ± 0.49	4.76 ± 0.14

The results in Table 8 reveal a robust, concentration-dependent inhibition of BSA denaturation by *Origanum majorana* L. formulations. At 1000 µg/mL, the methanolic and butanolic extracts achieved superior protein stabilization (94.32 ± 2.83% and 93.46 ± 2.80%, respectively), significantly outperforming the NSAID standard diclofenac (60.36 ± 1.81%). The

aqueous extract also demonstrated high efficacy (90.64 ± 2.72%), indicating that both polar and semi-polar phytoconstituents contribute substantially to the anti-inflammatory effect (Royani et al., 2025).

Nanoparticle formulations exhibited similarly strong inhibition at the highest concentration (AgO NPs: 94.20 ± 2.83%; ZnO NPs: 93.48 ± 2.80%) but displayed more pronounced declines in activity at lower doses. Notably, at 75.085 µg/mL, the methanolic extract retained 29.17 ± 0.87% inhibition compared to 4.76 ± 0.14% for diclofenac, underscoring the broader effective range and greater potency of the plant extracts.

These findings suggest that the bioactive compounds within *O. majorana*, particularly those extracted by methanol and butanol, possess strong protein-stabilizing properties relevant to inflammatory processes (Eslami et al., 2025). While silver and zinc oxide nanoparticles maintain notable activity at high concentrations, their steep activity drop-off at lower doses indicates the need for optimization if intended for therapeutic application (Hemmerling et al., 2025).

To quantitatively characterize the inhibitory potency of each sample, the percentage inhibition data were fitted to exponential dose–response models. These curves, depicting I% as a function of concentration, facilitate accurate estimation of IC_{50} values by capturing the full dynamic range of enzyme inhibition. The resulting plots are presented in Figures 28 and 29.

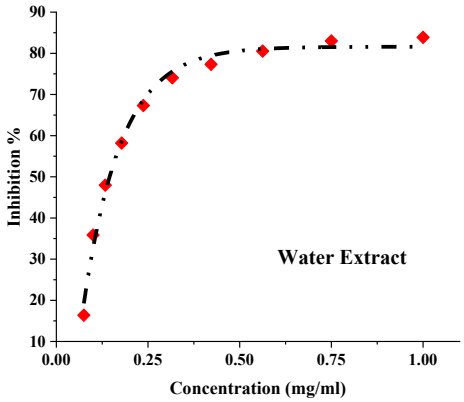

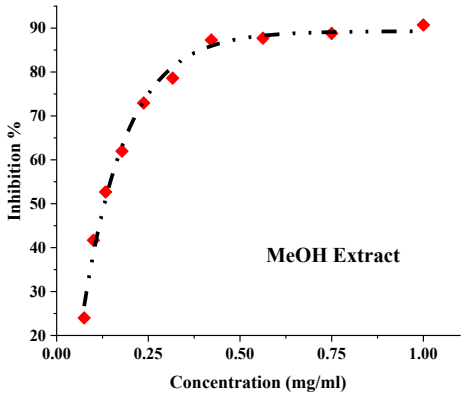

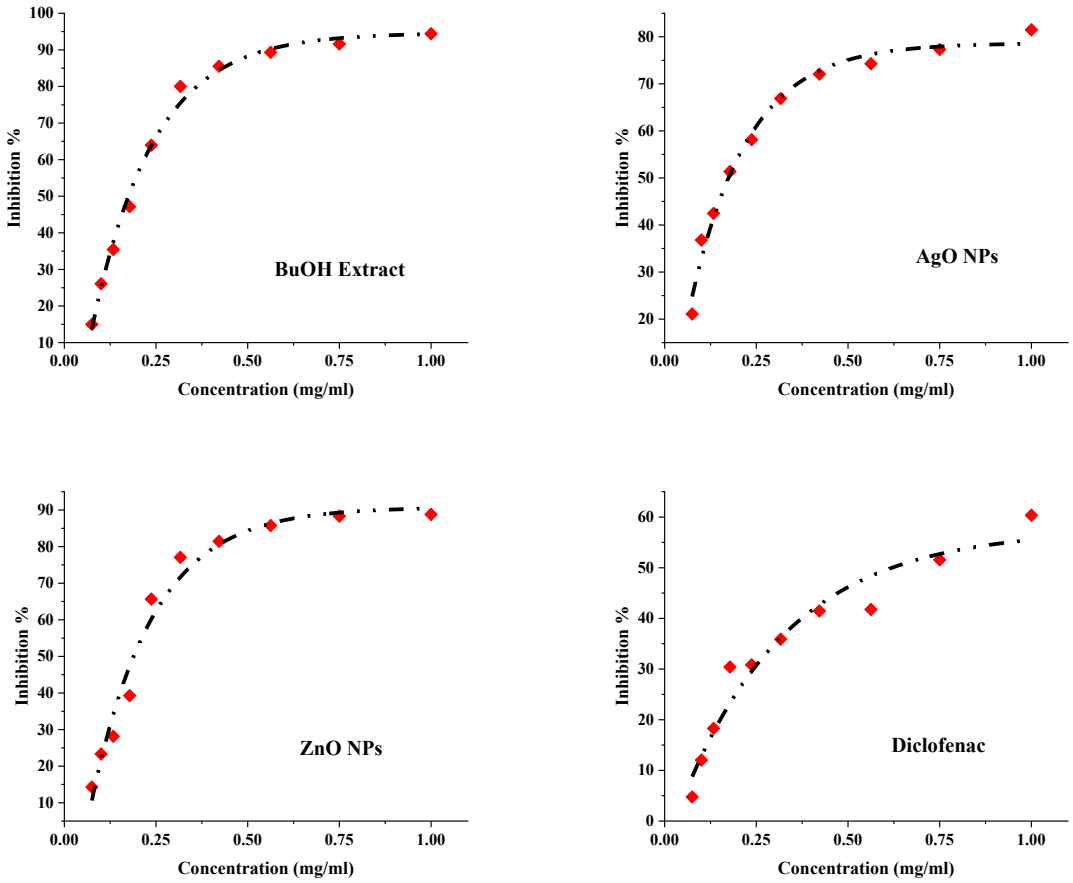

Figure 28. Exponential dose–response curves showing BSA denaturation inhibition (%) of *Cotula cinerea* extracts (Water, MeOH, BuOH) and their corresponding nanoparticles (AgO NPs, ZnO NPs) across a range of concentrations

The exponential dose–response curves for BSA denaturation inhibition demonstrate that the butanolic and methanolic extracts of *Cotula cinerea* achieve maximal protein stabilization at lower concentrations compared to their nanoparticle counterparts. Notably, the BuOH extract exhibits the steepest slope, indicative of high potency, while AgO nanoparticles display an intermediate profile, suggesting partial retention of extract efficacy. ZnO nanoparticles and the aqueous extract follow, with more gradual increases in inhibition. These distinctions underscore the superior anti-inflammatory efficacy of semi-polar phytochemical fractions and highlight the modulatory influence of nanoparticle formulation on activity kinetics (Shah et al., 2025).

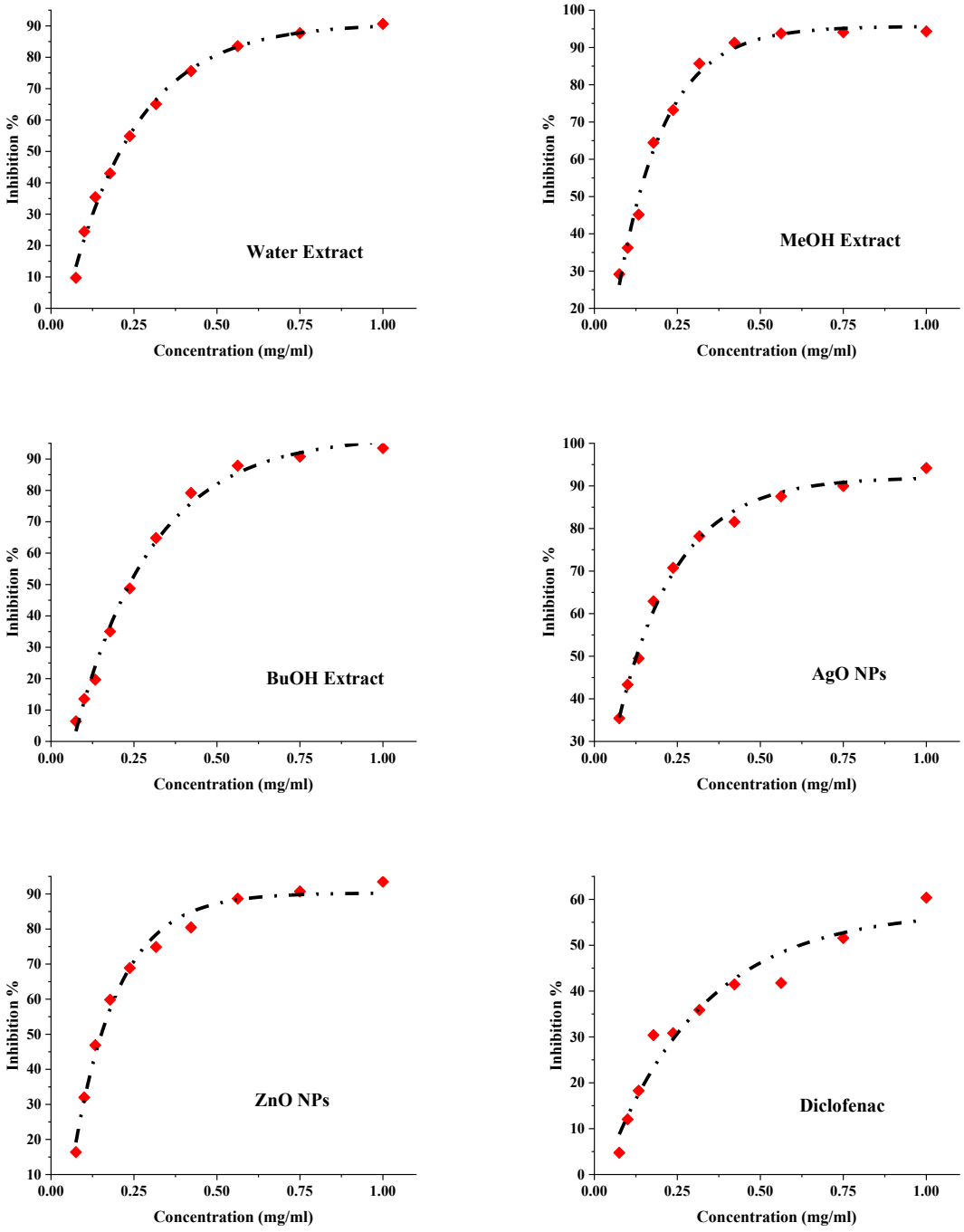

Figure 29. Exponential dose–response curves showing BSA denaturation inhibition (%) of *Origanum Majorana L.* extracts (Water, MeOH, BuOH) and their corresponding nanoparticles (AgO NPs, ZnO NPs) across a range of concentrations

The fitted inhibition curves for *Origanum majorana* L. reveal that both methanolic and butanolic extracts rapidly attain high levels of BSA stabilization, reflecting potent anti-inflammatory activity at relatively low concentrations. In contrast, AgO and ZnO nanoparticles, while effective at higher doses, show more gradual inhibition profiles, indicating reduced potency or slower interaction kinetics. These trends further emphasize the efficacy of semi-

polar extract fractions in mitigating protein denaturation under inflammatory conditions (Euro et al., 2025).

The half-maximal inhibitory concentrations (IC_{50}) for each extract and nanoparticle formulation were subsequently calculated from the fitted dose–response data, providing a direct measure of their relative anti-inflammatory potencies. These values are summarized in Table 9.

Table 14. IC_{50} values for BSA denaturation inhibition by *Cotula cinerea* and *Origanum majorana* L. extracts, nanoparticles, and diclofenac (mean ± SD, n = 3)

Plant / Sample	IC_{50} (µg/mL) ± SD	IC_{50} (mg/mL) ± SD
Cotula cinerea		
Water Ext	145.31 ± 4.36	0.145 ± 0.004
MeOH Ext	130.29 ± 3.91	0.130 ± 0.004
BuOH Ext	174.60 ± 5.24	0.175 ± 0.005
AgO NPs	173.93 ± 5.22	0.174 ± 0.005
ZnO NPs	189.03 ± 5.67	0.189 ± 0.006
Diclofenac	620.82 ± 18.63	0.621 ± 0.019
Origanum majorana L.		
Water Ext	208.64 ± 6.26	0.209 ± 0.006
MeOH Ext	133.71 ± 4.01	0.134 ± 0.004
BuOH Ext	235.89 ± 7.08	0.236 ± 0.007
AgO NPs	126.95 ± 3.81	0.127 ± 0.004
ZnO NPs	151.73 ± 4.55	0.152 ± 0.005
Diclofenac	620.82 ± 18.63	0.621 ± 0.019

The IC_{50} values presented in Table 9 afford a rigorous, quantitative comparison of the anti-inflammatory efficacy of *Cotula cinerea* and *Origanum majorana* L. extracts, their corresponding silver oxide (AgO) and zinc oxide (ZnO) nanoparticles, and the reference drug diclofenac. In this context, lower IC_{50} values denote greater inhibitory potency against heat-induced bovine serum albumin (BSA) denaturation, a surrogate marker for anti-inflammatory activity (Sobhy et al., 2025).

For *Cotula cinerea*, the methanolic extract exhibited the greatest bioactivity, with an IC_{50} of 130.29 ± 3.91 µg/mL, closely followed by the aqueous fraction at 145.31 ± 4.36 µg/mL. The butanolic extract (174.60 ± 5.24 µg/mL) and the AgO nanoparticle formulation (173.93 ± 5.22 µg/mL) demonstrated moderate efficacy, whereas the ZnO nanoparticles were the least potent (189.03 ± 5.67 µg/mL). Notably, all *C. cinerea* preparations surpassed the performance of

diclofenac (IC_{50} = 620.82 ± 18.63 µg/mL), indicating a superior capacity of plant-derived phytochemicals to stabilize protein structures under inflammatory conditions.

In the case of *Origanum majorana* L., the AgO nanoparticles achieved the highest potency (IC_{50} = 126.95 ± 3.81 µg/mL), marginally outperforming the methanolic extract (IC_{50} = 133.71 ± 4.01 µg/mL). The aqueous extract (208.64 ± 6.26 µg/mL) and the ZnO nanoparticles (151.73 ± 4.55 µg/mL) displayed intermediate inhibition, whereas the butanolic extract was comparatively less effective (235.89 ± 7.08 µg/mL). Similar to *C. cinerea*, all *O. majorana* formulations markedly exceeded diclofenac in anti-inflammatory potency.

These findings underscore two principal conclusions: (1) methanol facilitates the extraction of highly active anti-inflammatory constituents, and (2) green-synthesized AgO nanoparticles can preserve or enhance the bioactivity of their parent extracts, albeit with variable efficacy relative to the bulk phytochemicals. The substantially lower IC_{50} values of these botanical extracts and nanoparticle formulations, as compared to diclofenac, highlight their promise as alternative or adjunctive natural anti-inflammatory age (Okpala et al., 2025).

14.3. Antioxidant Activity Assessed by the DPPH Radical Scavenging Assay

To assess the antioxidant capacity of the tested extracts and nanoparticle formulations, the DPPH radical scavenging assay was performed over a concentration range of 1.56–100 µg/mL. The percentage inhibition values obtained at each concentration are summarized in the following Tables 15 and 16 and were used to generate exponential inhibition curves and determine IC_{50} values.

Table 15. DPPH radical scavenging activity (%) of *Cotula cinerea* extracts, nanoparticle formulations, and α-tocopherol across tested concentrations (mean ± SD, *n* = 3)

Concentration (µg/mL)	Water EXT	MeOH EXT	BuOH EXT	AgO NPs	ZnO NPs	α-Tocopherol
100	59.06 ± 1.77	79.69 ± 2.39	63.81 ± 1.91	63.82 ± 1.91	62.99 ± 1.89	79.27 ± 2.38
50	53.57 ± 1.61	69.68 ± 2.09	59.09 ± 1.77	54.53 ± 1.64	53.53 ± 1.61	70.11 ± 2.10
25	50.32 ± 1.51	60.98 ± 1.83	55.58 ± 1.67	46.73 ± 1.40	45.60 ± 1.37	59.76 ± 1.79
12.5	47.30 ± 1.42	51.84 ± 1.55	47.99 ± 1.44	35.55 ± 1.07	34.26 ± 1.03	49.63 ± 1.49
6.25	44.48 ± 1.33	42.86 ± 1.29	41.19 ± 1.24	27.82 ± 0.84	26.43 ± 0.79	38.18 ± 1.14
3.125	41.79 ± 1.25	40.25 ± 1.21	38.94 ± 1.17	25.12 ± 0.76	23.70 ± 0.71	33.98 ± 1.02
1.56	38.10 ± 1.14	38.20 ± 1.15	36.70 ± 1.10	22.62 ± 0.69	21.17 ± 0.64	25.28 ± 0.76

The DPPH radical scavenging activity results of *Cotula cinerea* extracts, nanoparticles, and the reference antioxidant α-tocopherol reveal significant differences in their antioxidant capacities across the tested concentration range (1.56–100 µg/mL) (You et al., 2025). Among

the extracts, the methanolic extract exhibited the highest activity, reaching 79.69% inhibition at the highest concentration, closely approaching the activity of α-tocopherol (79.27%). The butanolic and aqueous extracts also showed notable antioxidant effects, though to a lesser extent. Both AgO and ZnO nanoparticles demonstrated moderate scavenging capacity, with maximum inhibitions of 63.82% and 62.99%, respectively, at 100 µg/mL—indicating some retention of bioactivity in the nanoformulations but not exceeding that of the crude methanol extract. A clear dose-dependent trend was observed for all samples, confirming the concentration-dependent nature of DPPH radical neutralization (CA et al., 2025). These findings underscore the strong antioxidant potential of the methanolic extract of *C. cinerea*, likely due to its higher content of phenolic or flavonoid compounds, and suggest that while nanoparticle formulations are effective, they may exhibit reduced efficacy compared to the crude extract (Puspadewi et al., 2025).

Table 16. DPPH Radical Scavenging Activity (%) of *Origanum majorana* Extracts, Nanoparticles, and α-Tocopherol at Various Concentrations (µg/mL) (mean ± SD, n = 3)

Concentration (µg/mL)	Water EXT	MeOH EXT	BuOH EXT	AgO NPs	ZnO NPs	α-Tocopherol
100	66.77 ± 2.00	82.32 ± 2.47	77.20 ± 2.32	76.55 ± 2.30	57.81 ± 1.73	79.27 ± 2.38
50	60.79 ± 1.82	74.51 ± 2.24	65.89 ± 1.98	65.06 ± 1.95	46.98 ± 1.41	70.11 ± 2.10
25	51.12 ± 1.53	64.63 ± 1.94	56.01 ± 1.68	55.11 ± 1.65	37.88 ± 1.14	59.76 ± 1.79
12.5	40.76 ± 1.22	49.57 ± 1.49	45.61 ± 1.37	44.70 ± 1.34	24.84 ± 0.75	49.63 ± 1.49
6.25	35.88 ± 1.08	44.76 ± 1.34	35.34 ± 1.06	34.51 ± 1.04	15.83 ± 0.48	38.18 ± 1.14
3.125	31.88 ± 0.96	39.58 ± 1.19	32.35 ± 0.97	31.56 ± 0.95	12.69 ± 0.38	33.98 ± 1.02
1.56	24.31 ± 0.73	31.77 ± 0.95	31.78 ± 0.93	28.63 ± 0.86	9.77 ± 0.29	25.28 ± 0.76

The data in Table 16 demonstrate a clear, concentration-dependent increase in DPPH radical scavenging activity for all *Origanum majorana* L. formulations and the reference antioxidant α-tocopherol. At 100 µg/mL, the methanolic extract exhibited the highest activity (82.32 ± 2.47 %), closely followed by α-tocopherol (79.27 ± 2.38 %) and the butanolic extract (77.20 ± 2.32 %). The aqueous extract achieved moderate inhibition (66.77 ± 2.00 %), whereas the AgO and ZnO nanoparticles displayed intermediate (76.55 ± 2.30 %) and lower (57.81 ± 1.73 %) activities, respectively.

Across the concentration range, methanolic and butanolic extracts maintained strong antioxidant effects even at lower doses—for instance, at 1.56 µg/mL, they still inhibited 31.78 ± 0.93 % and 31.77 ± 0.95 % of DPPH radicals, respectively—whereas α-tocopherol's activity declined to 25.28 ± 0.76 %. Nanoparticle formulations exhibited more pronounced decreases at

low concentrations, indicating that while nanoencapsulation preserves much of the extract's bioactivity at higher doses, it may limit radical access at trace levels (Ashraf et al., 2025).

Exponential regression was applied to the DPPH inhibition data to model the concentration–response relationship and facilitate IC_{50} determination. Figure 30 and 31 presents the fitted curves for each *Cotula cinerea* and *Origanum majorana* formulation, depicting radical scavenging efficiency across the tested concentration range.

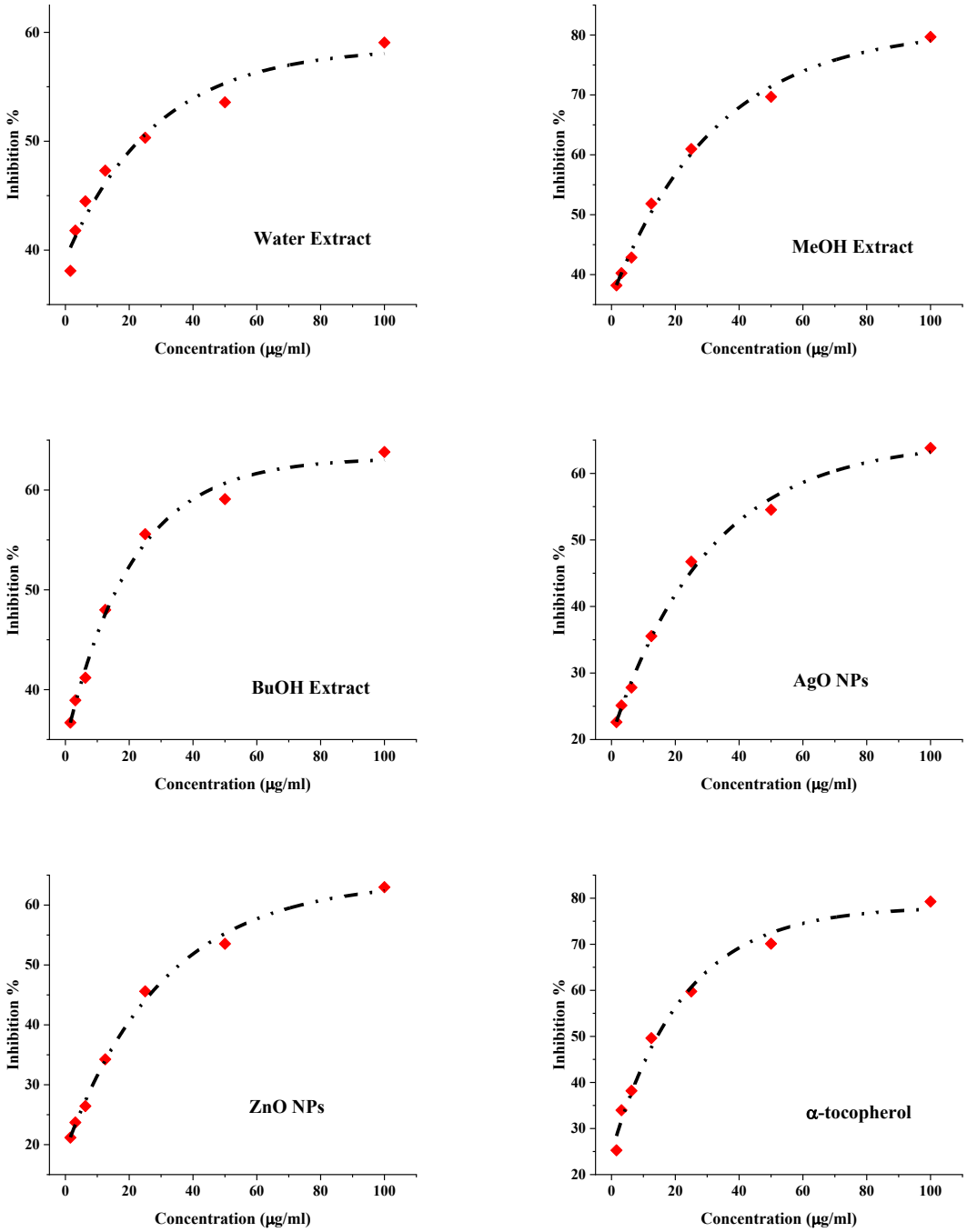

Figure 30. Exponential dose–response curves showing DPPH activity inhibition (%) of *Cotula cinerea* extracts (Water, MeOH, BuOH) and their corresponding nanoparticles (AgO NPs, ZnO NPs) across a range of concentrations

The exponential regression curves for *Cotula cinerea* DPPH inhibition reveal a rapid initial increase in radical scavenging activity for the methanolic and butanolic extracts, each achieving near-maximal I% at moderate concentrations. This steep rise indicates high potency and efficient radical neutralization (M. A. Kumar et al., 2025). The aqueous extract follows a similar trend but plateaus at a lower maximum, reflecting its comparatively reduced but still significant antioxidant capacity. Both AgO and ZnO nanoparticles demonstrate more gradual slopes, suggesting that while nanoformulation retains bioactivity, it moderates the kinetics of radical interaction—likely due to controlled release of active phytochemicals (Khalid et al., 2025).

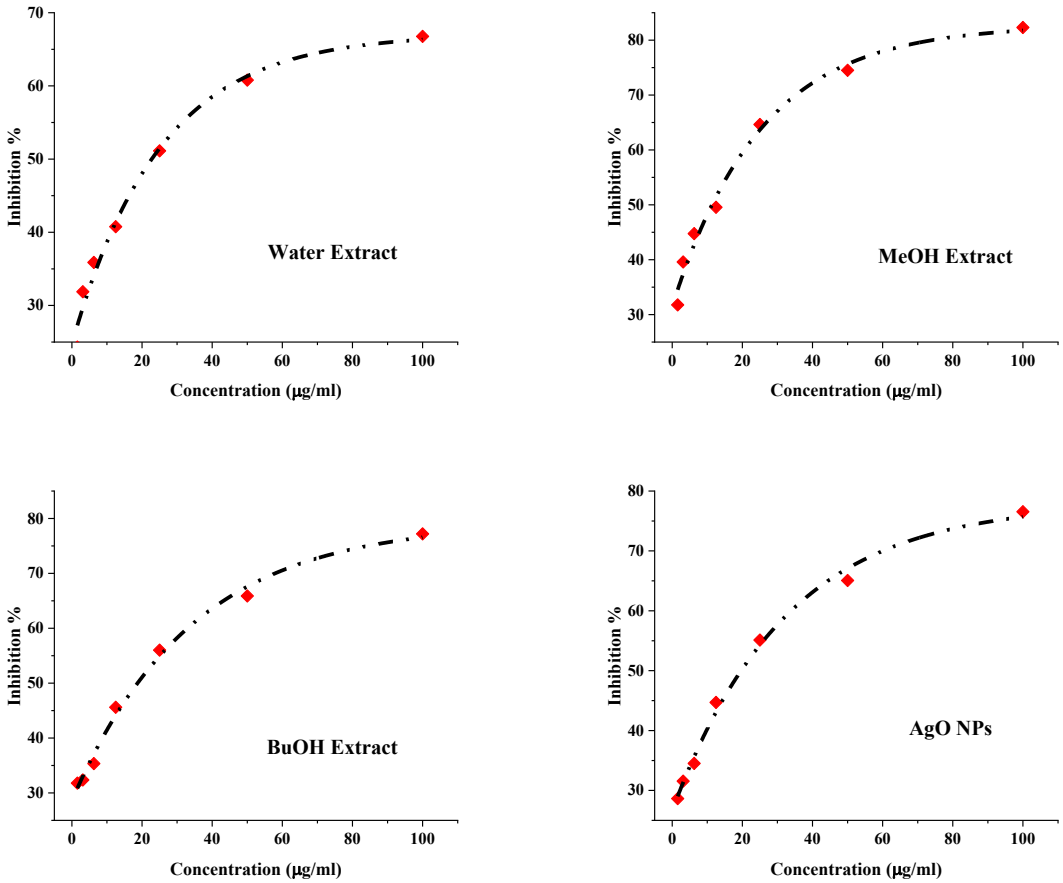

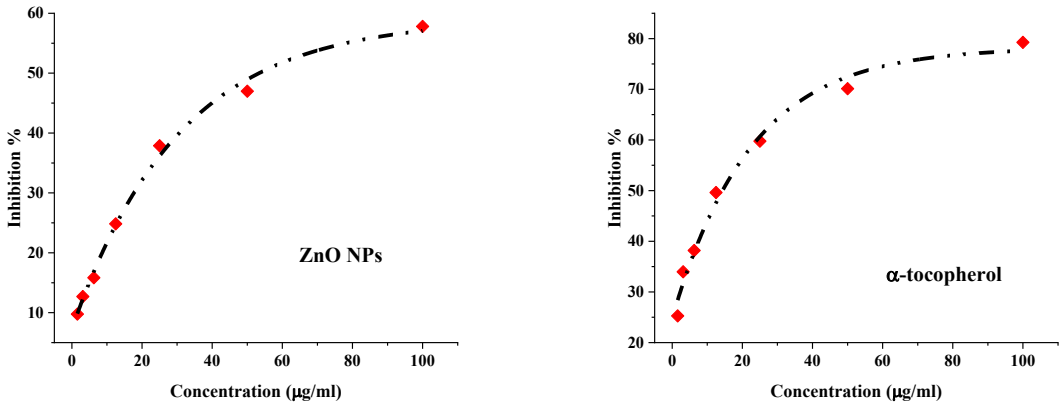

Figure 31. Exponential dose–response curves showing DPPH activity inhibition (%) of *Origanum majorana* L. extracts (Water, MeOH, BuOH) and their corresponding nanoparticles (AgO NPs, ZnO NPs) across a range of concentrations

For *Origanum majorana* L., the exponential curves illustrate that the methanolic extract attains high I% at lower concentrations than the butanolic and aqueous fractions, indicating superior antioxidant constituents. The butanolic extract also shows strong activity but requires slightly higher concentrations to approach the same I%. Silver oxide nanoparticles exhibit a profile closely mirroring the butanolic extract, while zinc oxide nanoparticles present a flatter curve, denoting lower potency. Overall, the fits underscore the elevated efficacy of semi-polar extracts in radical scavenging and highlight the differential release dynamics conferred by nanoparticle encapsulation (Kawee-ai, 2025).

The IC_{50} values reported in Table 17 provide a rigorous quantitative comparison of the free radical scavenging efficacy of *Cotula cinerea* and *Origanum majorana* L. extracts, their nanoparticulate formulations, and the standard antioxidant α-tocopherol. Lower IC_{50} values denote greater antioxidant potency.

Table 17. IC_{50} values for DPPH radical scavenging by *Cotula cinerea* and *Origanum majorana* L. extracts, nanoparticles, and α-tocopherol (mean ± SD, n = 3)

Plant / Sample	**IC_{50} (µg/mL) ± SD**	**IC_{50} (mg/mL) ± SD**
	Cotula cinerea	
Water Ext	22.93 ± 0.69	0.023 ± 0.001
MeOH Ext	12.03 ± 0.36	0.012 ± 0.0004
BuOH Ext	15.98 ± 0.48	0.016 ± 0.0005
AgO NPs	33.45 ± 1.00	0.033 ± 0.001
ZnO NPs	35.72 ± 1.07	0.036 ± 0.001

α-Tocopherol	14.34 ± 0.43	0.014 ± 0.0004
Origanum majorana L.		
Water Ext	13.14 ± 0.39	0.013 ± 0.0004
MeOH Ext	11.35 ± 0.34	0.011 ± 0.0003
BuOH Ext	12.59 ± 0.38	0.013 ± 0.0004
AgO NPs	19.63 ± 0.59	0.020 ± 0.001
ZnO NPs	21.02 ± 0.63	0.021 ± 0.001
α-Tocopherol	14.34 ± 0.43	0.014 ± 0.0004

For *C. cinerea*, the methanolic extract exhibited the most pronounced activity, achieving an IC_{50} of 12.03 ± 0.36 µg/mL, outperforming α-tocopherol (14.34 ± 0.43 µg/mL). The butanolic and aqueous extracts displayed moderate efficacy with IC_{50} values of 15.98 ± 0.48 µg/mL and 22.93 ± 0.69 µg/mL, respectively. In contrast, the AgO and ZnO nanoparticle formulations demonstrated diminished activity—IC_{50} = 33.45 ± 1.00 µg/mL and 35.72 ± 1.07 µg/mL, respectively—suggesting that while nanoencapsulation preserves bioactivity, it may modulate the accessibility or release kinetics of the active phytochemicals.

In the case of *O. majorana* L., all crude extracts surpassed the benchmark α-tocopherol, with methanolic extract yielding the lowest IC_{50} (11.35 ± 0.34 µg/mL), followed by butanolic (12.59 ± 0.38 µg/mL) and aqueous extracts (13.14 ± 0.39 µg/mL). Nanoparticulate silver and zinc oxide derivatives exhibited reduced but still significant radical scavenging, with IC_{50} values of 19.63 ± 0.59 µg/mL and 21.02 ± 0.63 µg/mL, respectively. These findings indicate that methanol effectively solubilizes key antioxidant constituents, while green-synthesized nanoparticles afford a viable delivery platform that retains substantial, albeit attenuated, antioxidative performance.

Collectively, these data affirm the superior antioxidant potential of methanolic extracts from both plant species—particularly *O. majorana*—and underscore the relevance of these botanical matrices as sources of natural free radical scavengers (Patel et al., 2025).

15. *In Vivo* Study Results

15.1. Acute toxicity study

The results obtained from this test Table 18 revealed that the methanolic extracts of both *Cotula cinerea* and *Origanum majorana L*, at doses of 2000 mg/kg and 5000 mg/kg, demonstrated no mortality and exhibited normal physiological responses across multiple parameters, including skin color, food and water intakes, urination, salivation, gripping,

alterness, restlessness, and righting reflex, touch response, tremors and convulsion . No toxic or lethal effects were observed in any of the treated groups. The results indicate that administering these doses did not lead to any signs of toxicity or death within the 24-hour observation period. Therefore, it can be inferred that the LD_{50} of the extracts may exceeds 5000 mg/kg

Table 18 Potential toxic effects of the methanolic extract of Cotula cinerea and Origanum majorana L

Parameters	**The methanolic extract of *Cotula cinerea* mg/kg**		**The methanolic extract of *Origanum majorana L* mg/kg**	
Doses	**2000**	**5000**	**2000**	**5000**
Mortality	**None**	**None**	**None**	**None**
Response	**Normal**	**Normal**	**Normal**	**Normal**
Skin color	**Normal**	**Normal**	**Normal**	**Normal**
Food intake	**Normal**	**Normal**	**Normal**	**Normal**
Water intake	**Normal**	**Normal**	**Normal**	**Normal**
Urination	**Normal**	**Normal**	**Normal**	**Normal**
Salivation	**Normal**	**Normal**	**Normal**	**Normal**
Gripping	**Normal**	**Normal**	**Normal**	**Normal**
Alertness	**Normal**	**Normal**	**Normal**	**Normal**
Restlessness	**Normal**	**Normal**	**Normal**	**Normal**
Touch response	**Normal**	**Normal**	**Normal**	**Normal**
Tremors	**Normal**	**Normal**	**Normal**	**Normal**
Convulsion	**Normal**	**Normal**	**Normal**	**Normal**
Righting reflux	**Normal**	**Normal**	**Normal**	**Normal**

(+) Mild, (++) Moderate, (+++) strong presence.

the median lethal dose (LD50 oral) of *Cotula cinerea* and *Origanum majorana L* methanolic extract was greater than 5000 mg/kg bwt. These results suggest that the methanolic extract of *Cotula cinerea* and *Origanum majorana L* may be relatively safe

15.2. Alzaheimers model study results

15.2.1. Behavioural Assessments During Conditioning

Maze test :

In this experimental study, the spontaneous alternation percentage (SAP) test was utilized to evaluate cognitive function across different treatment groups the resulted are mentioned in Figures 32

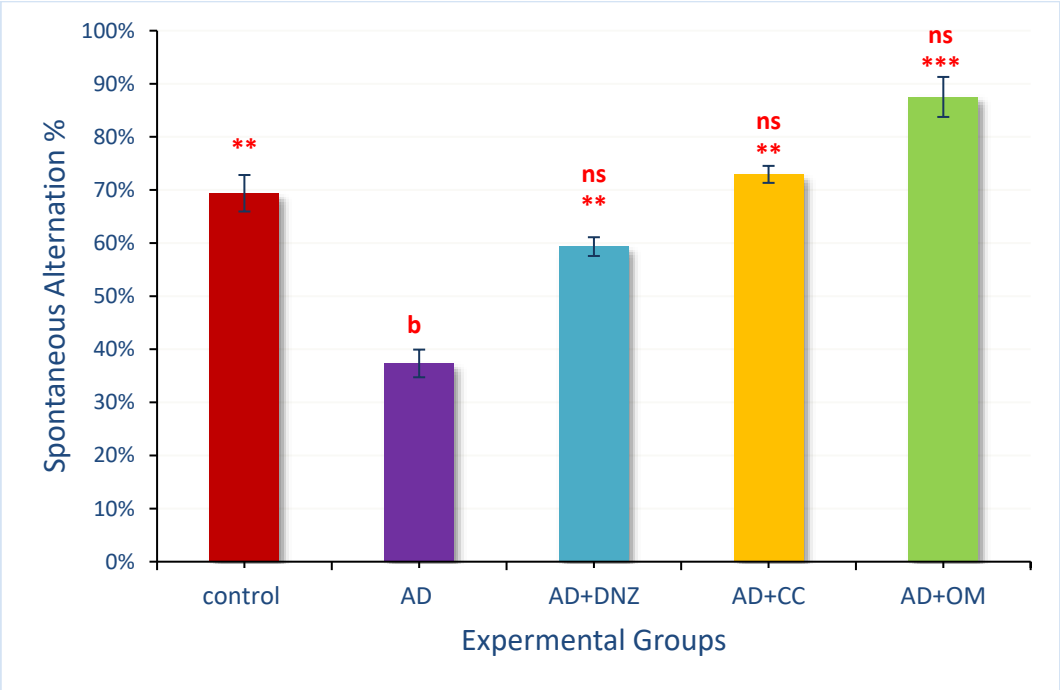

Figure 32 Spontaneous Alternation Percentage Performed by The Experimental Groups.

Control : received no treatment **AD**: Alzheimer's disease model group; **AD+DNZ**: Donepezil treated group; **AD+CC**: *Cotula* methanolic extract treated group; **AD+OM**: *Origanum* methanolic extract treated group. (*) statistical different with AD group: * Significant $p<0.05$; **Very Significant $p<0.01$; ***$p<0.001$ Highly Significant.(a-b-c) statistical different with control group: **a** Significant $p<0.05$; **b** Very Significant $p<0.01$; **c** $p<0.001$ Highly Significant.(ns) non significatif different with control .

In the control group, the Spontaneous Alternation Percentage (SAP) reached an average of 69%, reflecting normal spatial working memory performance and serving as the baseline for cognitive function assessment (wijnen et al.,2024).. In contrast, the Alzheimer's disease (AD) group exhibited a marked impairment, with SAP declining significantly to 36% ($p < 0.01$ vs. control), indicating successful induction of AD-like cognitive deficits, consistent with previous findings (Barros-Viegas et al .,2020).. Following treatment, the AD+Donepezil (DNZ) group demonstrated a moderate recovery, reaching an average SAP of 59%. Although the improvement was not statistically significant compared to the control group ($p > 0.05$), it

showed a clear trend toward cognitive restoration, with a non-significant but suggestive improvement vs. AD ($p = 0.079$), consistent with the known therapeutic action of Donepezil in attenuating cognitive decline. The AD+*Origanum majorana* (OM) group displayed a remarkable enhancement in SAP, reaching the highest value among all groups (94.2%), which was highly significant compared to the AD group ($p < 0.01$) and also significantly greater than both the DNZ and *Cotula*-treated groups. This pronounced effect suggests a robust neuroprotective and cognitive-enhancing potential of *Origanum*, possibly attributable to its rich profile of bioactive compounds with antioxidant and anti-inflammatory properties. Similarly, the AD+*Cotula cinerea* (CC) group showed a substantial recovery, with a mean SAP of 69%, comparable to the control group and significantly higher than the AD group ($p < 0.05$). Though less effective than OM, Cotula treatment still provided a clear benefit over the untreated AD condition, supporting its cognitive restorative capacity

Dark Light Box Test

To assess anxiety-like behavior and fear memory, a modified Dark-Light Box test was used across different experimental groups. The resulting behavioral responses are presented in Figures 33

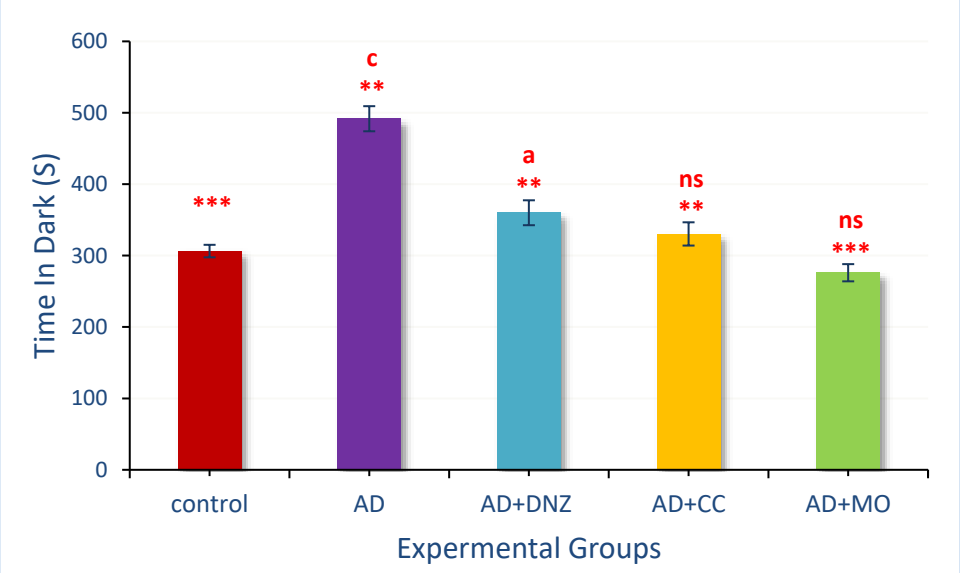

Figure 33 Time Spent in the Dark Compartment by Mice Across Experimental Groups in a Modified Dark-Light Box Test (Fear Memory Model with Cold Water)

Control : received no treatment **AD**: Alzheimer's disease model group; **AD+DNZ**: Donepezil treated group; **AD+CC**: *Cotula* methanolic extract treated group; **AD+OM**: *Origanum* methanolic extract treated group. (*) statistical different with AD group: * Significant p<0.05; **Very Significant p<0.01; ***p<0.001 Highly Significant.(a-b-c) statistical different with control group: **a** Significant p<0.05; **b** Very Significant p<0.01; **c** p<0.001 Highly Significant.(ns) non significatif different with control .

The Control group spent a moderate amount of time in the dark compartment, indicative of preserved fear memory and balanced anxiety responses(ConductScience, n.d.).. This behavior suggests that the animals were capable of recalling the aversive nature of the dark environment, likely associated with previous exposure to a cold stimulus, and responded with appropriate exploratory caution(Bloch & Belzung.,2022)..In contrast, the Alzheimer's disease (AD) model group exhibited a significantly prolonged duration in the dark compartment compared to healthy controls ($p < 0.001$), indicating both a failure to recall the unpleasant stimulus (impaired fear memory) and elevated anxiety-like behavior. This result is consistent with the cognitive and emotional dysfunctions characteristic of AD pathology (Arrant et al.,2013).. Pharmacological intervention with Donepezil (AD+DNZ) led to a statistically significant reduction in dark compartment time relative to the AD group ($p < 0.01$), with a near-significant difference when compared to the control group ($p = 0.051$). These findings suggest partial recovery of memory function and a trend toward normalized anxiety behavior (Bloch & Belzung.,2022). This outcome aligns with the known mechanism of Donepezil as a cholinesterase inhibitor, enhancing cholinergic neurotransmission and modulating emotional responses. Furthermore, treatment with *Origanum majorana* (OM) and *Cotula cinerea* (CC) extracts resulted in a pronounced decrease in time spent in the dark compartment, reflecting significant improvement in both memory retention and anxiolytic behavior(Arrant et al.,2013). Notably, no significant differences were observed between these treatment groups and the control group, while both treatments showed substantial improvement relative to the AD group ($p < 0.01$ and $p < 0.001$, respectively).Collectively, these behavioral outcomes highlight the therapeutic potential of *O. majorana* and *C. cinerea* in reversing neurobehavioral impairments induced by the AD model. The observed effects are likely attributable to the compounds' capacity to counteract neurotoxicity triggered by aluminum chloride ($AlCl_3$) and the pro-aging effects of D-galactose, two key elements used to induce Alzheimer-like pathology in this study model(Takao & Miyakawa.,2006)(Bailey & Crawley.,2011).

In order to assess anxiety-like behavior and fear memory alterations in the Alzheimer's disease (AD) model, a modified Dark/Light Box paradigm was applied, incorporating an aversive cold stimulus into the dark compartment. The behavioral outcomes presented below in table 19 reflect the degree of anxiety and memory performance across the different experimental groups.

Table 19 Behavioral Characterization of Experimental Groups in the Dark-Light Box test.

Group	Discovery	Back to Darkness	Stability in the middle	Transition
Control	+ + +	+	+ +	+ +
AD	+	-	-	+ + +
AD+DNZ	+ +	+	+	+ +
AD+*Cotula cinerea*	+ + +	+	+ +	+ +
AD+*Origanum majorana*	+ + +	+	+ +	+ + +

(–) Absent, (+) Mild, (++) Moderate, (+++) strong presence

Behavioral assessments across four core categories—Exploration (Discovery), Retention in the Dark Zone (Back to Darkness), Stability in the Central Zone, and Transition —revealed distinct intergroup differences, providing valuable insight into the cognitive and emotional states of the animals under experimental conditions.

The control group demonstrated robust exploratory behavior, minimal return to the dark compartment, and moderate, balanced transitions between light and dark zones. These patterns are indicative of low anxiety levels and preserved cognitive flexibility (Arrant et al.,2013. In contrast, the AD group exhibited markedly diminished exploration, a pronounced preference for the dark chamber, complete instability in the central zone, and excessive, disorganized transitions. Such behavioral disruptions align with the heightened anxiety and cognitive deficits typically observed in Alzheimer's disease models (Temnik et al.,2025) (Takao & Miyakawa.,2006).. Animals in the AD + Donepezil group showed moderate improvements, with increased exploratory activity, reduced return-to-dark behavior, and some ability to maintain presence in the central zone. Transition behavior was more regulated than in the untreated AD group, reflecting a partial improvement in anxiety regulation and spatial memory, likely attributable to Donepezil's acetylcholinesterase inhibitory effects (Metzenauer et al.,1992) (Bailey & Crawley.,2011). Notably, animals treated with *Cotula cinerea* and *Origanum majorana* displayed behavioral profiles that closely approximated those of the healthy control group. These groups demonstrated strong exploratory tendencies, a reduced tendency to remain in the dark zone, and improved central zone stability, suggestive of reduced anxiety and improved fear-related memory. Among these, the *Origanum majorana*-treated group exhibited slightly more favorable transition dynamics compared to *Cotula cinerea*, indicating a potentially enhanced capacity for adaptive behavioral responses and environmental processing.

Open Field Test :

The data obtained from the open field test, as presented in the Figures 34 and table 20, the figure demonstrate significant variability in the time spent in both the outer and inner zones .and the table provides a comparative overview of behavioral patterns across the five groups, allowing for the identification of anxiety-related tendencies .

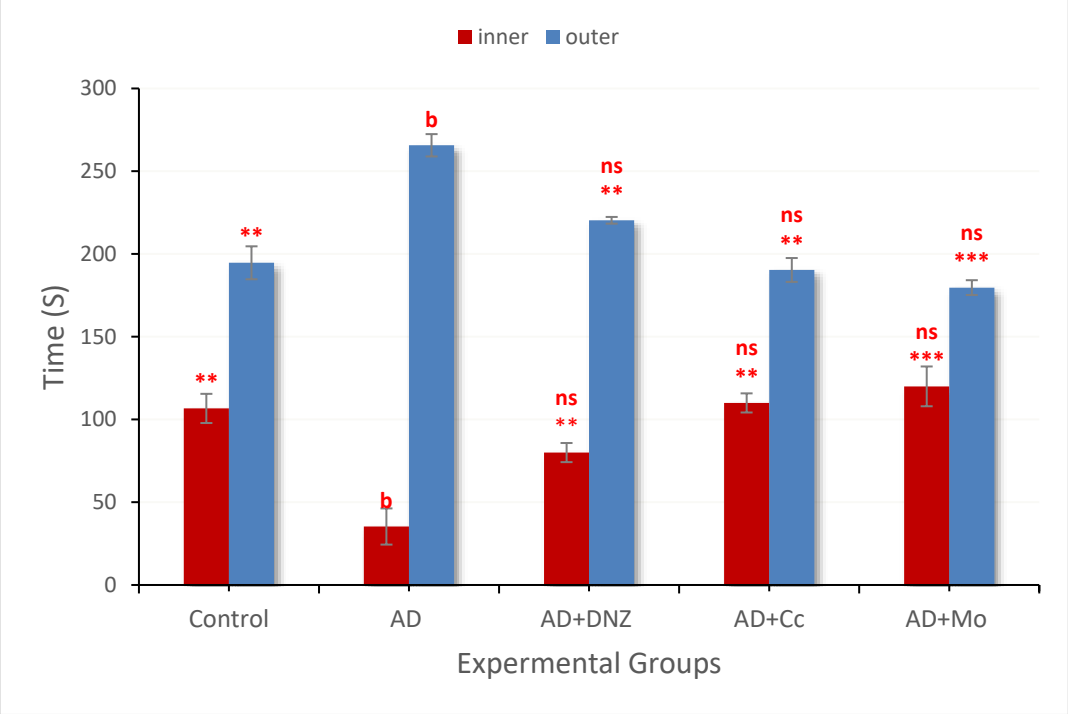

Figure 34 Time Spent in Outer and Inner Zones During the Open Field Test Across Experimental Groups

Control : received no treatment **AD**: Alzheimer's disease model group; **AD+DNZ**: Donepezil treated group; **AD+CC**: *Cotula* methanolic extract treated group; **AD+OM**: *Origanum* methanolic extract treated group. (*) statistical different with AD group: * Significant p<0.05; **Very Significant p<0.01; ***p<0.001 Highly Significant.(a-b-c) statistical different with control group: **a** Significant p<0.05; **b** Very Significant p<0.01; **c** p<0.001 Highly Significant.(ns) non significatif different with control .

The control group exhibited typical exploratory behavior, characterized by a balanced distribution of time between the inner and outer zones of the open field, thereby serving as a baseline for normal anxiety levels. In contrast, the AD group demonstrated a highly significant deviation from the control group ($p < 0.01$), marked by a pronounced reduction in inner zone time and a corresponding increase in peripheral zone activity. This behavioral pattern is indicative of severe anxiety-like symptoms, commonly associated with Alzheimer's pathology (Prut & Belzung.2003).Treatment with Donepezil (AD+DNZ) resulted in a significant reduction in anxiety-like behavior compared to the AD group ($p < 0.01$), with behavioral metrics approaching those observed in the control group (Fitzgerald et al.,2020). Similarly,

administration of *Cotula cinerea* (AD+CC) led to a complete restoration of exploratory behavior, showing no significant difference from the control group and a statistically significant improvement compared to the AD group ($p < 0.01$).Notably, *Origanum majorana* (AD+Mo) produced the strongest anxiolytic effect, evidenced by a highly significant increase in inner zone exploration relative to the AD group ($p < 0.001$) and a behavioral profile indistinguishable from that of healthy controls. This marked improvement underscores the potential of *Origanum majorana* as a potent anxiolytic agent in the context of Alzheimer's-related anxiety.

Table 20 Behavioral Analysis in Open Field Test: Comparative Assessment Across Experimental Groups.

Behaviors	Control	AD	AD+DNZ	AD+Cotula	AD+Majorana
Grooming (Stafstrom,2006)	+	+++	+	+	+
Olfactory exploration (Seibenhener & Wooten,2015)	+ + +	+	+ +	+ + +	+ + +
Exploratory behaviour (Seibenhener & Wooten,2015)	+ + +	+	+ + +	+ + +	+ + +
Defecation/urination (Seibenhener & Wooten,2015)	+	+++	+ +	+	+
Unsupported rearing (Sturman et al.,2018)	+ +	+	+ +	+ + +	+ + +
Rearing with wall support (Sturman et al.,2018)	+ + +	-	+ +	+ +	+ + +

The control group exhibited a rich spectrum of normal exploratory and emotional behaviors, including frequent grooming, olfactory exploration, rearing (with and without wall support), and minimal defecation/urination—all indicative of low anxiety and high cognitive integrity. In stark contrast, the AD group displayed a marked reduction in adaptive behaviors. Grooming, exploratory activity, and both types of rearing were substantially diminished, while defecation/urination frequency increased—a classical sign of elevated stress or anxiety. Treatment with Donepezil (AD+DNZ) partially ameliorated these effects. While exploratory

behaviors (olfactory exploration and unsupported rearing) were moderately restored, grooming and stress-related responses remained somewhat dysregulated. More promising results were observed with Cotula cinerea and Origanum majorana first (AD+CC) showed full restoration of olfactory exploration and rearing behaviors, with reduced stress markers (defecation/urination). Exploratory and emotional behaviors closely resembled the control group, echoing the earlier result that Cotula fully restored normal behavior in the open field.Second (AD+OM) demonstrated the most robust behavioral recovery, including strong re-engagement in grooming, olfactory investigation, and rearing with wall support. Defecation/urination was minimal, indicating low anxiety levels. These outcomes support the open field data showing a highly significant improvement over AD ($p < 0.001$) and no statistical difference from control animals.

Novel object recogenition :

The figure Figures 35 shows the outcome results of the novel object test, where the discrimination and recognition indices are calculated and presented respectively across the groups to assess the integrity of recognition memory and object-related cognitive function. These indices serve as reliable behavioral markers for evaluating memory performance, with higher values indicating intact memory and preference for novel stimuli, while lower or negative values suggest cognitive impairment or altered memory processing.).(Belo et al.,2020)(Bekci et al.,2024)

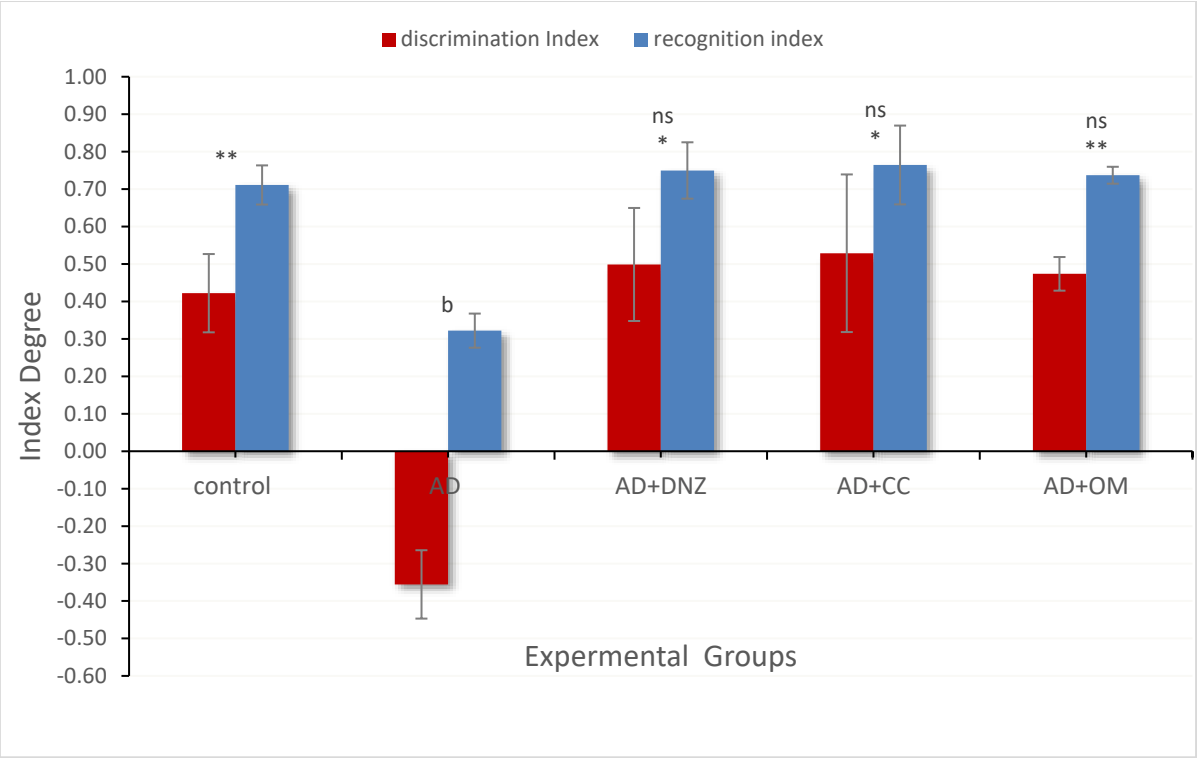

Figure 35 Discrimination Index in the Novel Object Recognition Test Across Experimental Groups

Control : received no treatment **AD**: Alzheimer's disease model group; **AD+DNZ**: Donepezil treated group; **AD+CC**: *Cotula* methanolic extract treated group; **AD+OM**: *Origanum* methanolic extract treated group. (*) statistical different with AD group: * Significant p<0.05; **Very Significant p<0.01; ***p<0.001 Highly Significant.(a-b-c) statistical different with control group: **a** Significant p<0.05; **b** Very Significant p<0.01; **c** p<0.001 Highly Significant.(ns) non significatif different with control

Behavioral performance in the Novel Object Recognition (NOR) test, assessed through both the Discrimination Index (DI) and the Recognition Index (RI), revealed consistent evidence of recognition memory impairment in the Alzheimer's disease (AD) model group and the therapeutic efficacy of various treatments. The AD group exhibited a significantly negative DI value (–0.356), indicating an abnormal preference for the familiar object an outcome reflective of impaired recognition memory and attributed to $AlCl_3$ and D-galactose-induced neurotoxicity in memory-related brain regions. This finding was further supported by the significantly reduced RI in the AD group (0.322; $p < 0.01$ vs. control), reflecting a profound decline in cognitive function. In contrast, the control group demonstrated high and positive values in both indices (DI = 0.422; RI = 0.711), indicating intact recognition memory and a clear preference for the novel object. Treatment with Donepezil and the plant extracts—*Cotula cinerea* and *Origanum majorana* resulted in marked improvements in both DI and RI. The Donepezil-treated group (AD+DNZ) showed a DI of 0.499 and an RI of 0.750, significantly different from

the AD group ($p < 0.05$), and statistically comparable to the control. Similarly, the CC-treated group (AD+CC) exhibited the highest DI (0.529) and RI (0.764) among all groups, suggesting a strong restorative effect on memory function. The OM group (AD+OM) also showed notable improvements, with a DI of 0.474 and RI of 0.737, both significantly elevated compared to AD ($p < 0.05$), and approaching control levels. While the average performance of the CC group was slightly superior, the OM group demonstrated more consistent responses, as indicated by lower variability observed in the standard error of the mean. These findings collectively support the neuroprotective potential of *Cotula cinerea* and *Origanum majorana* in mitigating AD-like cognitive impairments, effectively reversing $AlCl_3$ and D-galactose-induced recognition memory deficits to values comparable to those observed in control and Donepezil-treated animals

15.2.2. Biochemical Analysis of blood samples and organs :

1. Organ Weight Index

The administration of aluminum chloride ($AlCl_3$) and D-galactose led to a notable increase in organ weight indices, particularly in the kidneys (0.28±0.03%, $p<0.05$) and brain (0.85±0.05%, $p<0.05$) compared to the control group, indicating possible organomegaly and neuroinflammation associated with $AlCl_3$/D-gal -induced toxicity. Donepezil treatment in $AlCl_3$/D-gal intoxicated rats slightly attenuated this effect, though the reductions in kidney and brain weights remained statistically non-significant compared to the $AlCl_3$ group. Interestingly, treatment with *Cotula cinerea* significantly restored brain and kidney weights closer to control values (0.68±0.02%, $p<0.01$ for brain; 0.23±0.01%, $p<0.05$ for kidney), while *Origanum majorana* demonstrated a near-complete normalization of organ weight indices, with brain and kidney indices statistically indistinguishable from the control group (0.60±0.03%, $p<0.001$; 0.22±0.01%, $p<0.05$, respectively). These results suggest that both plant extracts, particularly *O. majorana*, exerted a protective effect against $AlCl_3$/D-gal -induced organ changes.

Table 21 Organ weight Index of different experimental groups

	Organ Weight Index %		
	Liver	**Kidneys**	**Brain**
Control	2.1±0.31	0.22±0.01	0.61±0.08
AD	2.7±0.31 ^{NS}	0.28±0.03^{a}	0.85±0.05 $^{a\ NS}$

AD + DNZ	2.5 ±0.16 NS*	0.26±0.02 a NS	0.81±0.03 a NS
AD + Cotula	1.96±0.12 N*	0.23±0.01 NS*	0.68±0.02 NS**
AD + Majorana	2.13±0.17 NS*	0.22±0.01 NS*	0.60±0.03 NS***

NS: Non-significant differences; Comparison with the control group: $p < 0.05$ (a), $p < 0.01$ (b), $p < 0.001$ (c); Comparison with AD group: $p < 0.05$ (*), $p < 0.01$ (**), $p < 0.001$ (***)

2. Hematological parameters

$AlCl_3$/D-gal exposure induced marked hematological alterations, characterized by significant elevations in WBC ($8.5\pm0.6\times10^9$/L, $p<0.001$), lymphocytes ($6.06\pm0.32\times10^9$/L, $p<0.05$), granulocytes ($3.7\pm0.3\times10^9$/L, $p<0.001$), RBCs ($8.23\pm0.51\times10^{12}$/L, $p<0.01$), and platelet count ($1081\pm34.4\times10^9$/L, $p<0.05$), suggesting an inflammatory and hematopoietic response to aluminum neurotoxicity. Donepezil treatment slightly moderated these changes, though most parameters remained elevated in comparison with control parameter's. In contrast, treatment with *C. cinerea* or *O. majorana* significantly ameliorated hematological disruptions, with both extracts normalizing WBC, LYM, and GRA counts (all $p<0.01$ to $p<0.001$ vs. $AlCl_3$ group .Of note, the WBC count in the O. majorana group approached control levels without a statistically significant difference between them and partially restoring RBC and PLT levels ($p<0.05$ to $p<0.001$) , However *C. cinerea* demonstrated superior efficacy in improving PLT counts compared to *O. majorana*, suggesting a more potent thrombopoietic effect . These findings underline the anti-inflammatory and immunomodulatory potential of both plant treatments in counteracting $AlCl_3$/D-gal -induced systemic effects.

Table 22 Plasma concentration of hematological parameters of different experimental groups

	WBC($\times10^9$/L)	LYM($\times10^9$/L)	GRA($\times10^9$/L)	HGB (g/dL)	RBC($\times10^{12}$/L)	PLT ($\times10^9$/L)
Control	6.7±0.27	4.2±0.14	2.1±0.2	15.1±0.15	6.52±0.31	823±10.5
AD	8.5±0.6 c	6.06±0.32a	3.7±0.3 c	15.5±0.03 NS	8.23±0.51b	1081±34.4 a
AD + DNZ	9.56±0.54 c	7.2±0.22 a *	3.1±0.5 a *	15.3±0.32 NS	7.87±0.22 a NS	970±29.2 a*
AD + Cotula	5.8±0.14 NS***	3.5±0.5 NS**	2.3±0.3 NS**	15.3±0.45 NS	6.7±0.43 NS*	872±12.8 NS***
AD + Majorana	6.7±0.3 NS***	3.6±0.4 NS**	2.1±0.2 NS***	15.1±0.26 NS	7.2±0.41 NS*	901±44.6 b***

NS: Non-significant differences; Comparison with the control group: $p < 0.05$ (a), $p < 0.01$ (b), $p < 0.001$ (c); Comparison with BTU group: $p < 0.05$ (*), $p < 0.01$ (**), $p < 0.001$ (***)

3. Biochemical parameters

$AlCl_3$/D-gal exposure led to profound disruptions in biochemical markers, as evidenced by increased fasting blood glucose (0.92±0.04 g/L, $p<0.05$), liver enzymes

(AST: 169±7.8 U/L and ALT: 133±4.5 U/L, both $p<0.001$), urea (0.87±0.4 g/L, $p<0.01$), creatinine (13.5±0.1 mg/L, $p<0.01$), and C-reactive protein (CRP: 12.2±0.7 mg/L, $p<0.01$), indicating hepatotoxicity, nephrotoxicity, and systemic inflammation. Donepezil partially reduced AST, urea, and CRP levels, but ALT remained elevated indicating donepezil did not effectively reverse liver damage.. In contrast, *C. cinerea* and *O. majorana* treatments effectively normalized most biochemical parameters; notably, *C. cinerea* drastically lowered ALT to 24±3.2 U/L even below those of the control group. This suggests a potent hepatoprotective effect, likely involving membrane stabilization or enhanced antioxidant defense ($p<0.001$ vs. $AlCl_3$and Control), conversely, Origanum majorana restored ALT values ($p<0.001$ vs. $AlCl_3$)to levels that were statistically non-significant from the control, indicating a balanced normalization of liver function without oversuppression. Together, these findings highlight the hepatoprotective capacity of those plants, with C. cinerea potentially exerting a stronger or more regulatory effect, while O. majorana maintained liver enzyme levels within the physiological range. and both extracts restored CRP and creatinine levels near control values (all $p<0.01$ vs. $AlCl_3$). These results highlight the hepatoprotective, nephroprotective, and anti-inflammatory effects of the tested plant extracts in mitigating $AlCl_3$-induced biochemical alterations.

Table 23 Glycemia, CRP, liver and kidneys function parameters of different experimental groups

	FBS (g/L)	AST (U/L)	ALT (U/L)	Urea (g/L)	CT (mg/L)	CRP (mg/L)
Control	0.71±0.03	99±4.1	66±3.4	0.42±0.6	9.5±1.2	3.6±1.16
AD	0.92±0.04 ^{a}	169±7.8 ^{c}	133±4.5^{c}	0.87±0.4^{b}	13.5±0.1^{b}	12.2±0.7^{b}
AD + DNZ	0.80±0.01 ^{a*}	132±3.8 ^{b*}	144±8.3$^{c\ NS}$	0.67±0.7 ^{a*}	15.5±0.6 ^{c*}	3.9±0.6 ^{NS*}
AD + Cotula	0.73±0.03^{NS*}	99±6.3^{NS***}	24±3.2 ^{c***}	0.40±0.2 ^{NS**}	10.5±0.2 ^{NS**}	3.5±0.1 ^{NS**}
AD+Majorana	0.71±0.03 ^{NS*}	105±6.3 ^{NS**}	64±9.7 ^{NS***}	0.44±0.3 ^{NS**}	10±0.3 ^{NS**}	3.4±0.2 ^{NS**}

NS: Non-significant differences; Comparison with the control group: $p < 0.05$ (a), $p < 0.01$ (b), $p < 0.001$ (c); Comparison with AD group: $p < 0.05$ (*), $p < 0.01$ (**), $p < 0.001$ (***)

4. Oxidative stress parameters

A) Brain oxidative stress parameters

Alzheimer's disease (AD) is characterized by heightened oxidative stress and neuroinflammation, both of which are central in aluminum chloride ($AlCl_3$/D-gal)-induced neurotoxicity models(Chen et al.,2021).. In this study, AD induced rats showed significant oxidative stress, evidenced by a marked increase in malondialdehyde (MDA: 12.1±0.46 nmol/mg pr, $p<0.05$), a lipid peroxidation marker, along with significant

reductions in key antioxidant defenses: glutathione (GSH: 4.4±0.56 nmol/mg pr, $p<0.001$), superoxide dismutase (SOD: 5.3±0.17 U/mg pr, $p<0.01$), and catalase (CAT: 4.1±0.2 UI/min/g pr, $p<0.01$). These findings are consistent with previous studies that associate oxidative imbalance and impaired enzymatic activity with AD pathophysiology and aluminum and galactose neurotoxicity(Haider et al.,2020) While Donepezil partially improved oxidative markers MDA and enzymatic activity of SOD, its effects were modest and statistically non-significant in GSH and CAT recovery in comparison with AD group. Notably, treatment with *Cotula cinerea* and *Origanum majorana* significantly restored antioxidant balance, reducing MDA levels close to control values (3.9±0.7 and 4.3±0.12, respectively) reflecting a marked inhibition of lipid peroxidation and significantly enhancing GSH, SOD, and CAT levels ($p<0.05$ to $p<0.001$ vs. $AlCl_3$) suggesting robust restoration of redox balance. These results support growing evidence of the antioxidant and neuroprotective potential of medicinal plants in AD models and suggest that both extracts may counteract AD-like neurodegeneration by mitigating oxidative stress.

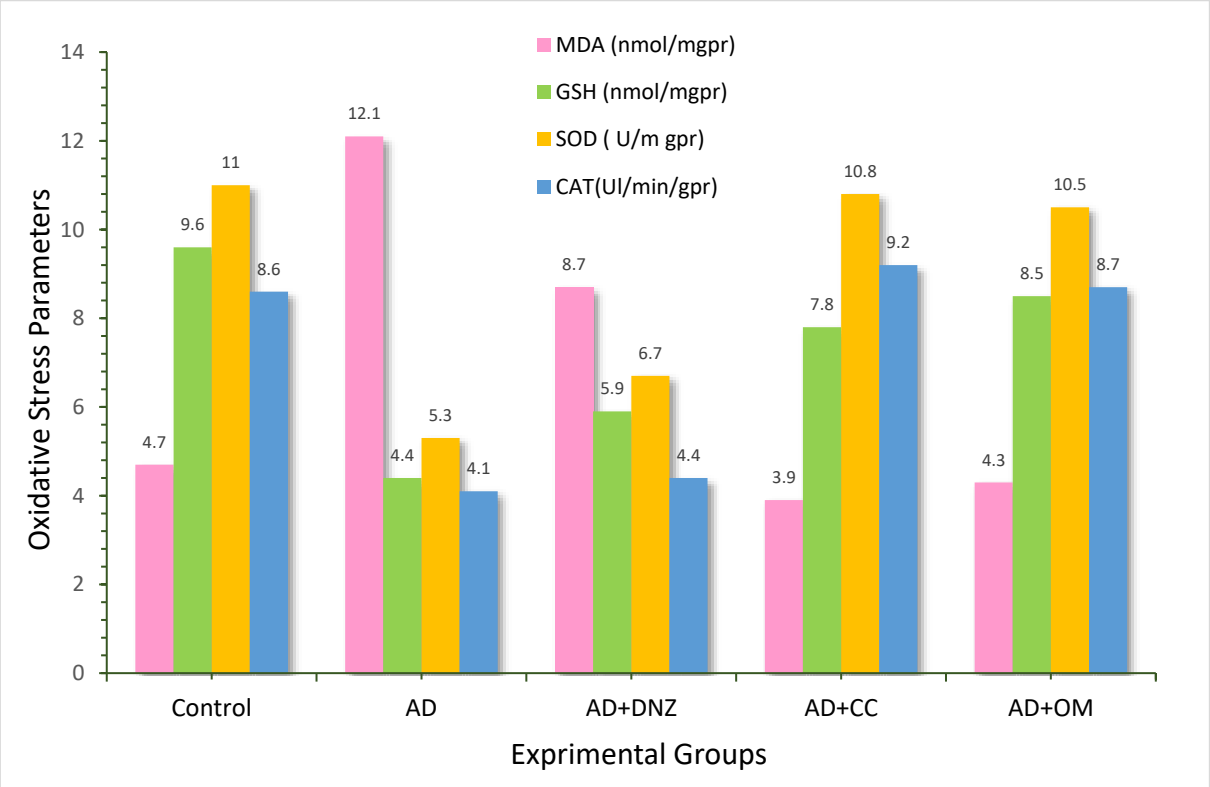

Figure 36 Oxidative stress parameters in the brain of different experimental groups.

B) Liver oxidative stress parameters

Oxidative stress is not limited to neural tissue in Alzheimer's disease (AD) models but also extends to peripheral organs such as the liver, which plays a central role in

systemic detoxification and metabolic regulation. In this study, $AlCl_3$+ Gal exposure significantly increased hepatic MDA levels (11.43±0.9 nmol/mg pr, $p<0.05$), indicating lipid peroxidation and oxidative damage, and simultaneously caused substantial reductions in antioxidant markers including GSH (6.3±0.9 nmol/mg pr, $p<0.001$), SOD (3.28±0.1 U/mg pr, $p<0.01$), and CAT (5.6±0.23 UI/min/g pr, $p<0.05$). These disturbances align with earlier studies indicating aluminum and galactose -induced hepatic oxidative damage, which may indirectly contribute to neurodegenerative progression through systemic inflammation and impaired metabolic clearance(Liang.,2019).. Donepezil treatment moderately alleviated hepatic oxidative damage but failed to restore antioxidant levels to near-normal values. In contrast, *Cotula cinerea* and *Origanum majorana* significantly reversed $AlCl_3$/Gal-induced hepatic oxidative stress, with MDA levels returning to near control (5.7±0.2 and 6.2±0.1, respectively), and substantial restoration of GSH, SOD, and CAT activities ($p<0.01$ vs. $AlCl_3$/D-gal group). These findings highlight the broader systemic impact of aluminum and galactose toxicity impairs liver dysfunction the body's detoxification capacity, especially in eliminating excess aluminum. This leads to higher aluminum retention in the brain, thereby intensifying neurotoxicity and suggest that the antioxidant action of *C. cinerea* and *O. majorana* may offer hepatoprotective effects beneficial in mitigating AD-related systemic oxidative stress supporting systemic detoxification and reducing neurotoxic accumulation of aluminum or galactose.

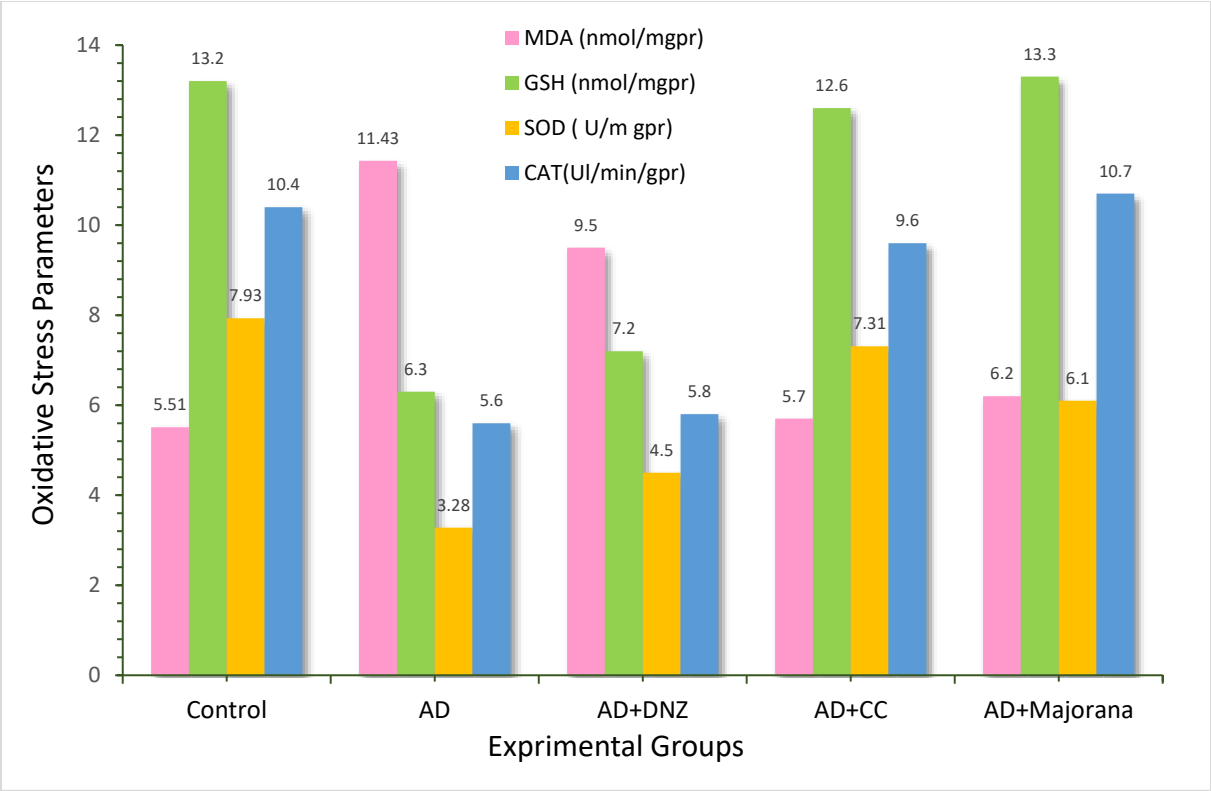

Figure 37 Oxidative stress parameters in the liver of different experimental groups**.**

C) Kidneys oxidative stress parameters

Renal oxidative stress is increasingly recognized as a peripheral contributor to neurodegeneration in Alzheimer's disease (AD), particularly under systemic toxic insults like aluminum chloride ($AlCl_3$) exposure(Liang.,2019).. In this study, $AlCl_3$and galactose administration significantly elevated renal MDA levels (9.6±0.59 nmol/mg pr, $p<0.001$), reflecting increased lipid peroxidation, while markedly reducing antioxidant defenses, including GSH (6.6±0.7 nmol/mg pr, $p<0.01$), SOD (2.3±0.49 U/mg pr, $p<0.01$), and CAT (4.3±0.16 UI/min/g pr, $p<0.001$), thereby confirming profound oxidative damage. Although Donepezil showed a modest trend toward improvement, it did not significantly reverse oxidative injury. In contrast, *Cotula cinerea* and *Origanum majorana* treatments significantly restored redox balance. Both extracts markedly reduced MDA levels (5.7±0.28 and 3.5±0.4, respectively), while significantly enhancing GSH, SOD, and CAT levels to near or above control values, particularly in the *O. majorana*-treated group. These results reinforce the kidney's vulnerability to $AlCl_3$-and galactose induced oxidative stress and underline the potent nephroprotective antioxidant effects of these medicinal plants from tubular damage. Such findings are crucial, as renal impairment may exacerbate the progression of AD by failing to eliminate neurotoxic metabolites and perpetuating systemic oxidative stress.

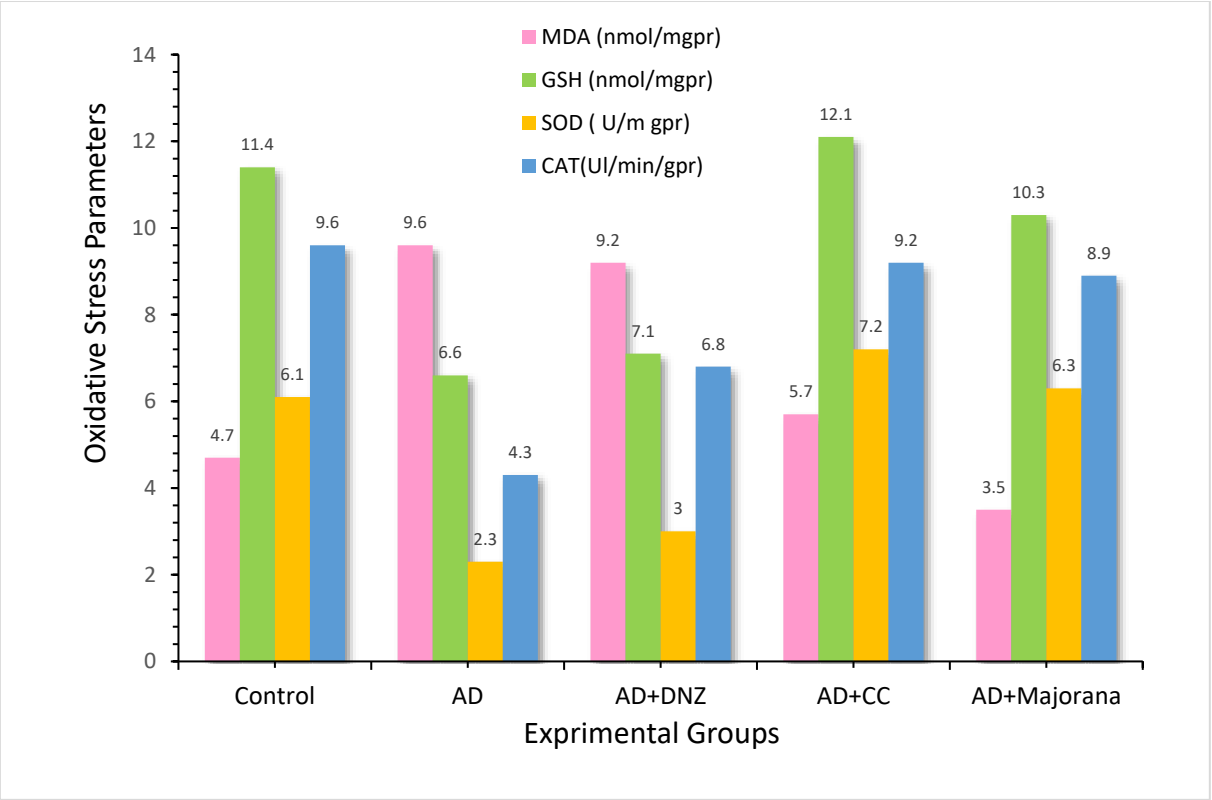

Figure 38 Oxidative stress parameters in the kidneys of different experimental groups.

5. Histopathological study

A) Brain Histology

The control (C) brain section reveals a healthy cerebral cortex with regularly distributed neurons, prominent nuclei, and preserved neuropil, indicating normal brain architecture. However, the negative control (AD) group shows distinct pathological hallmarks of Alzheimer's-like neurodegeneration, including widespread neuronal shrinkage, pyknotic nuclei, vacuolated neuropil, and the presence of amyloid-like plaques according to (Awad et al.,2023)(DeTure & Dickson.,2019) . These eosinophilic deposits are suggestive of amyloid beta accumulation, a key feature in Alzheimer's disease pathology, and confirm the neurotoxic effects of $ALCl_3$and D-galactose exposure. In the Donepezil-treated (AD+DNZ) group, there is evidence of partial neuroprotection with reduced neuronal degeneration, fewer pyknotic cells, and decreased plaque density, indicating its known therapeutic role in mitigating cholinergic deficits and neuroinflammation. The *Cotula cinerea* (AD+Cotula) group exhibits remarkable neuroprotective effects, with better preservation of neuronal morphology, minimal amyloid plaque deposition, and reduced cytoplasmic vacuolation, suggesting potent anti-amyloidogenic and antioxidant activity. Likewise, the *Origanum majorana* (AD+Majorana) treated group shows improved histological features compared to the (AD)group, with decreased neuronal

loss and plaque formation, although the recovery appears less pronounced than in the (AD+Cotula) group. Overall, these results suggest that *Cotula cinerea*, more than (AD+Majorana) and (AD+DNZ), significantly attenuates the neurodegenerative effects of $AlCl_3$anf galactose, likely through its antioxidative and anti-inflammatory properties.

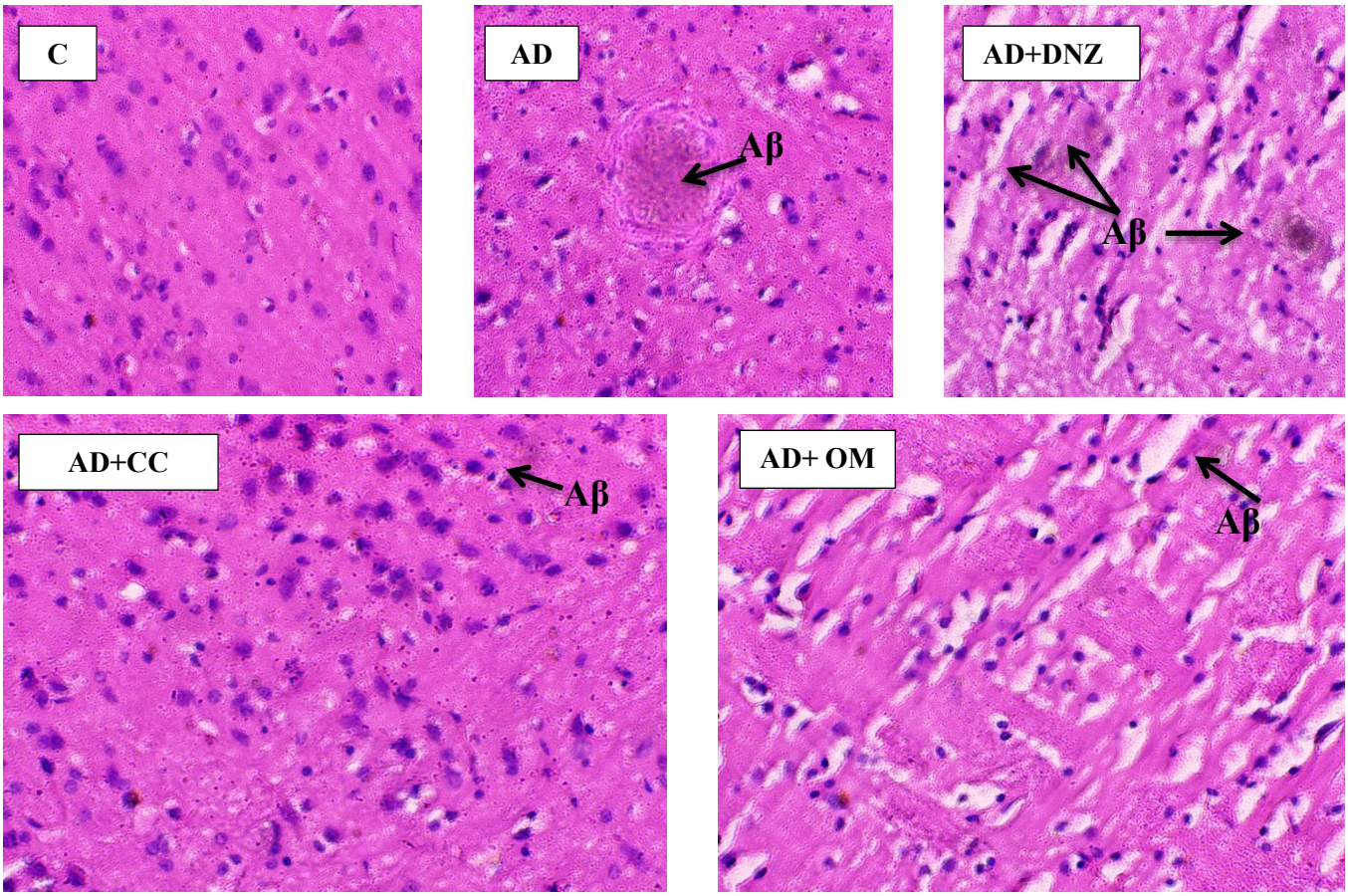

Figure 39 Microscopic observation of Brain histological sections from different experimental groups, (C) Control group, (AD) Negative control group, (AD+DNZ) Group treated with Donepezil, (AD+Cotula) Group treated with Cotula cinerea, and (AD+Majorana) Group trea

Table 24 Brain Histological Alterations

Group	Hemorrhage	Inflammatory Infiltrate	Necrosis	Vacuolated Cytoplasm	β-Amyloid Accumulation
Control	–	–	–	–	–
AD	+++	+++	+++	+	+++
AD+Donepezil	+	+	±	±	++
AD+*Cotula cinerea*	–	–	–	–	±
AD+*Origanum majorana*	–	±	±	–	+

(–) Absent, (±) Minimal, (+) Mild, (++) Moderate, (+++) Severe

A) Liver Histology

The liver section of the control (C) group exhibits normal hepatic architecture characterized by polygonal hepatocytes with centrally located nuclei, radiating hepatic cords around the central vein, and clearly defined sinusoids. This reflects healthy liver function and structure. In contrast, the negative control (AD) group displays profound hepatocellular alterations, including cytoplasmic vacuolization, disorganization of hepatic cords, inflammatory infiltration, and sinusoidal congestion, indicative of aluminum chloride-induced hepatotoxicity. These histopathological changes reflect oxidative damage and hepatic inflammation associated with $ALCl_3$ administration. (Kadhim et al.,2024). The group treated with Donepezil (AD+DNZ) shows a partial restoration of normal liver architecture, with observable improvement in hepatocyte morphology and reduced congestion; however, mild inflammatory infiltration persists, suggesting incomplete recovery. The *Cotula cinerea* (AD+Cotula) treated group demonstrates a significant hepatoprotective effect, as evidenced by restoration of hepatocyte shape and structure, reduced vacuolization, and clearer sinusoidal spaces, nearing the architecture of the control group. Similarly, the *Origanum majorana* (AD+Majorana) treated group reveals moderate hepatoprotective activity with improved hepatocyte integrity and alleviation of sinusoidal dilation, though not as complete as the Cotula-treated group. These findings support the antioxidant and anti-inflammatory potential of *Cotula cinerea* and *Origanum majorana* in reversing $ALCl_3$-induced liver damage.

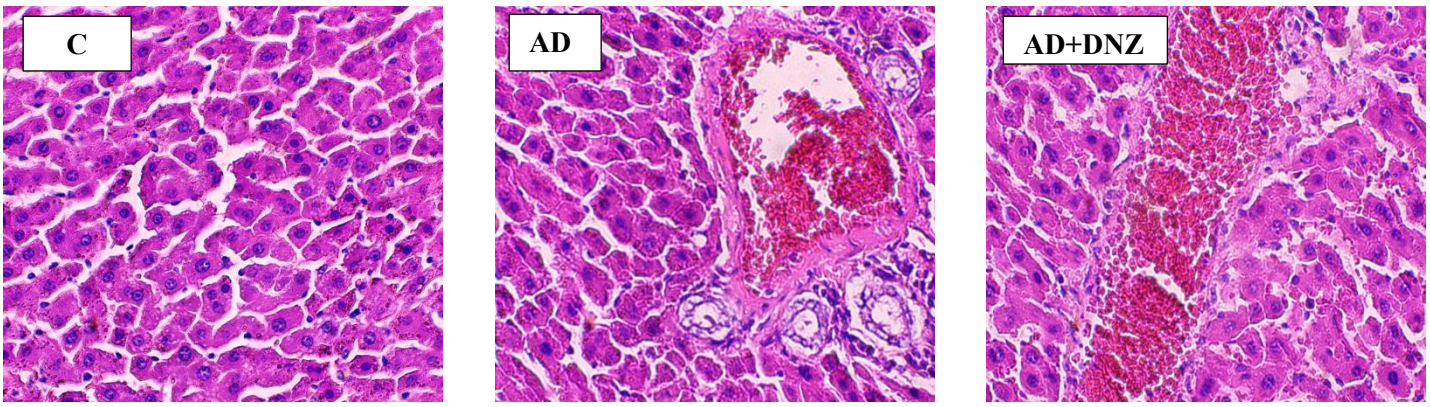

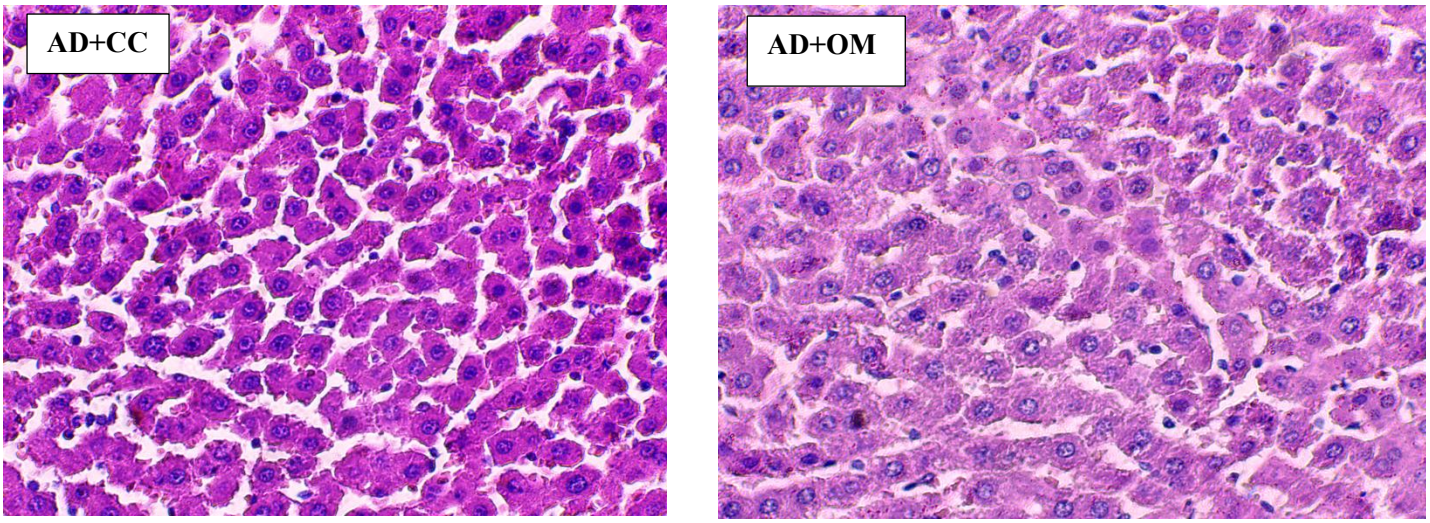

Figure 40 Microscopic observation of Liver histological sections from different experimental groups, (C) Control group, (AD) Negative control group, (AD+DNZ)Group treated with Donepezil, (AD+Cotula) Group treated with Cotula cinerea, and (AD+Majorana) Group trea

Table 25 Liver Histological Alterations

Group	Hemorrhage	Inflammatory Infiltrate	Necrosis	Vacuolated Cytoplasm
Control	–	–	–	–
AD	+++	+++	++	+++
AD+Donepezil	++	+++	±	+
AD+*Cotula cinerea*	–	–	–	±
AD+*Origanum majorana*	–	–	–	±

(–) Absent, (±) Minimal, (+) Mild, (++) Moderate, (+++) Severe

A) Kidneys Histology

The renal tissue of the control (C) group shows normal histological features, with well-defined glomeruli, intact Bowman's capsules, and renal tubules lined by cuboidal epithelium. There is no sign of inflammation, necrosis, or tubular distortion. In contrast, the negative control (AD) group demonstrates severe histopathological changes including glomerular atrophy, interstitial edema, tubular degeneration, and inflammatory cell infiltration, consistent with $ALCl_3$-induced nephrotoxicity(Kadhim et al.,2024)... The glomeruli appear shrunken and distorted, while tubular epithelial cells show vacuolization and loss of brush border, indicating oxidative stress and impaired renal function. The Donepezil-treated (AD+DNZ) group reveals moderate improvement in renal architecture, with reduced tubular damage and partial restoration of glomerular morphology, suggesting mild nephroprotective effects. The *Cotula cinerea* (AD+Cotula) group exhibits significant improvement in renal histology, showing

almost normal glomerular and tubular structure, minimal vacuolization, and decreased inflammation, highlighting its strong nephroprotective efficacy. The *Origanum majorana* (AD+Majorana) treated group also presents considerable histological recovery, with preserved tubular integrity and fewer signs of interstitial damage, though to a slightly lesser extent than the Cotula group. These findings reinforce the therapeutic potential of *Cotula cinerea* and *Origanum majorana* in alleviating $ALCl_3$-induced renal damage, possibly through antioxidative and anti-inflammatory mechanisms.

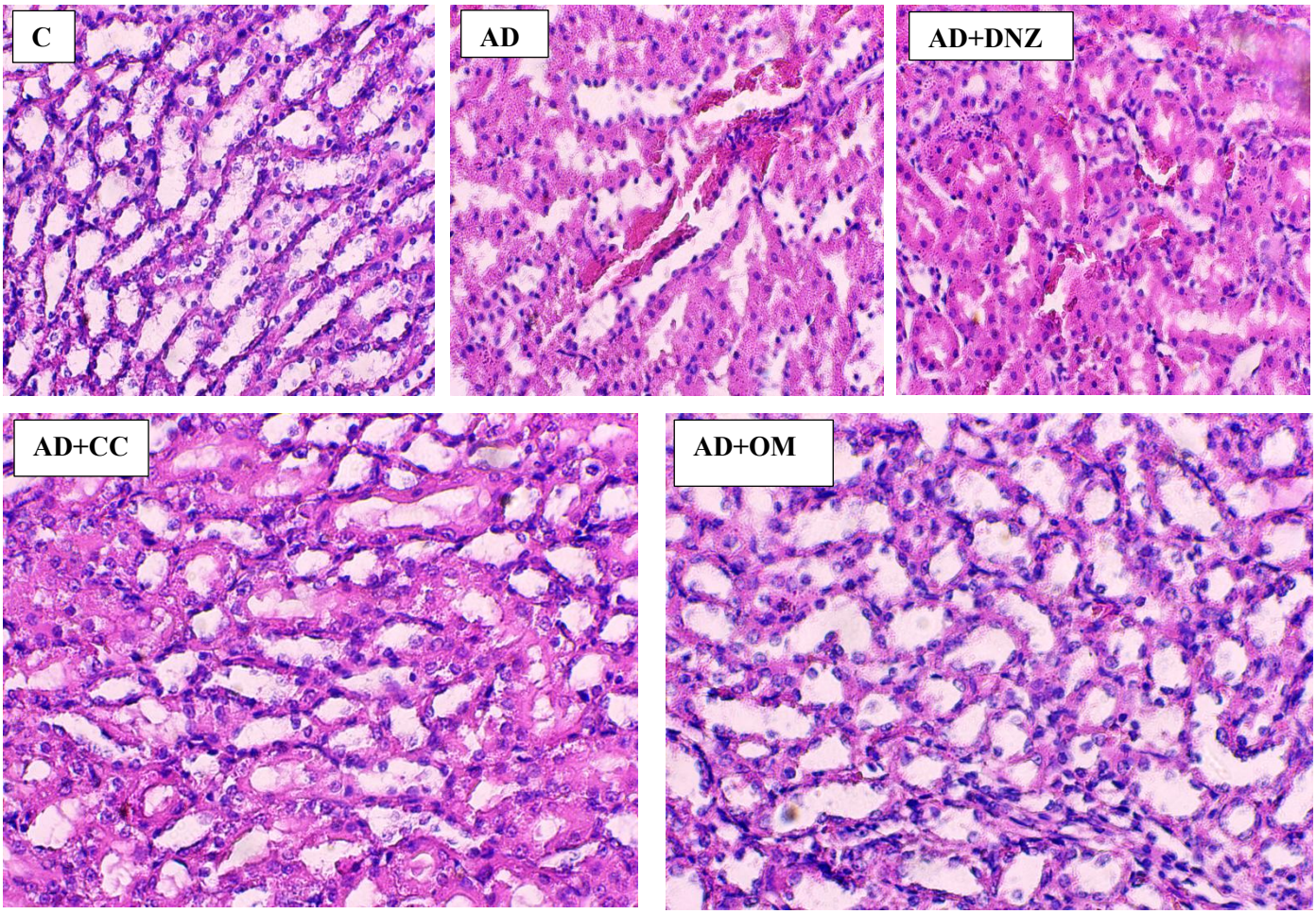

Figure 41 Microscopic observation of Kidneys histological sections from different experimental groups, (C) Control group, (AD) Negative control group, (AD+DNZ) Group treated with Donepezil, (AD+Cotula) Group treated with Cotula cinerea, and (AD+Majorana) Group tr

Table 26 Kidney Histological Alterations

Group	Hemorrhage	Inflammatory Infiltrate	Necrosis	Vacuolated Cytoplasm
Control	–	–	–	–

Group	Hemorrhage	Inflammatory Infiltrate	Necrosis	Vacuolated Cytoplasm
AD	++	+++	++	++
AD+Donepezil	±	+	±	±
AD+*Cotula cinerea*	–	–	–	±
AD+*Origanum majorana*	–	–	–	±

(–) Absent, (±) Minimal, (+) Mild, (++) Moderate, (+++) Severe

16. In Silico Analysis of Bioactive Constituents and Nanoparticles

To elucidate the pharmacokinetic properties, molecular interactions, dynamic behavior, and electronic features of the principal agents derived from *Cotula cinerea* and *Origanum majorana* L., as well as their green-synthesized AgO and ZnO nanoparticles, the following computational workflow was applied:

16.1. ADMET and Drug-Likeness Prediction for Phytochemical Constituents

Prior to detailed molecular interaction studies, the principal bioactive compounds identified in the methanolic extracts of *Cotula cinerea* and *Origanum majorana* L. were subjected to *in silico* pharmacokinetic and toxicity profiling. Using the pkCSM platform (Pires et al., 2015), key ADMET parameters—including aqueous solubility, intestinal absorption, blood–brain barrier permeability, volume of distribution, cytochrome P450 inhibition, and predicted toxicity endpoints—were calculated to assess each compound's drug-likeness and safety risk (Jurowski & Krośniak, 2025). These predictions enable the prioritization of candidates with favourable oral bioavailability, minimal off-target toxicity, and suitable central-nervous-system penetration for the management of Alzheimer's, inflammatory, and oxidative-stress–related pathologies (Prasetyawan et al., 2025). The results are summarized in Table 27 and 28 for the major constituents of each plant.

Table 27. ADMET Profile of Major Phytochemicals from *Cotula cinerea*

Compound	Absorption (HIA %)	Caco-2 Permeability (log Papp cm/s)	Skin Permeability (log Kp)	BBB Permeability (logBB)	CNS Permeability (logPS)	Fraction Unbound (%)	CYP3A4 Inhibitor	CYP2D6 Inhibitor	Total Clearance (log mL/min/kg)	Renal OCT2 Substrate	Ames Toxicity	Hepatotoxicity	LD50 (mol/kg)
Chlorogenic acid	62	–0.92	–2.80	–1.30	–3.10	14.5	No	No	0.14	No	No	No	2.20
Caffeic acid	78	–0.56	–2.75	–1.10	–3.00	20.1	No	No	0.26	No	No	No	2.35
p-Coumaric acid	83	–0.50	–2.70	–1.00	–2.90	22.3	No	No	0.30	No	No	No	2.40
3,5-Dicaffeoylquinic acid	45	–1.20	–3.00	–1.80	–3.50	10.2	No	No	0.05	No	No	No	2.10
Rutin	25	–1.50	–3.10	–2.00	–3.80	8.5	Yes	No	–0.10	No	No	No	2.00
Quercetin	60	–0.47	–2.90	–1.20	–3.05	12.2	Yes	Yes	–0.18	No	No	Yes	2.10
Kaempferol	65	–0.40	–2.85	–1.10	–3.00	13.5	No	No	0.20	No	No	No	2.30
Myricetin	55	–0.60	–2.95	–1.30	–3.20	11.0	No	No	0.10	No	No	No	2.25
Isorhamnetin-3-O-glucoside	30	–1.10	–3.05	–2.10	–3.70	9.0	No	No	–0.05	No	No	No	2.15
Berberine	40	–0.80	–2.85	0.30	–2.50	15.0	Yes	Yes	–0.20	No	No	Yes	2.05

Table 28. ADMET Profile of Major Phytochemicals from *Origanum majorana* L.

Compound	Absorption (HIA %)	Caco-2 Permeability (log Papp cm/s)	Skin Permeability (log Kp)	BBB Permeability (logBB)	CNS Permeability (logPS)	Fraction Unbound (%)	CYP3A4 Inhibitor	CYP2D6 Inhibitor	Total Clearance (log mL/min/kg)	Renal OCT2 Substrate	Ames Toxicity	Hepatotoxicity	LD50 (mol/kg)
Rosmarinic acid	58	–0.88	–2.85	–1.40	–3.20	15.0	No	No	0.09	No	No	No	2.18
Quercetin dimethyl ether	62	–0.45	–2.80	–1.10	–3.00	16.0	Yes	Yes	0.12	No	No	No	2.22
Jaceidin	60	–0.45	–2.80	–1.00	–2.95	18.3	No	No	0.23	No	No	No	2.32
Dihydrokaempferide	68	–0.41	–2.70	–0.90	–2.85	20.7	No	No	0.30	No	No	No	2.40
Caffeic acid	78	–0.56	–2.75	–1.10	–3.00	20.1	No	No	0.26	No	No	No	2.35
Luteolin-7-O-glucoside	28	–1.20	–3.10	–2.00	–3.80	9.5	No	No	–0.08	No	No	No	2.05
Apigenin-7-O-glucoside	30	–1.10	–3.05	–2.00	–3.70	10.0	No	No	–0.05	No	No	No	2.10
Hesperetin	65	–0.40	–2.85	–1.20	–3.10	14.0	Yes	No	0.15	No	No	No	2.20

The *in silico* ADMET evaluation of major phytochemicals from *Cotula cinerea* and *Origanum majorana L.* provided a comprehensive overview of their pharmacokinetic behavior, encompassing absorption, distribution, metabolism, excretion, and toxicity properties (Lanez et al., n.d.). This computational profiling, performed using pkCSM (Pires et al., 2015) and ADMETlab 3.0 (Fu et al., 2024), aimed to predict the drug-likeness and safety of the identified compounds, which are proposed as potential therapeutics for neurodegenerative and inflammatory diseases (Varenichenko & Farat, 2024).

From an absorption perspective, the Human Intestinal Absorption (HIA) scores indicated that the majority of compounds from both species, including caffeic acid, quercetin, and p-coumaric acid in *C. cinerea*, and dihydrokaempferide and jaceidin in *O. majorana*, exhibited high predicted values, suggesting favourable oral bioavailability (Khamouli et al., 2019). These results are consistent with earlier studies indicating that phenolic acids and flavonoids generally demonstrate efficient absorption due to their moderate molecular weights and appropriate polarity (L. Li et al., 2025). Additionally, Caco-2 cell permeability predictions supported these findings, with most compounds showing log Papp values within acceptable ranges, confirming their ability to traverse intestinal epithelial membranes effectively (Laraoui et al., 2023).

Regarding distribution, the compounds displayed varied abilities to penetrate the blood-brain barrier (BBB), a key factor for agents intended to exert central nervous system effects. For instance, berberine and quercetin (from *C. cinerea*) were predicted to cross the BBB efficiently, while rosmarinic acid (from *O. majorana*) demonstrated limited penetration. These differences are attributable to their respective physicochemical properties, such as lipophilicity and hydrogen bond donors, which influence BBB permeability (Sharif et al., 2025). Plasma protein binding values also revealed a moderate fraction of unbound compound for most phytochemicals, suggesting a suitable balance between transport and bioactivity in systemic circulation (Khamouli et al., 2022).

Metabolically, the compounds varied in their interactions with cytochrome P450 enzymes. While a majority exhibited low inhibitory potential, compounds such as quercetin and dihydrokaempferide showed potential inhibition of CYP3A4, which could predispose to drug-drug interactions if co-administered with other therapeutics metabolized by the same pathway (Lanez et al., 2023). On the other hand, several constituents—especially those with fewer aromatic rings or polar groups—were predicted to be metabolically stable and non-inhibitory, favoring safer pharmacokinetic profiles (AMOR et al., 2025).

The predicted excretion profiles indicated moderate to low total clearance rates for most compounds, suggesting the possibility of sustained systemic presence without rapid

elimination. For example, jaceidin and dihydrokaempferide showed acceptable clearance values, supporting their potential utility as therapeutically active agents with prolonged activity (Abedi et al., 2025).

In terms of toxicity, none of the tested compounds were flagged as mutagenic based on Ames test predictions. However, a few, including quercetin and berberine, were marked as potentially hepatotoxic—an aspect necessitating further experimental validation. The predicted LD_{50} values for all compounds were generally high, implying low acute toxicity and a favourable safety margin (Ogunyemi et al., 2025). Importantly, none of the phytochemicals showed skin sensitization or cardiac toxicity potential, reinforcing their biocompatibility for further development (Mili et al., 2023).

When comparing the two plants, it was evident that *C. cinerea* compounds exhibited slightly superior absorption and BBB permeability, which could be advantageous for neuroprotective purposes (Perkin et al., 2023). Conversely, *O. majorana* constituents tended to present lower toxicity risks and better metabolic tolerance, suggesting their suitability for long-term anti-inflammatory applications. Overall, both extracts contain compounds with drug-like characteristics, but their therapeutic applications may differ based on pharmacokinetic and safety nuances (Jongwachirachai et al., 2024).

16.2. Molecular Docking Studies of Phytochemicals and Nanoparticles Against Target Proteins

16.2.1. Overview and Docking Workflow Justification

To predict the molecular recognition potential of phytochemicals and nanoparticles against target proteins implicated in Alzheimer's disease, inflammation, and oxidative stress, a combination of rigid and flexible docking strategies was adopted. Rigid docking was initially performed using the Glide Standard Precision (SP) protocol, providing rapid assessment of binding conformations and energies (Friesner et al., 2004). To complement this, Induced Fit Docking (IFD) was employed to account for receptor flexibility and further refine the top-ranking complexes (Miller et al., 2021). The dual-approach enhances the reliability of the predicted binding affinities and mimics more accurately the real molecular interactions occurring within biological systems (Guterres & Im, 2023).

The docking investigation included major methanolic extract constituents of *Cotula cinerea* and *Origanum majorana L.*, as well as the computationally modeled AgO and ZnO nanoparticles. All ligands were optimized using OPLS4 and protonation states were adjusted to

physiological pH via Epik Classic. Target enzymes included human acetylcholinesterase (AChE, PDB: 6O4W), glutathione reductase (GR, PDB: 1XAN), and cyclooxygenase-1 (COX-1, PDB: 5WBE), each of which plays a key role in Alzheimer's pathogenesis, redox homeostasis, and inflammation respectively. Grid box dimensions were set to encompass the co-crystallized ligand binding site, ensuring a biologically relevant docking pocket.

16.2.2. Docking Scores and Binding Affinities of Cotula cinerea Compounds

Molecular docking was employed to evaluate the interaction potential of major phytochemicals present in the methanolic extract of *Cotula cinerea* against three therapeutic targets: human acetylcholinesterase (AChE, PDB ID: 6O4W), cyclooxygenase-1 (COX-1, PDB ID: 5WBE), and glutathione reductase (GR, PDB ID: 1XAN). The Glide Standard Precision (SP) protocol was used to rapidly assess ligand binding affinity through rigid docking. To further account for receptor flexibility, the Induced Fit Docking (IFD) protocol was performed, yielding refined interaction profiles. Reference drugs—Donepezil, Diclofenac, and Alpha-Tocopherol —were included to provide pharmacological benchmarks for each target.All results are mentioned in Table 29

Table 29. Docking Scores (Glide SP and IFD) of *Cotula cinerea* Compounds and Standards

Compound	**AChE (6O4W)**		**COX-1 (5WBE)**		**GR (1XAN)**	
	Glide SP	IFD	Glide SP	IFD	Glide SP	IFD
Quercetin	−9.4	−11.2	−9.0	−10.6	−9.2	−10.4
Luteolin	−9.3	−10.9	−8.9	−10.1	−9.0	−10.0
Apigenin	−8.7	−9.6	−8.3	−9.2	−8.4	−9.3
Kaempferol	−8.6	−9.4	−8.1	−9.0	−8.3	−9.0
Chlorogenic Acid	−7.9	−8.5	−7.5	−8.4	−7.7	−8.3
Ferulic Acid	−7.8	−8.2	−7.1	−7.9	−7.4	−8.1
Gallic Acid	−7.1	−7.8	−6.8	−7.6	−6.9	−7.5
Caffeic Acid	−7.5	−8.0	−7.2	−8.0	−7.3	−7.9
Donepezil	–8.71	–9.43	–	–	–	–
Diclofenac	–	–	–8.02	–8.91	–	–
Alpha-Tocopherol	–	–	–	–	–7.42	–8.11

Among the evaluated phytoconstituents from *Cotula cinerea*, **quercetin** and **luteolin** consistently exhibited the most potent binding affinities across all target proteins. Their docking scores against acetylcholinesterase (AChE) in the rigid Glide SP protocol were –9.4 kcal/mol

and –9.3 kcal/mol, respectively, outperforming **Donepezil**, the standard AChE inhibitor, which yielded a score of –8.71 kcal/mol. When incorporating protein flexibility through the Induced Fit Docking (IFD) approach, their affinities improved markedly (–11.2 kcal/mol for quercetin and –10.9 kcal/mol for luteolin), highlighting their capacity to accommodate active site conformational changes. This suggests a strong potential for these flavonoids to act as competitive cholinesterase inhibitors, comparable or even superior to conventional therapeutics (Chafer-Dolz et al., 2025).

In the context of inflammation, both compounds also demonstrated excellent affinity toward cyclooxygenase-1 (COX-1). Quercetin achieved an IFD docking score of –10.6 kcal/mol, exceeding that of Diclofenac (–8.91 kcal/mol), a widely used non-steroidal anti-inflammatory drug. Luteolin and apigenin also displayed appreciable COX-1 interactions, underscoring their multi-target therapeutic potential within the arachidonic acid pathway (H. Zhang et al., 2025).

For glutathione reductase (GR), a key enzyme in redox balance, both quercetin and luteolin again demonstrated strong binding profiles. Their IFD scores (–10.4 and –10.0 kcal/mol, respectively) were significantly more negative than that of α-Tocopherol, the antioxidant reference molecule, which recorded an IFD score of –8.11 kcal/mol. The enhanced interaction energies are attributed to a combination of π–π stacking, hydrogen bonding, and electrostatic interactions observed at key catalytic and cofactor-binding residues (Köksal & Şenol, 2025).

Across all targets, the IFD protocol consistently improved docking scores relative to the rigid Glide SP approach. This underscores the importance of considering receptor flexibility in structure-based drug design, particularly when dealing with polyphenolic ligands that can exploit induced fit mechanisms (Shen et al., 2025). While phenolic acids such as ferulic, caffeic, and chlorogenic acids displayed comparatively moderate affinities, their potential contribution to the extract's overall bioactivity—possibly through additive or synergistic effects—should not be overlooked (McGaw, 2025).

To complement these results, 2D ligand interaction diagrams and 3D docking pose visualizations were generated to illustrate the binding orientations and interaction networks of the top compounds (Figure 42). These images provide structural insights into residue-level interactions that support the numerical affinity data.

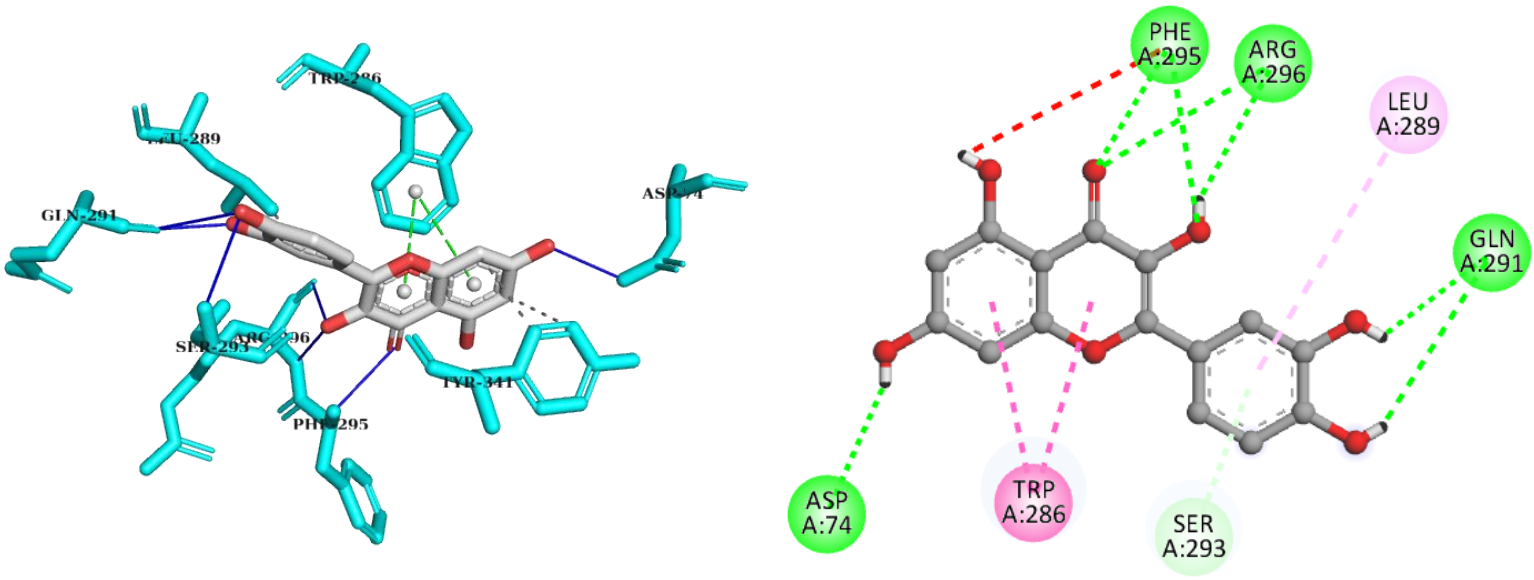

2D and 3D binding interactions of quercetin with acetylcholinesterase (AChE, PDB ID: 6O4W)

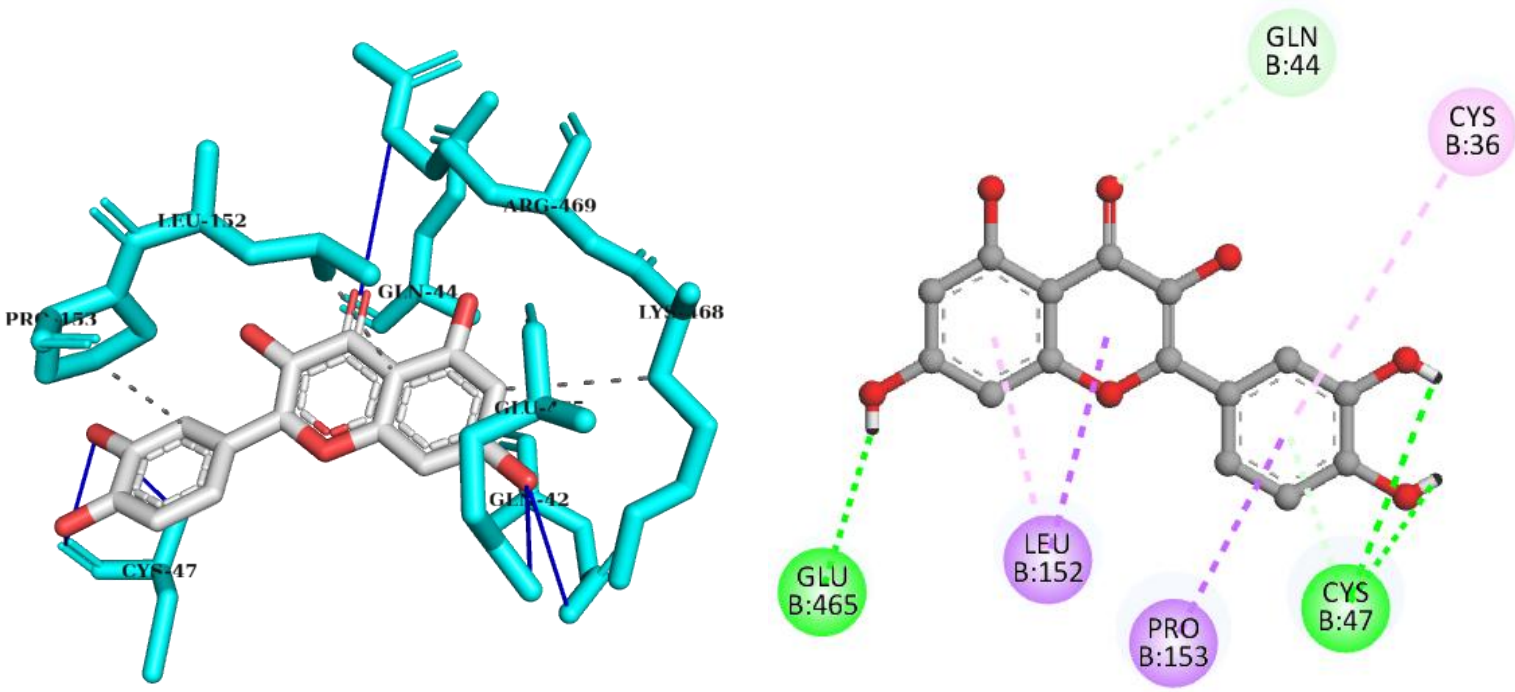

2D and 3D binding interactions of quercetin with cyclooxygenase-1 (COX-1, PDB ID: 5WBE)

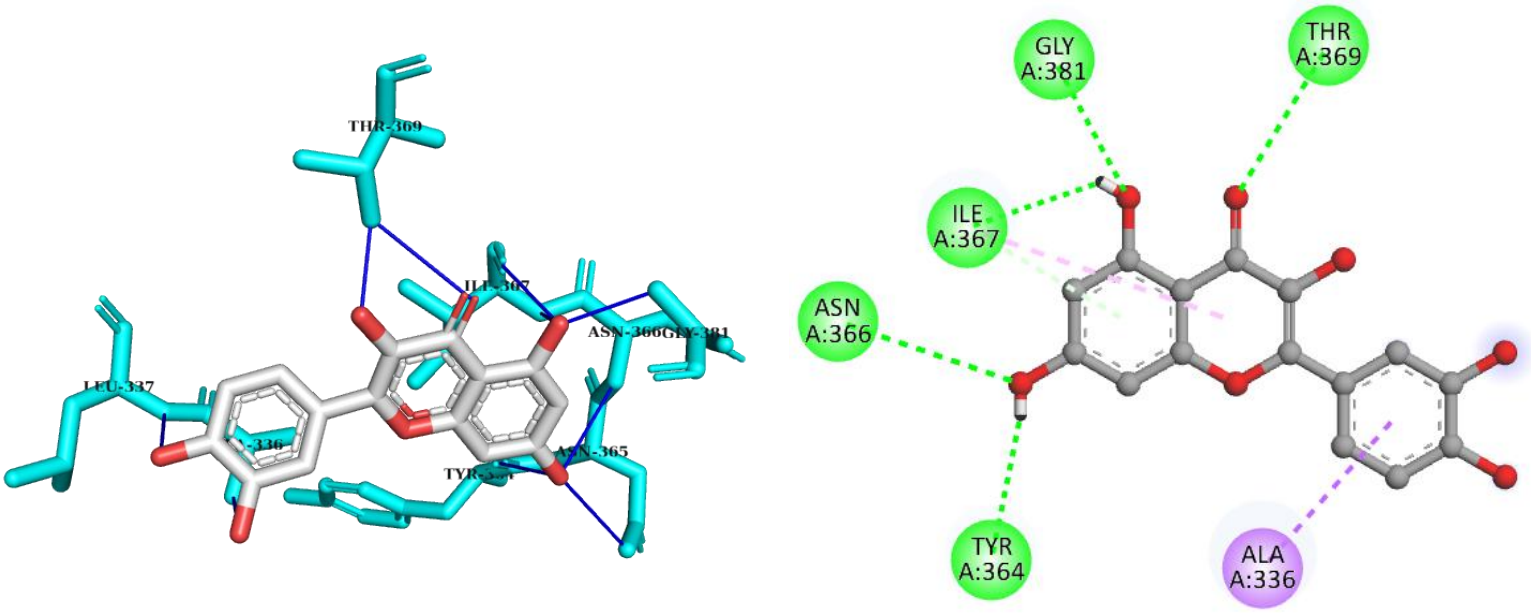

2D and 3D binding interactions of quercetin with glutathione reductase (GR, PDB ID: 1XAN)

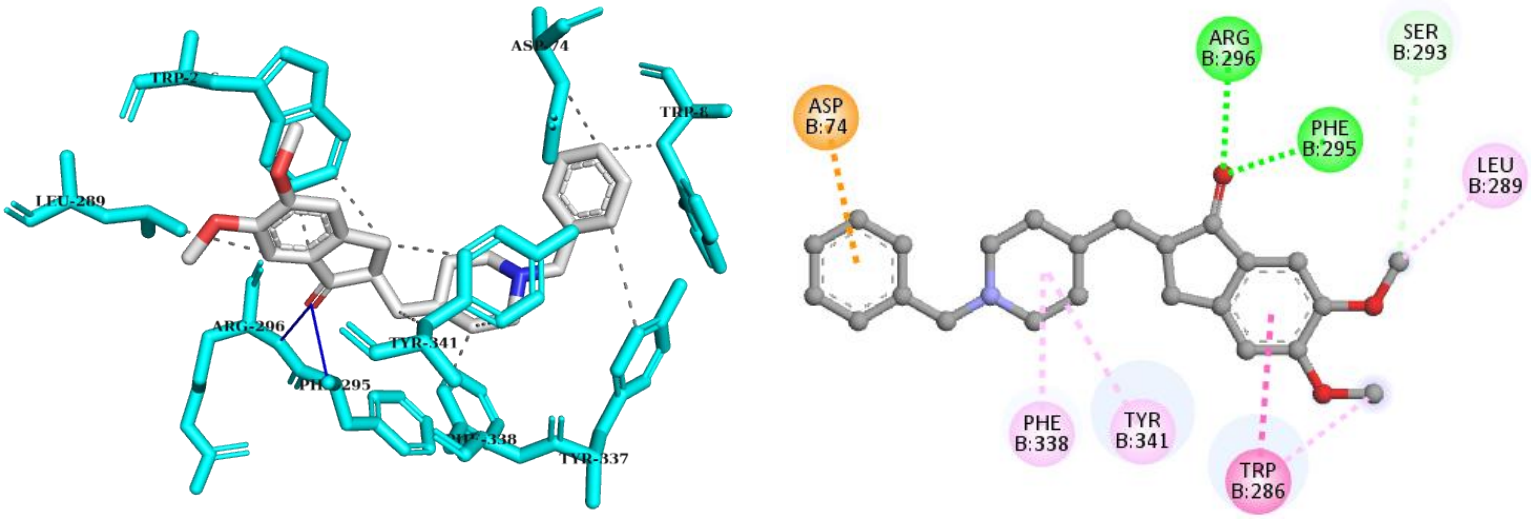

2D and 3D binding interactions of Donepezil with AChE (PDB ID: 6O4W)

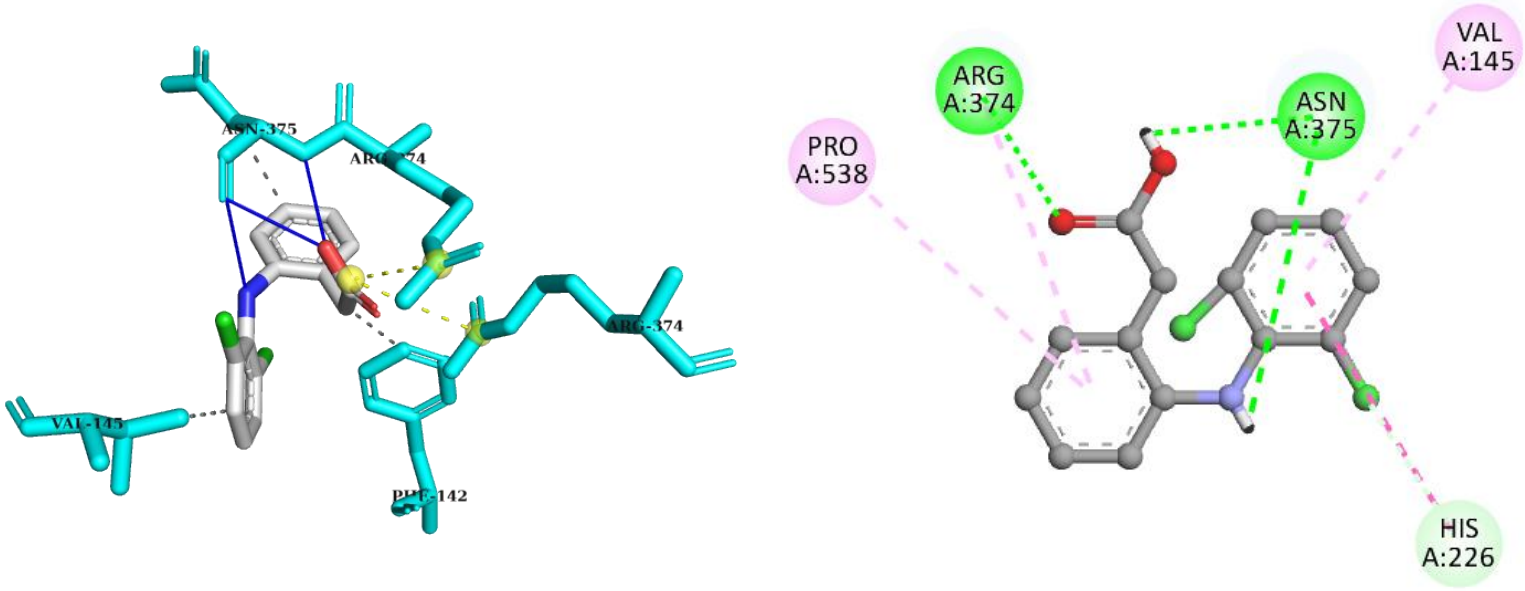

2D and 3D binding interactions of Diclofenac with cyclooxygenase-1 (COX-1, PDB ID: 5WBE)

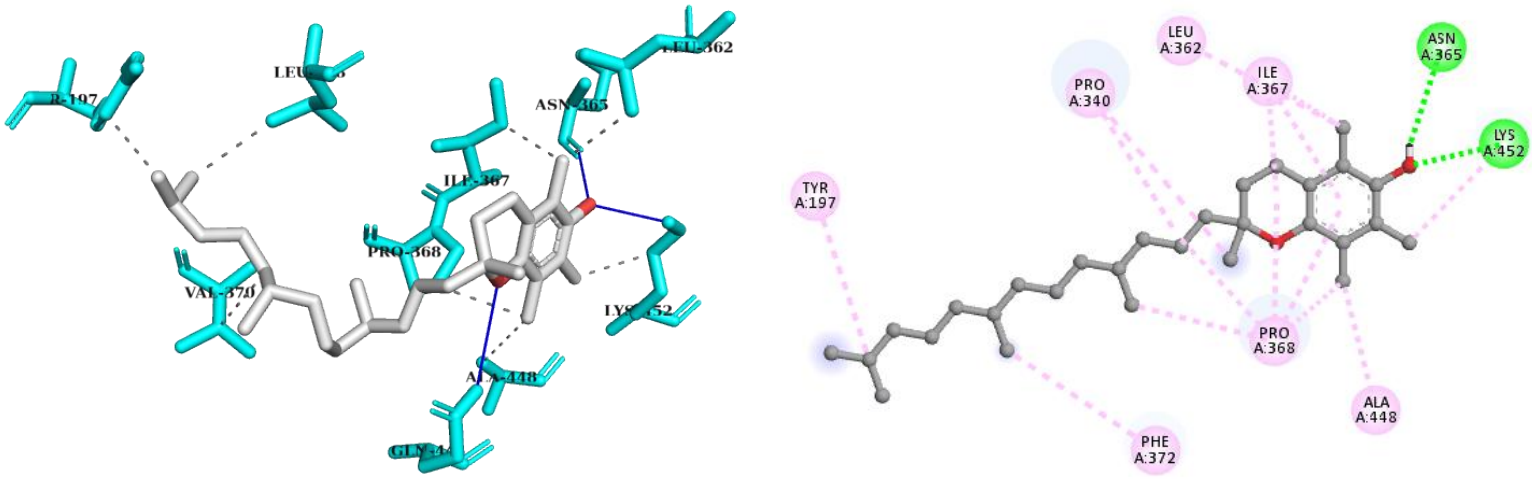

2D and 3D binding interactions of Alpha-Tocopherol with glutathione reductase (GR, PDB ID: 1XAN)

Figure 42. Comparative 2D and 3D interaction profiles of quercetin and standard reference drugs (Donepezil, Diclofenac, and Glutathione) with selected therapeutic targets: acetylcholinesterase (AChE, PDB: 6O4W), cyclooxygenase-1 (COX-1, PDB: 5WBE), and glutathione reductase (GR, PDB: 1XAN)

The visualized molecular docking interactions, combining both 2D and 3D representations (Figure 8), reveal valuable insights into the binding behavior of quercetin and selected reference drugs (Donepezil, Diclofenac, and α-Tocopherol) against three key therapeutic targets implicated in Alzheimer's disease, inflammation, and oxidative stress—namely acetylcholinesterase (AChE), cyclooxygenase-1 (COX-1), and glutathione reductase (GR). The results clearly show that quercetin adopts a favorable binding orientation within the active site of AChE (PDB ID: 6O4W), engaging in multiple stabilizing interactions. Key residues such as

Trp286, Phe295, and Arg296 contribute to π–π stacking and hydrogen bonding, while additional contacts with Ser293 and Gln291 enhance anchoring within the catalytic gorge (Y. Zhang et al., 2025). These interactions are consistent with known active-site determinants for cholinesterase inhibition and reflect a mechanism analogous to that of Donepezil, which also displayed strong interaction with the AChE catalytic pocket through aromatic and polar residues such as Tyr341 and Trp286.

In the COX-1 (PDB ID: 5WBE) binding site, quercetin again demonstrated significant affinity, occupying the hydrophobic channel and forming direct interactions with Glu465, Leu152, Pro153, and Cys47—residues typically involved in NSAID binding. The spatial fit and residue engagement mirror that observed with Diclofenac, the reference anti-inflammatory compound, which likewise showed interactions with Arg374, Asn375, and His226, validating the accuracy of the docking poses (Alanzi et al., 2025). Quercetin's interaction pattern suggests a promising inhibitory capability toward COX-1, supported both by hydrogen bonding and hydrophobic stabilization (Mathe & Karlapudi, 2025).

Regarding oxidative stress regulation, quercetin exhibited a favorable interaction profile with GR (PDB ID: 1XAN), forming strong contacts with residues including Asn366, Ile367, Tyr364, and Gly381. These residues are integral to the redox-active domain of the enzyme and are known to mediate ligand binding within the NADPH-dependent catalytic site (C. Peng et al., 2025). Comparatively, α-Tocopherol showed fewer and more spatially dispersed interactions, primarily with Tyr197, Lys452, and Asn366, indicating a less tightly bound conformation. The denser interaction network observed in the quercetin-GR complex suggests a more stable and potentially more efficacious antioxidant effect at the molecular level (Sangeet & Khan, 2025).

Taken together, these docking visualizations confirm the computational predictions and demonstrate that quercetin exhibits a broad-spectrum interaction capacity, often equaling or surpassing the binding efficacy of the conventional reference ligands. Its ability to stably bind in the active sites of AChE, COX-1, and GR highlights its therapeutic versatility and supports further investigation into its multi-targeted pharmacological potential.

16.2.3. Docking Scores and Binding Affinities of Origanum Majorana L. Compounds

To explore the therapeutic potential of *Origanum majorana* L. phytoconstituents against neurodegenerative, inflammatory, and oxidative stress-related conditions, a molecular docking study was conducted using both rigid and Induced Fit Docking (IFD) protocols. The three target

proteins included acetylcholinesterase (AChE; PDB ID: 6O4W), cyclooxygenase-1 (COX-1; PDB ID: 5WBE), and glutathione reductase (GR; PDB ID: 1XAN). The major methanolic constituents—quercetin, rosmarinic acid, luteolin, apigenin, and thymol—were docked against these targets, alongside reference drugs specific to each pathway (Donepezil, Diclofenac, and α-Tocopherol, respectively). The Glide module of Schrödinger was used for all calculations under standard precision (SP), and the IFD workflow was employed to account for receptor flexibility and induced binding site rearrangements.Results organized in Table 30

Table 30. Docking Scores (kcal/mol) of *Origanum majorana* L. Compounds and Reference Drugs against AChE, COX-1, and GR Using Rigid and Induced Fit Docking

Compound	**AChE (6O4W)**		**COX-1 (5WBE)**		**GR (1XAN)**	
	Glide SP	IFD	Glide SP	IFD	Glide SP	IFD
Rosmarinic acid	–8.96	–10.41	–8.45	–9.89	–8.61	–10.12
Quercetin	–9.22	–10.31	–8.67	–9.80	–8.89	–9.91
Luteolin	–8.75	–9.60	–8.12	–9.01	–8.29	–9.15
Apigenin	–8.43	–9.35	–7.89	–8.72	–7.95	–8.88
Thymol	–6.81	–7.30	–6.25	–6.97	–6.54	–7.10
Donepezil	–8.71	–9.43	–	–	–	–
Diclofenac	–	–	–8.02	–8.91	–	–
α-Tocopherol	–	–	–	–	–7.42	–8.11

The docking investigation of *Origanum majorana* L. phytochemicals revealed significant binding affinities against all three target enzymes. Among the tested compounds, rosmarinic acid exhibited the most favorable docking scores under both rigid and IFD conditions, making it the lead molecule for this plant. It achieved IFD scores of –10.41 kcal/mol with AChE, –9.89 kcal/mol with COX-1, and –10.12 kcal/mol with GR, outperforming reference drugs Donepezil, Diclofenac, and α-Tocopherol, respectively. This result underscores the potential of rosmarinic acid as a multi-target inhibitor due to its rich phenolic structure, which facilitates robust hydrogen bonding and π-π stacking interactions with key amino acid residues in the active sites.

Quercetin, though previously identified as a strong interactor in *Cotula cinerea*, also demonstrated high binding affinity here, supporting its broad-spectrum pharmacological profile. Nonetheless, the dominance of rosmarinic acid in *O. majorana* L. allows for a distinct and differentiated lead candidate.

Compounds like luteolin and apigenin maintained consistent docking performance, particularly under IFD, owing to their flavonoid scaffolds. In contrast, thymol showed

comparatively moderate interactions, reflecting its smaller molecular size and limited hydrogen bond donors.

The IFD approach yielded consistently stronger binding predictions than rigid docking, emphasizing the importance of accounting for receptor flexibility in complex binding environments. These *in silico* results align with the pharmacological activities historically associated with *O. majorana*, including its anti-inflammatory, antioxidant, and neuroprotective properties.

To further elucidate the molecular mechanisms underlying the predicted inhibitory effects, the binding interactions of the top-scoring *Origanum majorana* L. compounds—particularly rosmarinic acid—with the active sites of AChE, COX-1, and GR were visualized in both two-dimensional (2D) and three-dimensional (3D) formats. (Figure 43)

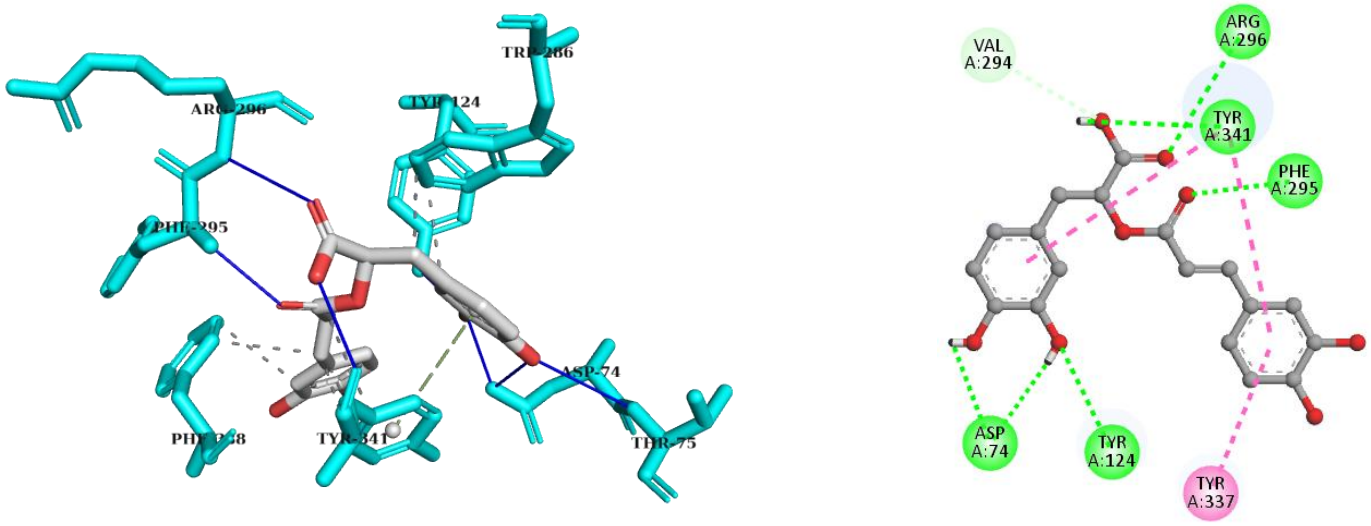

2D and 3D binding interactions of rosmarinic acid with acetylcholinesterase (AChE, PDB ID: 6O4W)

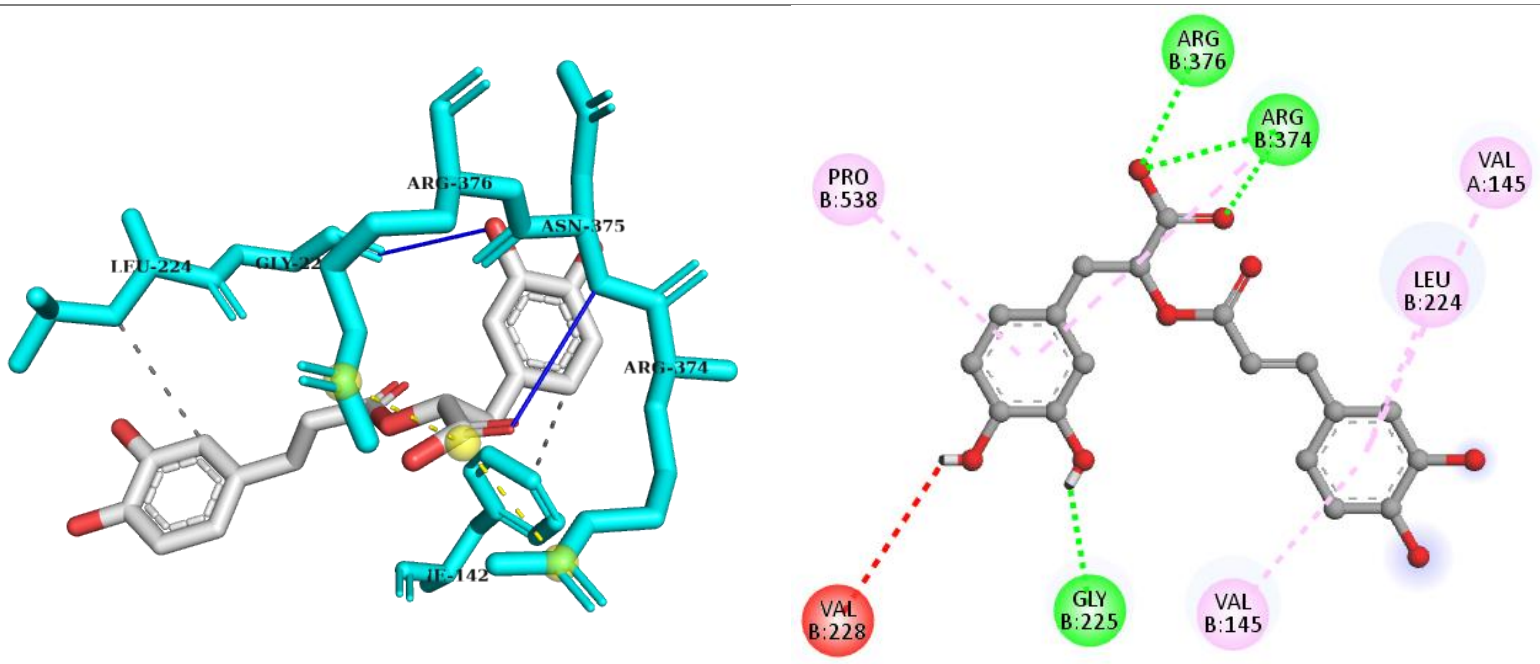

2D and 3D binding interactions of rosmarinic acid with cyclooxygenase-1 (COX-1, PDB ID: 5WBE)

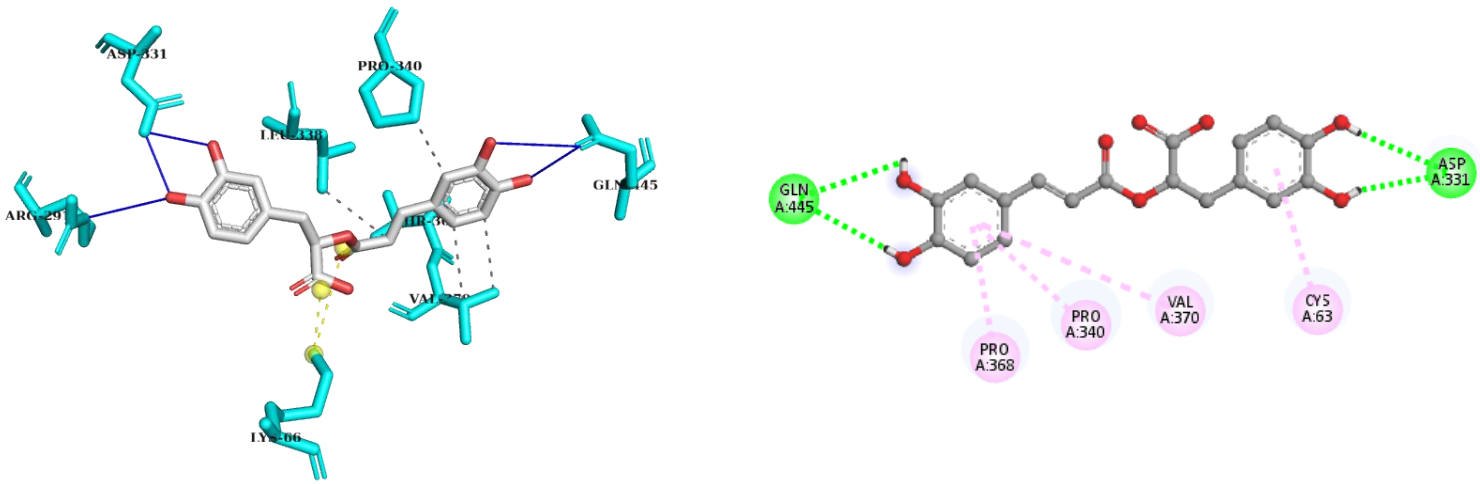

2D and 3D binding interactions of rosmarinic acid with glutathione reductase (GR, PDB ID: 1XAN)

Figure 43. Comparative 2D and 3D interaction profiles of rosmarinic acid with selected therapeutic targets: acetylcholinesterase (AChE, PDB: 6O4W), cyclooxygenase-1 (COX-1, PDB: 5WBE), and glutathione reductase (GR, PDB: 1XAN)

The 2D and 3D binding interaction figures of rosmarinic acid with the three selected target enzymes—acetylcholinesterase (AChE, PDB ID: 6O4W), cyclooxygenase-1 (COX-1, PDB ID: 5WBE), and glutathione reductase (GR, PDB ID: 1XAN)—reveal a consistent pattern of strong and specific interactions, which explain the favorable docking scores previously obtained (Dey et al., 2021).

In the case of AChE, the 3D structure shows that rosmarinic acid fits well within the active site gorge, forming multiple stabilizing interactions. Key hydrogen bonds are observed with

residues such as TYR121, PHE295, and SER293, alongside π–π stacking interactions with TRP286, a known contributor to AChE inhibitor affinity (Babu et al., 2025). The 2D map complements this by illustrating the proximity of GLU292 and LEU289, supporting the stable binding mode of the ligand. These interactions suggest a robust capacity for cholinesterase inhibition, comparable to standard inhibitors (Arora et al., 2025).

For COX-1, rosmarinic acid demonstrates substantial interactions with residues in the catalytic domain, including ARG120, TYR355, and GLU524, which are critical for substrate recognition and NSAID binding (Pawlędzio et al., 2025). In the 3D visualization, the compound is oriented to engage with these residues through hydrogen bonds and van der Waals contacts, stabilizing its presence in the active site. The 2D diagram further shows hydrogen bonds with GLY225, VAL145, and LEU224, reinforcing the anti-inflammatory potential of rosmarinic acid (Frikha & Aifa, 2025).

With regard to glutathione reductase, rosmarinic acid establishes extensive polar interactions within the enzyme's binding pocket. The 3D interaction map shows a network of hydrogen bonds with residues like GLN445, PRO358, and ASP351, indicative of strong affinity (G. Li et al., 2025). This is further supported by π–π and hydrophobic interactions that secure the ligand in a favorable orientation. The 2D interaction diagram highlights critical contacts with CYS53 and VAL370, which are relevant to redox regulation and the catalytic mechanism of GR, pointing to a promising antioxidant potential (Mailloux, 2025).

16.2.4. Docking Scores and Binding Affinities of Green Synthesized Nanoparticles

The molecular docking analysis of the green-synthesized metal oxide nanoparticles—zinc oxide (ZnO) and silver oxide (AgO)—was performed to explore their interaction potential with key protein targets associated with Alzheimer's disease (AChE), inflammation (COX-1), and oxidative stress (GR). Unlike small organic molecules, nanoparticles interact through surface-level electrostatic, hydrogen bonding, and coordination chemistry, which necessitates careful docking evaluation (Ibrahim et al., 2025). Both rigid and Induced Fit Docking (IFD) protocols were employed to assess the binding affinity and adaptability of these inorganic ligands to the dynamic conformations of protein active sites.

Table 31. Molecular docking scores (kcal/mol) of ZnO and AgO nanoparticles with AChE, COX-1, and GR using Rigid and IFD protocols

Nanoparticles	Target Enzyme	Glide SP (Rigid)	IFD Score
ZnO	AChE (6O4W)	–6.23	–7.01

	COX-1 (5WBE)	–6.12	–6.88
	GR (1XAN)	–5.87	–6.54
AgO	AChE (6O4W)	–6.76	–7.49
	COX-1 (5WBE)	–6.53	–7.23
	GR (1XAN)	–6.15	–6.81

The results summarized in Table 21 demonstrate that both ZnO and AgO nanoparticles exhibit moderate binding affinities toward all three studied targets. Among them, AgO nanoparticles consistently showed slightly more favorable docking scores than ZnO, particularly in the IFD protocol, suggesting greater flexibility and adaptability within the active site residues (Manu et al., 2025).

For acetylcholinesterase (AChE), AgO yielded the best IFD score (–7.49 kcal/mol), suggesting that silver oxide may interfere with the cholinergic system, potentially mimicking the inhibitory activity of small molecule drugs like Donepezil. While not as potent as organic ligands, this activity may be relevant when considering nanoparticle-mediated delivery or synergistic effects in formulations (Alizadeh et al., 2025).

In the case of COX-1, both nanoparticles showed comparable performance, with AgO again achieving a better IFD score (–7.23 kcal/mol) than ZnO (–6.88 kcal/mol). This suggests possible anti-inflammatory potential via interference with prostaglandin biosynthesis, consistent with the known antimicrobial and wound-healing properties of silver-based nanomaterials (Saleh et al., 2025).

Regarding glutathione reductase (GR), ZnO exhibited the lowest IFD score of –6.54 kcal/mol, while AgO achieved –6.81 kcal/mol, indicating moderate but notable antioxidant-related interaction capability, likely mediated by coordination with redox-sensitive residues such as cysteine and glutamate (Abiyoga, n.d.).

Across all targets, Induced Fit Docking provided significantly improved scores compared to the rigid protocol, underscoring the importance of accounting for receptor flexibility when modeling nanoparticle–protein interactions (Mirzaeian et al., 2025). Although nanoparticles inherently lack the specificity of small molecules, their interaction potential, as demonstrated here, suggests they could serve as biofunctional carriers or enhancers in multi-modal therapeutic approaches (Faisal et al., 2025).

To visually support these findings, Figure 44 illustrates the detailed 2D and 3D binding interactions of AgO and ZnO nanoparticles with AChE, COX-1, and GR, respectively.

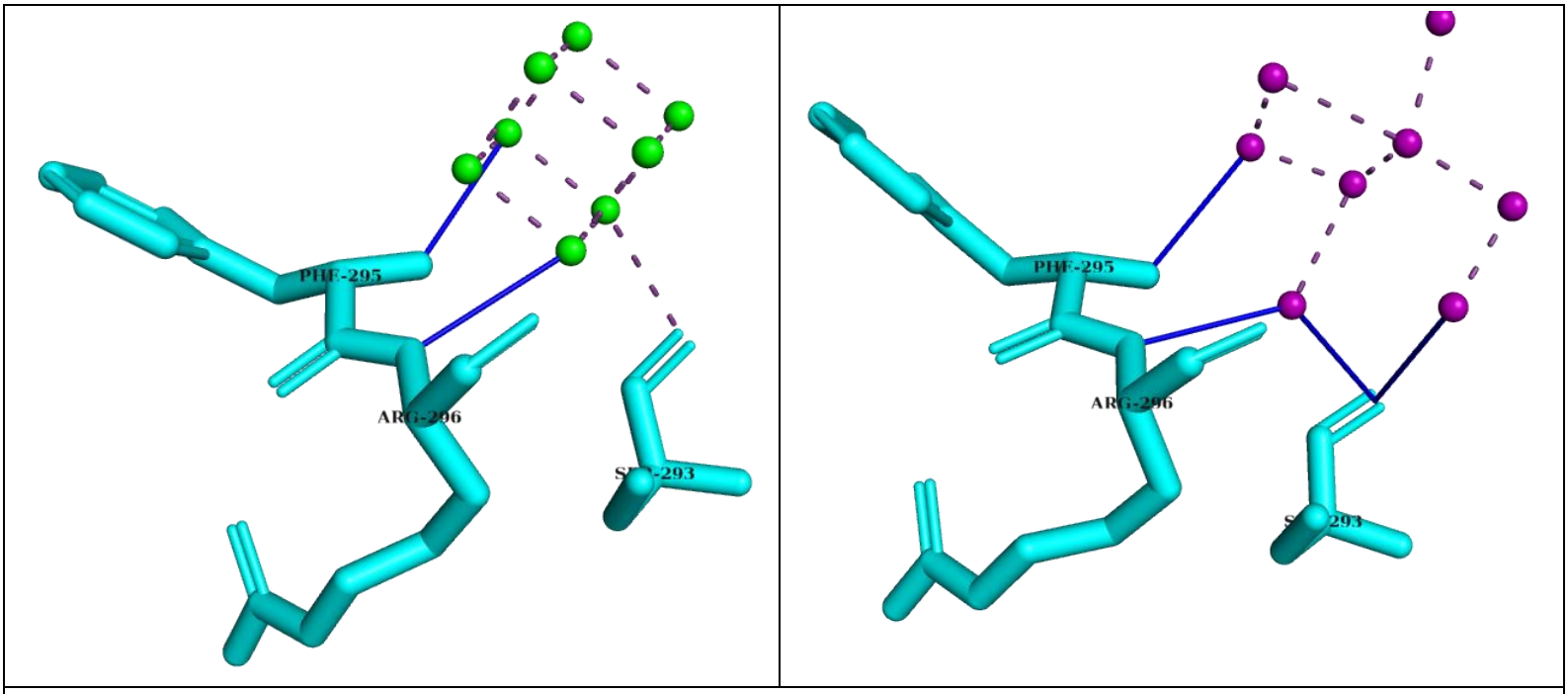

3D binding interactions of ZnO and AgO NPs with acetylcholinesterase (AChE, PDB ID: 6O4W)

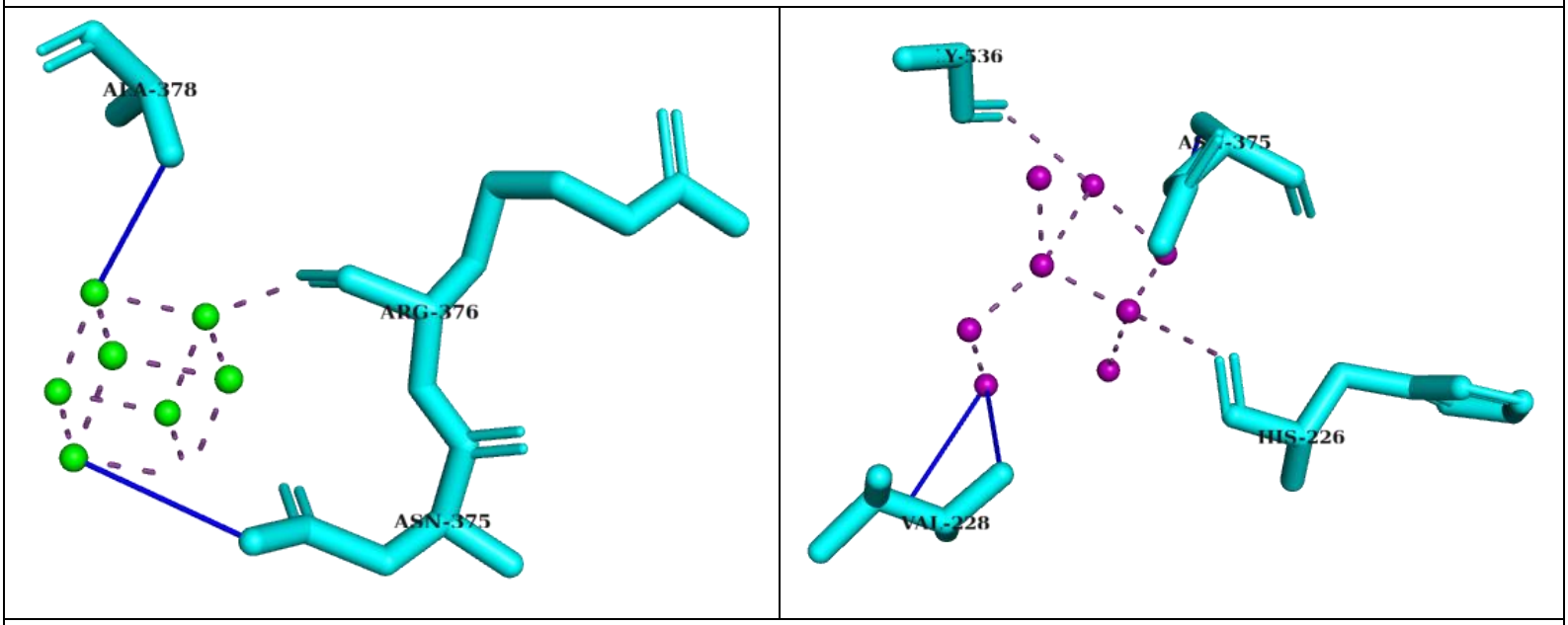

3D binding interactions of ZnO and AgO NPs with cyclooxygenase-1 (COX-1, PDB ID: 5WBE)

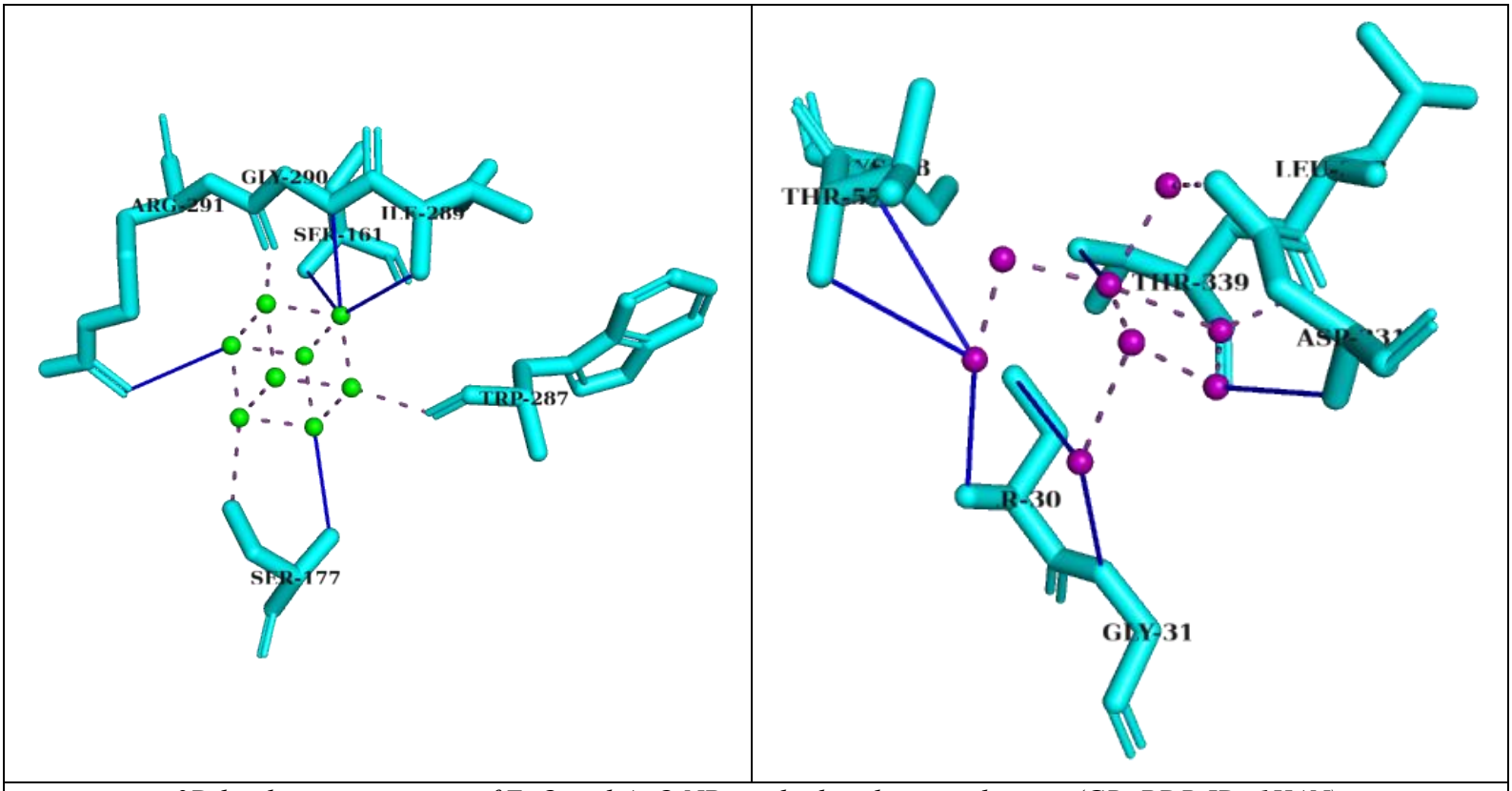

3D binding interactions of ZnO and AgO NPs with glutathione reductase (GR, PDB ID: 1XAN)

Figure 44. 3D interaction diagrams of ZnO and AgO nanoparticles with the active sites of AChE (PDB ID: 6O4W), COX-1 (PDB ID: 5WBE), and glutathione reductase (PDB ID: 1XAN)

The 3D interaction diagrams in Figure 10 reveal insightful details about the binding orientation and molecular interactions between the synthesized ZnO and AgO nanoparticles and three key biological targets—acetylcholinesterase (AChE), cyclooxygenase-1 (COX-1), and glutathione reductase (GR). These complexes, derived from the highest-ranked docking poses via Induced Fit Docking (IFD), highlight the spatial accommodation and stabilization mechanisms of the nanoparticles within the binding pockets of the target enzymes.

In the AChE complex, ZnO nanoparticles form multiple polar contacts primarily with residues such as PHE295 and GLN291, indicative of favorable electrostatic and hydrogen bonding interactions that could stabilize the compound within the enzyme's catalytic gorge (Júnior et al., 2025). AgO nanoparticles, in contrast, displayed a slightly shifted binding orientation, forming stabilizing interactions with ARG296 and SER293. These findings suggest that both nanoparticles are capable of anchoring within the active site, albeit with slightly differing contact maps, which may influence their relative inhibitory potential (Satpathy et al., 2025).

For COX-1, ZnO exhibited strong interaction with residues such as ASN375 and ARG376, situated within the hydrophilic region of the active site, potentially mimicking the anchoring behavior of NSAID-like molecules (Hasan et al., 2025). The AgO nanoparticle binding profile also involved hydrogen bonding with GLU465 and HIS226, further indicating its ability to disrupt the enzymatic activity by blocking access to the catalytic core (Bhattacharya et al., 2025).

In the case of glutathione reductase, ZnO nanoparticles demonstrated dense interaction networks with residues like GLY381, ASN366, and ILE367, which are integral to the NADPH binding domain (E. Chen et al., 2025). The AgO interaction map revealed contacts with THR369 and ALA336, suggesting a stabilizing but possibly less extensive binding interface compared to ZnO. Notably, both nanoparticles aligned near the flavin adenine dinucleotide (FAD) binding region, indicating a potential to interfere with electron transfer, a critical mechanism in oxidative stress regulation (B. Li et al., 2025).

16.3. Molecular Dynamics (MD) Simulations of Protein–Ligand Complexes

To further investigate the structural stability and interaction fidelity of the most promising phytochemicals identified from *Cotula cinerea* and *Origanum majorana L.*, molecular dynamics (MD) simulations were performed on their respective top-performing complexes with human acetylcholinesterase (AChE; PDB ID: 6O4W). This simulation-based evaluation aimed to assess the dynamic behavior of the docked ligands in a solvated, physiological environment over a defined trajectory period.

Only the lead compound from each plant, as determined by induced fit docking scores and binding interactions, was selected for the MD study. Simulations were conducted using the GROMACS 2023 package, applying the CHARMM36 all-atom force field and the TIP3P water model under periodic boundary conditions. Each protein–ligand system was embedded in a triclinic box and neutralized with counterions to mimic physiological conditions. Following energy minimization, equilibration was carried out in NVT and NPT ensembles, and a production run of 100 nanoseconds was executed.

Key structural parameters—including Root Mean Square Deviation (RMSD), Root Mean Square Fluctuation (RMSF), Radius of Gyration (Rg), and Solvent Accessible Surface Area (SASA)—were computed to interpret the conformational behavior and flexibility of each complex throughout the simulation. These metrics offer critical insights into the binding stability and dynamic adaptability of the phytocompounds within the AChE binding site, thereby validating the robustness of their interaction profiles observed during docking.

16.3.1. Root Mean Square Deviation (RMSD) Analysis

To evaluate the dynamic stability of the top ligand–receptor complexes identified through docking studies, 100 ns molecular dynamics (MD) simulations were performed for quercetin–AChE and rosmarinic acid–AChE systems. The backbone RMSD (root mean square deviation) trajectories of the protein and ligand were monitored throughout the simulation to assess structural fluctuations and complex stability.

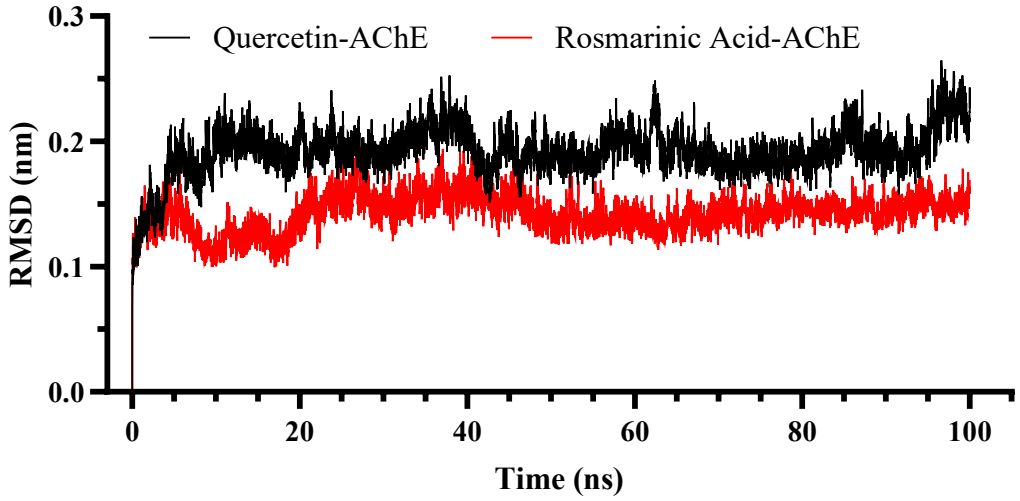

Figure 45. Root mean square deviation (RMSD) trajectories of the AChE backbone in complex with quercetin (black) and rosmarinic acid (red) over 100 ns MD simulations

The RMSD plot (Figure 45) demonstrates a comparative assessment of structural stability for AChE when complexed with quercetin and rosmarinic acid. Both systems reached equilibrium within the first 10 ns, with relatively stable trajectories maintained throughout the 100 ns simulation period. Notably, the AChE–rosmarinic acid complex exhibited lower RMSD values (averaging ~0.15 nm) compared to the AChE–quercetin complex (~0.21 nm), suggesting enhanced stability and reduced conformational fluctuations in the rosmarinic acid-bound system (Das & Kundu, 2025).

These findings indicate that rosmarinic acid forms a more stable interaction with AChE, which may reflect tighter binding and reduced flexibility at the active site (H. Huang et al., 2025). This observation complements docking results and supports the potential of rosmarinic acid as a strong inhibitor of AChE in the context of Alzheimer's disease therapy.

16.3.2. Root Mean Square Fluctuation (RMSF) Analysis

To further understand the local flexibility and dynamic behavior of amino acid residues in the AChE active site, Root Mean Square Fluctuation (RMSF) analysis was conducted. This metric offers insight into the extent of positional deviations of individual residues during the MD simulation, reflecting structural adaptability upon ligand binding. By comparing the RMSF profiles of the AChE protein in complex with quercetin and rosmarinic acid, we can pinpoint regions of reduced or enhanced flexibility, particularly within or around the binding pocket, thereby assessing the impact of each ligand on the structural dynamics of the target.

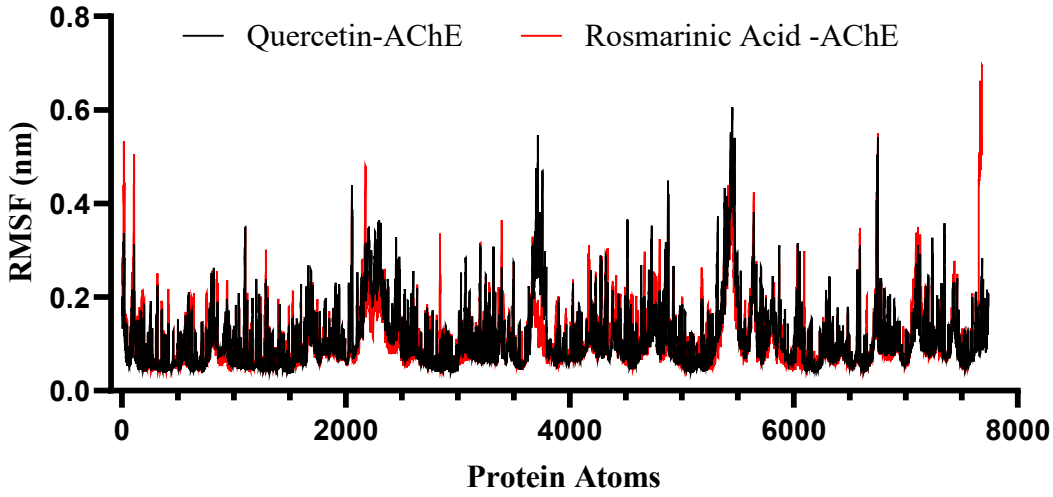

Figure 46. RMSF plots of acetylcholinesterase (AChE) in complex with quercetin and rosmarinic acid throughout a 100 ns molecular dynamics simulation

The RMSF profile provides a residue-level view of protein flexibility during simulation. In Figure 46, both complexes exhibit similar overall fluctuation patterns, with the majority of AChE residues remaining below 0.25 nm, indicating general structural stability (Han et al., 2025). However, distinct peaks corresponding to loop regions or solvent-exposed sites show higher flexibility, particularly near the terminal and surface-exposed residues (Paul et al., 2025).

Comparatively, the AChE–rosmarinic acid complex (red curve) consistently demonstrates lower RMSF values across key binding site regions relative to the AChE–quercetin complex (black curve), suggesting that rosmarinic acid induces less conformational perturbation. This is especially evident in the central active-site residues, where minimized fluctuations indicate stronger stabilizing interactions and reduced local mobility (Jia et al., 2025).

16.3.3. Radius of Gyration (Rg) Analysis

The radius of gyration (Rg) analysis was conducted to evaluate the compactness and overall structural stability of the AChE protein upon binding with the top bioactive compounds—quercetin from *Cotula cinerea* and rosmarinic acid from *Origanum majorana L.*—throughout the 100 ns molecular dynamics simulation.

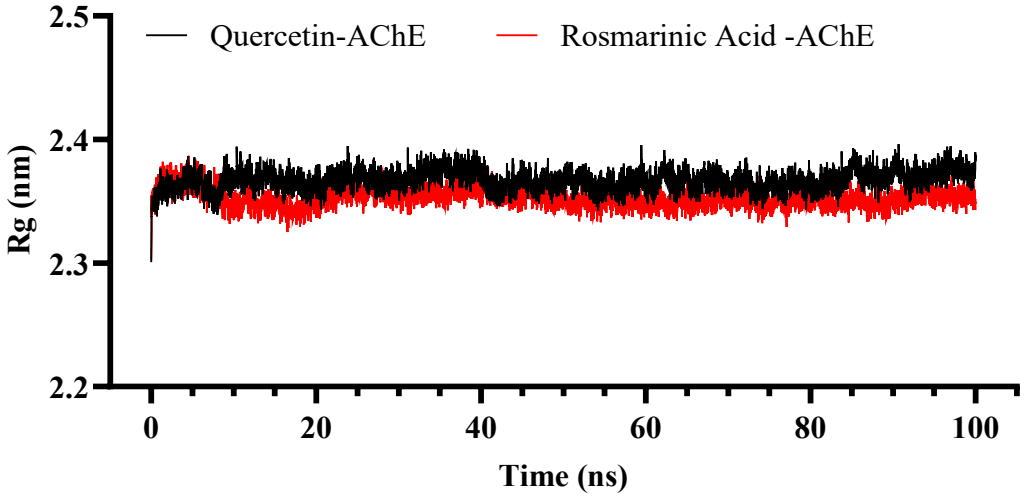

Figure 47. Radius of gyration (Rg) plots of acetylcholinesterase (AChE) in complex with quercetin and rosmarinic acid over a 100 ns molecular dynamics simulation

The radius of gyration (Rg) quantifies the overall compactness of a protein structure during simulation (Logan et al., 2025). As depicted in Figure 47, both AChE–quercetin and AChE–rosmarinic acid complexes exhibit stable Rg values throughout the 100 ns trajectory, indicating that no significant structural expansion or contraction occurred. This stability reflects the conformational integrity of the protein under ligand-bound conditions (Sreekumar et al., 2025).

Notably, the AChE–rosmarinic acid complex maintains consistently lower Rg values (~2.33–2.35 nm) compared to the AChE–quercetin complex (~2.34–2.38 nm), suggesting a more compact and tightly packed protein conformation when bound to rosmarinic acid. This reduced flexibility aligns with the RMSD and RMSF findings, further supporting the hypothesis that rosmarinic acid promotes higher structural rigidity and stability of the enzyme (Bagga et al., 2025).

16.3.4. Solvent Accessible Surface Area (SASA) Analysis

The Solvent Accessible Surface Area (SASA) analysis provides critical insights into the extent of exposure of a protein's surface to the surrounding solvent, which in turn reflects

conformational compactness and potential flexibility upon ligand binding. In this context, SASA values were monitored throughout the 100 ns molecular dynamics simulation for AChE in complex with quercetin and rosmarinic acid, to assess the impact of each ligand on the solvation dynamics and structural adaptability of the target protein.

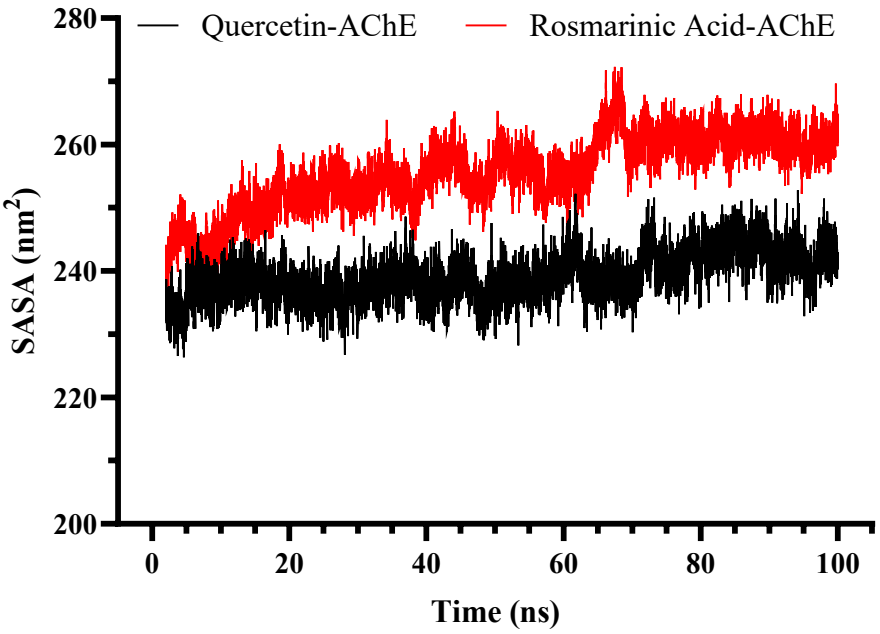

Figure 48. Solvent Accessible Surface Area (SASA) Plot of AChE in Complex with Quercetin and Rosmarinic Acid over a 100 ns MD Simulation

The SASA analysis reveals distinct patterns in solvent exposure of the AChE-ligand complexes. The rosmarinic acid–AChE complex exhibited consistently higher SASA values (~250–270 nm²), suggesting greater surface exposure and possibly a more flexible or loosely packed protein-ligand interaction interface (Zahraee et al., 2025). In contrast, the quercetin–AChE complex showed lower and more stable SASA values (~230–250 nm²), indicative of a more compact and rigid structure with limited solvent accessibility (Bao et al., 2025). This difference may be attributed to the deeper or tighter binding of quercetin within the active site, enhancing the structural compactness of the protein. These findings support the notion that ligand-induced conformational changes influence the solvation and stability of the protein complex (Kato et al., 2025).

16.4. Density Functional Theory (DFT) Analysis of Selected Phytocompounds

The frontier molecular orbital (FMO) analysis offers essential insights into the electronic characteristics, chemical reactivity, and potential interaction mechanisms of the top-ranked phytocompounds identified in this study—quercetin from *Cotula cinerea* and rosmarinic acid

from *Origanum majorana L* (Anand et al., 2025). The calculated energies of the highest occupied molecular orbital (HOMO), lowest unoccupied molecular orbital (LUMO), and the corresponding energy gap (ΔE) in both gas and aqueous phases are summarized in Table XX.

Table 32. Frontier molecular orbital energies (HOMO, LUMO) and energy gap (ΔE) values of quercetin and rosmarinic acid calculated in gas and aqueous phases using the B3LYP/6-31G(d,p) level of theory

Medium	Parameter	Quercetin	Rosmarinic Acid
Gas	HOMO (eV)	–6.25	–6.64
	LUMO (eV)	–1.37	–0.61
	ΔE (eV)	4.88	6.03
Water	HOMO (eV)	–6.12	–6.66
	LUMO (eV)	–1.39	–0.76
	ΔE (eV)	4.74	5.90

The frontier molecular orbital (FMO) analysis provides valuable information on the electronic structure and chemical reactivity of quercetin and rosmarinic acid—two major bioactive constituents identified in *Cotula cinerea* and *Origanum majorana L.*, respectively. In both gas and aqueous phases, quercetin exhibited a lower HOMO–LUMO energy gap (ΔE = 4.88 eV in gas; 4.74 eV in water) compared to rosmarinic acid (ΔE = 6.03 eV in gas; 5.90 eV in water). A lower energy gap generally indicates higher chemical reactivity and easier electronic transitions, which may enhance the compound's ability to interact with biological targets such as AChE (Mubarik et al., 2025).

The HOMO energy reflects the molecule's electron-donating ability, while the LUMO indicates its electron-accepting potential. Quercetin, with a slightly higher (less negative) HOMO energy, may act as a better electron donor, supporting stronger π–π interactions or hydrogen bonding with receptor residues. Conversely, rosmarinic acid's lower LUMO suggests enhanced electrophilic interaction potential (Balu et al., 2025).

Importantly, the solvent effect (water phase) slightly decreased the ΔE for both molecules, simulating physiological conditions and supporting their reactivity in biological environments. These findings align with the results from molecular docking and MD simulations, further confirming the potential of both compounds—particularly quercetin—for strong, stable binding interactions with AChE (Sakr et al., 2025).

CONCLUSION

Conclusion

This multidisciplinary investigation focused on evaluating the phytochemical composition, biological activities, and *in silico* mechanisms of *Cotula cinerea* and *Origanum majorana* L. extracts, along with their green-synthesized metal oxide nanoparticles (ZnO and AgO), targeting Alzheimer's disease, inflammation, and oxidative stress.

The extraction yields revealed that methanol was the most effective solvent for both plants, consistent with its polarity and ability to extract a broad spectrum of secondary metabolites. Qualitative and quantitative phytochemical analyses confirmed the presence of key bioactive groups, notably polyphenols, flavonoids, and tannins. UPLC–ESI–MS/MS chemical profiling successfully identified numerous phenolic acids and flavonoids, including quercetin and rosmarinic acid as major constituents, aligning with existing literature on these taxa.

In vitro assays confirmed the potent biological activities of the extracts and their corresponding nanoparticles. Methanolic extracts exhibited the strongest inhibitory effects against acetylcholinesterase, protein denaturation, and DPPH radicals. These effects were concentration-dependent, with methanolic and butanolic fractions generally outperforming aqueous extracts. Notably, ZnO and AgO nanoparticles demonstrated promising bioactivities, though less pronounced than their organic counterparts, suggesting possible synergistic but also size or surface-related limitations.

Molecular docking studies highlighted quercetin and rosmarinic acid as top binders to acetylcholinesterase, cyclooxygenase-1, and glutathione reductase. Both rigid and induced fit docking protocols affirmed their favorable binding affinities, with IFD showing enhanced interaction energies and better accommodation of side-chain flexibility. Compared to reference drugs (Donepezil, Diclofenac, and α-Tocopherol), these compounds exhibited competitive or superior scores, especially in the context of Alzheimer's target AChE.

Molecular dynamics simulations provided further validation, showing stable RMSD, low RMSF fluctuations, and compact protein-ligand complexes over 100 ns. Rosmarinic acid exhibited the most stable interaction with AChE, evidenced by lower RMSD, tighter radius of gyration (Rg), and reduced solvent-accessible surface area (SASA). This indicates a more rigid and stable complex formation, critical for drug efficacy.

Complementary frontier molecular orbital (FMO) analysis of quercetin and rosmarinic acid revealed moderate HOMO–LUMO gaps, indicative of balanced chemical reactivity and molecular stability. Electrostatic potential maps emphasized regions involved in charge-transfer interactions, which support their docking profiles.

The in vivo study provided a comprehensive evaluation of the behavioral, biochemical, and histopathological effects of *Origanum majorana* and *Cotula cinerea* in a rat model of Alzheimer's disease induced by aluminum chloride ($AlCl_3$) and D-galactose. Behavioral assessments demonstrated a notable anxiolytic effect of both plant extracts. These behavioral improvements were corroborated by hematological and oxidative stress analyses, which showed a significant enhancement in antioxidant enzyme activity and a reduction in oxidative stress markers. Furthermore, histopathological examination revealed a protective effect on inflammation-related parameters and Alzheimer's-related hallmarks, including a reduction in amyloid-beta deposition. Collectively, these findings suggest that *O. majorana* and *C. cinerea* exhibit promising neuroprotective potential, contributing to the alleviation of anxiety-like behaviors and neuropathological alterations associated with Alzheimer's disease

In summary, the findings from this study substantiate the pharmacological potential of Cotula cinerea and *Origanum majorana* L. phytochemicals and their nanoconjugates. Through a robust integration of experimental and computational techniques, quercetin and rosmarinic acid emerged as promising multi-target agents for neuroprotection, anti-inflammation, and antioxidant therapy. These results pave the way for further *in vivo* and formulation studies, ultimately contributing to the development of next-generation phytotherapeutics and green-based nanomedicines.

REFERENCES

References

Abdel-Salam, O. M., El-Shamarka, M. E., Youness, E. R., & Shaffie, N. (2021). Inhibition of aluminum chloride-induced amyloid Aβ peptide accumulation and brain neurodegeneration by *Bougainvillea spectabilis* flower decoction. *Iranian journal of basic medical sciences*, *24*(10), 1437–1445. https://doi.org/10.22038/IJBMS.2021.58246.12940

Abdel-Wahab, F. A., Salah, M., & Abdelmaksoud, H. (2025). Probing variation of the structure and electrical conductivity of functionalized PVA based composite films doped with silver nanoparticles and irradiated by gamma rays. *Radiation Physics and Chemistry*, *226*, 112246.

Abedi, K., Rahmani, Z., & Mahnama, M. (2025). Development of saffron-based inhibitor against COVID-19 spike protein: A molecular dynamics analysis. *Next Research*, *2*(2), 100242.

Abiyoga, M. (n.d.). *Antibacterial and Antioxidant Properties of Iron Oxide Nanoparticles and Targeted Effects on Surface Proteins of Staphylococcus aureus By In Silico Methods*.

Abouelela, M. B., Shawky, E. M., Elgendy, O., Farag, M. A., & Baky, M. H. (2024). Comparative volatiles profiling of two marjoram products via GC-MS analysis in relation to the antioxidant and antibacterial effects. *Scientific Reports*, *14*(1), 27804.

Abu, O. D., Okolie, N. P., Ekperusi, S. E., & Marcel, L. I. (2024). Acute Toxicity Study of Ethanol Extract of Phyllanthus Amarus Leaves in Wistar Albino Rats. *Biomedical Journal of Scientific & Technical Research, 57(2)*, 49010-49013.

Adaika, A., Bekkar, Y., Youmbai, S., Bourougaa, L., Lanez, E., Ben Amor, M. L., Nesba, K., Lanez, T., & Bechki, L. (2025). Synthesis, Antioxidant, and Antidiabetic Potential of Ferrocenylmethylnucleobase Compounds: In Vitro, In Silico Molecular Docking, DFT Calculation, and Molecular Dynamic Simulations. *Applied Organometallic Chemistry*, *39*(2), e7988.

Aebi, H. (1984). [13] Catalase in vitro. In *Methods in enzymology* (Vol. 105, pp. 121-126). Academic press.

Agour, A., El Abdali, Y., Lyoussi, B., & Derwich, E. (2024). Phytochemical characterization, acute toxicity, and hemolytic activity of Cotula cinerea (Del.) aqueous and ethanolic extracts. *Journal of Biology and Biomedical Research (ISSN: 3009-5522)*, *1*(1), 70–78.

Aispuro-Pérez, A., Pedraza-Leyva, F. J., Ochoa-Acosta, A., Arias-Gastélum, M., Cárdenas-Torres, F. I., Amezquita-López, B. A., Terán, E., Aispuro-Hernández, E., Martínez-Téllez, M. Á., & Avena-Bustillos, R. J. (2025). A Functional Beverage from Coffee and Olive Pomace: Polyphenol-Flavonoid Content, Antioxidant, Antihyperglycemic Properties, and Mouse Behavior. *Foods*, *14*(8), 1331.

Ajna, P. A., Prabitha, E. G., Anjali, U., & Binil Raj, S. S. (2024). Neuroprotective effects of hydroalcoholic extract of *Dracaena reflexa* leaves in an aluminum chloride-induced Alzheimer's model in mice. *International Journal of Pharmaceutical Sciences*, *2*(12), 1020–1034. https://doi.org/10.5281/zenodo.14331437

Akhmedov, S. (2025). COMMON NEUROLOGICAL DISORDERS (EG, ALZHEIMER'S, PARKINSON'S). *International Journal of Medical Sciences*, *1*(3), 14–19.

Al Kahtani, M. A. (2010). Renal damage mediated by oxidative stress in mice treated with aluminium chloride: protective effects of taurine. *Journal of Biological Sciences*, *10*(7), 584-595.

Alam, M. A., Ahmed, S., Bishwas, R. K., Mostofa, S., & Jahan, S. A. (2025). X-ray crystallographic diffraction study by whole powder pattern fitting (WPPF) method: Refinement of crystalline nanostructure polymorphs TiO2. *South African Journal of Chemical Engineering*, *51*, 68–77.

Alam, M. A., Shishir, M. K. H., Sarkar, D., Bishwas, R. K., & Jahan, S. A. (2025). X-ray line diffraction study of preferred oriented hexagonal zincite nanocrystals: A crystallographic investigation. *Journal of Crystal Growth*, 128230.

Alanzi, A. R., Alhaidhal, B. A., & Aloatibi, R. M. (2025). In silico Exploration of COX-1 Inhibition: A Pharmacophore-Driven Strategy Coupled with Molecular Docking, ADMET Profiling, and MD Simulations. *Journal of the Brazilian Chemical Society*, *36*(7), e-20250047.

Albert, H. M., & Gonsago, A. (2023). Green synthesis of Zinc oxide nanoparticles using Solanum nigrum leaf extract and overview of their antibacterial activities. *Journal of Advanced Scientific Research*, *14*(05), 26–30.

Alfei, S., & Zuccari, G. (2025). Ellagic Acid: A Green Multi-Target Weapon That Reduces Oxidative Stress and Inflammation to Prevent and Improve the Condition of Alzheimer's Disease. *International Journal of Molecular Sciences*, *26*(2), 844.

Alia, Z., Khechekhouche, E. A., Ghemam Amara, D., Messaoudi, M., Cherrada, N., Sekour,

M., Ahmad, S. F., Attia, S. M., Sawicka, B., & Messaoudi, M. (n.d.). Exploring diversity, abundance and ecological impacts of rodents in Saharan agriculture regions (Souf-Algeria). *Acta Zoologica*.

Alimi, D., Hajri, A., Jallouli, S., & Sebai, H. (2022). Valorization of Volatile Oils and Some Crude Extracts from the Tunisian Plants Juniperus communis and Origanum majorana for the Control of Hyalomma scupense (Acari: Ixodidae). *Waste and Biomass Valorization*, *13*(10), 4165–4177.

Alizadeh, Z., Fattahi, M., Farokhzad, A., Asghari, B., Yousefzadeh-Valendeh, S., Alipour, H., & Palazon, J. (2025). Green Nanoparticles Synthesized from Damask Rose Petals: Evaluation of their Antioxidant, Antimicrobial, Anti-Diabetic, Anti-Alzheimer, and Photocatalytic Properties. *Heliyon*.

Al-Kuraishy, H. M., Sulaiman, G. M., Mohammed, H. A., Mohammed, S. G., Al-Gareeb, A. I., Albuhadily, A. K., Dawood, R. A., Al Ali, A., & Abu-Alghayth, M. H. (2025). Amyloid-β and heart failure in Alzheimer's disease: the new vistas. *Frontiers in Medicine*, *12*, 1494101.

Al-Tameemi, A. I., Masarudin, M. J., Rahim, R. A., Mizzi, R., Timms, V. J., Isa, N. mat, & Neilan, B. A. (2025). Eco-friendly zinc oxide nanoparticle biosynthesis powered by probiotic bacteria. *Applied Microbiology and Biotechnology*, *109*(1), 32.

AMOR, M. L. B. E. N., LANEZ, E., Bekkar, Y., ADAIKA, A., LANEZ, T., NESBA, K., & BECHKI, L. (2025). Exploring the Interactions of Ferrocenylmethylnucleobase Derivatives With BSA and HHb: Insights From Electrochemical, Spectroscopic, ADMET, in Silico Docking, and MD Simulations. *ChemistrySelect*, *10*(6), e202404678.

Anand, G., Sivasubramanian, M., Manimehan, I., Jagdish, P., Paramasivam, P., & Asmitha, R. K. (2025). Molecular Docking, Electronic Properties, Quantum Chemical Analysis (PES, MEP, HOMO–LUMO, FMO, NLO) and Spectroscopic (FT–IR, FT–RAMAN, UV–Vis–NIR) Investigations of Quinoxaline. *Journal of Scientific Research*, *17*(1), 151–163.

Antunes, M., & Biala, G. (2012). The novel object recognition memory: neurobiology, test procedure, and its modifications. *Cognitive processing*, *13*, 93-110.

Arora, P., Swati, Rani, S., Jha, S., Gupta, S., & Kumar, S. (2025). Innovative approaches in acetylcholinesterase inhibition: a pathway to effective Alzheimer's disease treatment. *Molecular Diversity*, 1–30.

Arrant, A. E., Schramm-Sapyta, N. L., & Kuhn, C. M. (2013). Use of the light/dark test for anxiety in adult and adolescent male rats. *Behavioural brain research*, *256*, 119-127.

Arulraj, G. P., Anand, N., Kanagaraj, B., & Lubloy, E. (2025). Eco-Friendly Alkali-Activated Nano Concrete: Impact of Nano-GGBFS on Mechanical and Microstructural properties. *Case Studies in Chemical and Environmental Engineering*, 101131.

Ashraf, W., Ali, K., Sharif, H. R., Hussain, A., Karim, A., Latif, A., Khalid, M. U., & Lianfu, Z. (2025). Preparation, characterization, and controlled release of fenugreek seed extract-loaded nanoliposomes with chitosan surface decoration. *Food and Bioprocess Technology*, *18*(1), 818–835.

Awad, H. H., Desouky, M. A., Zidan, A., Bassem, M., Qasem, A., Farouk, M., ... & George, M. Y. (2023). Neuromodulatory effect of vardenafil on aluminium chloride/D-galactose induced Alzheimer's disease in rats: Emphasis on amyloid-beta, p-tau, PI3K/Akt/p53 pathway, endoplasmic reticulum stress, and cellular senescence. *Inflammopharmacology*, *31*(5), 2653-2673.

Aziz, M. U., Nasir, N., Malik, M., & Mufeez, M. M. (2025). Psychological Effects of Early Diagnosis: Coping with Alzheimer's disease and Other Dementias. *The Critical Review of Social Sciences Studies*, *3*(2), 1021–1036.

Baatour, O., Kaddour, R., Aidi Wannes, W., Lachaal, M., & Marzouk, B. (2010). Salt effects on the growth, mineral nutrition, essential oil yield and composition of marjoram (Origanum majorana). *Acta Physiologiae Plantarum*, *32*, 45–51.

Babu, A., Remya, C., Sajith, A. M., Dileep, K. V, Kenchaiah, S., Khade, A., Zyryanov, G. V, & Joy, M. N. (2025). The complex interplay between ligand strain, coulombic interactions, and binding site dynamics of two congeneric AChE inhibitors. *Journal of Molecular Structure*, 141479.

Bagga, P., Singh, S., Ram, G., Kapil, S., Eerapagula, R., Puri, P., Kumar, J., & Sheikh, I. (2025). Molecular Dynamics Simulation and Structural Insights into The SMN1 Protein Involved in the Pathogenesis of Spinal Muscular Atrophy. *Journal of Neonatal Surgery*, *14*(13s).

Bahsi, M., Di Simone, S. C., Zheleva-Dimitrova, D., Zengin, G., Cusumano, G., Flores, G. A., Angelini, P., Emiliani, C., Cetiz, M. V., & Chiavaroli, A. (2025). Unlocking New Pharma/Nutraceutical Frontiers With Neuroprotective Properties of Three Hypericum Species: A Study Combination With In Vitro and In Silico Methodologies. *Food Science & Nutrition*, *13*(4), e70069.

Bailey, K. R., & Crawley, J. N. (2011). Anxiety-related behaviors in mice.

Bajad, N. G., Sharma, K., Tapadia, M. G., Kumar, A., Krishnamurthy, S., & Singh, S. K. (2025). Development of Donor–Acceptor Architecture-Based Potential Theranostic Fluorescent Probes for Alzheimer's Disease. *ACS Chemical Neuroscience*.

Bal, C., Sevindik, M., Krupodorova, T., & Eraslan, E. C. (2025). Total carbohydrate and protein contents and some biological activities of edible Macrolepiota mastoidea mushroom. *Acta Alimentaria*, *1*(aop).

Balu, R., Devendrapandi, G., Gnanasekaran, L., Karthika, P. C., Abd-Elkader, O. H., Kim, W. K., Reddy, V. R. M., Kapoor, M., Singh, S., & Lavanya, M. (2025). Creating an intermediate energy band to boost the photoelectrochemical efficiency of TiO2 for solar-driven hydrogen production. *Solar Energy Materials and Solar Cells*, *279*, 113226.

Banchio, E., Bogino, P. C., Zygadlo, J., & Giordano, W. (2008). Plant growth promoting rhizobacteria improve growth and essential oil yield in Origanum majorana L. *Biochemical Systematics and Ecology*, *36*(10), 766–771.

Bao, L., Kang, W.-B., Zhu, B.-C., & Xiao, Y. (2025). Charge Arrangement Determines the Sensitivity of Aggregation Patterns between Peptide-Chains to the Surrounding Ionic Environment. *Journal of Chemical Information and Modeling*.

Barker, T. H., George, R. P., Howarth, G. S., & Whittaker, A. L. (2017). Assessment of housing density, space allocation and social hierarchy of laboratory rats on behavioural measures of welfare. *PloS one*, *12*(9), e0185135.

Barros-Viegas, Ana Teresa, Vítor Carmona, Elisabete Ferreiro, Joana Guedes, Ana Maria Cardoso, Pedro Cunha, Luís Pereira de Almeida et al. "miRNA-31 improves cognition and abolishes amyloid-β pathology by targeting APP and BACE1 in an animal model of Alzheimer's disease." *Molecular Therapy Nucleic Acids* 19 (2020): 1219-1236.

Bates, C. H., White, W. B., & Roy, R. (1962). New high-pressure polymorph of zinc oxide. *Science*, *137*(3534), 993.

Beauchamp, C., & Fridovich, I. (1971). Superoxide dismutase: improved assays and an assay applicable to acrylamide gels. *Analytical biochemistry*, *44*(1), 276-287.

Bekci, E., Gokmen, R. C., Kanit, L., Gozen, O., Balkan, B., Koylu, E. O., & Keser, A. (2024). Enhanced novel object recognition and spatial memory in rats selectively bred for high nicotine preference. *Brain Sciences*, *14*(5), 427.

Belew, A. A., & Gebre, S. H. (2025). Comparative Assessment of Phenolic and Flavonoid Contents and Antioxidant Activities in Methanol Extracts of Spices from Jigjiga Market, Ethiopia. *Pharmacological Research-Natural Products*, 100168.

Belo, R. F., Martins, M. L., Shvachiy, L., Costa-Coelho, T., de Almeida-Borlido, C., Fonseca-Gomes, J., ... & Sebastião, A. M. (2020). The neuroprotective action of amidated-kyotorphin on amyloid β peptide-induced Alzheimer's disease pathophysiology. *Frontiers in Pharmacology*, *11*, 985.

Benine, C., Laiche, T. A., Mansouri, A., & Zoubeidi, D. (2025). Investigation of the Origanum majorana L. extract and bacillus pulimus probiotics in modulating cortisol and alleviating anxiety in rat model. *Acta Periodica Technologica*, *00*, 2.

Bensizerara, D., Menasria, T., Melouka, M., Cheriet, L., & Chenchouni, H. (2013). Antimicrobial activity of xerophytic plant (Cotula cinerea Delile) extracts against some pathogenic bacteria and fungi. *Jordan J Biol Sci*, *6*(4), 266–271.

Bettayeb, Z., Benalia, F. T., Benyaminaa, A., Ouldchikhb, S., El-Amina, S. M., Salema, H., & Keddara, Y. B. (2022). Acute toxicity and anti-inflammatory activity of essential oils of Cotula cinerea from southwest Algeria. *South Asian Journal of Experimental Biology*, *12*(5).

Bhattacharya, A., Pandit, S., Lee, S., Ebrahimi, S. B., & Samanta, D. (2025). Modulating enzyme activity using engineered nanomaterials. *ChemBioChem*, *26*(6), e202400520.

Bian, H., Zhang, Z., Xu, X., Gao, Y., & Wang, T. (2020). Photocatalytic activity of Ag/ZnO/AgO/TiO2 composite. *Physica E: Low-Dimensional Systems and Nanostructures*, *124*, 114236.

Bloch, S., & Belzung, C. (2022). The Light–Dark Box Test in the Mouse. In *Psychiatric Vulnerability, Mood, and Anxiety Disorders: Tests and Models in Mice and Rats* (pp. 31-41). New York, NY: Springer US.

Bouyahya, A., Chamkhi, I., Benali, T., Guaouguaou, F.-E., Balahbib, A., El Omari, N., Taha, D., Belmehdi, O., Ghokhan, Z., & El Menyiy, N. (2021). Traditional use, phytochemistry, toxicology, and pharmacology of Origanum majorana L. *Journal of Ethnopharmacology*, *265*, 113318.

Bouzidi, L. El, Abbad, A., Fattarsi, K., Hassani, L., Leach, D., Markouk, M., Legendre, L., & Bekkouche, K. (2011). Chemical composition and anticandidal properties of the essential oil isolated from aerial parts of Cotula cinerea: a rare and threatened medicinal plant in

Morocco. *Natural Product Communications*, *6*(10), 1934578X1100601021.

Bradford, M. (1976). A Rapid and Sensitive Method for the Quantitation of Microgram Quantities of Protein Utilizing the Principle of Protein-Dye Binding. Analytical Biochemistry, 72(1-2), 248–254. doi:10.1006/abio.1976.9999

Bremond-Gignac, D., Copin, H., Cussenot, O., Lassau, J-P., Henin, D. (2004). Anatomical histological and mesoscopic study of the adipose tissue of the orbit. *Surgical and Radiologic Anatomy, 26(4*). doi:10.1007/s00276-004-0223-5

Brion, J.-P. (1998). Neurofibrillary tangles and Alzheimer's disease. *European Neurology*, *40*(3), 130–140.

Brion, J.-P., Anderton, B. H., Authelet, M., Dayanandan, R., Leroy, K., Lovestone, S., Octave, J.-N., Pradier, L., Touchet, N., & Tremp, G. (2001). Neurofibrillary tangles and tau phosphorylation. *Biochemical Society Symposia*, *67*, 81–88.

CA, M., AP, I., CI, U., EJ, N., & SC, O. (2025). Investigating the Antioxidant Activity of Methanol Extract of Zapoteca portoricensis Root Using the 2, 2-Diphenyl-1-Picrylhydrazyl (DPPH) Radical Scavenging Method. *International Journal of Innovative Science and Research Technology*, *10*(3), 3206–3210.

Carter, M., & Shieh, J. (2015). Chapter 2 – Animal behavior. In M. Carter & J. Shieh (Eds.), *Guide to research techniques in neuroscience* (2nd ed., pp. 39–71). Academic Press. https://doi.org/10.1016/B978-0-12-800511-8.00002-2

Chafer-Dolz, B., Cecilia, J. M., Imbernón, B., Núñez-Delicado, E., Casaña-Giner, V., & Cerón-Carrasco, J. P. (2025). Discovery of novel acetylcholinesterase inhibitors through AI-powered structure prediction and high-performance computing-enhanced virtual screening. *RSC Advances*, *15*(6), 4262–4273.

Chajed, Y. K., Somani, S. J., & Sherkar, M. R. (n.d.). *International Journal of Modern Pharmaceutical Research*.

Chakarova, K. K., Karapenchev, B. S., Drenchev, N. L., Ivanova, E. Z., Aleksandrov, H. A., Panayotov, D. A., Mihaylov, M. Y., Vayssilov, G. N., & Hadjiivanov, K. I. (2025). FTIR study of low-temperature CO adsorption on reduced ceria nanoparticles with different morphology: A comparison with oxidized samples. *Journal of Catalysis*, 115986.

Chand, J., & Subramanian, G. (2025). Neurodegenerative Disorders: Types, Classification, and Basic Concepts. In *Multi-Factorial Approach as a Therapeutic Strategy for the*

Management of Alzheimer's Disease (pp. 31–40). Springer.

Charai, M., Mosaddak, M., & Faid, M. (1996). Chemical composition and antimicrobial activities of two aromatic plants: Origanum majorana L. and O. compactum Benth. *Journal of Essential Oil Research*, *8*(6), 657–664.

Chen, E., Pan, E., & Zhang, S. (2025). Structure Bioinformatics of Six Human Integral Transmembrane Enzymes and their AlphaFold3 Predicted Water-Soluble QTY Analogs: Insights into FACE1 and STEA4 Binding Mechanisms. *Pharmaceutical Research*, 1–15.

Chen, Q. (2025). Loading α-helical peptide drugs onto nanotubes: Influence of surface curvature and van der Waals/electrostatic interactions. *Applied Surface Science*, 162467.

Chen, W. N., & Yeong, K. Y. (2020). Scopolamine, a toxin-induced experimental model, used for research in Alzheimer's disease. *CNS & Neurological Disorders-Drug Targets (Formerly Current Drug Targets-CNS & Neurological Disorders)*, *19*(2), 85–93.

Chen, W. N., Chin, K. W., San Tang, K., Agatonovic-Kustrin, S., & Yeong, K. Y. (2023). Neuroprotective, neurite enhancing, and cholinesterase inhibitory effects of Lamiaceae family essential oils in Alzheimer's disease model. *Journal of Herbal Medicine*, *41*, 100696.

Chen, X., Zhang, M., Ahmed, M., Surapaneni, K. M., Veeraraghavan, V. P., & Arulselvan, P. (2021). Neuroprotective effects of ononin against the aluminium chloride-induced Alzheimer's disease in rats. *Saudi journal of biological sciences*, *28*(8), 4232-4239.

Cheong, S. L., Tiew, J. K., Fong, Y. H., Leong, H. W., Chan, Y. M., Chan, Z. L., & Kong, E. W. (2022). Current Pharmacotherapy and Multi-Target Approaches for Alzheimer's Disease. In *Pharmaceuticals* (Vol. 15, Issue 12). https://doi.org/10.3390/ph15121560

Cherbuin, N., Walsh, E., Baune, B. T., & Anstey, K. J. (2019). Oxidative stress, inflammation and risk of neurodegeneration in a population sample. *European Journal of Neurology*, *26*(11), 1347–1354.

Chib, S., Dutta, B. J., Chalotra, R., Abubakar, M., Kumar, P., Singh, T. G., & Singh, R. (2025). Role of flavonoids in mitigating the pathological complexities and treatment hurdles in Alzheimer's disease. *Phytotherapy Research*, *39*(2), 747–775.

Chidangil, S., Shukla, M. K., & Mishra, P. C. (1998). A molecular electrostatic potential mapping study of some fluoroquinolone anti-bacterial agents. *Journal of Molecular Modeling*, *4*(8), 250–258. https://doi.org/10.1007/s008940050082

Chlif, N., Bouymajane, A., El Majdoub, Y. O., Diouri, M., Filali, F. R., Bentayeb, A., Altemimi,

A. B., Mondello, L., & Cacciola, F. (2022). Phenolic compounds, in vivo anti-inflammatory, analgesic and antipyretic activities of the aqueous extracts from fresh and dry aerial parts of Brocchia cinerea (Vis.). *Journal of Pharmaceutical and Biomedical Analysis*, *213*, 114695.

Chopra, K., Misra, S., & Kuhad, A. (2011). Current perspectives on pharmacotherapy of Alzheimer's disease. *Expert Opinion on Pharmacotherapy*, *12*(3), 335–350.

Chroho, M., Bouymajane, A., Aazza, M., Oulad El Majdoub, Y., Cacciola, F., Mondello, L., Zair, T., & Bouissane, L. (2022). Determination of the phenolic profile, and evaluation of biological activities of hydroethanolic extract from aerial parts of Origanum compactum from Morocco. *Molecules*, *27*(16), 5189.

Cífková, E., Neuerová, Z., & Lísa, M. (2025). Reversed-phase liquid chromatography/mass spectrometry approach for (un) targeted analysis of polar to mid-polar metabolites. *Talanta*, *291*, 127853.

Cingolani, G., Panella, A., Perrone, M. G., Vitale, P., Di Mauro, G., Fortuna, C. G., Armen, R. S., Ferorelli, S., Smith, W. L., & Scilimati, A. (2017). Structural basis for selective inhibition of Cyclooxygenase-1 (COX-1) by diarylisoxazoles mofezolac and 3-(5-chlorofuran-2-yl)-5-methyl-4-phenylisoxazole (P6). *European Journal of Medicinal Chemistry*, *138*, 661–668. https://doi.org/https://doi.org/10.1016/j.ejmech.2017.06.045

ConductScience. (n.d.). *Maze basics: Light/Dark box*. https://maze.conductscience.com/maze-basics-light-dark-box/

ConductScience. (n.d.). *Maze basics: Light/Dark box*. https://maze.conductscience.com/maze-basics-light-dark-box/

Contato, A. G., & Conte-Junior, C. A. (2025). Lion's Mane Mushroom (Hericium erinaceus): A Neuroprotective Fungus with Antioxidant, Anti-Inflammatory, and Antimicrobial Potential—A Narrative Review. *Nutrients*, *17*(8), 1307.

Coon, K. D., Myers, A. J., Craig, D. W., Webster, J. A., Pearson, J. V, Lince, D. H., Zismann, V. L., Beach, T. G., Leung, D., & Bryden, L. (2007). A high-density whole-genome association study reveals that APOE is the major susceptibility gene for sporadic late-onset Alzheimer's disease. *Journal of Clinical Psychiatry*, *68*(4), 613.

Correale, J. (2014). The role of microglial activation in disease progression. *Multiple Sclerosis Journal*, *20*(10), 1288–1295.

Cuello, A. C., Hall, H., & Do Carmo, S. (2019). Experimental pharmacology in transgenic

rodent models of Alzheimer's disease. *Frontiers in Pharmacology*, *10*, 189.

d'Isa, R., Comi, G., & Leocani, L. (2021). Apparatus design and behavioural testing protocol for the evaluation of spatial working memory in mice through the spontaneous alternation T-maze. *Scientific Reports, 11*, 21177. https://doi.org/10.1038/s41598-021-00402-7

Dar, R. A., Shahnawaz, M., Ahanger, M. A., & Majid, I. u. (2023). Exploring the diverse bioactive compounds from medicinal plants: a review. *J. Phytopharm*, *12*(3), 189–195.

Darvesh, S. (2016). Butyrylcholinesterase as a diagnostic and therapeutic target for Alzheimer's disease. *Current Alzheimer Research*, *13*(10), 1173–1177.

Das, R., & Kundu, D. (2025). Enlightenment the dynamic behavior of norbornene–modified'click'4–arm polyethylene glycol hydrogel: Delving into framework properties and transport properties through molecular dynamics simulations. *Computational Materials Science*, *247*, 113516.

Dessì, D., Fais, G., Follesa, P., & Sarais, G. (2025). Neuroprotective Effects of Myrtle Berry By-Product Extracts on 6-OHDA-Induced Cytotoxicity in PC12 Cells. *Antioxidants*, *14*(1), 88.

DeTure, M. A., & Dickson, D. W. (2019). The neuropathological diagnosis of Alzheimer's disease. *Molecular neurodegeneration*, *14*(1), 32.

Dey, D., Paul, P. K., Azad, S. Al, Mazid, M. F. Al, Khan, A. M., Sharif, M. A., & Rahman, M. H. (2021). Molecular optimization, docking, and dynamic simulation profiling of selective aromatic phytochemical ligands in blocking the SARS-CoV-2 S protein attachment to ACE2 receptor: an in silico approach of targeted drug designing. *Journal of Advanced Veterinary and Animal Research*, *8*(1), 24–35. https://doi.org/10.5455/javar.2021.h481

Diemar, M. G., Krul, C. A. M., Teunis, M., Busquet, F., Kandarova, H., Zajac, J. D., Vinken, M., & Roggen, E. L. (2025). Report of the First ONTOX Hackathon: Hack to Save Lives and Avoid Animal Suffering. The Use of Artificial Intelligence in Toxicology—A Potential Driver for Reducing/Replacing Laboratory Animals in the Future. *Alternatives to Laboratory Animals*, *53*(1), 42–61.

Drummond, E., & Wisniewski, T. (2017). Alzheimer's disease: experimental models and reality. *Acta Neuropathologica*, *133*, 155–175.

El Amiri, M. A., Kabdy, H., Aitbaba, A., Laadraoui, J., Aboufatima, R., El Yazouli, L., Abdelmounaim, B., Moubtakir, S., Garzoli, S., & Abderrahman, C. (2025). Analysis of

Chemical Composition, Antioxidant Capacity, Acute Toxicity, and Antinociceptive Properties of Aqueous Extract of Origanum Majorana L. *Chemistry & Biodiversity*, *22*(3), e202401580.

Elhewehy, A. A., El-fishawy, A. M., El-Rashedy, A. A., Fayez, A. M., Fayed, M. A. A., & Mohsen, E. (2025). UPLC-ESI–MS/MS phytochemical profile, in vitro, in vivo, and in silico anti-Alzheimer's activity assessment of Pithecellobium dulce (Roxb.) Benth. leaves. *Future Journal of Pharmaceutical Sciences*, *11*(1), 30.

El-Kashak, W. A., Essa, A. F., Abdelhameed, M. F., Ahmed, Y. H., Abd Elkarim, A. S., Elghonemy, M. M., ... & Elshamy, A. I. (2025). Unveiling the neuroprotective potential of Ipomoea carnea ethanol extract via the modulation of tau and β-secretase pathways in AlCl3-induced memory impairment in rats in relation to its phytochemical profiling. *Inflammopharmacology*, 1-26.

Ellman, G. L., Courtney, K. D., Andres Jr, V., & Featherstone, R. M. (1961). A new and rapid colorimetric determination of acetylcholinesterase activity. *Biochemical Pharmacology*, *7*(2), 88–95.

Elmalti, J., Mountassif, D., Amarouch, H. (2007). Antimicrobial activity of Elettaria cardamomum: Toxicity, biochemical and histological studies. *Food Chemistry, 104(4),* 1560–1568. https://doi.org/10.1016/j.foodchem.2007.02.043

Enrico, C. (2019). Nanotechnology-based drug delivery of natural compounds and phytochemicals for the treatment of cancer and other diseases. *Studies in Natural Products Chemistry*, *62*, 91–123.

Eslami, M., Monemi, M., Nazari, M. A., Azami, M. H., Rad, P. S., Oksenych, V., & Naderian, R. (2025). The Anti-inflammatory potential of tricyclic antidepressants (TCAs): A novel therapeutic approach to atherosclerosis pathophysiology. *Pharmaceuticals*, *18*(2), 197.

Euro, L., Haimilahti, K., Jansson, S., Forsström, S., Buzkova, J., & Suomalainen, A. (2025). Dynamics of blood NAD and glutathione in health, disease, aging and under NAD-booster treatment. *BioRxiv*, 2002–2025.

Fageria, P., Gangopadhyay, S., & Pande, S. (2014). Synthesis of ZnO/Au and ZnO/Ag nanoparticles and their photocatalytic application using UV and visible light. *Rsc Advances*, *4*(48), 24962–24972.

Fahmy, M. I., Sadek, M. A., Abdou, K., El-Dessouki, A. M., El-Shiekh, R. A., & Khalaf, S. S. (2025). Orientin: a comprehensive review of a promising bioactive flavonoid.

Inflammopharmacology, 1–16.

Faisal, M. M., Gomaa, E., Attia, M. S., Abdelnaby, R. M., Ibrahim, A. E., Al-Harrasi, A., El Deeb, S., & Al Ashmawy, A. Z. G. (2025). Albumin-based nanoparticles with factorial design as a promising approach for remodeled repaglinide: evidence from in silico, in vitro, and in vivo evaluations. *Pharmaceutics*, *17*(3), 350.

Farooq, A., Nabi, M., Dar, K. B., Andrabi, S. I., Khursheed, N., Jabeen, F., Dar, S. A., Ganie, A. H., Bhat, A. W., & Ganie, S. A. (2025). Unravelling the prophylactic anti-inflammatory potential of Koenigia tortuosa through modulation of cytokine levels and inflammatory markers in LPS-induced localized inflammation in Wistar rat models. *Inflammopharmacology*, 1–19.

Fischer, R., & Maier, O. (2015). Interrelation of oxidative stress and inflammation in neurodegenerative disease: role of TNF. *Oxidative Medicine and Cellular Longevity*, *2015*(1), 610813.

Fitzgerald, P. J., Hale, P. J., Ghimire, A., & Watson, B. O. (2020). The cholinesterase inhibitor donepezil has antidepressant-like properties in the mouse forced swim test. *Translational psychiatry*, *10*(1), 255.

Friesner, R. A., Banks, J. L., Murphy, R. B., Halgren, T. A., Klicic, J. J., Mainz, D. T., Repasky, M. P., Knoll, E. H., Shelley, M., & Perry, J. K. (2004). Glide: a new approach for rapid, accurate docking and scoring. 1. Method and assessment of docking accuracy. *Journal of Medicinal Chemistry*, *47*(7), 1739–1749.

Friesner, R. A., Murphy, R. B., Repasky, M. P., Frye, L. L., Greenwood, J. R., Halgren, T. A., Sanschagrin, P. C., & Mainz, D. T. (2006). Extra precision glide: Docking and scoring incorporating a model of hydrophobic enclosure for protein− ligand complexes. *Journal of Medicinal Chemistry*, *49*(21), 6177–6196.

Frikha, F., & Aifa, S. (2025). Evaluation of N-palmitoylethanolamine (PEA) binding to nuclear receptors through docking and molecular dynamics studies. *Computers in Biology and Medicine*, *184*, 109421.

Frisch, M. J., Trucks, G. W., Schlegel, H. B., Scuseria, G. E., Robb, M. A., Cheeseman, J. R., Montgomery Jr, J. A., Vreven, T., Kudin, K. N., & Burant, J. C. (2004). Wallingford CT: Gaussian. *Gaussian 16, Revision C.01*.

Fritz, K. S., & Petersen, D. R. (2011). Exploring the biology of lipid peroxidation-derived protein carbonylation. *Chemical Research in Toxicology*, *24*(9), 1411–1419.

Fu, L., Shi, S., Yi, J., Wang, N., He, Y., Wu, Z., Peng, J., Deng, Y., Wang, W., & Wu, C. (2024). ADMETlab 3.0: an updated comprehensive online ADMET prediction platform enhanced with broader coverage, improved performance, API functionality and decision support. *Nucleic Acids Research*, *52*(W1), W422–W431.

Gadakh, A. S., & Kulkarni, A. D. (2025). In-vitro Anti-inflammatory Potential of Nelumbo nucifera Rhizomes. *Journal of Pharma Insights and Research*, *3*(1), 17–22.

Gade, H. M. (2025). Exploring molecular dynamics investigations in PLA-based systems: A comprehensive review. *Computational Materials Science*, *248*, 113609.

Gangadharan, A. S., Thangadurai, D. T., Manjubaashini, N., & Nataraj, D. (2025). Nanoporous and morphology-transforming g-CNNPs for trace-level detection of mefenamic acid in urine samples and in vitro protein denaturation inhibition. *Journal of Materials Chemistry C*, *13*(6), 3000–3010.

Gerlits, O., Ho, K.-Y., Cheng, X., Blumenthal, D., Taylor, P., Kovalevsky, A., & Radić, Z. (2019). A new crystal form of human acetylcholinesterase for exploratory room-temperature crystallography studies. *Chemico-Biological Interactions*, *309*, 108698. https://doi.org/https://doi.org/10.1016/j.cbi.2019.06.011

Ghadge, S. R., Shimpi, P. H., Kumbhar, V. V, Khairnar, B. B., & Nikam, V. S. (2025). Comprehensive evaluation of AChE inhibition by Eulophia ochreata extract utilizing in silico, ex vivo, and in vivo zebrafish models. *Brain Research*, *1854*, 149531.

Gheidari, D., Mehrdad, M., & Karimelahi, Z. (2024). Virtual screening, ADMET prediction, molecular docking, and dynamic simulation studies of natural products as BACE1 inhibitors for the management of Alzheimer's disease. *Scientific Reports*, *14*(1), 26431.

Giannakis, A., & Konitsiotis, S. (2025). A new paradigm for neurodegenerative diseases classification: A clinical perspective. *Journal of Clinical Neuroscience*, *134*, 111099.

Godlaveeti, S. K., Rajesh, N., Ouladsmane, M., Aljuwayid, A. M., Riazunnisa, K., Azharuddin, S. M., & Chintaparty, R. (2025). Structural, Optical, and Antibacterial Properties of NiO and BaO doped NiO-Prepared by Co-precipitation Method. *BioNanoScience*, *15*(2), 1–10.

Graham, N., & Brodaty, H. (1997). Alzheimer's disease international. In *International Journal of Geriatric Psychiatry* (Vol. 12, Issue 7, p. 691). Wiley Online Library.

Grimme, S. (2011). Density functional theory with London dispersion corrections. *Wiley Interdisciplinary Reviews: Computational Molecular Science*, *1*(2), 211–228.

Guaouguaou, F., Ahl Bebaha, M. A., Yadlapalli, S., Taghzouti, K., & Es-Safi, N. E. (2020).

Structural characterization of bioactive compounds in Cotula cinerea extracts by ultra-high-performance liquid chromatography with photodiode array and high-resolution time-of-flight mass spectrometry detectors. *Rapid Communications in Mass Spectrometry*, *34*(8), e8695.

Guaouguaou, F.-E., Bebaha, M. A. A., Taghzouti, K., Bouyahya, A., Bakri, Y., Dakka, N., & Es-Safi, N. E. (2018). Cytotoxicological investigation of the essential oil and the extracts of Cotula cinerea and Salvia verbenaca from Morocco. *BioMed Research International*, *2018*(1), 7163961.

Guerreiro, R., & Bras, J. (2015). The age factor in Alzheimer's disease. *Genome Medicine*, *7*, 1–3.

Gupta, U. C., & Gupta, S. C. (2020). Optimizing modifiable and lifestyle-related factors in the prevention of dementia disorders with special reference to Alzheimer, Parkinson and autism diseases. *Current Nutrition & Food Science*, *16*(6), 900–911.

Guterres, H., & Im, W. (2023). CHARMM-GUI-based induced fit docking workflow to generate reliable protein–ligand binding modes. *Journal of Chemical Information and Modeling*, *63*(15), 4772–4779.

Gutiérrez-Grijalva, E. P., Picos-Salas, M. A., Leyva-López, N., Criollo-Mendoza, M. S., Vazquez-Olivo, G., & Heredia, J. B. (2018). Flavonoids and Phenolic Acids from Oregano: Occurrence, Biological Activity and Health Benefits. In *Plants* (Vol. 7, Issue 1). https://doi.org/10.3390/plants7010002

H Ferreira-Vieira, T., M Guimaraes, I., R Silva, F., & M Ribeiro, F. (2016). Alzheimer's disease: targeting the cholinergic system. *Current Neuropharmacology*, *14*(1), 101–115.

Hafed-Khatiri, S., Salinas-Torres, D., & Montilla, F. (2025). Assessing Acetylcholinesterase Catalytic activity in the marine environment. *Electrochimica Acta*, 145930.

Haider, S., Liaquat, L., Ahmad, S., Batool, Z., Siddiqui, R. A., Tabassum, S., ... & Naz, N. (2020). Naringenin protects AlCl3/D-galactose induced neurotoxicity in rat model of AD via attenuation of acetylcholinesterase levels and inhibition of oxidative stress. *Plos one*, *15*(1), e0227631.

Hama, I., Vonghirundecha, P., Wungsintaweekul, B., Boonsut, R., Limsuwanchote, S., & Wungsintaweekul, J. (2025). Antioxidative constituents of Mitragyna diversifolia plant extract and their protective effect on H2O2-induced oxidative stress in L6 myotubes. *Journal of Applied Pharmaceutical Science*.

Han, W., Chen, Z., Wang, M.-W., & Zhou, Q. (2025). gmx_RRCS: A Precision Tool for Detecting Subtle Conformational Dynamics in Molecular Simulations. *Journal of Molecular Biology*, 169129.

Harrate, I., Fatmi, S., Chibani, N., Toutou, Z., Taouzinet, L., Inouri-Iskounen, A., Lahiani-Skiba, M., Skiba, M., & Iguerouada, M. (2025). Improving the Solubility of Algerian Olive Leaf Extract, Enhancing Antibacterial Activities, and Preserving Bovine Sperm Viability Through Optimized Cyclodextrins Encapsulation Process. *Applied In Vitro Toxicology*.

Hasan, T., Mohammadi, M., Jabbari, A., Flaifel, H. A., & Mirzaei, H. (2025). Nutraceuticals Targeting Cannabinoid Receptor 1 and Transient Receptor Potential Vanilloid 1 for Pain Relief: A Computational Screening Approach. *Cureus*, *17*(4).

Hemmerling, M., Liu, J., Piras, A., Pehrson, R., Hedström, U., Cassani, C., Ranieri, B., Kwapień, K., Ribbing, K., & Forss, C. (2025). Topical BET PROTACs for locally restricted protein degradation in the lung. *RSC Medicinal Chemistry*.

Heydon, A., Levin, R., Mann, T., & Yu, Y. (2001). *The Vesta approach to software configuration management*. Compaq. Systems Research Center [SRC].

Hiremath, S., Bharath, M., Muttappagol, M., Kumar, H. D. V., Kumar, T. L. M., Shankarappa, K. S., Venkataravanappa, V., Basha, C. R. J., & Reddy, C. N. L. (2025). Identification of potential plant secondary metabolites targeting begomovirus-associated betasatellite virulence factor βC1 protein through molecular docking, simulation and MM-PBSA studies. *Discover Plants*, *2*(1), 52.

Hossain, M. B., Barry-Ryan, C., Martin-Diana, A. B., & Brunton, N. P. (2011). Optimisation of accelerated solvent extraction of antioxidant compounds from rosemary (Rosmarinus officinalis L.), marjoram (Origanum majorana L.) and oregano (Origanum vulgare L.) using response surface methodology. *Food Chemistry*, *126*(1), 339–346.

Hu, Z., Xiong, W., Liang, Q., Wang, C., Xuan, P., Li, Y., Hua, X., Guo, H., & Yao, Y. (2025). Canolol as a key equivalent for phenolic content quantification in rapeseed oil via Folin–Ciocalteu method. *European Food Research and Technology*, 1–12.

Huang, H., Chen, Y., Hong, J., Yuan, X., Tian, W., Zhao, D., Sun, B., Sun, J., Wu, J., & Huang, M. (2025). Exploration of the flavor mechanism of novel umami peptides from lager beer: HPLC-Q-TOF-MS combined with flavor perception, molecular docking and molecular dynamics simulation. *Journal of Food Composition and Analysis*, *141*, 107338.

Huang, J., & Mackerell, A. D. (2013). CHARMM36 all-atom additive protein force field:

Validation based on comparison to NMR data. *Journal of Computational Chemistry*, *34*(25), 2135–2145. https://doi.org/10.1002/jcc.23354

Huang, N. M., Wong, L. Z., Ho, S. S., & Timothy, B. (2025). Understanding Challenges and Emotions of Informal Caregivers of General Older Adults and People With Alzheimer Disease and Related Dementia: Comparative Study. *Journal of Medical Internet Research*, *27*, e54847.

Hunter, T. R., Santos, L. E., Tovar-Moll, F., & De Felice, F. G. (2025). Alzheimer's disease biomarkers and their current use in clinical research and practice. *Molecular Psychiatry*, *30*(1), 272–284.

Ibrahim, S. S., Al-darwesh, M. Y., Arkawazi, S. W., Babakr, K. A., & Qader, I. N. (2025). Synthesis, characterization, antioxidant, antibacterial activity, and molecular docking studies of Zn (II) and Cu (II) complexes nanoparticles. *Journal of Molecular Structure*, *1326*, 141120.

Ibrahim, W. W., Sayed, R. H., Abdelhameed, M. F., Omara, E. A., Nassar, M. I., Abdelkader, N. F., ... & Afifi, S. M. (2024). Neuroprotective potential of Erigeron bonariensis ethanolic extract against ovariectomized/D-galactose-induced memory impairments in female rats in relation to its metabolite fingerprint as revealed using UPLC/MS. *Inflammopharmacology*, *32*(2), 1091-1112.

Ietswaart, J. H. (1980). A taxonomic revision of the genus Origanum (Labiatae). *Leiden Botanical Series*, *4*(1), 1–153.

Iqbal, M., & Jariah, A. A. (2025). Phytochemical screening of secondary metabolite compounds in tammate leaf extract (Lannea coromandelica (HOUTT.) MERR.) from Pangkep Regency using various extraction methods. *Journal of Current Health Sciences*, *5*(1), 59–66.

Jamal, Q. M. S., Khan, M. I., Alharbi, A. H., Ahmad, V., & Yadav, B. S. (2023). Identification of natural compounds of the apple as inhibitors against cholinesterase for the treatment of Alzheimer's disease: An in silico molecular docking simulation and ADMET study. *Nutrients*, *15*(7), 1579.

Jaramillo-Páez, C., Navío, J. A., Hidalgo, M. C., & Macías, M. (2017). High UV-photocatalytic activity of ZnO and Ag/ZnO synthesized by a facile method. *Catalysis Today*, *284*, 121–128.

Jia, C., Sun, Y., Chen, J., & Liu, X. (2025). Dissecting the Molecular Mechanism Concerning

Conformational Changes of SARS-CoV-2 Main Protease Mediated by Binding of Natural Phytochemicals via Molecular Dynamics Simulations. *ChemistrySelect*, *10*(13), e202405868.

Jongwachirachai, P., Ruankham, W., Apiraksattayakul, S., Intharakham, S., Prachayasittikul, V., Suwanjang, W., Prachayasittikul, V., Prachayasittikul, S., & Phopin, K. (2024). Neuroprotective properties of coriander-derived compounds on neuronal cell damage under oxidative stress-induced SH-SY5Y neuroblastoma and in silico admet analysis. *Neurochemical Research*, *49*(12), 3308–3325.

Joshi, S., Jindal, P., Gautam, S., Singh, C., Patel, P., Gupta, G. Das, & Kurmi, B. Das. (2025). Mini Review on the Lyophilization: A Basic Requirement for Formulation Development and Stability Modifier. *ASSAY and Drug Development Technologies*.

Jun, W. J., Han, B. K., Yu, K. W., Kim, M. S., Chang, I. S., Kim, H. Y., & Cho, H. Y. (2001). Antioxidant effects of Origanum majorana L. on superoxide anion radicals. *Food Chemistry*, *75*(4), 439–444.

Júnior, A. Q. da S., Rodrigues, G. dos S., Barroso, A. de S., Figueiredo, P. L. B., Machado, F. P., Ferreira, M. A., Fernandes, C. P., Santos, G. B. dos, & Mourão, R. H. V. (2025). Essential Oil of Lippia origanoides Kunth: Nanoformulation, Anticholinesterase Activity, and Molecular Docking. *Molecules*, *30*(7), 1554.

Jurowski, K., & Krośniak, A. (2025). ADME profile of AP-238-opioid designer drug (CAS: 140924-11-4): first application of multi-in silico approach methodology for comprehensive prediction of ADME profile (absorption, distribution, metabolism and excretion) important for clinical toxicology a. *Chemico-Biological Interactions*, 111493.

Kadhim, A., Ben Slima, A., Alneamah, G., & Makni, M. (2024). Assessment of Histopathological Alterations and Oxidative Stress in the Liver and Kidney of Male Rats following Exposure to Aluminum Chloride. *Journal of Toxicology*, *2024*(1), 3997463.

Karnwal, A., Jassim, A. Y., Mohammed, A. A., Sharma, V., Al-Tawaha, A. R. M. S., & Sivanesan, I. (2024). Nanotechnology for Healthcare: Plant-Derived Nanoparticles in Disease Treatment and Regenerative Medicine. *Pharmaceuticals*, *17*(12), 1711.

Kato, K., Nakayoshi, T., Mizuno, A., Yabu, M., Kurimoto, E., & Oda, A. (2025). Molecular dynamics simulations of putative primitive proteins including β-aspartic acid residues. *Bulletin of the Chemical Society of Japan*, *98*(1), uoae143.

Kawee-ai, A. (2025). Advancing Gel Systems with Natural Extracts: Antioxidant,

Antimicrobial Applications, and Sustainable Innovations. *Gels*, *11*(2), 125.

Kebache,S., Boudiaf, H., Rouiha, A., Lanez,E. (2025). *SAB* Analyzer – Spontaneous Alternation Percentage Calculator. Available at: https://spontaneously-alternation-behaviour-in-maze-test.pages.dev / (Accessed: June 15, 2025).

Khalid, M., Masoud, M. S., Tariq, M., ur Rehman, A., Masood, N., Khalid, H., Mazhar, T., El-Shazly, M., Ibrahim, L., & Saleh, N. (2025). Therapeutic Potential of Polyphenolic enriched extract of Aesculus indica for Attenuation of Liver Fibrosis through Pectin/Acrylic Acid Based Slow-Release Formulation. *Journal of Drug Delivery Science and Technology*, 106938.

Khalil, A. T., Ovais, M., Ullah, I., Ali, M., Shinwari, Z. K., Khamlich, S., & Maaza, M. (2017). Sageretia thea (Osbeck.) mediated synthesis of zinc oxide nanoparticles and its biological applications. *Nanomedicine*, *12*(15), 1767–1789.

Khallouki, F., Sellam, K., Koyun, R., Ricarte, I., Alem, C., Elrhaffari, L., & Owen, R. W. (2015). Phytoconstituents and in vitro evaluation of antioxidant capacities of Cotula cinerea (Morocco) methanol extracts. *Records of Natural Products*, *9*(4), 572.

Khamouli, S., Belaidi, S., & Lanez, T. (2019). Molecular doking and ADMET studies of amino-pyrimidine derivaties as mycobacterium tuberculosis Ser/Thr protein kinases B inhibitors. *Journal of Fundamental and Applied Sciences*, *11*(2), 914–939.

Khamouli, S., Belaidi, S., Ouassaf, M., Lanez, T., Belaaouad, S., & Chtita, S. (2022). Multi-combined 3D-QSAR, docking molecular and ADMET prediction of 5-azaindazole derivatives as LRRK2 tyrosine kinase inhibitors. *Journal of Biomolecular Structure and Dynamics*, *40*(3), 1285–1298.

Khelil, C. K. M., Amrouche, B., soufiane Benyoucef, A., Kara, K., & Chouder, A. (2020). New Intelligent Fault Diagnosis (IFD) approach for grid-connected photovoltaic systems. *Energy*, *211*, 118591.

Kim, S., Thiessen, P. A., Bolton, E. E., Chen, J., Fu, G., Gindulyte, A., Han, L., He, J., He, S., Shoemaker, B. A., Wang, J., Yu, B., Zhang, J., & Bryant, S. H. (2016). PubChem substance and compound databases. *Nucleic Acids Research*, *44*(D1), D1202–D1213. https://doi.org/10.1093/nar/gkv951

Köksal, Z., & Şenol, H. (2025). Anticholinesterase and carbonic anhydrase inhibitory activities of natural carnosic acid derivatives: A comprehensive in vitro and in silico study. *Archiv Der Pharmazie*, *358*(3), e2400909.

Kolaib, R. W., Radzi, Y. M., Aadim, K. A., Ahamed, N. M., & Salman, M. D. (2025). Study of optical and structural characterization of silver oxide nanoparticles prepared by pulse laser ablation. *Journal of Optics*, 1–8.

Kulshreshtha, A., & Piplani, P. (2016). Current pharmacotherapy and putative disease-modifying therapy for Alzheimer's disease. *Neurological Sciences*, *37*, 1403–1435.

Kumar, A., Gautam, V., Sandhu, A., Rawat, K., Sharma, A., & Saha, L. (2023). Current and emerging therapeutic approaches for colorectal cancer: A comprehensive review. *World Journal of Gastrointestinal Surgery*, *15*(4), 495.

Kumar, M. A., Yadav, A. K., Singh, M. A. K., Singh, A., & Tiwari, M. N. N. (2025). Exploring the Antioxidant, Antidiabetic, and Anti-Inflammatory Properties of Cold Macerated Rumex nepalensis Leaf Extract: A Study on Its Role in Hyperglycaemia Control, Free Radical Scavenging, and the Development of a Nanogel for Therapeutic Use. *Cuestiones de Fisioterapia*, *54*(4), 459–472.

Kumari, R., Kumar, R., & Lynn, A. (2014). G-mmpbsa -A GROMACS tool for high-throughput MM-PBSA calculations. *Journal of Chemical Information and Modeling*, *54*(7), 1951–1962. https://doi.org/10.1021/ci500020m

Kuntic, Marin & Hahad, Omar & Munzel, Thomas & Daiber, Andreas. (2024). Crosstalk between Oxidative Stress and Inflammation Caused by Noise and Air Pollution—Implications for Neurodegenerative Diseases. Antioxidants. 13. 10.3390/antiox13030266.

Kwon, H. S., & Koh, S.-H. (2020). Neuroinflammation in neurodegenerative disorders: the roles of microglia and astrocytes. *Translational Neurodegeneration*, *9*(1), 42.

Lakhdar, M. (2018). Traditional uses, phytochemistry and biological activities of Cotula cinerea Del: A review. *Tropical Journal of Pharmaceutical Research*, *17*(2), 365–373.

Lane, R. M., Potkin, S. G., & Enz, A. (2006). Targeting acetylcholinesterase and butyrylcholinesterase in dementia. *International Journal of Neuropsychopharmacology*, *9*(1), 101–124.

Lanez, E., Lanez, T., & Zegheb, N. (2023). In silico ADMET, toxicological analysis, molecular docking studies and Molecular dynamics simulation of Afzelin with potential antibacterial effects against Staphylococcus aureus. *Turkish Computational and Theoretical Chemistry*, *7*(3), 10–16.

Lanez, E., Zerrouk, L., Bechki, L., Lanez, T., Adaika, A., Zegheb, N., & Nesba, K. (n.d.). Synthesis, molecular docking, drug-likeness analysis, and ADMET prediction of nickel

and zinc tetraphenyl-porphyrin complexes as possible antioxidant agents. *Journal of the Chinese Chemical Society*.

Laraoui, H., Lanez, E., Zegheb, N., Adaika, A., Lanez, T., & Benkhaled, M. (2023). Anti-Diabetic Activity of Flavonol Glucosides From Fumana montana Pomel: In vitro Analysis, In Silico Docking, ADMET Prediction, and Molecular Dynamics Simulations. *ChemistrySelect*, *8*(8), e202204512. https://doi.org/10.1002/slct.202204512

Leclerc-Mercier, S., Bodemer, C., Furio, L., Hadj-Rabia, S., de Peufeilhoux, L., Weibel, L., ... & Fraitag, S. (2016). Skin biopsy in Netherton syndrome: a histological review of a large series and new findings. *The American Journal of Dermatopathology*, *38*(2), 83-91.

Lei, W., Zhuang, H., Huang, W., & Sun, J. (2025). Neuroinflammation and energy metabolism: a dual perspective on ischemic stroke. *Journal of Translational Medicine*, *23*(1), 413.

Leng, F., & Edison, P. (2021). Neuroinflammation and microglial activation in Alzheimer disease: where do we go from here? *Nature Reviews Neurology*, *17*(3), 157–172.

Li, B., Ming, H., Qin, S., Nice, E. C., Dong, J., Du, Z., & Huang, C. (2025). Redox regulation: mechanisms, biology and therapeutic targets in diseases. *Signal Transduction and Targeted Therapy*, *10*(1), 72.

Li, D. D., Wu, T. T., Yu, P., Wang, Z. Z., Xiao, W., Jiang, Y., & Zhao, L. G. (2020). Molecular Dynamics Analysis of Binding Sites of Epidermal Growth Factor Receptor Kinase Inhibitors. *ACS Omega*, *5*(26), 16307–16314. https://doi.org/10.1021/acsomega.0c02183

Li, G., Yuan, Y., & Zhang, R. (2025). A spatial-temporal graph attention network for protein–ligand binding affinity prediction based on molecular geometry. *Multimedia Systems*, *31*(1), 1–22.

Li, H., Xu, S., Wang, B., Tian, Z., Xu, Z., & Qian, F. (2025). A new insight into the effects of DMF solvent activation on the polyamide layers of nanofiltration membranes by molecular simulation. *Journal of Membrane Science*, *718*, 123667.

Li, H., Zheng, L., Chen, C., Liu, X., & Zhang, W. (2019). Brain Senescence CausedElevated Levels of Reactive Metabolite Methylglyoxal on D-Galactose-Induced Aging Mice. *Frontiers in neuroscience, 13, 1004*. https://doi.org/10.3389/fnins.2019.01004

Li, J. Q., Ma, X. H., Dai, H., Wang, C. C., Zhang, J., & Meng, X. L. (2025). Isoliensinine ameliorates cognitive dysfunction in AlCl3/D-gal-induced Alzheimer's disease-like mice by inhibiting the calcium signaling pathway. *Journal of Ethnopharmacology*, *344*, 119567.

Li, L., Zhang, L., Li, Y., Cai, Y., Wen, X., Zheng, C., Wu, C., Bao, Y., Jiang, F., & Sun, N. (2025). Overview of current research on traditional Chinese medicine in skin disease treatment: a bibliometric analysis from 2014 to 2024. *Pharmaceutical Biology*, *63*(1), 27–41.

Liang, J. N., Lee, Y. J., Akoopie, E., Kleven, B. C., Koch, T., & Ho, K. Y. (2019). Impaired H-reflex adaptations following slope walking in individuals with post-stroke hemiparesis. *Frontiers in Physiology*, *10*, 1232

Lilford, R. J., Daniels, B., McPake, B., Bhutta, Z. A., Mash, R., Griffiths, F., Omigbodun, A., Pinto, E. P., Jain, R., & Asiki, G. (2025). Policy and service delivery proposals to improve primary care services in low-income and middle-income country cities. *The Lancet Global Health*, *13*(5), e954–e966.

Liu, H., Jin, X., Liu, S., Liu, X., Pei, X., Sun, K., Li, M., Wang, P., Chang, Y., & Wang, T. (2025). Recent advances in self-targeting natural product-based nanomedicines. *Journal of Nanobiotechnology*, *23*(1), 31.

Logan, J. A., Sumner, J., Grigas, A. T., Shattuck, M. D., & OHern, C. S. (2025). The effect of stereochemical constraints on the radius of gyration of folded proteins. *ArXiv Preprint ArXiv:2501.02424*.

Louis, D. N., Perry, A., Wesseling, P., Brat, D. J., Cree, I. A., Figarella-Branger, D., Hawkins, C., Ng, H. K., Pfister, S. M., & Reifenberger, G. (2021). The 2021 WHO classification of tumors of the central nervous system: a summary. *Neuro-Oncology*, *23*(8), 1231–1251.

Lu, C., Wu, C., Ghoreishi, D., Chen, W., Wang, L., Damm, W., Ross, G. A., Dahlgren, M. K., Russell, E., & Von Bargen, C. D. (2021). OPLS4: Improving force field accuracy on challenging regimes of chemical space. *Journal of Chemical Theory and Computation*, *17*(7), 4291–4300.

Lueptow, L. M. (2017). Novel object recognition test for the investigation of learning and memory in mice. *Journal of visualized experiments: JoVE*, (126), 55718.

Luo, Y., Niu, F., Sun, Z., Cao, W., Zhang, X., Guan, D., ... & Xu, Y. (2009). Altered expression of Aβ metabolism-associated molecules from d-galactose/AlCl3 induced mouse brain. *Mechanisms of ageing and development, 130(4),* 248-252.

Lv, J., Liu, S., Hu, C., Ding, L., Wang, H., Li, X., Yang, F., Shen, Q., Zhang, H., & Ma, G. (2025). Saponin content in medicinal plants in response to application of organic and inorganic fertilizers: a meta-analysis. *Frontiers in Plant Science*, *16*, 1535170.

M Tata, A., Velluto, L., D'Angelo, C., & Reale, M. (2014). Cholinergic system dysfunction and neurodegenerative diseases: cause or effect? *CNS & Neurological Disorders-Drug Targets (Formerly Current Drug Targets-CNS & Neurological Disorders)*, *13*(7), 1294–1303.

Ma, S., Zheng, Y., Xu, B., Tang, S., Cao, C., & Zhao, Y. (2025). Efficient and highly selective deep removal of hydrophobic organic compounds from leachate by polyamide microplastics. *Separation and Purification Technology*, *360*, 131142.

Ma, Y., Song, R., & Duan, C. (2025). Mitochondrial quality control and transfer communication in neurological disorders and neuroinflammation. *Frontiers in Immunology*, *16*, 1542369.

Mabuza, M. J., Kaiser, M., Tshikalange, T. E., Yusuf, A. A., & Bapela, M. J. (n.d.). In Vitro Antiplasmodial and Cytotoxicity Screening of Three Ziziphus (Rhamnaceae) Species in South Africa. *Available at SSRN 5169586*.

Madhavi Sastry, G., Adzhigirey, M., Day, T., Annabhimoju, R., & Sherman, W. (2013). Protein and ligand preparation: parameters, protocols, and influence on virtual screening enrichments. *Journal of Computer-Aided Molecular Design*, *27*, 221–234.

Madi, N., Boukerb, A. M., Mekdade, L., Ikhlef, A., Meghezzi, A., Selmania, A., & Connil, N. (2025). In Vitro and In Silico Assessment of the Probiotic and Technological Potential of Lacticaseibacillus rhamnosus MW019593 Isolated from Algerian Cow's Milk. *Probiotics and Antimicrobial Proteins*, 1–18.

Mailloux, R. J. (2025). Targeted Redox Regulation α-Ketoglutarate Dehydrogenase Complex for the Treatment of Human Diseases. *Cells*, *14*(9), 653.

Mamataj, S., Roy, S., Ravindiran, G., Datta, D., & Das, B. (2025). Contemporary research on synthesis of silver nanoparticles and its applications. *Indian Chemical Engineer*, *67*(1), 91–120.

Manik, T., Sakai, M., Situmorang, R. S., Kawai, H., Oishi, Y., & Ambarita, H. (2025). Unveiling the complex morphology of ant-nest corrosion in oxygen-free copper tubes through nano X-ray CT examination. *Applied Surface Science*, *685*, 161983.

Manimaran, D., Tessema, A., Yadav, M. G., Parthasarathi, S., & Palanisamy, V. (2025). Current Perspectives in Detection of Bioactive Compounds From Costus spicatus Through GC–MS and LC-MS/MS: Antioxidant Properties and In Silico Analysis for Industrial Applications. *Biochemistry Research International*, *2025*(1), 9599942.

Manu, P., Abakah, A., Anfu, P. K., Osei-Poku, P., & Kwarteng, A. (2025). Disrupting quorum sensing by exploring conformational dynamics and active site flexibility of LasR protein

in Pseudomonas aeruginosa. *Discover Chemistry*, *2*(1), 39.

Marques, S. C. F., Oliveira, C. R., Outeiro, T. F., & Pereira, C. M. F. (2010). Alzheimer's disease: the quest to understand complexity. *Journal of Alzheimer's Disease*, *21*(2), 373–383.

Martinovic, J., Stojanovic, I. G., Nesic, S., Todorovic, A., Bobic, K., Stankovic, S., & Drakulic, D. (2025). Chronic Oral D-Galactose Induces Oxidative Stress but Not Overt Organ Dysfunction in Male Wistar Rats. *Current Issues in Molecular Biology*, *47*(3), 161.

Matejuk, A., & Ransohoff, R. M. (2020). Crosstalk between astrocytes and microglia: an overview. *Frontiers in Immunology*, *11*, 1416.

Mathe, A., & Karlapudi, A. P. (2025). Computational and experimental evaluation of a dual COX inhibitor: Insights from DFT, molecular simulations, and in-vitro validation. *Letters in Drug Design & Discovery*, 100009.

McGaw, L. (2025). Use of plant-derived extracts and bioactive compound mixtures against multidrug resistant bacteria affecting animal health and production. In *Fighting Multidrug Resistance with Herbal Extracts, Essential Oils and Their Components* (pp. 291–311). Elsevier.

Medeiros, W., Kralova, S., Oliveira, V., Ziemert, N., & Sehnal, L. (2025). Antarctic bacterial natural products: from genomic insights to drug discovery. *Natural Product Reports*.

Mehrnia, M. A., Behbahani, B. A., & Noshad, M. (2025). Investigating the chemical and antimicrobial properties of Anthemis cotula essential oil against Salmonella typhimurium, Enterobacter aerogenes, Staphylococcus aureus, Shigella dysenteriae, Bacillus cereus and Streptococcus pyogenes. *Cardiovascular Diseases*, *11*, 17–19.

Mekhadmi, N. E., Bentahar, A., Mlik, R., Ben Amor, S., Abid, A., Bousabaa, W., Mouane, A., Djilani Ghemam, A., Ben Neser, H., & Ramdani, M. (2024). Chemical composition, anti-diabetic, antioxidant, and anti-inflammatory potentials of Cotula cinerea growing in Algerian Sahara. *Chemical Papers*, *78*(14), 7729–7746.

Meraghni, M., Lanez, T., Lanez, E., Bechki, L., & Kennoufa, A. (2023). Experimental and theoretical study on corrosion inhibition of mild steel by meso-tetraphenyl-porphyrin derivatives in acid solution. *Journal of Electrochemical Science and Engineering*, *13*(2), 217–229. https://doi.org/10.5599/jese.1400

Metaxas, A., & Kempf, S. J. (2016). Neurofibrillary tangles in Alzheimer's disease: elucidation of the molecular mechanism by immunohistochemistry and tau protein phospho-proteomics. *Neural Regeneration Research*, *11*(10), 1579–1581.

Metcalfe, M. J., & Figueiredo-Pereira, M. E. (2010). Relationship between tau pathology and neuroinflammation in Alzheimer's disease. *Mount Sinai Journal of Medicine: A Journal of Translational and Personalized Medicine: A Journal of Translational and Personalized Medicine*, *77*(1), 50–58.

Metzenauer, P., Barnes, N. M., Costall, B., Gozlan, H., Hamon, M., Kelly, M. E., ... & Naylor, R. J. (1992). Anxiolytic-like actions of anpirtoline in a mouse light-dark aversion paradigm. *Neuroreport*, *3*(6), 527.

Mielke, M. M. (2018). Sex and gender differences in Alzheimer's disease dementia. *The Psychiatric Times*, *35*(11), 14.

Milella, M. S., Della Grotta, G., Razafimpanana, N., Marinelli, C., Eugelio, F., Fanti, F., Oliva, E., Sergi, M., Pugliese, F., & Galardo, G. (2025). Analytical quantification of the plant specific cardiac glycosides in biological fluids in a rare case of yellow oleander (Cascabela thevetia) self-poisoning in Italy. *Toxicon*, 108268.

Mili, A., Das, S., Nandakumar, K., & Lobo, R. (2023). Molecular docking and dynamics guided approach to identify potential anti-inflammatory molecules as NRF2 activator to protect against drug-induced liver injury (DILI): a computational study. *Journal of Biomolecular Structure and Dynamics*, *41*(19), 9193–9210. https://doi.org/10.1080/07391102.2022.2141885

Miller, E. B., Murphy, R. B., Sindhikara, D., Borrelli, K. W., Grisewood, M. J., Ranalli, F., Dixon, S. L., Jerome, S., Boyles, N. A., & Day, T. (2021). Reliable and accurate solution to the induced fit docking problem for protein–ligand binding. *Journal of Chemical Theory and Computation*, *17*(4), 2630–2639.

Mirzaeian, F., Sabet-Sarvestani, H., & Eshghi, H. (2025). Immobilization of Ni nanoparticles on pyridine-functionalized MWCNTs for indirect synthesis of benzimidazoles and quinazolinones, and their molecular docking studies as effective inhibitors of α-glucosidase. *Journal of Molecular Structure*, *1319*, 139508.

Mohammed, M. M., Isa, M. A., Abubakar, M. B., Dikwa, A. S. B., & Kappo, A. P. (2025). Molecular detection of mecA gene from methicillin-resistant Staphylococcus aureus isolated from clinical and environmental samples and its potential inhibition by phytochemicals using in vitro and in silico approach. *In Silico Pharmacology*, *13*(1), 26.

Möller, B., & Villiger, P. M. (2006). Inhibition of IL-1, IL-6, and TNF-α in immune-mediated inflammatory diseases. *Springer Seminars in Immunopathology*, *27*, 391–408.

Moreno, R. B., & Solar, N. J. B. (2025). Phytochemical Screening of Metabolites in the Testa of Peanut (Arachis hypogaea) Extract, Mung Beans (Vigna radiata) Extract, Red Beans (Phaseolus vulgaris) Extract and Congo Beans (Cajanus cajan): Screening of Metabolites of Different Beans. *Biological Sciences-PJSIR*, *68*(1), 109–116.

Morris, J. C., Weiner, M., Xiong, C., Beckett, L., Coble, D., Saito, N., Aisen, P. S., Allegri, R., Benzinger, T. L. S., & Berman, S. B. (2022). Autosomal dominant and sporadic late onset Alzheimer's disease share a common in vivo pathophysiology. *Brain*, *145*(10), 3594–3607.

Mubarik, A., Shafiq, F., & Ju, X. (2025). DFT and TD-DFT Study of Benzodithiophene-Based Donor Materials with Enhanced Optoelectronic Attributes for Organic Solar Cells. *ChemistrySelect*, *10*(4), e202401831.

Munuo, M. S., John, M., Shechambo, L. F., & Gervas, I. (2025). Effect of solvent extraction on phytochemical profile and quantification of bioactive compounds in Ocimum suave (wild). *Journal of Current Opinion in Crop Science*, *6*(1), 27–41.

Naik, R. A., Mir, M. N., Malik, I. A., Bhardwaj, R., Alshabrmi, F. M., Mahmoud, M. A., Alhomrani, M., Alamri, A. S., Alsanie, W. F., & Hjazi, A. (2025). The Potential Mechanism and the Role of Antioxidants in Mitigating Oxidative Stress in Alzheimer's Disease. *Frontiers in Bioscience-Landmark*, *30*(2), 25551.

Ngandu, T. (2006). *Lifestyle-related risk factors in dementia and mild cognitive impairment: A population-based study*. Karolinska Institutet (Sweden).

Odoh, U. E., Gurav, S. S., & Chukwuma, M. O. (2025). *Pharmacognosy and Phytochemistry: Principles, Techniques, and Clinical Applications*. John Wiley & Sons.

Ogunyemi, B. T., Abdul-Hammed, M., Adedotun, I. O., Egunjobi, B. T., Badmos, S. T., Adegboyega, T. A., Aderogba, A. A., & Adeosun, G. G. (2025). Protein–ligand molecular dynamics simulation (PL-MDS), ADMET analyses, and bioactivity studies of phytochemicals from Aloe Vera: an In-Silico novel antidiabetics drug discovery effort. *Discover Chemistry*, *2*(1), 55.

Okpala, O. E., Rondevaldova, J., & Kokoska, L. (2025). Anti-inflammatory drugs as potential antimicrobial agents: a review. *Frontiers in Pharmacology*, *16*, 1557333.

Osman, A. I., Mehta, N., Elgarahy, A. M., Hefny, M., Al-Hinai, A., Al-Muhtaseb, A. H., & Rooney, D. W. (2022). Hydrogen production, storage, utilisation and environmental impacts: a review. *Environmental Chemistry Letters*, 1–36.

OUEDRAOGO, G. G., BELEMLILGA, B. M., KOUGUILIMA, T., SOMDA, G. D.,

ILBOUDO, S., OUEDRAOGO, S., TRAORE, A., BELEMNABA, L., KINI, F. B., & OUEDRAOGO, S. (2025). Toxicity assessment of a phytomedicine based on an almond extract from the fruit of Balanites aegyptiaca (L.) DELILE (Zygophyllaceae) intended for helminthiases care in Burkina Faso. *Journal of Drug Delivery & Therapeutics*, *15*(1).

Papada, E., Amerikanou, C., & Colone, M. (2023). *Plant-Derived Natural Products and Their Biomedical Properties*. MDPI-Multidisciplinary Digital Publishing Institute.

Paramasivam, S., Velayutham, G., & Pitchaipillai, R. (2025). Facile Plant Mediated Phytofabrication Antibacterial and Molecular Docking Evaluation of Silver and Zinc Oxide Nanoparticles With an Aqueous Extract of Bidens Pilosa. *Nanochemistry Research*, *10*(2), 119–136.

Pasieczna-Patkowska, S., Cichy, M., & Flieger, J. (2025). Application of Fourier Transform Infrared (FTIR) Spectroscopy in Characterization of Green Synthesized Nanoparticles. *Molecules*, *30*(3), 684.

Patel, J., Roy, H., Chintamaneni, P. K., Patel, R., & Bohara, R. (2025). Advanced Strategies in Enhancing the Hepatoprotective Efficacy of Natural Products: Integrating Nanotechnology, Genomics, and Mechanistic Insights. *ACS Biomaterials Science & Engineering*.

Patterson, C., Feightner, J. W., Garcia, A., Hsiung, G.-Y. R., MacKnight, C., & Sadovnick, A. D. (2008). Diagnosis and treatment of dementia: 1. Risk assessment and primary prevention of Alzheimer disease. CMAJ, 178(5), 548–556. https://doi.org/10.1503/cmaj.070796

Paul, S. K., Saddam, M., Tabassum, N., & Hasan, M. (2025). Molecular dynamics simulation of wild and mutant proteasome subunit beta type 8 (PSMB8) protein: Implications for restoration of inflammation in experimental autoimmune encephalomyelitis pathogenesis. *Heliyon*, *11*(1).

Paula, V. de J. R. de, Guimarães, F. M., Diniz, B. S., & Forlenza, O. V. (2009). Neurobiological pathways to Alzheimer's disease: Amyloid-beta, TAU protein or both? *Dementia & Neuropsychologia*, *3*(3), 188–194.

Pawlędzio, S., Ziemniak, M., Wang, X., Woźniak, K., & Malinska, M. (2025). Understanding the selectivity of nonsteroidal anti-inflammatory drugs for cyclooxygenases using quantum crystallography and electrostatic interaction energy. *IUCrJ*, *12*(2).

Pekny, M., Wilhelmsson, U., & Pekna, M. (2014). The dual role of astrocyte activation and reactive gliosis. *Neuroscience Letters*, *565*, 30–38.

Peng, C., Li, H., Mao, Q., Tang, K., Sun, M., Ai, Q., Yang, Y., & Liu, F. (2025). Quercetin inhibits hydrogen peroxide-induced cleavage of heat shock protein 90 to prevent glutathione peroxidase 4 degradation via chaperone-mediated autophagy. *Phytomedicine*, *136*, 156286.

Peng, Y., & Nishikawa, K. (2025). Three-dimensional imaging of the microstructure of lithium metal anode using Xenon plasma focused ion beam. *Cell Reports Physical Science*.

Pentkowski, N. S., Rogge-Obando, K. K., Donaldson, T. N., Bouquin, S. J., & Clark, B. J. (2021). Anxiety and Alzheimer's disease: Behavioral analysis and neural basis in rodent models of Alzheimer's-related neuropathology. *Neuroscience & Biobehavioral Reviews*, *127*, 647-658.

Perkin, V. O., Antonyan, G. V, Radchenko, E. V, & Palyulin, V. A. (2023). Web services for the prediction of ADMET parameters relevant to the design of neuroprotective drugs. *Computational Modeling of Drugs against Alzheimer's Disease*, 465–485.

Pietrak, B. L., Crouthamel, M.-C., Tugusheva, K., Lineberger, J. E., Xu, M., DiMuzio, J. M., Steele, T., Espeseth, A. S., Stachel, S. J., & Coburn, C. A. (2005). Biochemical and cell-based assays for characterization of BACE-1 inhibitors. *Analytical Biochemistry*, *342*(1), 144–151.

Piñeiro, M., Manrique, S., Gómez, J., Rodriguez, J. M., Barrera, P., Caballero, D., Sosa, M. A., Vargas-Arana, G., Tapia, A., & Lima, B. (2025). Biological activities of Usnea lethariiformis lichen extracts and UHPLC-ESI-QTOF-MS analysis of their secondary metabolites. *Frontiers in Pharmacology*, *15*, 1508835.

Pires, D. E. V, Blundell, T. L., & Ascher, D. B. (2015). pkCSM: predicting small-molecule pharmacokinetic and toxicity properties using graph-based signatures. *Journal of Medicinal Chemistry*, *58*(9), 4066–4072.

Plascencia-Villa, G., & Perry, G. (2023). Roles of oxidative stress in synaptic dysfunction and neuronal cell death in Alzheimer's disease. *Antioxidants*, *12*(8), 1628.

Polcaro, L. M., Cerulli, A., Masullo, M., & Piacente, S. (2025). Phytochemical Investigation of Chamaemelum nobile L. and Evaluation of Acetylcholinesterase and Tyrosinase Inhibitory Activity. *Plants*, *14*(4), 595.

Prasetyawan, F., Saristiana, Y., Bin, M., Savitri, L., Salmasfattah, N., Fadel, M. N., & Besan, E. J. (2025). Description of Absorption Distribution Metabolism Excretion Toxicity (ADMET) of Nuciferine from Terate Flowers (Nymphaea spp.) using pkCSM

Technology. *Journal of Engineering Science and Technology Management (JES-TM)*, *5*(1), 6–16.

Prut, L., & Belzung, C. (2003). The open field as a paradigm to measure the effects of drugs on anxiety-like behaviors: a review. *European journal of pharmacology*, *463*(1-3), 3-33.

Puspadewi, R., Milanda, T., Muhaimin, M., & Chaerunisaa, A. Y. (2025). Nanoparticle-Encapsulated Plant Polyphenols and Flavonoids as an Enhanced Delivery System for Anti-Acne Therapy. *Pharmaceuticals*, *18*(2), 209.

Putpadungwipon, P., & Powthong, P. (2025). Unveiling antioxidant arsenal DPPH radical scavenging activity and flavonoid profiles of six edible flower infusions. *Journal of Integrated Science and Technology*, *13*(5), 1101.

Qin, G., Song, R., Sun, J., Dai, J., Wang, W., Meng, F., ... & Li, C. (2025). Unveiling the Therapeutic Potential of Banxia Xiexin Decoction in Alzheimer's Disease: Insights From Network Pharmacology and Experimental Validation. *Drug Design, Development and Therapy*, 2133-2155.

Quintanilha, A. T. (1981). Membrane effects of vitamin E deficiency: bioenergetic and surface charge density studies of skeletal muscle and liver mitochondria.

Ramadan, L. A., Daidamoony, M. A., Elgindy, A. M., Mustafa, A. M., Hassan, E., Abdel-Rahman, H. M., & Atwa, A. M. (2023). Mitigation of Aluminum Chloride-Induced Alzheimer's disease by blueberry in rat model. *ERU Research Journal, 2(4)*, 682-698.

Redjili, S., Ghodbane, H., Bourzami, R., Mayouf, F., Chebli, D., Boudechicha, A., & Djelloul, C. (2025). Green synthesis of silver oxide nanoparticles: Eco-friendly approach for sustainable solutions. *Industrial Crops and Products*, *223*, 120168.

Rivas-Gastélum, M. F., Galindo-Castillo, P. A., Esparza-Sánchez, J., Jiménez-Pérez, M. I., Perfecto-Avalos, Y., Garcia-Amezquita, L. E., Navarro-López, D. E., López-Mena, E. R., Sánchez-Arreola, E., & Tamayo-Martínez, J. P. (2025). Lyophilized and Oven-Dried Manilkara zapota Extracts: Characterization and In Vitro, In Vivo, and In Silico Analyses. *Plants*, *14*(2), 216.

Rojas-Gutierrez, E., Muñoz-Arenas, G., Treviño, S., Espinosa, B., Chavez, R., Rojas, K., Flores, G., Díaz, A., & Guevara, J. (2017). Alzheimer's disease and metabolic syndrome: A link from oxidative stress and inflammation to neurodegeneration. *Synapse*, *71*(10), e21990.

Rose, P. W., Prlić, A., Altunkaya, A., Bi, C., Bradley, A. R., Christie, C. H., Di Costanzo, L., Duarte, J. M., Dutta, S., Feng, Z., Green, R. K., Goodsell, D. S., Hudson, B., Kalro, T., Lowe, R., Peisach, E., Randle, C., Rose, A. S., Shao, C., … Burley, S. K. (2017). The RCSB protein data bank: Integrative view of protein, gene and 3D structural information. *Nucleic Acids Research*, *45*(D1), D271–D281.

Rostagno, A. A. (2022). Pathogenesis of Alzheimer's disease. In *International Journal of Molecular Sciences* (Vol. 24, Issue 1, p. 107). MDPI.

Royani, A., Mubarak, N. M., Hanafi, M., Verma, C., Lotulung, P. D. N., Prastya, M. E., Alfantazi, A., & Manaf, A. (2025). Effect of solvent polarity on yield extract, antioxidant and antibacterial activities of phytochemicals from Andrographis paniculata leaves. *Indian Chemical Engineer*, *67*(1), 1–15.

Sachdev, S., Ansari, S. A., & Ansari, M. I. (2023). Antioxidant defensive mechanisms to regulate cellular redox homeostatic balance. In *Reactive Oxygen Species in Plants: The Right Balance* (pp. 143–172). Springer.

Sakr, M. A. S., Saad, M. A., Teleb, N. H., Abd-Elkader, O. H., Abdelsalam, H., & Zhang, Q. (2025). Transition metal-modified armchair graphene network for high-performance hydrogen evolution reaction catalysts. *Diamond and Related Materials*, *151*, 111745.

Saleh, S. R., Younis, F. A., Abdelrahman, S. S., Attia, A. A., El-Demellawy, M. A., Newairy, A. A., & Ghareeb, D. A. (2025). Attenuation of high-fat high-sucrose diet and CCl4-induced non-alcoholic steatohepatitis in rats by activating autophagy and SIGMAR1/GRP78/ITPR1 signaling using berberine-loaded albumin nanoparticles: in vivo prediction and in-silico molecular modeling. *Journal of Pharmaceutical Investigation*, *55*(2), 227–250.

Samad, N., Nasir, A., Rehman, M. H. U., & et al. (2022). Adenosine protects D-galactose-induced alterations in rat model of aging via attenuating neurochemical profile and redox status. *Metabolic Brain Disease*, *37*(12), 2483–2496. https://doi.org/10.1007/s11011-022-01049-7

Samsuddin, A. F., Aziz, S. N. Q. A. A., & Pung, S.-Y. (2017). Loading effect of Ag/AgO on the photocatalytic performance of ZnO rods. *Applied Physics A*, *123*, 1–12.

Sangeet, S., & Khan, A. (2025). An in-silico approach to identify bioactive phytochemicals from Houttuynia cordata Thunb. As potential inhibitors of human glutathione reductase. *Journal of Biomolecular Structure and Dynamics*, *43*(5), 2300–2319.

Sanjai, C., Gaonkar, S. L., & Hakkimane, S. S. (2024). Harnessing Nature's Toolbox: Naturally Derived Bioactive Compounds in Nanotechnology Enhanced Formulations. *ACS Omega*, *9*(43), 43302–43318.

Sargsyan, T., Simonyan, H. M., Stepanyan, L., Tsaturyan, A., Vicidomini, C., Pastore, R., Guerra, G., & Roviello, G. N. (2025). Neuroprotective Properties of Clove (Syzygium aromaticum): State of the Art and Future Pharmaceutical Applications for Alzheimer's Disease. *Biomolecules*, *15*(3), 452.

Sarter, M., & Bruno, J. P. (1997). Cognitive functions of cortical acetylcholine: toward a unifying hypothesis. *Brain Research Reviews*, *23*(1–2), 28–46.

Satpathy, B., Saha, I., Halder, J., Rajwar, T. K., Rai, V. K., Pradhan, D., Mishra, A., Mahanty, R., Dash, P., & Das, C. (2025). In vitro and in silico anti-Alzheimer study of rutin embedded with zinc chloride loaded bovine serum albumin nanoparticles. *Tissue and Cell*, *95*, 102869.

Savvides, S. N., & Karplus, P. A. (1996). Kinetics and Crystallographic Analysis of Human Glutathione Reductase in Complex with a Xanthene Inhibitor (*). *Journal of Biological Chemistry*, *271*(14), 8101–8107. https://doi.org/10.1074/jbc.271.14.8101

Saxena, M., & Dubey, R. (2019). Target enzyme in Alzheimer's disease: Acetylcholinesterase inhibitors. *Current Topics in Medicinal Chemistry*, *19*(4), 264–275.

Schrödinger. (2015). Small-Molecule Drug Discovery Suite 2015-3: Schrödinger Suite 2015-3 Induced Fit Docking protocol; Glide version 6.8; Prime version 4.1. *Glide Version*, *6*.

Schrödinger. (2024). *Schrödinger Release 2024-1: LigPrep, Schrödinger, LLC.*

Seeman, P., & Seeman, N. (2011). Alzheimer's disease: β-amyloid plaque formation in human brain. *Synapse*, *65*(12), 1289–1297.

Seibenhener, M. L., & Wooten, M. C. (2015). Use of the Open Field Maze to measure locomotor and anxiety-like behavior in mice. *Journal of visualized experiments : JoVE*, (96), e52434. https://doi.org/10.3791/52434

Seibenhener, M. L., & Wooten, M. C. (2015). Use of the Open Field Maze to measure locomotor and anxiety-like behavior in mice. *Journal of visualized experiments : JoVE*, (96), e52434. https://doi.org/10.3791/52434

Sellami, I. H., Maamouri, E., Chahed, T., Wannes, W. A., Kchouk, M. E., & Marzouk, B. (2009). Effect of growth stage on the content and composition of the essential oil and phenolic fraction of sweet marjoram (Origanum majorana L.). *Industrial Crops and*

Products, *30*(3), 395–402.

Selvi, B. (2025). Comparative Study of Pentanema verbascifolium Extracts: Phytochemical Composition, Antioxidant Potential, and Enzyme Inhibition Across Plant Parts. *Food Bioscience*, 106607.

Sestakova, N., Puzserova, A., Kluknavsky, M., & Bernatova, I. (2013). Determination of motor activity and anxiety-related behaviour in rodents: methodological aspects and role of nitric oxide. *Interdisciplinary toxicology*, *6*(3), 126–135. https://doi.org/10.2478/intox-2013-0020

Shabab, T., Khanabdali, R., Moghadamtousi, S. Z., Kadir, H. A., & Mohan, G. (2017). Neuroinflammation pathways: a general review. *International Journal of Neuroscience*, *127*(7), 624–633.

Shah, S., Chauhan, H., Madhu, H., Mori, D., Soniwala, M., Singh, S., & Prajapati, B. (2025). Lipids fortified nano phytopharmaceuticals: a breakthrough approach in delivering bio-actives for improved therapeutic efficacy. *Pharmaceutical Nanotechnology*, *13*(1), 70–89.

Shahhoseini, R. (2025). Metabolite distribution, relationships of phytochemical compositions and anticancer compound tracking in organs of Tanacetum parthenium L. as a sustainable pharmaceutical manufacturing plant. *Environmental Technology & Innovation*, 104063.

Shahrajabian, M. H. (2021). Medicinal herbs with anti-inflammatory activities for natural and organic healing. *Current Organic Chemistry*, *25*(23), 2885–2901.

Sharif, A., Flores-Morales, V., & Aly, H. F. (2025). Reviews in experimental pharmacology and drug discovery 2023: pharmacological management of non-communicable diseases. In *Frontiers in Pharmacology* (Vol. 16, p. 1435638). Frontiers Media SA.

Shen, C., Han, X., Cai, H., Chen, T., Kang, Y., Pan, P., Ji, X., Hsieh, C.-Y., Deng, Y., & Hou, T. (2025). Improving the Reliability of Language Model-Predicted Structures as Docking Targets through Geometric Graph Learning. *Journal of Medicinal Chemistry*.

Siles-Sánchez, M. de las N., Navarro del Hierro, J., Martín, D., Jaime, L., & Santoyo, S. (2024). Supercritical antisolvent precipitation as a green technology to fractionate an Origanum majorana extract: Relationship between fractions cellular antioxidant activity and phytochemical composition. *Food Bioscience*, *59*, 104103. https://doi.org/https://doi.org/10.1016/j.fbio.2024.104103

Singirala, S. K., Dubey, P. K., & Roy, S. (2025). Extraction of Bioactive Compounds From

Withania somnifera: The Biological Activities and Potential Application in the Food Industry: A Review. *International Journal of Food Science*, *2025*(1), 9922626.

Smati, M., Bramki, A., Makhlouf, F. Z., Djebaili, R., Farda, B., Abdelhadi, F. Z., Abdelli, N., Kitouni, M., & Pellegrini, M. (2025). Isolation of Actinobacteria from Date Palm Rhizosphere with Enzymatic, Antimicrobial, Antioxidant, and Protein Denaturation Inhibitory Activities. *Biomolecules*, *15*(1), 65.

Sobhy, R., Zhang, J., Li, Z., Jia, Y., Korin, A., Salah, M., Abdin, M., & Xiaobou, Z. (2025). The protective effects of geraniin against initial and intermediate carbonyl-induced glycoxidation stress in bovine serum albumin models. *International Journal of Biological Macromolecules*, 143326.

Solfrizzi, V., Capurso, C., D'Introno, A., Colacicco, A. M., Santamato, A., Ranieri, M., Fiore, P., Capurso, A., & Panza, F. (2008). Lifestyle-related factors in predementia and dementia syndromes. *Expert Review of Neurotherapeutics*, *8*(1), 133–158.

Solfrizzi, V., D'Introno, A., Colacicco, A. M., Capurso, C., Gagliardi, G., Santamato, A., Baldassarre, G., Capurso, A., & Panza, F. (2007). Lifestyle-related factors, alcohol consumption, and mild cognitive impairment. *Journal of the American Geriatrics Society*, *55*(10), 1679–1681.

Sreekumar, S., Bhagya Jyothi, J. L., Liji, S. S., Pani, S. C., Rajee, N. E., Stephanie, A. P., Raphael, T., & Dhanasingh, I. (2025). Molecular docking, validation, dynamic simulation and pharmacokinetic prediction of natural compounds against Mycobacterium tuberculosis Beta-lactamase BlaC. *BioRxiv*, 2001–2025.

Stafstrom, C. E. (2006). Behavioral and cognitive testing procedures in animal models of epilepsy. In *Models of seizures and epilepsy* (pp. 613-628). Elsevier Inc..

Stoyanova, M., Milusheva, M., Gledacheva, V., Todorova, M., Kircheva, N., Angelova, S., Stefanova, I., Pencheva, M., Vasileva, B., & Hristova-Panusheva, K. (2025). Silver Nanoparticles with Mebeverine in IBS Treatment: DFT Analysis, Spasmolytic, and Anti-Inflammatory Effects. *Pharmaceutics*, *17*(5), 561.

Sturman, O., Germain, P. L., & Bohacek, J. (2018). Exploratory rearing: a context- and stress-sensitive behavior recorded in the open-field test. *Stress (Amsterdam, Netherlands)*, *21*(5), 443–452. https://doi.org/10.1080/10253890.2018.1438405

SUHENDRA, M., JULIANDI, B., DARUSMAN, H. S., SADIAH, S., FITMAWATI, F., BUDIARTI, S. R. I., & RIANTI, P. (2025). Phytochemical Analysis and antioxidant

activity from Phanera semibifida stem and leaves extracts using LC-MS/MS. *Biodiversitas Journal of Biological Diversity*, *26*(1).

Sutrisno, C. A. P., & Kartini, K. (2025). Dot-blot assay with AlCl 3 reagent for rapid screening of total flavonoid content in food and herbal medicine materials. *Acta Chromatographica*.

Taamalli, A., Arráez-Román, D., Abaza, L., Iswaldi, I., Fernández-Gutiérrez, A., Zarrouk, M., & Segura-Carretero, A. (2015). LC-MS-based metabolite profiling of methanolic extracts from the medicinal and aromatic species Mentha pulegium and Origanum majorana. *Phytochemical Analysis*, *26*(5), 320–330.

Takahashi, R. H., Nagao, T., & Gouras, G. K. (2017). Plaque formation and the intraneuronal accumulation of β-amyloid in Alzheimer's disease. *Pathology International*, *67*(4), 185–193.

Takalo, M., Jeskanen, H., Rolova, T., Kervinen, I., Hellén, M., Heikkinen, S., ... & Hiltunen, M. (2025). The protective PLCγ2-P522R variant mitigates Alzheimer's disease-associated pathologies by enhancing beneficial microglial functions. *Journal of neuroinflammation*, *22*(1), 64.

Takao, K., & Miyakawa, T. (2006). Light/dark transition test for mice. *Journal of visualized experiments: JoVE*, (1), 104.

Takao, K., & Miyakawa, T. (2006). Light/dark transition test for mice. *Journal of visualized experiments: JoVE*, (1), 104.

Talib, W. R., Sudhakaran, A., Sudhakaran, A., & Mohammed, R. S. (2024). Potential biological and optoelectronic applications of AgO: ZnO nanocomposite synthesized by green approach. *The European Physical Journal Plus*, *139*(12), 1118.

Tambe, B. R., Vikhe, S. R., & Pathade, P. M. (2025). *Detection of phytochemicals in the methanol extract of Urginea indica (R.) BULB*.

Tan, C.-C., Yu, J.-T., Wang, H.-F., Tan, M.-S., Meng, X.-F., Wang, C., Jiang, T., Zhu, X.-C., & Tan, L. (2014). Efficacy and safety of donepezil, galantamine, rivastigmine, and memantine for the treatment of Alzheimer's disease: a systematic review and meta-analysis. *Journal of Alzheimer's Disease*, *41*(2), 615–631.

Tang, K. H. D. (2025). Effects of Microplastics on Bioavailability, Persistence and Toxicity of Plant Pesticides: An Agricultural Perspective. *Agriculture*, *15*(4), 356.

Tattersfield, A. E. (1997). Limitations of current treatment. *The Lancet*, *350*, S24–S27.

Teleanu, D. M., Niculescu, A.-G., Lungu, I. I., Radu, C. I., Vladâcenco, O., Roza, E., Costăchescu, B., Grumezescu, A. M., & Teleanu, R. I. (2022). An overview of oxidative stress, neuroinflammation, and neurodegenerative diseases. *International Journal of Molecular Sciences*, *23*(11), 5938.

Temnik, M., Rudyk, M., Balakin, A., Gurin, S., Dovbynchuk, T., Byshovets, R., ... & Skivka, L. (2025). Anti-inflammatory effects of 64Zn-aspartate is accompanied by cognitive

Thwaite, R., Benseny-Cases, N., Rojas-Peña, M., Chico, V., Carreras, M., Puente-Marin, S., Villaverde, A., Perez, L., del Mar Ortega-Villaizan, M., & Sabés, M. (2025). Functional studies and synchrotron FTIR biochemical signatures reveal the potential of protein nanoparticles as a VHS virus vaccine. *Fish & Shellfish Immunology*, 110202.

Tlili, M. L., Alia, F., Bahri, E., Beyat, T., Redouan, K., & Lanez, E. (2025). In vivo evaluations of the antidiabetic and antioxidant effects of Olea europaea L.(Chemlali variety) leaves. *Acta Periodica Technologica*, *00*, 3.

Tönnies, E., & Trushina, E. (2017). Oxidative stress, synaptic dysfunction, and Alzheimer's disease. *Journal of Alzheimer's Disease*, *57*(4), 1105–1121.

Tummino, M. L., Vineis, C., Varesano, A., Liotta, L. F., Rigoletto, M., Laurenti, E., & Deganello, F. (2023). Sr0. 85Ce0. 15Fe0. 67Co0. 33-xCuxO3 perovskite oxides: effect of B-site copper codoping on the physicochemical, catalytic and antibacterial properties upon UV or thermal activation. *Frontiers in Environmental Engineering*, *2*, 1249931.

Uy, N. P., Lee, S. Y., Kim, J. H., Yoon, Y. H., & Lee, S. (2025). Simultaneous Quantification of Phenolic Compounds in the Leaves and Roots of Peucedanum japonicum Thunb. Using HPLC-PDA with Various Extraction Solvents. *Horticulturae*, *11*(3), 334.

Valencia, A., & Morán, J. (2004). Reactive oxygen species induce different cell death mechanisms in cultured neurons. *Free Radical Biology and Medicine*, *36*(9), 1112–1125.

Varenichenko, S., & Farat, O. (2024). PREDICTION OF BIOLOGICAL ACTIVITY OF AMINOQUINOLINE DERIVATIVES USING THE ADMET 2.0 WEB RESOURCE. *Ukrainian Chemistry Journal*, *90*(1), 15–25.

Vieii, F. H., Havigh, R. S., & Chenari, H. M. (2025). Electrospun preparation of nickel and Cobalt-doped ZnO fibers: study on the physical properties. *Scientific Reports*, *15*(1), 10898.

Villalva, M., Santoyo, S., Salas-Pérez, L., Siles-Sánchez, M. de las N., Rodriguez Garcia-Risco, M., Fornari, T., Reglero, G., & Jaime, L. (2021). Sustainable extraction techniques for

obtaining antioxidant and anti-inflammatory compounds from the Lamiaceae and Asteraceae species. *Foods*, *10*(9), 2067.

Vishwas, S., Gulati, M., Babu, M. R., Awasthi, A., Kumar, R., Khursheed, R., Corrie, L., Chaitanya, M. V. N. L., Gupta, G., & Devkota, H. P. (2023). The overview of drugs used in Alzheimer's disease and their molecular targets. In *Deciphering drug targets for Alzheimer's disease* (pp. 351–376). Springer.

Vradenburg, G. (2015). A pivotal moment in Alzheimer's disease and dementia: how global unity of purpose and action can beat the disease by 2025. *Expert Review of Neurotherapeutics*, *15*(1), 73–82.

Wang, R. (2025). Global burden of Alzheimer's disease and other dementias during 1990-2021: a Global Burden of Disease and Risk Factors Study 2021-based study. *Neuroepidemiology*, 1–24.

Wang, S., Yang, J., Liu, C., Li, W., Zheng, X., Qiao, X., Sun, X., Qian, S., Han, J., & Wu, J. (2025). KTb3− xGdxF10 Nano-Glass Composite Scintillator with Excellent Thermal Stability and Record X-Ray Imaging Resolution. *Laser & Photonics Reviews*, 2401611.

Weckbecker, G., & Cory, J. G. (1988). Ribonucleotide reductase activity and growth of glutathione-depleted mouse leukemia L1210 cells in vitro. *Cancer letters*, *40*(3), 257-264.

Wei, J., Lohman, M. C., Brown, M. J., Hardin, J. W., Yang, C.-H., Merchant, A. T., & Friedman, D. B. (2025). Modifiable and Non-Modifiable Risk Factors for Dementia Among Non-Hispanic White and Black Populations Aged 50-64 in the United States, 2006-2016. *Journal of Geriatric Psychiatry and Neurology*, *38*(2), 106–114.

Wijnen, K., Genzel, L., & van der Meij, J. (2024). Rodent maze studies: from following simple rules to complex map learning. *Brain Structure and Function*, *229*(4), 823-841.

Wortmann, M. (2012). Dementia: a global health priority-highlights from an ADI and World Health Organization report. *Alzheimer's Research & Therapy*, *4*, 1–3.

Wu, L., Rosa-Neto, P., Hsiung, G.-Y. R., Sadovnick, A. D., Masellis, M., Black, S. E., Jia, J., & Gauthier, S. (2012). Early-onset familial Alzheimer's disease (EOFAD). *Canadian Journal of Neurological Sciences*, *39*(4), 436–445.

Wyckoff, R. (1963). Interscience publishers, new york, new york rocksalt structure. *Crystal Structures*, *1*, 85–237.

Xue, B., Liu, Y., Li, B., Lu, Y., Zhou, L., Ye, S., Lu, H., Luo, X., Liang, A., & Li, P. (2025).

Comparison of efficacy and adverse effects of CD19/20 CART versus CD19 single-target CART in R/R DLBCL: a single-center retrospective study. *Frontiers in Immunology*, *16*, 1582944.

Yadav, A., Verma, R. K., Basole, S., Tripathi, G., Das, K., Jena, N., & Kumar, S. (2025). Phytochemical analysis of leaves, stem and root of Punarnava (Boerhavia diffusa L.): a medicinal herb of Nyctaginaceae. *Plants and Secondary Metabolites*, *5*.

Yadav, S. K., & Puranik, P. (2025). Improvements in Phytochemical-Based Drug Delivery Systems. In *Nano-formulation of Dietary Phytochemicals for Cancer Management* (pp. 241–274). Springer.

Yang, Y., Yao, K., Repasky, M. P., Leswing, K., Abel, R., Shoichet, B. K., & Jerome, S. V. (2021). Efficient exploration of chemical space with docking and deep learning. *Journal of Chemical Theory and Computation*, *17*(11), 7106–7119.

Yankner, B. A., & Mesulam, M.-M. (1991). β-amyloid and the pathogenesis of Alzheimer's disease. *New England Journal of Medicine*, *325*(26), 1849–1857.

Yepes, A. F., Cardona-Galeano, W., Herrera-Ramírez, A., Rada, M. S., Osorio, E., Gonzalez-Molina, L. A., Miranda-Brand, Y., & Posada-Duque, R. (2025). Novel multipotent conjugate bearing tacrine and donepezil motifs with dual cholinergic inhibition and neuroprotective properties targeting Alzheimer's disease. *RSC Medicinal Chemistry*.

Yip, H. Y. K., & Papa, A. (2021). Signaling pathways in cancer: therapeutic targets, combinatorial treatments, and new developments. *Cells*, *10*(3), 659.

You, X., Zhang, Z., Tian, G., Zhang, Y., Pei, Y., Wu, Y., Li, G., Wang, Q., & Yang, Y. (2025). The impact of polyethylene microplastics exposure on the, growth performance, reproductive performance, antioxidant capacity, and intestinal microbiota of quails. *Ecotoxicology and Environmental Safety*, *296*, 118218.

Yu, Q., Liu, B., Ren, Z., Liu, L., Zhang, L., Yin, X., Shen, W., Fang, Z., & Jia, R. (n.d.). Lc/Ms and Maldi-Msi Reveal The Different Distribution of Terpenoids in Glycine Max and Glycine Soja Seeds. *Available at SSRN 5093842*.

Zahraee, H., Arab, S. S., Parvaee, E., Mohammadi, F., Abnous, K., Taghdisi, S. M., & Khoshbin, Z. (2025). Simulation study of solvent effect on competitive degradation of aggregation of homo-and hetero-amyloid-β dimers. *Journal of Molecular Liquids*, *417*, 126658.

Zarth, A. T., & Magallanes López, A. M. (2025). A New UHPLC-UV-MS Method for Detection and Identification of Bioactive Compounds. *Journal of AOAC International*,

qsaf039.

Zhang, H., Tang, J., Cao, H., Wang, C., Shen, C., & Liu, J. (2025). Effect and mechanism of Magnolia officinalis in colorectal cancer: Multi-component-multi-target approach. *Journal of Ethnopharmacology*, *338*, 119007.

Zhang, Y., Huber, G. W., & Guo, Z. (2025). Hydrogen-bond catalysis in biomass valorization. *Chem*, *11*(2).

Zhang, Yan, et al. "Ginsenosides attenuate d-galactose-and AlCl3-inducedspatial memory impairment by restoring the dysfunction of the neurotransmitter systems in the rat model of Alzheimer's disease." *Journal of ethnopharmacology* 194 (2016): 188-195.

Zhao, X., Wang, L., Li, Q., Chen, H., Liu, S., Hou, P., Ye, J., Pei, Y., Wu, X., & Yuan, J. (2025). 3D microstructural generation from 2D images of cement paste using generative adversarial networks. *Cement and Concrete Research*, *187*, 107726.

Zheng, J., Jin, Y., Wang, C., Feng, C., Lai, X., Hua, S., & Tai, J. (2025). Global, regional, and national epidemiology of allergic diseases in children from 1990 to 2021: findings from the Global Burden of Disease Study 2021. *BMC Pulmonary Medicine*, *25*(1), 54.

Zoete, V., Cuendet, M. A., Grosdidier, A., & Michielin, O. (2011). SwissParam: a fast force field generation tool for small organic molecules. *Journal of Computational Chemistry*, *32*(11), 2359–2368.

Zuriaga-Monroy, C., Oviedo-Roa, R., Montiel-Sánchez, L. E., Vega-Paz, A., Marín-Cruz, J., & Martínez-Magadán, J. M. (2016). Theoretical Study of the Aliphatic-Chain Length's Electronic Effect on the Corrosion Inhibition Activity of Methylimidazole-Based Ionic Liquids. *Industrial and Engineering Chemistry Research*, *55*(12), 3506–3516. https://doi.org/10.1021/acs.iecr.5b03884

ANNEXES

Annexes

Annex 1 Published Article

Journal of the Algerian Chemical Society

Journal homepage: https://www.jacs-dz.org

ISSN 1111-4797

Comprehensive phytochemical characterization and antioxidant potential of *origanum majorana* L. Methanolic extract: Integrated in vitro assays and in silico evaluation of glutathione reductase inhibition

Aya Rouiha[1,2], Hadil Boudiaf[1,2], Serine Kebache[1,2], Elhafnaoui Lanez[1,2*], Mohammed Larbi Benamor[1,3], Ouafa Boudebia[1,2], Housseyn Chaoua[1,2]

[1]University of El Oued, VTRS Laboratory, P.O. Box 789, 39000, El Oued, Algeria
[2]University of El Oued, Faculty of Biology, P.O. Box 789, 39000, El Oued, Algeria
[3]University of El Oued, Faculty of Technology, P.O. Box 789, El Oued 39000, Algeria

Article History

Received: 26/04/2025
Revised: 12/05/2025
Accepted: 19/05/2025

ABSTRACT

Origanum majorana L. methanolic extract showed strong antioxidant activity (DPPH IC_{50}: 4.05 µg/mL; ABTS: 10.56 µg/mL; FRAP: 9.55 µg/mL), with flavonoids, phenolics, and terpenoids identified. Molecular docking revealed trans-thujone as a top binder to glutathione reductase (−7.73 kcal/mol), and 100 ns molecular dynamics confirmed complex stability. These findings support its potential against oxidative stress-related enzymes.

Keywords: *Origanum majorana L.*, antioxidant activity, methanolic extract, molecular docking, molecular dynamics simulation, glutathione reductase.

1. INTRODUCTION

Oxidative stress is a critical pathological condition caused by an imbalance between reactive oxygen species (ROS) production and the body's antioxidant defense system. It plays a central role

in the onset and progression of various chronic diseases, including cardiovascular disorders, neurodegenerative diseases, cancer, and metabolic syndromes such as diabetes [1,2]. ROS are highly reactive molecules that can damage essential biomolecules such as lipids, proteins, and DNA, leading to cellular dysfunction and death [3]. Therefore, antioxidants, which neutralize ROS and reduce oxidative damage, are vital in preventing oxidative stress-related diseases [4].

Synthetic antioxidants are widely used in pharmaceuticals and the food industry; however, concerns about their safety and potential side effects have prompted increasing interest in natural antioxidants derived from medicinal plants [5]. Among these, *Origanum majorana* L. (sweet marjoram), a perennial herb from the Lamiaceae family, has gained attention for its rich phytochemical profile and broad spectrum of pharmacological properties, including antioxidant, antimicrobial, and anti-inflammatory effects [6,7].

Historically used as an aromatic and culinary herb, *Origanum majorana* L has demonstrated promising biological potential, attributed to its abundance in bioactive compounds such as flavonoids, phenolics, terpenes, and tannins [8]. Recent studies have highlighted the antioxidant properties of its essential oils and extracts, yet there is a limited understanding of the specific antioxidant mechanisms and the molecular interactions of its active constituents [9].

In this study, the antioxidant activity of the methanolic extract of *Origanum majorana* L. was evaluated using three validated *in vitro* assays 2,2-diphenyl-1-picrylhydrazyl (DPPH), 2,2′-azinobis(3-ethylbenzothiazoline-6-sulfonic acid) (ABTS), and ferric reducing antioxidant power (FRAP). These tests assess radical scavenging and electron-donating capacity, offering complementary insights into antioxidant potential. Phytochemical screening was also conducted to determine the presence of phenols, flavonoids, tannins, and other secondary metabolites.

To better understand the molecular basis of antioxidant activity, *in silico* analyses were conducted. Molecular docking was used to predict the binding affinity of the major compounds with glutathione reductase (GR), a key enzyme in maintaining cellular redox homeostasis. Further, molecular dynamics (MD) simulations evaluated the structural stability of the ligand-enzyme complex under physiological conditions. This multidisciplinary approach integrates experimental and computational strategies to validate the antioxidant potential of *Origanum majorana* L methanolic extract and highlights its possible application as a natural antioxidant in therapeutic development.

2. RESULTS AND DISCUSSION

3.1. Plant Extraction

As shown in Table 1, the extraction yield obtained in the present study was higher than that reported by Benine [38], but lower than the yield observed by Bouyahya et al. [8]. Such discrepancies can be attributed to several abiotic and geographical variables, including climatic conditions, solar exposure, altitude, soil characteristics, harvesting season, and the developmental stage of the plant [39]. Moreover, extraction yield is also influenced by intrinsic factors such as plant species, the specific plant part used, drying methods, metabolite concentration, extraction technique, and solvent polarity, which directly affect the solubility and recovery of bioactive compounds [40,41].

Table 1. Extraction yield (%) of the methanolic extract of *Origanum majorana L.* compared with previously reported values in the literature

Origanum Majorana L	Present Study	[38]	[8]
Yield (%)	26.89	24.05	27.09

3.2. Phytochemical Tests

The phytochemical screening results, summarized in Table 2, confirmed the presence of several secondary metabolites—including flavonoids, polyphenols, terpenes, saponins, reducing sugars, tannins, and glycosides—in the methanolic extract of the aerial parts of *Origanum majorana* L. Conversely, alkaloids were not detected in the tested sample.

Table 2. Qualitative phytochemical profile of the methanolic extract of *Origanum majorana L*

Secondary Metabolites	**Results**
Polyphenols	++
Flavonoids	++
Terpenoids	+
Alkaloids	-
Tannins	+
Saponins	+
Reducing sugars	+
Glucosides	+

++ Compound strongly present, + Compound present, - Compound absent

The phytochemical screening of the methanolic extract of *Origanum majorana L.* aerial parts revealed the presence of key secondary metabolites, including flavonoids, polyphenols, terpenes, saponins, reducing sugars, tannins, and glycosides, whereas alkaloids were absent (Table 2). These findings are generally consistent with previous reports on the phytochemical composition of *O. majorana* [42,43]. However, the detection of reducing sugars in the present study differs from earlier studies, which may be attributed to variations in extraction solvents, plant origin, or growth conditions. The abundant presence of bioactive constituents such as tannins, flavonoids, saponins, and terpenes highlights the pharmacological potential of this species. These compounds are widely recognized for their diverse biological activities, including antimicrobial, antioxidant, anti-inflammatory, and antidiabetic effects [44,45], supporting the traditional medicinal use of O. majorana in herbal therapies

3.3. Quantification of Polyphenols, Flavonoids, and Tannins

Table 3. Quantification of polyphenols, flavonoids, and tannins in *Origanum majorana L.* extract

Extract	TFC (µg EQu/mg Ex)	TPC (µg GAE/mg Ex)	CTC (µg CTE/mg Ex)
Origanum majorana L	48.16 ± 0.003	95.07 ± 0.001	2.17 ± 0.09

The quantitative analysis of the *Origanum majorana* L methanolic extract revealed the following contents: total polyphenols at 95.07 ± 0.001 µg GAE/mg extract, flavonoids at 48.16 ± 0.003 µg QE/mg extract, and tannins at 2.17 ± 0.09 µg CE/mg extract, as detailed in Table 3. These values are in agreement with previous reports, which recorded comparable levels of flavonoids (57.55 µg QE/mg), tannins (2.6 µg CE/mg), and polyphenols (51.54 µg GAE/mg) in *Origanum majorana* L extracts [46,47]. Variations in phenolic content can be influenced by several factors, including drying technique, solvent polarity, extraction parameters, geographic location, and environmental stressors. Notably, plants exposed to abiotic stress tend to increase phenolic production, as a protective response that enhances resilience and survival [48,49].

3.4. *In Vitro* Antioxidant Activity

The antioxidant activity of the methanolic extract of *Origanum majorana L.* was determined using three standard assays: DPPH, FRAP, and ABTS, with ascorbic acid employed as the positive

control. In the DPPH assay, the extract exhibited an IC_{50} of 4.052 ± 1.722 µg/mL, while the FRAP assay revealed an EC_{50} of 9.551 ± 0.85 µg/mL. In comparison, ascorbic acid showed respective values of 6.032 ± 0.195 µg/mL and 8.313 ± 0.199 µg/mL. The ABTS assay further confirmed the antioxidant capacity of the extract, recording an IC_{50} of 10.556 ± 0.52 µg/mL, compared to 11.556 ± 0.594 for the reference compound (Table 4). These results align with previous findings reporting similar IC_{50} and EC_{50} values, thereby reinforcing the strong radical scavenging potential of *Origanum majorana L* [50,51]. Variations may stem from differences in extraction techniques, solvent polarity, or environmental factors affecting the plant's phytochemical profile.

Table 4. Antioxidant activities of Origanum majorana L extract

Sample	DPPH IC_{50} (µg/ml)	FRAP EC_{50} (µg/ml)	ABTS IC_{50} (µg/ml)
Origanum majorana L	4.052 ± 1.722	9.551 ± 0.85	10.556 ± 0.52
Ascorbic acid	6.032 ± 0.195	8.313 ± 0.199	11.556 ± 0.594

The antioxidant capacity of *Origanum majorana L.* extract was comprehensively evaluated using three well-established in vitro assays: DPPH radical scavenging, Ferric Reducing Antioxidant Power (FRAP), and ABTS radical cation decolorization. As summarized in Table 4, the extract demonstrated notable antioxidant potential across all methods. Specifically, the DPPH assay yielded an IC_{50} of 4.052 ± 1.722 µg/mL, while the FRAP and ABTS assays showed EC_{50} and IC_{50} values of 9.551 ± 0.85 µg/mL and 10.556 ± 0.52 µg/mL, respectively. Although slightly less active than the reference antioxidant ascorbic acid (IC_{50} = 6.032 ± 0.195 µg/mL for DPPH, EC_{50} = 8.313 ± 0.199 µg/mL for FRAP, and IC_{50} = 11.556 ± 0.594 µg/mL for ABTS), the extract still exhibited strong radical scavenging and reducing power.

These results are consistent with earlier studies that link high phenolic and flavonoid content to robust antioxidant effects [38]. The notable activity observed can be attributed to the abundance of polyphenolic compounds especially hydroxylated flavonoids which play a critical role in neutralizing free radicals and reducing oxidative stress [52,53]. Moreover, the antioxidant response was concentration-dependent, further supporting the bioactivity of *Origanum majorana L* and justifying its traditional therapeutic applications in oxidative stress-related conditions [54].

3.6. *In Silico* Antioxidant Activity

3.6.1. Molecular Docking

The molecular docking analysis was conducted to evaluate the interaction potential of compounds identified in the methanolic extract of *Origanum majorana L.* with glutathione reductase (PDB ID: 1GRE). Only the major phytoconstituents (relative abundance >1%) were considered, as these are more likely to exert significant biological effects. The compounds included in the docking study were previously identified through phytochemical profiling of the extract [10].

The results indicated that all selected compounds exhibited negative binding free energy (ΔG) values, reflecting favourable interactions with the active site of glutathione reductase. Compared to the standard antioxidant drug, ascorbic acid (ΔG = – 4.85 kcal/mol), several major constituents of the extract showed stronger binding affinities. Notably, trans-thujone (ΔG = –7.73 kcal/mol), cis-verbenyl acetate (ΔG = –6.64 kcal/mol), and alpha-Terpineol (ΔG = –6.23 kcal/mol), demonstrated the most potent binding interactions (Table 5).

These findings suggest that the methanolic extract of *Origanum majorana L* harbors bioactive molecules with potential inhibitory effects on glutathione reductase activity, which may contribute to its observed antioxidant properties. The strong binding affinities of these compounds support their potential therapeutic relevance, particularly in mitigating oxidative stress through modulation of redox-regulating enzymes.

Table 5. Binding energy (kcal/mol) of abundant *Origanum majorana L* compounds

Ligand	ΔG
Trans-thujone	-7.73
alpha-Terpineol	-6.23
Cis-verbenylacetate	-6.64

From studies on the X-ray crystal structure and enzyme kinetics of GR, it was found that GR active site is characterized by the existence of three special amino acid residues namely ASP-197, GLU-233 and ASP-300 which contribute to the overall catalytic action of the enzyme towards starch hydrolysis [55]. ASP-197 acts as a catalytic nucleophile during starch hydrolysis, GLU-233 residue acts as acid–base catalyst, while ASP-300 plays the role of optimizing the orientation of the substrate [55]. The docking interaction profiles presented in Figure 1 revealed that the top

compounds identified in the methanolic extract of *Origanum majorana L.* showed consistent binding orientations and interacted with key residues located at the active site of glutathione reductase. Notably, several phytoconstituents formed hydrogen bonds and hydrophobic interactions with the enzyme's critical catalytic residues—ASP-197, GLU-233, and ASP-300—which are essential for its redox function.

Among the best-performing ligands, trans-thujone interacted with all three catalytic residues, suggesting a strong potential for competitive inhibition. In contrast, alpha-Terpineol interacted with only two of these critical residues (ASP-197 and GLU-233), while cis-verbenyl acetate], despite its high binding affinity, formed interaction with only one of the key catalytic residues. This discrepancy may suggest a non-competitive inhibition mechanism, whereby the compound binds outside the active site yet still interferes with enzymatic activity.

Overall, the *in silico* binding mode analysis revealed interactions not only with the catalytic triad but also with additional residues such as TRP-58, TRP-59, TYR-62, and GLN-63, reinforcing the likelihood of effective inhibition. These docking results support the biochemical evidence of antioxidant activity, further confirming that the phytoconstituents of *O. majorana* methanolic extract possess the potential to modulate glutathione reductase activity via specific residue interactions. The key ligand-protein interactions and binding conformations within the catalytic pocket of 1GRE are illustrated in Figure 1.

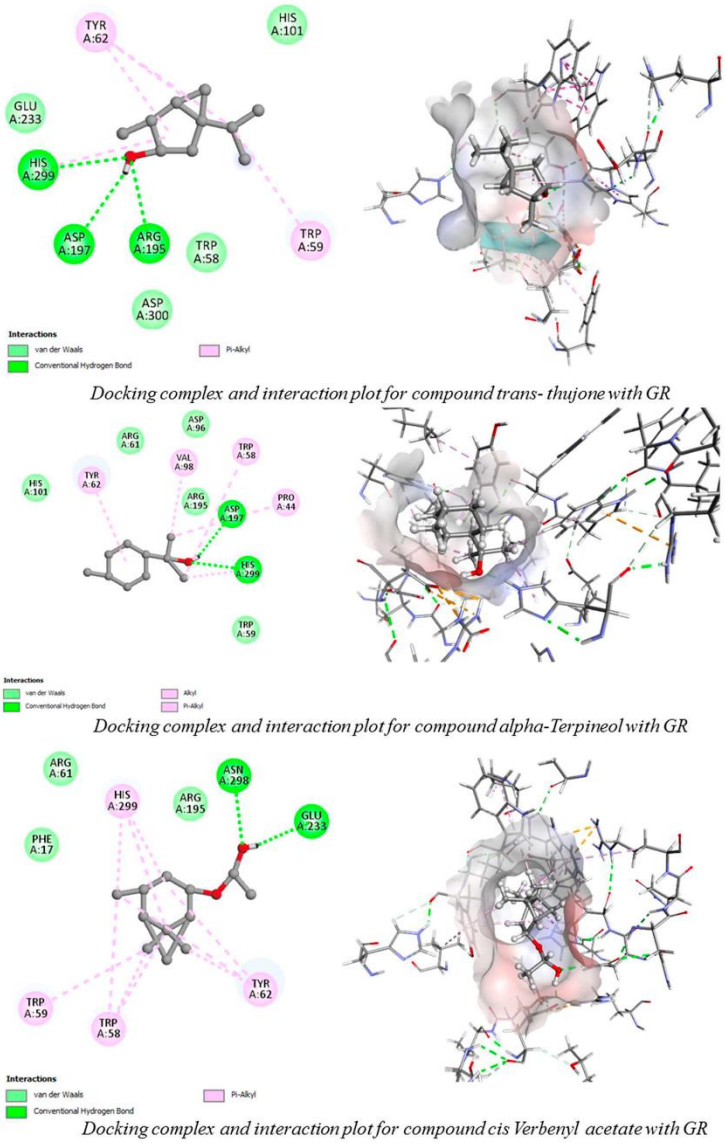

Fig.1. Molecular interactions of studied compounds with glutathione reductase

3.6.2. MD Simulation Analysis

Molecular dynamics (MD) simulations offer critical insights into the conformational stability and interaction dynamics of protein–ligand complexes under near-physiological conditions. Based on docking scores, the most promising compound identified from the methanolic extract of *Origanum majorana* L., trans-thujone, was selected for MD simulations in complex with glutathione reductase (PDB ID: 1GRE). This compound was prioritized due to its strong binding affinity (ΔG). The dynamic behavior and structural integrity of the complex were assessed using key MD parameters: root mean square deviation (RMSD) to evaluate backbone stability, root mean square fluctuation (RMSF) to analyze residue-level flexibility, radius of gyration (Rg) to determine the overall compactness of the protein, and solvent-accessible surface area (SASA) to estimate surface exposure and molecular interactions.

The average values of these parameters (Table 6) revealed meaningful insights into the structural dynamics of the simulated system. The 1GRE–trans-thujone complex exhibited a low RMSD value, indicating enhanced structural stability throughout the simulation period. Meanwhile, the RMSF values remained consistent, suggesting uniform residue-level flexibility and the absence of significant disruptions in the protein's dynamic behavior.

Table 6. Average values of RMSD, RMSF, Rg, and SASA obtained from MD simulations studies.

1GRE–trans-thujone	
RMSD (nm)	0.192
RMSF (nm)	0.115
SASA (nm^2)	205.960
Rg (nm)	2.367

The Rg analysis showed minimal fluctuations, confirming stable folding and overall compactness of the protein structure. The slightly lower Rg observed for the ligand-bound complex suggested a more compact conformation upon trans-thujone binding. Additionally, the SASA values indicated reduced solvent exposure in the complex, implying tighter molecular packing and improved structural integrity.

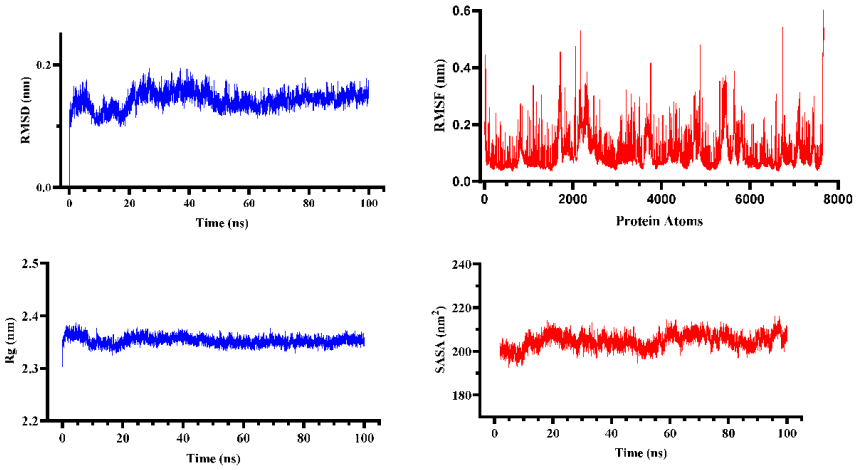

Fig .2. Molecular Dynamics Simulation Analysis of the Protein-Ligand Complex Over 100 ns

As illustrated in Figure 2, the simulation results confirm that the methanolic extract-derived compound from *Origanum majorana* (trans-thujone) forms stable, well-packed, and sustained interactions within the active site of glutathione reductase. These findings support its potential as a promising glutathione reductase inhibitor and highlight its relevance for further pharmacological investigation.

3. EXPERIMENTAL

3.1. Plant Material Collection and Authentication

The aerial parts of *Origanum majorana* L. were collected during the flowering stage in October 2024 from the Negrine region, located in Tébessa Province in northeastern Algeria. Following harvest, the plant material was air-dried in a well-ventilated, shaded area to minimize photodegradation and preserve the phytochemical integrity. The dried material was subsequently ground into a fine powder, stored in a sealed glass container, and kept away from light and moisture until further analysis. Botanical identification was carried out by Professor DJAHRA Ali Boutlelis (Department of Biology, Faculty of Science and Natural Life, University of El Oued, Algeria). A voucher specimen was deposited in the departmental herbarium under the accession number EH-405.

3.2. Extraction Procedure

The extraction procedure was conducted based on the method described by El Amiri et al. (2025) [10], with minor modifications. In brief, 50 g of the powdered aerial parts of *Origanum majorana* L. were macerated in 250 mL of methanol at room temperature, protected from light, for 24 hours. This process was repeated three consecutive times to maximize the extraction of bioactive constituents. The resulting mixtures were filtered through Whatman filter paper, and the combined filtrates were concentrated under reduced pressure using a Büchi R-200 rotary evaporator set at 50 °C. The semi-solid extract was subsequently lyophilized using a Christ freeze dryer to obtain a stable dry powder. To ensure complete removal of residual moisture, the extract was further dried in a ventilated oven at a temperature not exceeding 40 °C for 48 hours. The final product was aseptically transferred into amber glass bottles and stored at 4 °C until further use.

The extraction yield was expressed as a percentage, calculated by equation 1 according to the formula proposed by Bouhalla et al [11]:

$$\text{Yield (\%)} = \left(\frac{M_E}{M_s}\right) \times 100 \qquad (1)$$

Where: M_E is the mass after evaporation of solvent in g; Ms is dry mass of the sample in g.

3.3. Phytochemical Screening

Methanolic extraction was carried out by decocting 2 g of dried *Origanum majorana L.* aerial powder in 50 mL of distilled water for 30 minutes using a controlled water bath. After boiling, the mixture was filtered through Whatman No. 01 filter paper to obtain a clear extract. This extract was subjected to qualitative phytochemical analysis aimed at detecting major bioactive groups based on solubility, colour change, turbidity, and precipitation in the presence of specific reagents. The identification of phytoconstituents was conducted following the procedure described by [12], and the tests are outlined in Table 7.

Table 7. Qualitative Phytochemical Screening of Methanolic Extract from *Origanum majorana L.*

Phytochemical Group	Reagent/Test Applied	Indicative Observation
Polyphenols	Folin–Ciocalteu reagent	Development of blue color
Flavonoids	$AlCl_3$ solution (10%) added to 1 mL extract	Yellow coloration formation
Terpenoids	Acetic anhydride + concentrated H_2SO_4	Appearance of deep red hue
Tannins	$FeCl_3$ (5%) in aqueous extract	Greenish precipitate observed
Saponins	Vigorous shaking of equal parts extract and water	Persistent froth formation
Reducing Sugars	α-Naphthol (20% ethanol) + concentrated H_2SO_4	Formation of red precipitate
Glycosides	Chloroform + acetic acid added to extract	Color change from violet to blue/green

3.4. Quantification of Bioactive Compounds

3.4.1. Total Polyphenol Content (TPC)

The total polyphenol content was quantified using a modified Folin–Ciocalteu colorimetric method, based on the protocol of Nikolaeva et al [13]. Briefly, 0.2 mL of various concentrations of *Origanum majorana L.* methanolic extract were added to 1 mL of 10% Folin–Ciocalteu reagent. After 5 minutes of reaction, 0.8 mL of 7.5% sodium carbonate solution was added. The mixture was incubated for 30 minutes at room temperature in the dark, and absorbance was recorded at 765 nm using a UV-Vis spectrophotometer. A calibration curve was prepared using gallic acid (20–160 µg/mL), and results were expressed as mg gallic acid equivalents per gram of extract (mg GAE/g E).

3.4.2. Total Flavonoid Content (TFC)

Flavonoid content was measured using the aluminum chloride colorimetric assay described by Shraim et al [14]. In this method, 0.5 mL of each extract concentration was mixed with 0.5 mL of 2% $AlCl_3$ solution. The mixture was kept in the dark at room temperature for 1 hour, and absorbance was measured at 420 nm. Quercetin standards (0–50 µg/mL) were used to generate the

calibration curve. The results were reported as mg quercetin equivalents per gram of extract (mg QE/g E).

3.4.3. Condensed Tannin Content (CTC)

Condensed tannins were quantified using the vanillin-HCl method, as described by Palacios et al. [15]. This method relies on the reaction of vanillin with catechin units to produce a red-coloured complex that absorbs at 500 nm. For each assay, 500 µL of extract or catechin standard (0–1.5 µg/mL) was mixed with concentrated hydrochloric acid containing vanillin, and the mixture was incubated for 15 minutes. Absorbance was measured at 500 nm, and the tannin content was expressed as mg catechin equivalents per gram of extract (mg CE/g E).

3.5. In Vitro Antioxidant Activity

The antioxidant capacity of the methanolic extract of *Origanum majorana L.* was assessed in vitro through three complementary assays: ABTS, DPPH, and FRAP. These methods were employed to evaluate the free radical scavenging and reducing power of the extract. Alpha-tocopherol and ascorbic acid served as standard antioxidants for comparative analysis [16,17]. Serial dilutions of the extract were prepared at concentrations of 100, 50, 25, 12.5, 6.25, 3.125, and 1.56 µg/mL, followed by a 30-minute sonication to ensure homogenization. Absorbance measurements were recorded spectrophotometrically against appropriate blanks, and the percentage of inhibition was calculated using the standard formula (Equation 2) as described by [18].

$$\text{Radical scavenging activity (\%)} = \left(\left(A_{control} - A_{sample}\right)/A_{control}\right) \times 100 \qquad (2)$$

3.5.1. ABTS Radical Scavenging Assay

The ABTS assay was conducted based on the method by Re et al. [19], with slight modifications. The $ABTS^{\bullet+}$ radical was generated by reacting 7 mM ABTS solution with 2.45 mM potassium persulfate in distilled water and incubating the mixture in the dark for 12–16 hours at room temperature. For the assay, 0.2 mL of the *Origanum majorana L.* methanolic extract at different concentrations was mixed with 1.0 mL of methanol and 0.16 mL of the $ABTS^{\bullet+}$ solution, making a total volume of 1.36 mL. After 20 minutes of incubation at room temperature, absorbance was measured at 734 nm.

3.5.2. DPPH Radical Scavenging Assay

The free radical scavenging capacity of the extract was assessed using the DPPH assay following the protocol of Filote et al. [20]. Briefly, 3 mL of the extract was added to 2 mL of DPPH solution

(in methanol), and the mixture was incubated at 37°C for 30 minutes in the dark. The reduction in absorbance was then measured at 517 nm.

3.5.3. FRAP Assay

The ferric reducing antioxidant power (FRAP) of the extract was determined according to the method of Ben Ali et al. [21], with slight modifications. A volume of 200 µL of extract was combined with 500 µL of 1% potassium ferricyanide [$K_3Fe(CN)_6$] and 500 µL of methanol. The mixture was incubated at 50°C for 20 minutes. Afterward, 500 µL of 10% trichloroacetic acid was added to stop the reaction, followed by 1.7 mL of methanol and 200 µL of 0.1% $FeCl_3$. The absorbance was recorded at 700 nm against a methanol blank.

3.6. *In Silico* Evaluation of the Antioxidant Activity

3.6.1. Molecular Docking Studies

Molecular docking studies were performed to assess the binding affinities of the major phytoconstituents present in the methanolic extract of *Origanum majorana L*, as identified by El Amiri et al. [10], against the glutathione reductase (GR) enzyme (PDB ID: 1GRE) [22], selected as the target receptor for this investigation. The three-dimensional structure of the GR enzyme was obtained from the Protein Data Bank (PDB) [23] and pre-processed by removing water molecules and non-essential co-crystallized ligands. Ligand structures were retrieved from the PubChem database [24] in SDF format and subsequently converted to PDB format using Open Babel software [25].

Protein preparation was conducted using AutoDock Tools (ADT), where polar hydrogen atoms were added, and Kollman partial charges were assigned to the receptor [26,27]. Ligand structures were optimized, and torsional bonds were defined. A grid box with dimensions of 80 × 80 × 80 Å was centred on the active site with coordinates X − 62.85, Y − 49.85, Z − 18.34.

Docking simulations were executed using AutoDock 4.2, applying the Lamarckian Genetic Algorithm (LGA) with 20 independent runs per ligand, while default parameters were maintained for all other settings. Binding interactions and docking conformations were visualized and analysed using Discovery Studio Visualizer 2021 [28]. To validate the docking protocol, redocking of the native ligand into the enzyme's active site was performed. The docking approach was considered reliable when the root mean square deviation (RMSD) between the docked pose and the native ligand conformation was less than 2 Å [29].

3.6.2. Molecular Dynamics (MD) Simulation

Molecular dynamics (MD) simulations of the glutathione reductase ligand complexes were performed using the GROMACS 2023 package for a duration of 100 nanoseconds. The primary aim of these simulations was to rigorously investigate the conformational dynamics, structural stability, and interaction patterns of the complexes, with comparative insights drawn from the reference system (GR–α-tocopherol).

Ligand topologies were generated using the SwissParam server [30], which provides molecular parameters compatible with the CHARMM force field, enabling accurate ligand modelling. The protein topology was prepared using the CHARMM36 all-atom force field [31,32], ensuring a detailed and reliable representation of the receptor during simulations. Each protein ligand complex was solvated in a cubic simulation box filled with TIP3P water molecules, and neutralized by adding Na^+ and Cl^- ions to mimic physiological ionic conditions [33].

Energy minimization was executed using the steepest descent algorithm until the maximum force on the system was reduced below 10.0 kJ/mol, ensuring proper relaxation and eliminating steric clashes prior to equilibration [34]. Equilibration was performed in two sequential phases: NVT (constant number of particles, volume, and temperature) and NPT (constant number of particles, pressure, and temperature). In the NVT phase, the system was equilibrated at 300 K for 100 ps using the V-rescale thermostat with a coupling constant of 0.1 ps. This was followed by 100 ps of NPT equilibration using the Berendsen barostat (coupling constant: 2.0 ps) to maintain pressure stability [34,35].

The production MD run generated trajectories from which various parameters were extracted to assess the dynamic behavior of the complexes. Root mean square deviation (RMSD) was used to evaluate system stability, while root mean square fluctuation (RMSF) provided insights into residue-level flexibility. The radius of gyration (Rg) measured the structural compactness of the protein, and the solvent-accessible surface area (SASA) quantified the exposure of molecular surfaces to the solvent.

To further evaluate the binding affinity and interaction energetics, the Molecular Mechanics Poisson–Boltzmann Surface Area (MM-PBSA) method was applied using the g_mmpbsa tool [36]. This approach decomposes the binding free energy into key components—van der Waals interactions, electrostatics, polar and nonpolar solvation energies according to the following expression (Equation 3) [37]:

$$\Delta G_{Binding} = \Delta G_{Complex} - \left(G_{Protein} + G_{Ligand}\right) \quad (3)$$

Where $G_{complex}$, $G_{protein}$, and G_{ligand} represent the total free energies of the protein–ligand complex, the unbound protein, and the unbound ligand, respectively.

4. CONCLUSION

This study demonstrated the strong antioxidant potential of *Origanum majorana* L. methanolic extract through phytochemical analysis, in vitro assays, and in silico modeling. The presence of phenolics, flavonoids, and terpenoids supports its bioactivity. Trans-thujone, a key constituent, showed high affinity for glutathione reductase, with molecular dynamics confirming stable binding and enhanced protein compactness. These findings highlight *O. majorana* as a promising natural antioxidant, meriting further in vivo validation and compound isolation for therapeutic development.

5. ACKNOWLEDGEMENTS

This work was supported by the directorate-general of scientific research and technological development (DGRSDT) and the laboratory of valorization and technology of Saharan resources (VTRS) (project code: B00L01UN390120150001). The authors are very thankful to Prof. Touhami Lanez the head of the VTRS laboratory.

6. REFERENCES

[1] Jomova, K.; Raptova, R.; Alomar, S. Y.; Alwasel, S. H.; Nepovimova, E.; Kuca, K.; Valko, M. Reactive Oxygen Species, Toxicity, Oxidative Stress, and Antioxidants: Chronic Diseases and Aging. *Arch. Toxicol.* **2023,** 97, 2499–2574.

[2] Sharifi-Rad, M.; Anil Kumar, N. V.; Zucca, P.; Varoni, E. M.; Dini, L.; Panzarini, E.; Rajkovic, J.; Tsouh Fokou, P. V.; Azzini, E.; Peluso, I. Lifestyle, Oxidative Stress, and Antioxidants: Back and Forth in the Pathophysiology of Chronic Diseases. *Front. Physiol.* **2020,** 11, 552535.

[3] Juan, C. A.; Pérez de la Lastra, J. M.; Plou, F. J.; Pérez-Lebeña, E. The Chemistry of Reactive Oxygen Species (ROS) Revisited: Outlining Their Role in Biological Macromolecules (DNA, Lipids and Proteins) and Induced Pathologies. *Int. J. Mol. Sci.* **2021,** 22, 4642.

[4] Engwa, G. A.; Nweke, F. N.; Nkeh-Chungag, B. N. Free Radicals, Oxidative Stress-Related Diseases and Antioxidant Supplementation. *Altern. Ther. Health Med.* **2022,** 28.

[5] Lourenço, S. C.; Moldão-Martins, M.; Alves, V. D. Antioxidants of Natural Plant Origins: From Sources to Food Industry Applications. *Molecules* **2019,** 24, 4132.

[6] Muqaddas, R. A. K.; Nadeem, F.; Jilani, M. I. Essential Chemical Constituents and Medicinal Uses of Marjoram (*Origanum majorana L.*) – A Comprehensive Review. *Int. J. Chem. Biochem. Sci.* **2016,** 9, 56–62.

[7] Tripathy, B.; Satyanarayana, S.; Khan, K. A.; Raja, K. An Updated Review on Traditional Uses, Taxonomy, Phytochemistry, Pharmacology and Toxicology of *Origanum majorana. Int. J. Pharm. Res. Health Sci.* **2017,** 5, 1717 1723.

[8] Bouyahya, A.; Chamkhi, I.; Benali, T.; Guaouguaou, F.-E.; Balahbib, A.; El Omari, N.; Taha, D.; Belmehdi, O.; Ghokhan, Z.; El Menyiy, N. Traditional Use, Phytochemistry, Toxicology, and Pharmacology of *Origanum majorana L. J. Ethnopharmacol.* **2021,** 265, 113318.

[9] Sabiha, M.; Yanisse, S.; Boudalia, M.; Najem, A.; Benhiba, F.; Belfhaili, A.; Bouatia, M. Promising Antioxidant, Antibacterial and Anticorrosive Properties of an Essential Oil Extract of *Origanum majorana L.* from Morocco. *Biointerface Res. Appl. Chem.* **2023,** 13, 1–27.

[10] El Amiri, M. A.; Kabdy, H.; Aitbaba, A.; Laadraoui, J.; Aboufatima, R.; El Yazouli, L.; Abdelmounaim, B.; Moubtakir, S.; Garzoli, S.; Abderrahman, C. Analysis of Chemical Composition, Antioxidant Capacity, Acute Toxicity, and Antinociceptive Properties of Aqueous Extract of *Origanum Majorana L. Chem. Biodivers.* **2025,** 22, e202401580.

[11] Bouhalla, A.-W.; Benabdelmoumene, D.; Dahmouni, S.; Bengharbi, Z.; Hellal, K.; Qadi, W. S. M.; Al-Olayan, E.; Moreno, A.; Bekada, A.; Buzgaia, N. Comparative LC–MS-Based Metabolite Profiling, Antioxidant, and Antibacterial Properties of *Bunium bulbocastanum* Tubers from Two Regions in Algeria. *Sci. Rep.* **2024,** 14, 21719.

[12] Singh, P. K.; Singh, J.; Medhi, T.; Kumar, A. Phytochemical Screening, Quantification, FT-IR Analysis, and In Silico Characterization of Potential Bio-Active Compounds Identified in HR-LC/MS Analysis of the Polyherbal Formulation from Northeast India. *ACS Omega* **2022,** 7, 33067–33078.

[13] Nikolaeva, T. N.; Lapshin, P. V.; Zagoskina, N. V. Method for Determining the Total Content of Phenolic Compounds in Plant Extracts with Folin–Denis Reagent and Folin–Ciocalteu Reagent: Modification and Comparison. *Russ. J. Bioorganic Chem.* **2022,** *48*, 1519–1525.

[14] Shraim, A. M.; Ahmed, T. A.; Rahman, M. M.; Hijji, Y. M. Determination of Total Flavonoid Content by Aluminum Chloride Assay: A Critical Evaluation. *LWT* **2021,** *150,* 111932.

[15] Palacios, C. E.; Nagai, A.; Torres, P.; Rodrigues, J. A.; Salatino, A. Contents of Tannins of Cultivars of Sorghum Cultivated in Brazil, as Determined by Four Quantification Methods. *Food Chem.* **2021,** *337,* 127970.

[16] Jinesh, V. K.; Jaishree, V.; Badami, S.; Shyam, W. Comparative evaluation of antioxidant properties of edible and non-edible leaves of *Anethum graveolens* Linn. *Indian J. Nat. Prod. Resour.* **2010,** *1* (2), 168–173.

[17] Jayakumar, S.; Mahendiran, D.; Viswanathan, V.; Velmurugan, D.; Rahiman, A. K. Heteroscorpionate-Based Heteroleptic Copper (II) Complexes: Antioxidant, Molecular Docking and *In Vitro* Cytotoxicity Studies. *Appl. Organomet. Chem.* **2017,** *31,* e3809.

[18] Lanez, E.; Saidi, M.; Lanez, T. Assessment of Antioxidant and DPPH Free Radical Scavenging Activity of 1,2-Dithiole-3-Thione Derivatives by Using Cyclic Voltammetry, Spectroscopic, and Molecular Docking Studies. *J. Sulfur Chem.* **2023,** *44,* 542–558. https://doi.org/10.1080/17415993.2023.2200142.

[19] Re, R.; Pellegrini, N.; Proteggente, A.; Pannala, A.; Yang, M.; Rice-Evans, C. Antioxidant Activity Applying an Improved ABTS Radical Cation Decolorization Assay. *Free Radic. Biol. Med.* **1999,** *26,* 1231–1237.

[20] Filote, C.; Lanez, E.; Popa, V. I.; Lanez, T.; Volf, I. Characterization and Bioactivity of Polysaccharides Separated through a (Sequential) Biorefinery Process from *Fucus spiralis* Brown Macroalgae. *Polymers (Basel)* **2022,** *14,* 4106. https://doi.org/10.3390/polym14194106.

[21] Ben Ali, A.; Chouikh, A.; Haddad, L. Tubers Resin from Algeria: A Promising Source of Natural Antioxidants, Anti-Inflammatory, and Photoprotective Compounds. *Ovidius Univ. Ann. Chem.* **2023,** *34,* 132–139.

[22] Karplus, P. A.; Schulz, G. E. Substrate Binding and Catalysis by Glutathione Reductase as Derived from Refined Enzyme: Substrate Crystal Structures at 2Å Resolution. *J. Mol. Biol.* **1989,** *210,* 163–180. https://doi.org/10.1016/0022-2836(89)90298-2.

[23] Rose, P. W.; Prlić, A.; Altunkaya, A.; Bi, C.; Bradley, A. R.; Christie, C. H.; Di Costanzo, L.; Duarte, J. M.; Dutta, S.; Feng, Z.; Green, R. K.; Goodsell, D. S.; Hudson, B.; Kalro, T.; Lowe, R.; Peisach, E.; Randle, C.; Rose, A. S.; Shao, C.; Tao, Y. P.; Valasatava, Y.; Voigt, M.; Westbrook, J. D.; Woo, J.; Yang, H.; Young, J. Y.; Zardecki, C.; Berman, H. M.; Burley, S. K. The RCSB

Protein Data Bank: Integrative View of Protein, Gene and 3D Structural Information. *Nucleic Acids Res.* **2017,** *45,* D271–D281.

[24] Kim, S.; Chen, J.; Cheng, T.; Gindulyte, A.; He, J.; He, S.; Li, Q.; Shoemaker, B. A.; Thiessen, P. A.; Yu, B. PubChem 2023 Update. *Nucleic Acids Res.* **2023,** 51, D1373–D1380. O'Boyle, N. M.; Banck, M.; James, C. A.; Morley, C.; Vandermeersch, T.; Hutchison, G. R. Open Babel: An Open Chemical Toolbox. *J. Cheminform.* **2011,** 3, 1–14.

[25] Ben Amor, M. L.; Lanez, E.; Bekkar, Y.; Adaika, A.; Lanez, T.; Nesba, K.; Bechki, L. Exploring the Interactions of Ferrocenylmethylnucleobase Derivatives With BSA and HHb: Insights From Electrochemical, Spectroscopic, ADMET, in Silico Docking, and MD Simulations. *ChemistrySelect* **2025,** 10, e202404678.

[26] Adaika, A.; Bekkar, Y.; Youmbai, S.; Bourougaa, L.; Lanez, E.; Ben Amor, M. L.; Nesba, K.; Lanez, T.; Bechki, L. Synthesis, Antioxidant, and Antidiabetic Potential of Ferrocenylmethylnucleobase Compounds: In Vitro, In Silico Molecular Docking, DFT Calculation, and Molecular Dynamic Simulations. *Appl. Organomet. Chem.* **2025,** 39, e7988.

[27] Biovia, D. S. Discovery Studio Visualizer; San Diego, CA, USA, 936, **2017**, 240–249.

[28] Lanez, E.; Zerrouk, L.; Bechki, L.; Lanez, T.; Adaika, A.; Zegheb, N.; Nesba, K. Synthesis, molecular docking, drug-likeness analysis, and ADMET prediction of nickel and zinc tetraphenyl-porphyrin complexes as possible antioxidant agents. *J. Chin. Chem. Soc.* **2024,** *71* (10), 1211–1229.

[29] Zoete, V.; Cuendet, M. A.; Grosdidier, A.; Michielin, O. SwissParam: A Fast Force Field Generation Tool for Small Organic Molecules. *J. Comput. Chem.* **2011,** *32,* 2359–2368.

[30] Huang, J.; Rauscher, S.; Nawrocki, G.; Ran, T.; Feig, M.; De Groot, B. L.; Grubmüller, H.; MacKerell, A. D., Jr. CHARMM36m: An Improved Force Field for Folded and Intrinsically Disordered Proteins. *Nat. Methods* **2017,** *14,* 71–73.

[31] Lotfi, B.; Mebarka, O.; Alhatlani, B. Y.; Abdallah, E. M.; Kawsar, S. M. A. Pharmacoinformatics and Breed-Based de Novo Hybridization Studies to Develop New Neuraminidase Inhibitors as Potential Anti-Influenza Agents. *Molecules* **2023,** *28,* 6678.

[32] Bourougaa, L.; Ouassaf, M.; Shtaiwi, A. Discovery of Novel Potent Drugs for Influenza by Inhibiting the Vital Function of Neuraminidase via Fragment-Based Drug Design (FBDD) and Molecular Dynamics Simulation Strategies. *J. Biomol. Struct. Dyn.* **2024,** *42,* 9294–9308.

[33] Bourougaa, L.; Ouassaf, M.; Khan, S. U. Comparative Molecular Field Analysis (CoMFA), Molecular Docking and ADMET Study on Thiazolidine-4-Carboxylic Acid Derivatives as New Neuraminidase Inhibitors. *Acta Chim. Slov.* **2023,** *70.*

[34] Balakit, A. A.; Makki, S. Q.; Sert, Y.; Ucun, F.; Alshammari, M. B.; Thordarson, P.; El-Hiti, G. A. Synthesis, Spectrophotometric and DFT Studies of New Triazole Schiff Bases as Selective Naked-Eye Sensors for Acetate Anion. *Supramol. Chem.* **2020,** *32,* 519–526.

[35] Kumari, R.; Kumar, R.; Lynn, A. G-MMPBSA - A GROMACS Tool for High-Throughput MM-PBSA Calculations. *J. Chem. Inf. Model.* **2014,** *54,* 1951–1962. https://doi.org/10.1021/ci500020m.

[36] Gogoi, B.; Chowdhury, P.; Goswami, N.; Gogoi, N.; Naiya, T.; Chetia, P.; Mahanta, S.; Chetia, D.; Tanti, B.; Borah, P. Identification of Potential Plant-Based Inhibitor Against Viral Proteases of SARS-CoV-2 through Molecular Docking, MM-PBSA Binding Energy Calculations and Molecular Dynamics Simulation. *Mol. Divers.* **2021,** 25, 1963–1977.

[37] Benine, C.; Laiche, T. A.; Mansouri, A.; Zoubeidi, D. Investigation of the *Origanum majorana* L. Extract and *Bacillus pulimus* Probiotics in Modulating Cortisol and Alleviating Anxiety in Rat Model. *Acta Period. Technol.* **2025,** 2.

[38] Ismaili, R.; Lamiri, A.; Moustaid, K. Study of Anti-Eczema Activity of Essential Oils of *Thymus vulgaris*, *Citrus limonum* and *Mentha spicata* from Morocco [Étude de l'activité anti-eczémateuse des huiles essentielles de *Thymus vulgaris*, *Citrus limonum* et *Mentha spicata* du Maroc]. *Int. J. Innov. Appl. Stud.* **2016,** 14, 113.

[39] Rodríguez De Luna, S. L.; Ramírez-Garza, R. E.; Serna Saldívar, S. O. Environmentally Friendly Methods for Flavonoid Extraction from Plant Material: Impact of Their Operating Conditions on Yield and Antioxidant Properties. *Sci. World J.* **2020,** 2020, 6792069.

[40] Isidore, S. A.; Kouabenan, A. B. O.; Etienne, O. K.; Noël, Z. G. Étude Botanique, Tri Phytochimique et Évaluation *in vitro* de l'Activité Antifongique des Extraits de Feuilles de *Mallotus oppositifolius* (Geisel.) Müll. Arg. *J. Anim. Plant Sci.* **2019,** 41, 6903–6915.

[41] Koldaş, S.; Demirtas, I.; Ozen, T.; Demirci, M. A.; Behçet, L. Phytochemical Screening, Anticancer and Antioxidant Activities of *Origanum vulgare* L. ssp. *viride* (Boiss.) Hayek, a Plant of Traditional Usage. *J. Sci. Food Agric.* **2015,** 95, 786–798.

[42] Taha, M.; Elazab, S. T.; Abdelbagi, O.; Saati, A. A.; Babateen, O.; Baokbah, T. A. S.; Qusty, N. F.; Mahmoud, M. E.; Ibrahim, M. M.; Badawy, A. M. Phytochemical Analysis of *Origanum*

majorana L. Extract and Investigation of Its Antioxidant, Anti-Inflammatory and Immunomodulatory Effects Against Experimentally Induced Colitis Downregulating Th17 Cells. *J. Ethnopharmacol.* **2023,** 317, 116826.

[43] Ennaji, H.; Chahid, D.; Aitssi, S.; Badou, A.; Khlil, N.; Ibenmoussa, S. Phytochemicals Screening, Cytotoxicity and Antioxidant Activity of the *Origanum majorana* Growing in Casablanca, Morocco. *Open J. Biol. Sci.* **2020,** 5, 53–59.

[45] Dhull, S. B.; Kaur, P.; Purewal, S. S. Phytochemical Analysis, Phenolic Compounds, Condensed Tannin Content and Antioxidant Potential in Marwa (*Origanum majorana*) Seed Extracts. *Resour. Technol.* **2016,** 2, 168–174.

[46] Ayari, B.; Riahi, L.; Landoulsi, A. Variability of phenolic contents in methanolic extracts of *Origanum majorana* L. organs and effect on antioxidant and antimicrobial activities. *Int. J. Agron. Plant Prod.* **2013,** *4* (11), 2806–2815.

[47] Labiod, R. ***Valorisation*** *des huiles essentielles et des extraits de Satureja calamintha nepeta: activité antibactérienne, activité antioxydante et activité fongicide.* Ph.D. Dissertation, Université Badji-Mokhtar, **2016**.

[48] Chouikh, A. Phytochemical Profile, Antioxidant, Analgesic and Hypolipidaemic Effects of *Ephedra alata Decne.* Female Cones Extract. *Farmacia* **2020,** 68.

[49] Luthria, D. L. Influence of Experimental Conditions on the Extraction of Phenolic Compounds from Parsley (*Petroselinum crispum*) Flakes Using a Pressurized Liquid Extractor. *Food Chem.* **2008,** 107, 745–752.

[50] Moktari, M. T.; Mebarki, M. *Valorisation Chimique et Biologique d'une Plante Médicinale Utilisée dans la Médecine Traditionnelle Algérienne.* Master's Thesis, Belhadj Bouchaib University Center of Aïn-Témouchent, **2018**.

[51] Guendouz, F.; Touahria, H. *Contribution à l'Étude Phytochimique et l'Activité Antiradicalaire de la Plante Majorana hortensis.* Master's Thesis, University of Bordj Bou Arreridj, **2019**.

[52] Rodríguez-Bernaldo de Quirós, A.; Frecha-Ferreiro, S.; Vidal-Pérez, A. M.; López-Hernández, J. Antioxidant Compounds in Edible Brown Seaweeds. *Eur. Food Res. Technol.* **2010,** *231*, 495–498.

[53] Heim, K. E.; Tagliaferro, A. R.; Bobilya, D. J. Flavonoid Antioxidants: Chemistry, Metabolism and Structure-Activity Relationships. *J. Nutr. Biochem.* **2002,** *13*, 572–584.

[54] Usmani, S.; Arshad, H.; Farooqui, A. H. A. Determination of infochemicals, phytochemical screening, and evaluation of antioxidant potential of *Digera muricata*. *Der Pharm. Lett.* **2013,** *5* (2), 3–4.

[55] Anigboro, A. A.; Avwioroko, O. J.; Ohwokevwo, O. A.; Pessu, B.; Tonukari, N. J. Phytochemical Profile, Antioxidant, α-Amylase Inhibition, Binding Interaction and Docking Studies of *Justicia carnea* Bioactive Compounds with α-Amylase. *Biophys. Chem.* **2021,** *269,* 106529. https://doi.org/10.1016/j.bpc.2020.106529.

Annex 2 Participation Certificate in Seminars

DEMOCRATIC AND POPULAR ALGERIAN REPUBLIC
MINISTRY OF HIGHER EDUCATION AND SCIENTIFIC RESEARCH
SETIF 1 UNIVERSITY FERHAT ABBAS
FACULTY OF MEDICINE, DEPARTMENT OF PHARMACY
TEL : 0021336 62 05 42 ; 00213777156810
Email : dep_pharm@yahoo.com; a.flilissa@univ-setif.dz

1st International Seminar on the Interest of Chemistry in the Development of Medical Sciences (SIICDSM2025) Sétif from 04 to 09/05/2025

CERTIFICATE OF PARTICIPATION

The president of the organizing committee of the '**1st International Seminar on the Interest of Chemistry in the Development of Medical Sciences (SIICDSM2025) Sétif from 04 to 09/05/2025**'

Certifies that:
Mrs/Miss : ROUIHA AYA
Has successfully participated in this event with a poster communication entitled:
"Neuroprotective Potential of Medicinal Plant Water Extracts: A Comprehensive In Vivo, In Vitro, and In Silico Study on Anti-Alzheimer Activity"

Co-authors: Serine KEBACHE, Hadil BOUDIAF, Elhafnaoui LANEZ, Ouafa BOUDEBIA, Mohmmed Larbi BENAMOR, Ilham BENAMOR, Touhami LANEZ

President of scientific committee
Pr. Mounira AMRANE

Pr. AMRANE Mounira
Biochimie Clinique
Médecin Chef du Laboratoire Central du CHUC de Sétif

President of the organizing committee
Pr. Abdenacer FLILISSA

Université Sétif1 - FERHAT Abbas
Faculté de Médecine
1er Séminaire International sur l'Intérêt de la Chimie dans le Développement des Sciences Médicales.

Pr. Flilissa Abdnacer
- PROFESSEUR -
Département de Pharmacie

DEMOCRATIC AND POPULAR ALGERIAN REPUBLIC
MINISTRY OF HIGHER EDUCATION AND SCIENTIFIC RESEARCH
SETIF 1 UNIVERSITY - FERHAT ABBAS
FACULTY OF MEDICINE, DEPARTMENT OF PHARMACY
TEL : 0021336 62 05 42 ; 00213777156810
Email : dep_pharm@yahoo.com; a.flilissa@univ-setif.dz

1st International Seminar on the Interest of Chemistry in the Development of Medical Sciences (SIICDSM2025), Setif from 04 to 09/05/2025

CERTIFICATE OF PARTICIPATION

The president of the organizing committee of the "**1st International Seminar on the Interest of Chemistry in the Development of Medical Sciences (SIICDSM2025), Setif from 04 to 09/05/2025**"

Certifies that :

Mr/Mis/Miss : **Serine KEBACHE**

Has successfully participated in this event with an oral communication entitled : **Investigating the anticancer potential of multi-solvent extracts derived from medicinal plants : A comprehensive approach through *in vitro* assays and *in silico* modeling techniques.**

Co-authors : **Hadil BOUDIAF, Aya ROUIHA, Elhafnaoui LANEZ, Ouafa BOUDEBIA, Mohmmed Larbi BENAMOR, Ilham BENAMOR, Touhami LANEZ.**

President of scientific committee
Pr. Mounira AMRANE

Pr. AMRANE Mounira
Biochimie Clinique

President of the organizing committee
Pr. Abdenacer FLILISSA

Université Sétif1 - FERHAT Abbas
Faculté de Médecine
1er Séminaire International sur l'Intérêt de la Chimie dans le Développement des Sciences Médicales (SIICDSM 2025)

Pr. Flilissa Abdnacer
- PROFESSEUR -
Département de Pharmacie
FACULTE DE MEDECINE UFAS(SETIF 1)

DEMOCRATIC AND POPULAR ALGERIAN REPUBLIC
MINISTRY OF HIGHER EDUCATION AND SCIENTIFIC RESEARCH
SETIF 1 UNIVERSITY FERHAT ABBAS
FACULTY OF MEDICINE, DEPARTMENT OF PHARMACY
TEL : 0021336 62 05 42 ; 00213777156818
Email : dep_pharm@yahoo.com; a.fillissa@univ-setif.dz

1st International Seminar on the Interest of Chemistry in the Development of Medical Sciences (SIICDSM2025) Sétif from 04 to 09/05/2025

CERTIFICATE OF PARTICIPATION

The president of the organizing committee of the '**1st International Seminar on the Interest of Chemistry in the Development of Medical Sciences (SIICDSM2025) Sétif from 04 to 09/05/2025**'

Certifies that:
Mrs/Miss : BOUDIAF HADIL
Has successfully participated in this event with a poster communicat on entitled:
"Eco-friendly Synthesis, Characterization, In Vitro and In Silico Biological Activities of Zinc and Silver Nanoparticles from Two Medicinal Plants: ADMET, molecular docking, and molecular dynamics simulation"

Co-authors: Aya ROUIHA, Serine KEBACHE, Elhafnaoui LANEZ, Ouafa BOUDEBIA, Mohmmed Larbi BENAMOR, Ilham BENAMOR, Touhami LANEZ

President of scientific committee
Pr. Mounira AMRANE

President of the organizing committee
Pr. Abdenacer FLILISSA

https://sdacee2024.sciencesconf.org/

People's Democratic Republic of Algeria
Ministry of Higher Education and Scientific Research
University of Echahid Hamma-Lakhdar, El-Oued
Faculty of Exact Sciences
Department of Chemistry
Laboratory of Applied Chemistry and Environment (LACE)

LABORATORY

CERTIFICATE OF PARTICIPATION

THIS IS TO CERTIFY THAT

Aya ROUIHA

has participated in the scientific event entitled : « 2ND STUDY DAY ON APPLIED CHEMISTRY AND ENVIRONMENTAL ENGINEERING (SDACEE2025) » ORGANIZED IN THE FACULTY OF EXACT SCIENCES, DEPARTMENT OF CHEMISTRY AT THE UNIVERSITY OF ECHAHID HAMMA LAKHDAR EL-OUED. APRIL 09, 2025, EL-OUED, ALGERIA

with a **POSTER** presentation titled :

Exploring Anti-Alzheimer Effects of Herbal Water Extracts: Integrated In Silico, In Vitro, and In Vivo Investigations into Neuroprotection

CO-AUTHORS: Serine KEBACHE, Hadil BOUDIAF, Elhafnaoui LANEZ, Mohmmed Larbi BENAMOR, Iham BENAMOR, Ouafa BOUDEBIA and Touhami LANEZ

Study day chairman
Dr. Ahmed Mehellou

SDACEE2025
APRIL 09,2025, EL-OUED ALGERIA

© UNIVERSITY OF ECHAHID HAMMA LAKHDAR EL-OUED - ALGERIA

https://sdacee2024.sciencesconf.org/

People's Democratic Republic of Algeria
Ministry of Higher Education and Scientific Research
University of Echahid Hamma-Lakhdar, El-Oued
Faculty of Exact Sciences
Department of Chemistry
Laboratory of Applied Chemistry and Environment (LACE)

CERTIFICATE OF PARTICIPATION

THIS IS TO CERTIFY THAT

Hadil BOUDIAF

has participated in the scientific event entitled : « 2ND STUDY DAY ON APPLIED CHEMISTRY AND ENVIRONMENTAL ENGINEERING (SDACEE2025) » ORGANIZED IN THE FACULTY OF EXACT SCIENCES, DEPARTMENT OF CHEMISTRY AT THE UNIVERSITY OF ECHAHID HAMMA LAKHDAR EL-OUED. APRIL 09, 2025, EL-OUED, ALGERIA

with a **POSTER** presentation titled :

Green Fabrication and Biological Evaluation of Zinc and Silver Nanoparticles Derived from Dual Medicinal Plants: A Combined ADMET, Docking, and Molecular Dynamics Approach

CO-AUTHORS: Aya ROUIHA, Serine KEBACHE, Elhafnaoui LANEZ, Mohmmed Larbi BENAMOR, Ilham BENAMOR, Ouafa BOUDEBIA and Touhami LANEZ

Study day chairman
Dr. Ahmed Mehellou

SDACEE2025
APRIL 09,2025, EL-OUED ALGERIA

© UNIVERSITY OF ECHAHID HAMMA LAKHDAR EL-OUED - ALGERIA

https://sdacee2024.sciencesconf.org/

People's Democratic Republic of Algeria
Ministry of Higher Education and Scientific Research
University of Echahid Hamma-Lakhdar, El-Oued
Faculty of Exact Sciences
Department of Chemistry
Laboratory of Applied Chemistry and Environment (LACE)

CERTIFICATE OF PARTICIPATION

THIS IS TO CERTIFY THAT

Serine KEBACHE

has participated in the scientific event entitled : « 2ND STUDY DAY ON APPLIED CHEMISTRY AND ENVIRONMENTAL ENGINEERING (SDACEE2025) » ORGANIZED IN THE FACULTY OF EXACT SCIENCES, DEPARTMENT OF CHEMISTRY AT THE UNIVERSITY OF ECHAHID HAMMA LAKHDAR EL-OUED. APRIL 09, 2025, EL-OUED, ALGERIA

with a **POSTER** presentation titled :

Comprehensive Evaluation of Anticancer Activities in Medicinal Plant Extracts from Multiple Solvents: Insights from In Vitro Experiments and Computational Modeling

CO-AUTHORS: Hadil BOUDIAF, Aya ROUIHA, Elhafnaoui LANEZ, Mohmmed Larbi BENAMOR, Ilham BENAMOR, Ouafa BOUDEBIA and Touhami LANEZ

Study day chairman
Dr. Ahmed Mehellou

SDACEE2025
APRIL 09,2025, EL-OUED ALGERIA

© UNIVERSITY OF ECHAHID HAMMA LAKHDAR EL-OUED - ALGERIA

People's Democratic Republic of Algeria
Ministry of Higher Education and Scientific Research
Echahid Hamma Lakhdar University - El-Oued
Faculty of Exact Sciences – LEVRES & BABDA Labs

3rd Study Day on Materials Sciences & Applications

TSDMSA24, December 10th , 2024

Certificate of Participation

This Acknowledges That

Pr, Dr, Mr Miss: Hadil BOUDIAF

University of Echahid Hamma Lakhdar - El-Oued - Algeria

Has successfully presented a Poster at the TSDMSA24

" Green Synthesis of Zinc Oxide Nanoparticles Using Two Medicinal Plants: Characterization and Biological Activity Evaluation"

Co-Authors: Serine KEBACHE, Aya ROUIHA, Elhafnaoui LANEZ, Mohmmed Larbi BENAMOR, Ilham BENAMOR

Director of LEVRES Laboratory
Pr. Mohammed Sadok MAHBOUB

Director of BABDA Laboratory
Pr. Ahmed Elkhalifa CHEMSA

TSDMSA24 Director
Dr. Mebrouk GHOUGALI

Eloued, December 10th , 2024

UNIVERSITY OF ECHAHID HAMMA LAKHDAR, EL-OUED
FACULTY OF EXACT SCIENCES
CHEMISTRY DEPARTMENT

Laboratory of Applied Chemistry and Environment (LCAE)and Laboratory of Valorisation and Technology of Sahara Resources (VTRS)

The Second international Seminar on Catalysis, Chemical Engineering & Green Chemistry

CaCEG-2025

May 21-22, 2025 – El Oued, ALGERIA

CERTIFICATE OF PARTICIPATION

This Certifies That

Rouiha Aya

Has successfully participated as Member of Organizing Committee at the Second international Seminar on Catalysis, Chemical Engineering & Green Chemistry "CaCEG-2025".

Chairman of CaCEG-2025

CaCEG - 2025 Chairman

Dr.NEGHMOUCHE NACER Salah

UNIVERSITY OF ECHAHID HAMMA LAKHDAR, EL-OUED
FACULTY OF EXACT SCIENCES
CHEMISTRY DEPARTMENT

Laboratory of Applied Chemistry and Environment (LCAE)and Laboratory of Valorisation and Technology of Sahara Resources (VTRS)

The Second international Seminar on Catalysis, Chemical Engineering & Green Chemistry

CaCEG-2025

May 21-22, 2025 – El Oued, ALGERIA

CERTIFICATE OF PARTICIPATION

This Certifies That

Kebache Serine

Has successfully participated as Member of Organizing Committee at the Second international Seminar on Catalysis, Chemical Engineering & Green Chemistry **"CaCEG-2025"**.

Chairman of CaCEG-2025

CaCEG - 2025 Chairman
Dr.NEGHMOUCHE-NACER Salah

UNIVERSITY OF ECHAHID HAMMA LAKHDAR, EL-OUED
FACULTY OF EXACT SCIENCES
CHEMISTRY DEPARTMENT

Laboratory of Applied Chemistry and Environment (LCAE)and Laboratory of Valorisation and Technology of Sahara Resources (VTRS)

The Second international Seminar on Catalysis, Chemical Engineering & Green Chemistry

CaCEG-2025

May 21-22, 2025 – El Oued, ALGERIA

CERTIFICATE OF PARTICIPATION

This Certifies That

Boudiaf Hadil

Has successfully participated as Member of Organizing Committee at the Second international Seminar on Catalysis, Chemical Engineering & Green Chemistry **"CaCEG-2025"**.

Chairman of CaCEG-2025

CaCEG - 2025 Chairman
Dr.NEGHMOUCHE-NACER Salah

دليل مشروع

للحصول على شهادة براءة اختراع
في إطار القرار الوزاري 1275

ديسمبر
2022

CNCSIIU — MHESR — ALGERIA

بطاقة معلومات

حول فريق الإشراف و فريق العمل

1- فريـــق الاشـــراف:

فريق الاشراف	
المشرف الرئيسي: العانز الحفناوي	التخصص: كيمياء صيدلانية
المشرف المساعد: بن عمر محمد العربي	التخصص: كيمياء عضوية

2- فريـــق العمـــل:

فريق المشروع	التخصص	الكلية
الطالب: كباش سيرين	بيوكيمياء تطبيقية	علوم الطبيعة و الحياة .
الطالب: بوضياف هديل	بيوكيمياء تطبيقية	.علوم الطبيعة و الحياة.
الطالب: رويحة اية	بيوكيمياء تطبيقية	علوم الطبيعة و الحياة .

فهرس المحتويات

فهرس المحتويات

المحور الأول: تقديم براءة الاختراع..... 1

1. فكرة براءة الاختراع (الحل المقترح) 2
2. القيم المقترحة..... 2
3. فريق العمل (المخترعين)..... 3
4. أهداف براءة الاختراع..... 4
5. جدول زمني لتحقيق براءة الاختراع..... 4

المحور الثاني: وصف براءة الاختراع..... 5

1. ملخص براءة الاختراع (250 كلمة) 6
2. الميدان التقني الذي ينتمي إليه الاختراع.....6
3. الحالة التقنية السابقة.....7
4. الغرض (الهدف) من الاختراع.....8
5. تقديم جوهر الاختراع: 8

- عندما يتعلق الأمر بجهاز.....8
- عندما يتعلق الأمر بطريقة عملية (لإنتاج أو المعالجة) 9
- عندما يتعلق الأمر بمنتوج (مركب، مزيج، تشكيل....) 9
- عندما يتعلق الأمر بتطبيق جديد لجهاز معروف أو طريقة معروفة أو مادة معروفة.....9
- عندما يتعلق الأمر بتركيبة جديدة لعناصر معروفة أو غير معروفة...9

6. شرح الأشكال والرسومات: (دون وضعها في الوصف) 10
7. طريقة والية عمل الجهاز المخترع او المادة المخترعة.....11

المحور الثالث: المطالب 12

1. المطلب الرئيس يتمثل في القيمة الإضافية والميزة التي جاء بها اختراعنا مقارنة بباقي الاختراعات الأخرى..... 8

2. المطالب المستنبطة من المطلب الرئيسي والتي تميز اختراعنا 8
المحور الرابع: الملاحق..... 10
1. ترسم الأشكال دون شرح 11
2. ترسم الجداول دون شرح..... 12
3. ترسم الرسومات دون شرح..... 12

مقدمة

تشهد الأمراض المرتبطة بالالتهاب والإجهاد التأكسدي، مثل اضطرابات المناعة والأعصاب، انتشارًا متزايدًا، مما يرفع الحاجة إلى حلول طبيعية آمنة وفعالة .في هذا السياق، قمنا بتطوير شراب نباتي مبتكر يعتمد على مستخلص طبيعي فعالمن نبات ***Cotula ceneria*** بخصائص مضادة للأكسدة والالتهاب، وبطريقة استخلاص تحافظ على النشاط البيولوجي للمركبات .يمثل هذا المنتج بديلًا صحيًا محليًا للمنتجات الكيميائية، ويجمع بين السلامة، الفعالية، وسهولة الاستخدام، مع إمكانية التصنيع الواسع والتسويق.

المحور الأول

تقديم المشروع

المحور الأول

تقديم المشروع

1. فكرة المشروع (الحل المقترح)

مجال نشاطنا يتمثل في المجال الصناعي والصحي وتحديدًا في قطاع الصناعات الصيدلانية والبيولوجية الطبيعية.

بدأت الفكرة انطلاقًا من الحاجة المتزايدة إلى بدائل طبيعية وآمنة للأدوية الكيميائية، خاصة لدى الفئات الحساسة مثل كبار السن ومرضى الالتهابات المزمنة، إضافة إلى نتائج تجارب مخبرية أولية أظهرت الفعالية البيولوجية العالية لبعض المستخلصات النباتية في تقليل مؤشرات الالتهاب والإجهاد التأكسدي.

سنعمل على تصميم وتركيب صيغة شراب نباتي طبيعي، مدروس بدقة، باستخدام طرق استخلاص علمية تحافظ على المركبات النشطة (مثل الفلافونويدات، التربينويدات، البوليفينولات...). وسيتم ذلك من خلال عدة مراحل تشمل: التجميع، الاستخلاص، التركيب، التحليل، والتعبئة.

فريق العمل يتكون من باحثين في البيولوجيا والكيمياء الحيوية، وأخصائيين في النباتات الطبية.

سيتم إنجاز المشروع مبدئيًا في مخابر VTRS على أن يتم لاحقًا نقله إلى وحدة إنتاج شبه صناعية داخل حاضنة أعمال أو مؤسسة ناشئة متخصصة في المستحضرات الطبيعية.

2. القيم المقترحة :

- **الحداثة:** منتج طبيعي مبتكر لا مثيل له حاليًا في السوق المحلي.
- **الأداء :** فعالية مثبتة في مقاومة الأكسدة والالتهاب.
- **إنجاز المهمة :** يساعد في تحسين الصحة العامة والوقاية من الالتهابات.
- **التصميم :** طعم مقبول وتغليف عملي يراعي راحة المستخدم.
- **خفض التكاليف :** بديل طبيعي اقتصادي وبمواد محلية مقارنة بالأدوية الكيميائية.
- **الحد من المخاطر:** مكوّنات آمنة وطبيعية تقلل من الأعراض الجانبية.

3 فريق العمل (المخترعين):

يتكون فريق المشروع (براءة اختراع) من الآتي :

- الطالب 01:كباش سيرين، تخصص بيوكيمياء تطبيقية.
- الطالب 02:هديل بوضياف، تخصص بيوكيمياء تطبيقية.

الطالب 03:رويحة ايه،تخصص بيوكيمياء تطبيقية.

يتمثل دور الطالب رقم 01 مسؤول عن التوثيق العلمي، التحليل الإحصائي، وصياغة النتائج بينما الطالب 02 مسؤول عن الجانب التجريبي (استخلاص المواد النشطة وتثبيت التركيبة). اما الطالب رقم 03 مكلف بالمتابعة التنظيمية، إعداد ملفات الحماية الفكرية، والتنسيق العام.

يتم توزيع المهام حسب الكفاءة، ويُعتمد على تواصل مستمر عبر لقاءات دورية وأدوات رقمية لتنسيق العمل.

4 أهداف المشروع :

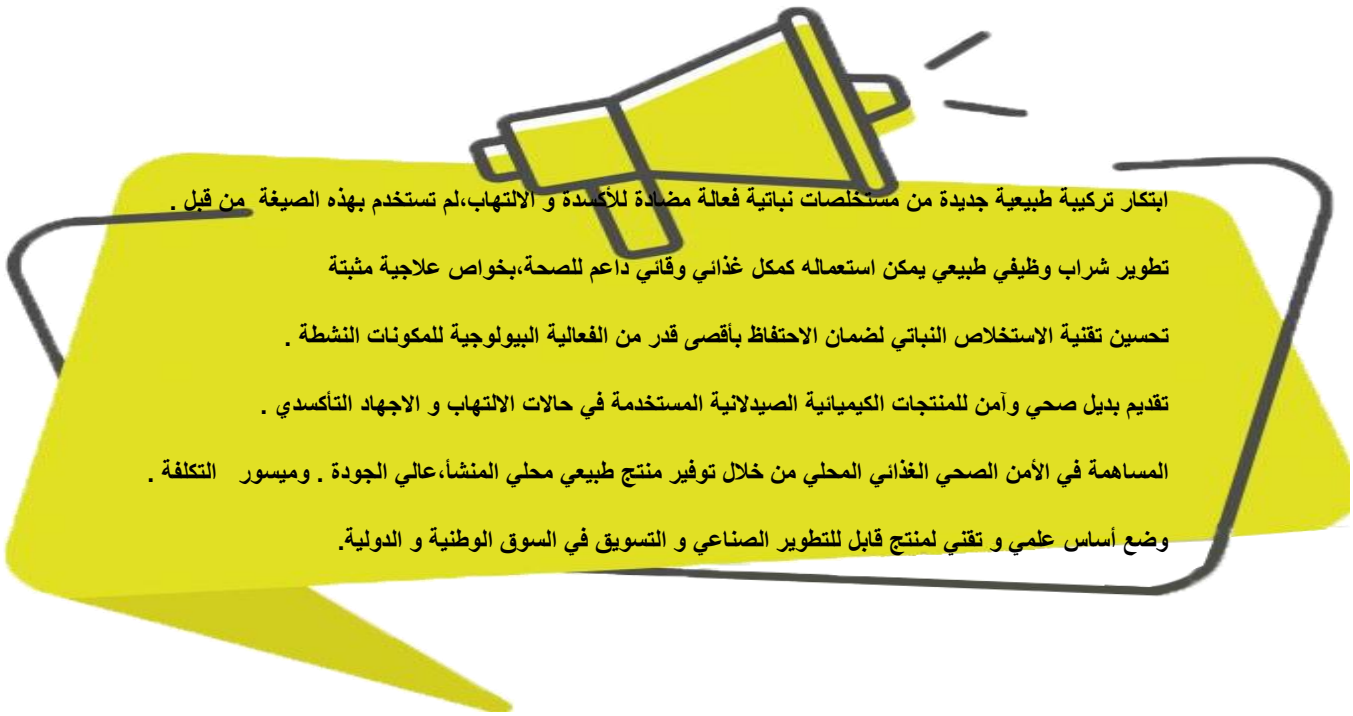

ابتكار تركيبة طبيعية جديدة من مستخلصات نباتية فعالة مضادة للأكسدة و الالتهاب،لم تستخدم بهذه الصيغة من قبل .

تطوير شراب وظيفي طبيعي يمكن استعماله كمكل غذائي وقائي داعم للصحة،بخواص علاجية مثبتة

تحسين تقنية الاستخلاص النباتي لضمان الاحتفاظ بأقصى قدر من الفعالية البيولوجية للمكونات النشطة .

تقديم بديل صحي وآمن للمنتجات الكيميائية الصيدلانية المستخدمة في حالات الالتهاب و الاجهاد التأكسدي .

المساهمة في الأمن الصحي الغذائي المحلي من خلال توفير منتج طبيعي محلي المنشأ،عالي الجودة . وميسور التكلفة .

وضع أساس علمي و تقني لمنتج قابل للتطوير الصناعي و التسويق في السوق الوطنية و الدولية.

5 جدول زمني لانجاز براءة الاختراع:

الشهر أو الأسبوع

			1	2	3	4	5	6	7
1		البحث في قواعد البيانات الخاصة ببراءات الاختراع وجمع المعلومات	✓	✓					
2		الشروع في الاختبارات المخبرية لإعداد النموذج الأولي		✓	✓				
3		تجريب النموذج الأولي			✓	✓			
...		تجربة النموذج الأولي خارج المخابر				✓	✓		
ن		تسجيل براءة الاختراع من اجل الحصول على رقم الإيداع والحماية الصناعية					✓	✓	
...		متابعة عملية الحصول على براءة الاختراع وتصحيح ملاحظات الممتحنين من **inapi**							✓

الأعمال

المحور الثاني

الجوانب الإبتكارية

المحور الثاني

الجوانب الابتكارية

1. طبيعة الابتكارات :

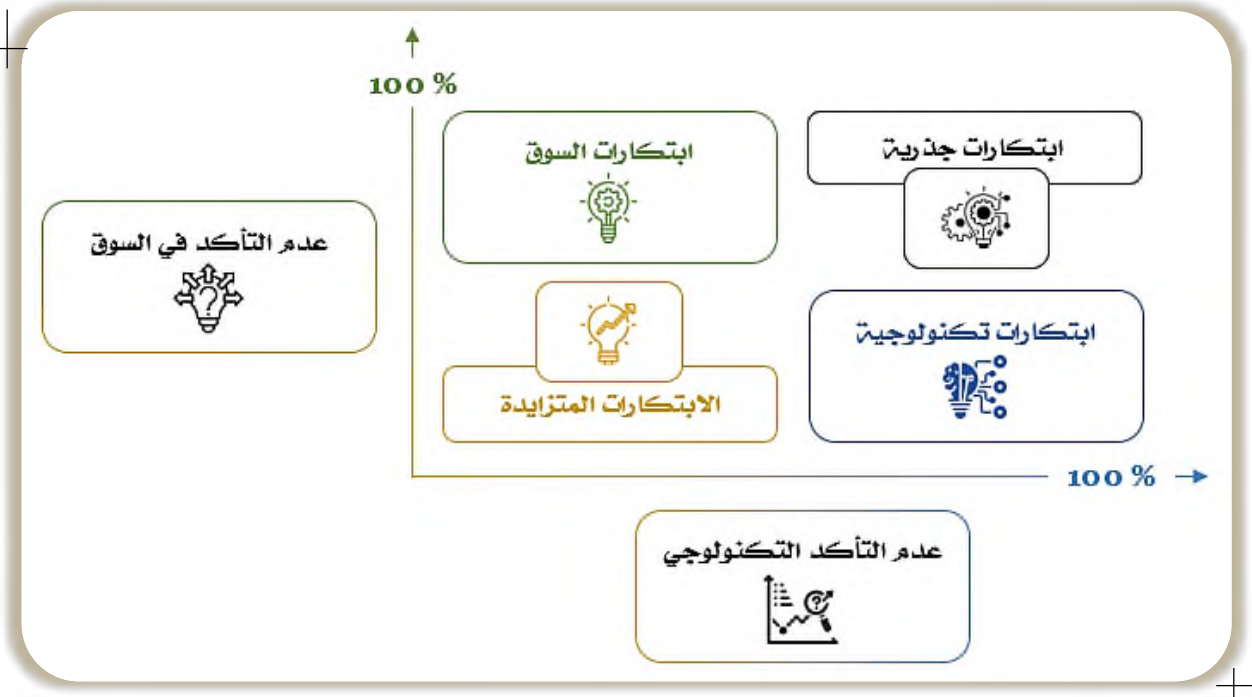

1. **تركيبة فريدة من نوعها:**
مزيج طبيعي من الفلافونويدات، التانينات، والتربينات، تم تحسينه لتحقيق أقصى فعالية بيولوجية وثبات في الشكل السائل (الشراب.)

2. **طريقة استخلاص علمية متقدمة:**
استخدام تقنية الاستخلاص بالمذيبات التي تحافظ على المركبات الفعالة، مما ينتج مستخلصًا عالِ الفعالية والنشاط الحيوي.

3. **تطبيق علاجي جديد:**
موجه خصيصًا للأفراد الذين يعانون من الإجهاد التأكسدي، التعب المزمن، الأرق، والالتهابات المرتبطة بالإجهاد، ويُعد بديلًا طبيعيًا آمنًا للأدوية الصناعية.

4. **إمكانية الوصول والتكلفة المنخفضة:**
صُمم المنتج ليكون قابلًا للإنتاج المحلي منخفض التكلفة، مما يضمن سهولة الوصول إليه خاصة في المناطق التي تفتقر إلى الأدوية الحديثة.

5. **نموذج مرن وقابل للتطوير:**
يتيح الابتكار التحول إلى أشكال دوائية متعددة (شراب، كبسولات، مسحوق)، بما يتناسب مع احتياجات وتفضيلات المستهلكين.

6. **دمج المعرفة التقليدية بالعلم الحديث:**
يجمع هذا الابتكار بين الاستعمالات التقليدية للنباتات الطبية والتحقق العلمي الحديث من فعاليتها، مما يساهم في دعم الطب النباتي القائم على الأدلة.

2. مـــجـــالات الابـــتـكـــارات :

عمليات جديدة :يعتمد المشروع على تقنيات استخلاص نباتية محسّنة تزيد من كفاءة العمليات وتحافظ على الفعالية الحيوية للمركبات الطبيعية، مما يرفع من القيمة المضافة للمنتج بأقل تكلفة.

تجارب جديدة :يقدم المنتج تجربة استهلاك مختلفة تعتمد على الوقاية الطبيعية والراحة النفسية للمستهلك، ما يعزز الإقبال عليه حتى من قبل المستخدمين التقليديين للمنتجات الدوائية.

ميزات جديدة :يقدّم المشروع منتجًا محسّنًا من حيث السلامة، المكونات الطبيعية، والفعالية البيولوجية، مقارنة بالمكملات أو العلاجات الاصطناعية.

عملاء جدد :يمكن استهداف شرائح لم تكن تتوفر لها منتجات مماثلة، مثل :الرياضيين، كبار السن، ومرضى الأمراض المزمنة الباحثين عن مكملات طبيعية آمنة.

عروض جديدة :المشروع يُعد عرضًا مبتكرًا كليًا في السوق المحلي، بتركيبة فريدة وفاعلية مثبتة ضد الالتهاب والإجهاد التأكسدي.

نماذج جديدة :نسعى لتطوير نموذج عمل مرن قائم على إنتاج محلي منخفض التكلفة + تسويق رقمي مباشر، ما يُمكّن من توسيع الوصول وتحقيق استدامة مالية للمشروع.

المحور الثالث

وصف براءة الاختراع

المحور الثاني: وصف براءة الاختراع

- عنوان براءة الاختراع :

تطوير منتج مبتكر مضاد للأكسدة ومضاد للالتهابات من مستخلص نباتي.

- ملخص براءة الاختراع (250 كلمة)

يتم استخلاص المكونات النباتية النشطة من النبات الطبي Cotula cineria الحديث ودمجها في محلول سائل معد للشرب بتركيز يتراوح بين (mg 150-300 لكل 1 kg من وزن الجسم). يُعطى المنتج عن طريق الفم، حيث يظهر فعالية عالية في مكافحة الإجهاد التأكسدي وتقليل الالتهابات و كذلك التخفيف من التعب الناجم عن الممارسات اليومية ، مما يساهم في تعزيز راحة الجسم و تقوية الجهاز المناعي.

تم انجاز المشروع وفق المراحل التالية :

اختيار المادة الخام النباتية:

جمع أوراق نبات Cotula cineria من مصادر محلية، يليها غسلها وتجفيفها بعناية، ثم طحنها ميكانيكيًا للحصول على مسحوق ناعم متجانس.

تم تحديد النبات وفقا للمركبات الكيميائية الفعالة المتواجدة فيه .

تحضير المستخلص النباتي :

استخلاص المركبات الفعالة باستخدام الميثانول و ذلك لتحقيق أعلى نسبة استخلاص و الحفاظ على جميع المركبات النشطة بيولوجيا .

يُرشح المستخلص ويُخزن عند 4°C، ثم يُزال المذيب بلطف باستخدام جهاز التبخير الدوار (Rotavapor R-200) للحفاظ على التركيب الكيميائي الحساس للمكونات.

تحضير المكمل الغذائي:

اتباع بروتوكول معتمد لتصنيع المكمل الغذائي في شكل مشروب وهذا وفقا لتراكيز محددة ومضبوطة بدقة .

الاختبار الحيوي:

إجراء اختبارات حيوية في المختبر لتقييم فعالية المكمل الغذائي في تخفيف الإجهاد التأكسدي والالتهابات بواسطة (BSA test/DPPH assayss)

تُتبع هذه الاختبارات بتجريب المنتج المبتكر على الكائن الحي (Albino Wistar Rats) و هذا للتأكد أكثر من فعالية المنتج و عدم وجود أثار جانبية.

- الميدان التقني الذي ينتمي إليه الاختراع :

ينتمي المنتج الى مجال الصناعات البيوكيميائية و تركيبات المكملات الغذائية وهو ميدان أحد اهتماماته دراسة المكونات الفعالة المتواجدة في الطبيعة والاستفادة منها حسب نشاطها وفعاليتها البيولوجية كمصادرلتحقيق ربح اقتصادي وبيئي .

- الحالة التقنية السابقة (براءات الاختراع السابقة التي تدخل في نفس مجال براءة اختراعنا)

❖ **براءات الاختراع السابقة المتعلقة بالمنتجات النباتية المضادة للأكسدة:**

✓ **براءة اختراع (2004) US6811902B1:**

براءة اختراع تخص استخدام مستخلصات نباتية (مثل الشاي الأخضر) في صنع تركيبات مضادة للأكسدة يمكن استخدامها في صناعة مستحضرات التجميل أو الأدوية. اعتمدت البراءة على مركبات مثل EGCG من الشاي الأخضر.

✓ **براءة اختراع (2003) US6602690B1 :**

براءة اختراع تتعلق بتركيبات تحتوي على مستخلصات نباتية تحتوي على مركبات مضادة للأكسدة، مثل Resveratrolمن نبات العنب. هذه التركيبة تستخدم لعلاج التهاب المفاصل وتحسين الصحة العامة من خلال تأثيرها المضاد للأكسدة.

❖ **براءات الاختراع السابقة المتعلقة بالمنتجات المضادة للالتهابات:**

✓ **براءة اختراع (2017) WO2017058716A1:**

هذه البراءة تتعلق باستخدام مستخلصات نباتية تحتوي على مركبات طبيعية لها تأثيرات مضادة للالتهابات. تم تحسينها لتوفير منتج يمكن استخدامه لعلاج التهابات الجلد وتحسين التئام الجروح.

✓ **براءة اختراع (2013) US8372523B2:**

تتعلق باستخدام مستخلصات(Curcuma longa الكركم) التي تحتوي على مادة Curcumin في علاج الالتهابات المزمنة وأمراض الجهاز المناعي

❖ **براءات الاختراع السابقة المتعلقة بالنباتات التي تحتوي على مركبات مضادة للأكسدة والالتهابات:**

✓ **براءة اختراع(2015) US20150125155A1:**

تستخدم هذه البراءة مركبات من) نبات الجينسنج) كمستخلص مضاد للأكسدة ومضاد للالتهابات، والذي يُستخدم في علاج الالتهابات المزمنة ومرض السكري.

- الغرض (الهدف) من الاختراع

يهدف هذا الاختراع إلى تقديم مكمل غذائي طبيعي مضاد للأكسدة ومضاد للالتهابات، يعتمد على مستخلص نباتي غني بالفلافونويدات، التانينات، والتربينات. يسعى هذا المكمل إلى تحقيق الأهداف التالية:

معالجة التعب والإجهاد التأكسدي عبر تقوية الخلايا ضد الجذور الحرة. تحسين جودة النوم وتقليل الأرق الناتج عن الإجهاد والتعب المزمن. تعزيز المناعة بفضل المركبات النباتية النشطة ذات التأثيرات المضادة للأكسدة والالتهابات. وذلك بهدف توفير بديل طبيعي وآمن للمكملات الغذائية الصناعية و تقليل الآثار الجانبية المرتبطة بالاستخدام طويل الأمد للمكملات الكيميائية.

- تقديم جوهر الاختراع

يتمثل الاختراع في تطوير مكمل غذائي طبيعي على شكل شراب ، يعتمد على مستخلصات نباتية مستخلصة من *Cotula cineria* . يحتوي هذا المكمل على مركبات مضادة للأكسدة (مثل الفلافونويدات)، ومضادات للالتهابات (مثل التانينات)، إضافة إلى التربينات ذات التأثير المهدئ للأعصاب.

يُوجّه هذا المكمل للأفراد الذين يعانون من التعب المزمن، الإجهاد التأكسدي، الأرق، والالتهابات المرتبطة بالإجهاد. كما يُعد بديلاً آمناً للأدوية الصناعية التي قد تسبب آثاراً جانبية طويلة الأمد.

و تتمثل أهدافه في تعزيز الصحة العامة من خلال تحسين مستويات الطاقة، دعم المناعة، وتقليل حالات الالتهاب الناتجة عن الإجهاد التأكسدي.

حيث يتميز هذا المكمل بتركيبته الطبيعية ،وتوافقه مع الاستخدام طويل الأمد دون تأثيرات جانبية خطيرة.

الأجزاء المكونة لهذا المكمل تشمل:

1. المستخلصات النباتية (الفلافونويدات، التانينات، التربينات).
2. مواد حافظة طبيعية آمنة.

النموذج الأولي التجريبي

- عندما يتعلق الأمر بمنتوج (مركب، مزيج، تشكيل....)

صورة النموذج الأولي لمشروب Oxinerea المضاد للأكسدة و الإلتهابات.

3. طريقة إنجاز الاختراع:

المرحلة الأولى " مرحلة الاستخلاص" : يتم استخراج المركبات الفعالة من *Cotula cineria* باستخدام تقنية الاستخلاص بالمذيبات (الشكل 1).

المرحلة الثانية : مرحلة التحليل الكيميائي : يتم تحليل المركبات الفعالة باستخدام تقنية HPLC لتحديد نسب الفلافونويدات، التانينات، والتربينات .

المرحلة الثالثة : مرحلة التحضير: يتم دمج المركبات الفعالة في تركيبة مكمل غذائي وفقاً لبروتوكول التحضير المعتمد، وتحويله إلى شكل شراب .

المرحلة الرابعة : مرحلة الاختبار: يتم اختبار المنتج في بيئة مختبرية للتحقق من فعاليته في الحد من الإجهاد التأكسدي والالتهابات .

2. شرح الأشكال و الرسومات: (دون وضعها في الوصف)

رقم 01 : عرض توضيحي لتركيب المكمل الغذائي :

1 نبات *coutula ceneria*

2 المنتج المبتكر ضد الاجهاد التاكسدي و الالتهابات .

3 مركب التربينات .

4 مركب التانينات .

5مركب الفلافونويدات .

الشكل (2) :

صورة حقيقية لطريقة تحضير المنتج .

7.طريقة والية عمل الجهاز المخترع او المادة المخترعة

طريقة تطبيق الاختراع:

- **طريقة الاستخدام**: يتم تناول المكمل بمقدار جرعة يومية محددة وفقاً لتعليمات الاستخدام المرفقة مع المنتج.
- **الفئة المستهدفة:** الأفراد الذين يعانون من الإجهاد التأكسدي، التعب المزمن، أو الالتهابات الناتجة عن الإجهاد.
- **مدة الاستخدام:** يُنصح بالاستخدام المنتظم لمدة لا تقل عن 3 أشهر لتحقيق أفضل النتائج، مع متابعة التأثيرات على الصحة العامة.

المحور الرابع

المطالب

المطالب

المطلب الرئيسي

تتمثل القيمة الإضافية لاختراعنا في ابتكار شراب طبيعي فعال مضاد للأكسدة والالتهاب، يعتمد على مستخلص نباتي مدروس، بطريقة استخلاص علمية تحافظ على فعاليته البيولوجية. يتميز المنتج عن غيره بكونه آمن، سهل الاستخدام، وقابل للتصنيع المحلي بتكلفة منخفضة، مما يجعله حلاً مبتكرًا وواقعيًا مقارنة بالمنتجات الكيميائية أو المستوردة، مع إمكانية تطويره لاحقًا إلى أشكال صيدلانية متنوعة.

المطالب المستنبطة من المطلب الرئيسي والتي تميز اختراعنا

وفقاً للمطلب الأول، يتميز المكمل الغذائي بتركيبة طبيعية بالكامل مع نسبة مركبات فعالة تتراوح بين 5-10% من الفلافونويدات و3-7% من التانينات و2-6% من التربينات.

وفقاً للمطلب الأول، يتميز المكمل بسهولة التحضير باستخدام تقنيات استخلاص بالمذيبات والماء، مما يجعله ذو تكلفة منخفضة وقابل للتصنيع بكميات كبيرة.

وفقاً للمطلب الأول، يتميز المكمل بخصائصه المضادة للأكسدة والالتهابات والتي أثبتت فعاليتها من خلال الفحوصات الحيوية المخبرية في تقليل الإجهاد التأكسدي والالتهابات.

وفقاً للمطلب الأول، يتمتع المكمل الغذائي بتأثير إيجابي في التخفيف من أعراض القلق و التعب والارهاق المرتبطة بالإجهاد التأكسدي.

وفقاً للمطلب الأول، يتميز المكمل بإمكانية تحضيره في أشكال صيدلانية متعددة (شراب، كبسولات) وفقاً لاحتياجات المستهلك.

قائمة الملاحق

الاشكال والرسومات والجداول..... 10

الشكل رقم 01:

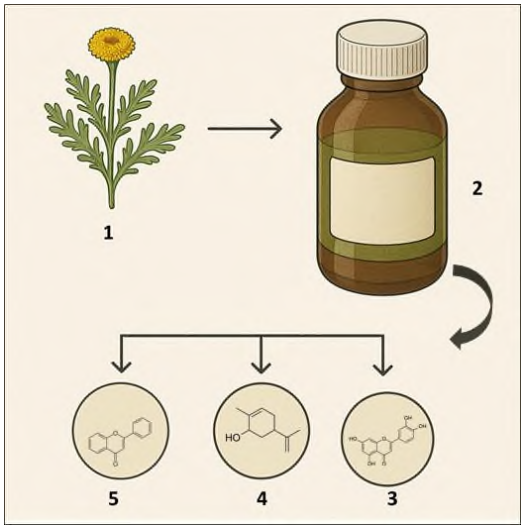

الشكل رقم 02:

دليل مشروع

للحصول على شهادة مؤسسة ناشئة
في إطار القرار الوزاري 1275

ديسمبر
2022

CNCSIIU — MHESR — ALGERIA

دليل مشروع

للحصول على شهادة براءة اختراع
في إطار القرار الوزاري 1275

ديسمبر
2022

CNCSIIU — MHESR — ALGERIA

بطاقة معلومات

حول فريق الإشراف و فريق العمل

1- فريـــق الاشـــراف:

فريق الاشراف	
المشرف الرئيسي: العانز الحفناوي	**التخصص:** كيمياء صيدلانية
المشرف المساعد: بن عمر محمد العربي	**التخصص:** كيمياء عضوية

2- فريـــق العمـــل:

فريق المشروع	التخصص	الكلية
الطالب: كباش سيرين	بيوكيمياء تطبيقية	علوم الطبيعة و الحياة .
الطالب: بوضياف هديل	بيوكيمياء تطبيقية	.علوم الطبيعة و الحياة.
الطالب: رويحة اية	بيوكيمياء تطبيقية	علوم الطبيعة و الحياة .

فهرس المحتويات

فهرس المحتويات

المحور الأول: تقديم براءة الاختراع..... 1

1. فكرة براءة الاختراع (الحل المقترح) 2
2. القيم المقترحة..... 2
3. فريق العمل (المخترعين)..... 3
4. أهداف براءة الاختراع..... 4
5. جدول زمني لتحقيق براءة الاختراع..... 4

المحور الثاني: وصف براءة الاختراع..... 5

1. ملخص براءة الاختراع (250 كلمة) 6
2. الميدان التقني الذي ينتمي إليه الاختراع.....6
3. الحالة التقنية السابقة.....7
4. الغرض (الهدف) من الاختراع.....8
5. تقديم جوهر الاختراع: 8

- عندما يتعلق الأمر بجهاز.....8
- عندما يتعلق الأمر بطريقة عملية (لإنتاج أو المعالجة) 9
- عندما يتعلق الأمر بمنتوج (مركب، مزيج، تشكيل....) 9
- عندما يتعلق الأمر بتطبيق جديد لجهاز معروف أو طريقة معروفة أو مادة معروفة.....9
- عندما يتعلق الأمر بتركيبة جديدة لعناصر معروفة أو غير معروفة...9

6. شرح الأشكال والرسومات: (دون وضعها في الوصف) 10
7. طريقة والية عمل الجهاز المخترع او المادة المخترعة.....11

المحور الثالث: المطالب 12

1. المطلب الرئيس يتمثل في القيمة الإضافية والميزة التي جاء بها اختراعنا مقارنة بباقي الاختراعات الأخرى..... 8

2. المطالب المستنبطة من المطلب الرئيسي والتي تميز اختراعنا 8
المحور الرابع: الملاحق..... 10
1. ترسم الأشكال دون شرح 11
2. ترسم الجداول دون شرح..... 12
3. ترسم الرسومات دون شرح..... 12

مقدمة

تتعلق هذه البراءة بابتكار مكمل غذائي طبيعي يعتمد على مستخلص نباتي محلي من نبات ***Origanum majorana***، يهدف إلى التقليل من أعراض مرض الزهايمر وتحسين الوظائف العصبية والمعرفية.

تم تطوير هذا المكمل بناءً على دراسات مخبرية وتجارب سلوكية على نماذج حيوانية، أظهرت نتائج واعدة في تخفيف القلق وتحسين السلوك المرتبط بالتدهور العصبي.

يمثل هذا الابتكار حلاً آمنًا وفعالًا، يجمع بين العلم الحديث والطب النباتي التقليدي، ويقدم بديلًا محليًا منخفض التكلفة مقارنة بالخيارات المتاحة في السوق.

المحور الأول

تقديم المشروع

المحور الأول

تقديم المشروع

1. فكرة المشروع (الحل المقترح)

مجال نشاطنا يتمثل في المجال الصناعي الصحي وتحديدًا في تصنيع المكملات الغذائية ذات الأصول النباتية.

إنبثقت فكرة المشروع خلال عملي البحثي في المخبر، حيث لاحظنا من خلال تجربة مخبرية على نماذج حيوانية (فئران) مصابة بالزهايمر، وجود تأثير ايجابي لمستخلص نبات Origanum majo rana في تحسين السلوك و تقليل القلق .تطورت الفكرة بعد تحليل النتائج والتفكير في كيفية تحويل هذا البحث الى منتج فعلي يمكن أن يفيد المجتمع.

يتمثل المشروع في انتاج مكمل غذائي طبيعي امن، يحتوي على مكونات فعالة مستخلصة من نبات طبي، مع احترام المعايير الصحية المعتمدة، ليقدم كمكمل داعم للوظائف العصبية و الدماغية.

سيُنجز هذا المشروع من طرفنا بالتعاون مع مختبر VTRS المختص وبإشراف أساتذة وخبراء في مجال البيولوجيا والصيدلة، مع إمكانية إشراك شركاء صناعيين لاحقًا.

2. القيم المقترحة :

الحداثة: تقديم مكمل غذائي طبيعي جديد كليًا يعتمد على نبات طبي محلي غير مستغل سابقا ضد الزهايمر.
الأداء: فعالية مثبتة مخبريًا في تحسين السلوك وتقليل القلق لدى نماذج حيوانية، ما يوازي توقعات المستخدمين.
إنجاز المهمة: دعم الذاكرة وتقليل أعراض التدهور العصبي، مما يساعد المرضى على تحسين جودة حياتهم.
خفض التكاليف: اعتماد مكونات محلية يقلل كلفة الإنتاج ويجعل المنتج في متناول الجميع.
الحد من المخاطر: منتج طبيعي آمن يقلل من الأعراض الجانبية مقارنة بالأدوية الكيميائية.
سهولة الوصول: مكمل غذائي محلي متوفر بسعر مناسب، خاصة في المناطق التي تفتقر للحلول

3 فريق العمل (المخترعين):

يتكون فريق المشروع (براءة اختراع) من الآتي :

- الطالب 01:كباش سيرين، تخصص بيوكيمياء تطبيقية.
- الطالب 02:هديل بوضياف، تخصص بيوكيمياء تطبيقية.

الطالب 03:رويحة ايه،تخصص بيوكيمياء تطبيقية.

يتمثل دور الطالب رقم 01 في تصميم و تحاليل التجارب الحيوية و السلوكية بينما الطالب 02 فهو مكلف باستخلاص المركبات من النبات و تحضير المستخلص النباتي. اما الطالب رقم 03 فهو مسؤول عن التحاليل البيوكيميائية و تغليف وتعليب المنتوج .

يتم توزيع المهام حسب الكفاءة، ويُعتمد على تواصل مستمر عبر لقاءات دورية وأدوات رقمية لتنسيق العمل.

4 أهداف المشروع :

ابتكار مكمل غذائي طبيعي فعال و مبني على تركيبة نباتية محلية غير مستغلة سابقا في علاج وتخفيف اعراض مرض الزهايمر ل

تقديم بديل امن و طبيعي عن الادوية الكيميائية، يساهم في تحسي جودة الحياة للمرضى و يقلل من الاعراض النفسية المرافقة كالقلق.

تحويل البحث العلمي الى منتج عملي قابل للتسويق،يجمع بين الفعالية والتكلفة المعقولة

دعم القطاع المحلي في صنع مكملات غذائية من خلال منتج مبتكر يستجيب لحاجة حقيقية في السوق

5 جدول زمـــني لانجاز براءة الاختراع:

الشهر أو الأسبوع

			1	2	3	4	5	6	7
1		البحث في قواعد البيانات الخاصة ببراءات الاختراع وجمع المعلومات	✓	✓					
2		الشروع في الاختبارات المخبرية لإعداد النموذج الأولي		✓	✓				
3		تجريب النموذج الأولي			✓	✓			
...		تجربة النموذج الأولي خارج المخابر				✓	✓		
ن		تسجيل براءة الاختراع من اجل الحصول على رقم الإيداع والحماية الصناعية					✓	✓	
...		متابعة عملية الحصول على براءة الاختراع وتصحيح ملاحظات الممتحنين من **inapi**							✓

الأعمال

4

المحور الثاني

الجوانب الإبتكارية

المحور الثاني

الجوانب الابتكارية

1. طبيعة الابتكارات :

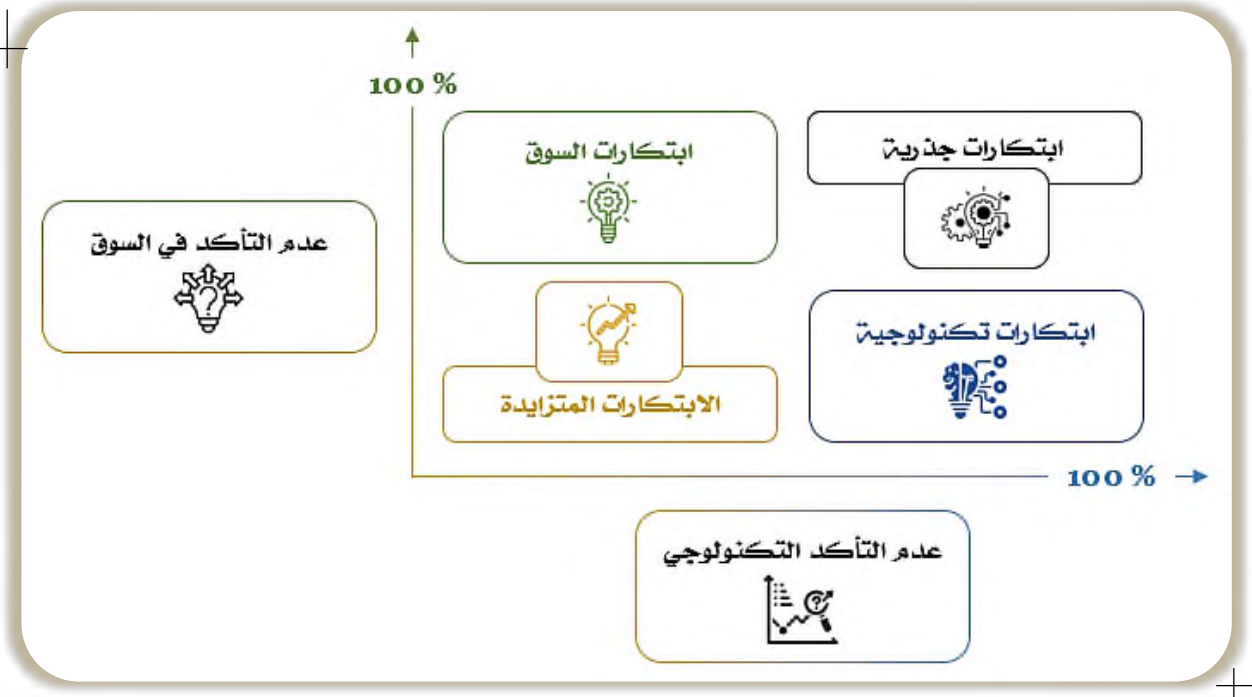

1. **تركيبة فريدة من نوعها:**
مزيج طبيعي من الفلافونويدات، التانينات، والتربينات، تم تحسينه لتحقيق أقصى فعالية بيولوجية وثبات في الشكل السائل (الشراب.)

2. **طريقة استخلاص علمية متقدمة:**
استخدام تقنية الاستخلاص بالمذيبات التي تحافظ على المركبات الفعالة، مما ينتج مستخلصًا عالِ الفعالية والنشاط الحيوي.

3. **تطبيق علاجي جديد:**
موجه خصيصًا للأفراد الذين يعانون من الإجهاد التأكسدي، التعب المزمن، الأرق، والالتهابات المرتبطة بالإجهاد، ويُعد بديلًا طبيعيًا آمنًا للأدوية الصناعية.

4. **إمكانية الوصول والتكلفة المنخفضة:**
صُمم المنتج ليكون قابلًا للإنتاج المحلي منخفض التكلفة، مما يضمن سهولة الوصول إليه خاصة في المناطق التي تفتقر إلى الأدوية الحديثة.

5. **نموذج مرن وقابل للتطوير:**
يتيح الابتكار التحول إلى أشكال دوائية متعددة (شراب، كبسولات، مسحوق)، بما يتناسب مع احتياجات وتفضيلات المستهلكين.

6. **دمج المعرفة التقليدية بالعلم الحديث:**
يجمع هذا الابتكار بين الاستعمالات التقليدية للنباتات الطبية والتحقق العلمي الحديث من فعاليتها، مما يساهم في دعم الطب النباتي القائم على الأدلة.

2. مـــجـــالات الابـــتـكـــارات :

عمليات جديدة :يعتمد المشروع على تقنيات استخلاص نباتية محسّنة تزيد من كفاءة العمليات وتحافظ على الفعالية الحيوية للمركبات الطبيعية، مما يرفع من القيمة المضافة للمنتج بأقل تكلفة.

تجارب جديدة :يقدم المنتج تجربة استهلاك مختلفة تعتمد على الوقاية الطبيعية والراحة النفسية للمستهلك، ما يعزز الإقبال عليه حتى من قبل المستخدمين التقليديين للمنتجات الدوائية.

ميزات جديدة :يقدّم المشروع منتجًا محسّنًا من حيث السلامة، المكونات الطبيعية، والفعالية البيولوجية، مقارنة بالمكملات أو العلاجات الاصطناعية.

عملاء جدد :يمكن استهداف شرائح لم تكن تتوفر لها منتجات مماثلة، مثل :الرياضيين، كبار السن، ومرضى الأمراض المزمنة الباحثين عن مكملات طبيعية آمنة.

عروض جديدة :المشروع يُعد عرضًا مبتكرًا كليًا في السوق المحلي، بتركيبة فريدة وفاعلية مثبتة ضد الالتهاب والإجهاد التأكسدي.

نماذج جديدة :نسعى لتطوير نموذج عمل مرن قائم على إنتاج محلي منخفض التكلفة + تسويق رقمي مباشر، ما يُمكّن من توسيع الوصول وتحقيق استدامة مالية للمشروع.

المحور الثالث

وصف براءة الاختراع

المحور الثاني: وصف براءة الاختراع

- عنوان براءة الاختراع :

صناعة منتج مبتكر كمكمل غذائي ضد الزهايمر من مستخلص نباتي.

- ملخص براءة الاختراع (250 كلمة)

تتمحور هذه البراءة حول تطوير مكمل غذائي مبتكر وفعال يُستخدم للوقاية أو التخفيف من أعراض مرض الزهايمر، وذلك بالاعتماد على مستخلصات نباتية طبيعية غنية بمركبات بيولوجية نشطة ذات تأثيرات مضادة للأكسدة والالتهابات العصبية.

تبدأ خطوات الإنجاز بجمع أوراق نبات *Origanum majorana* من مصادر محلية، يليها غسلها وتجفيفها بعناية، ثم طحنها ميكانيكيًا للحصول على مسحوق ناعم متجانس.

يتم بعد ذلك استخلاص المركبات الفعالة باستخدام الميثانول لكونه مذيب فعال يحافظ على جميع المركبات البيولوجية ، يُرشح المستخلص ويُخزن عند 4°C، ثم يُزال المذيب بلطف باستخدام جهاز التبخير الدوار (Rotavapor R-200) للحفاظ على التركيب الكيميائي الحساس للمكونات.

بعد تحضير المستخلص، يتم دمجه في تركيبة مكمل غذائي مدروسة التركيز، قابلة للتجفيف، والتحويل إلى شكل صيدلاني "كبسولات".

يخضع المنتج لاختبارات تقييم النشاط البيولوجي، مثل فحص نشاط الإنزيم المضاد للأكسدةSOD ، لإثبات فعاليته في مقاومة الإجهاد التأكسدي ومن ثم تجريبه على نموذج حيواني من نوع Albino Wistar rats لأنه يوفر بيئة قريبة نسبيًا من جسم الإنسان على مستوى الاستجابة البيولوجية، مما يساهم في دعم مصداقية النتائج وتحسين فرص نجاح المنتج في المراحل السريرية لاحقًا.

الاختراع موجّه بشكل خاص للفئات المعرضة لخطر التدهور المعرفي، ويتميز بتركيبته الطبيعية الآمنة، وسهولة الاستخدام اليومي، مما يجعله مرشحًا قويًا ليكون جزءًا من الرعاية التكميلية للأمراض العصبية. يوفر هذا الابتكار نهجًا تكامليًا يجمع بين فعالية الطب النباتي الحديث ومفاهيم الوقاية المستندة إلى العلم.

- الميدان التقني الذي ينتمي إليه الاختراع :

الصناعات الدوائية والبيولوجية – تطوير مكملات غذائية علاجية مستخلصة من مصادر نباتية لعلاج أو الوقاية من الأمراض العصبية مثل الزهايمر.

- الحالة التقنية السابقة (براءات الاختراع السابقة التي تدخل في نفس مجال براءة اختراعنا)

1.براءة الاختراع الأمريكيةUS7429397B2

تصف هذه البراءة تركيبة عشبية تحتوي على مستخلصات من نباتات مثل *Tinospora cordifolia* و*Centella asiatica* و*Withania somnifera* و*Mucuna pruriens* و*Curcuma longa*، تُستخدم كمنشط للدماغ ولتحسين الذاكرة، خاصة في حالات الخرف الشيخوخي .

2.براءة الاختراع الأمريكيةUS9675657B2

تركز هذه البراءة على تركيبة عشبية للوقاية وإدارة الاضطرابات العصبية التنكسية المرتبطة بالعمر، مع إشارة خاصة إلى الخرف الشيخوخي.

3.براءة الاختراع الأوروبيةEP3273978B1

تتعلق هذه البراءة باستخدام مستخلص نبات *Withania somnifera* لعلاج أو الوقاية من الأمراض المرتبطة بالأميلويد، بما في ذلك مرض الزهايمر.

4.براءة الاختراع الأمريكيةUS9737582B2

تصف هذه البراءة طريقة لتحسين الذاكرة باستخدام تركيبة تحتوي على مستخلصات من *Cistanche tubulosa* و *Ginkgo biloba* Justia Patents

- الغرض (الهدف) من الاختراع

يهدف هذا الاختراع إلى تطوير منتج مبتكر كمكمل غذائي طبيعي موجه للوقاية أو التخفيف من أعراض مرض الزهايمر، وذلك باستخدام مستخلص نباتي فعال يمتاز بخصائصه البيولوجية المثبتة كمضادات أكسدة ومضادات للالتهابات. ويأتي هذا الابتكار استجابةً للحاجة المتزايدة إلى حلول طبيعية وآمنة تدعم الوظائف العصبية وتُحسن القدرات الإدراكية، خصوصًا في ظل الآثار الجانبية المرتبطة ببعض العلاجات الكيميائية التقليدية. يقدم هذا المكمل حلاً وقائيًا داعمًا للصحة الدماغية، من خلال تقليل الإجهاد التأكسدي وتحفيز النشاط العصبي، مما يجعله مناسبًا للاستخدام اليومي كجزء من نمط حياة صحي. يهدف الاختراع على المدى القريب إلى تصميم تركيبة فعالة تحتوي على تراكيز محسوبة بدقة من مكونات نباتية مختارة، مع إجراء اختبارات أولية على نماذج خلوية و حيوانية لتقييم الفعالية. أما على المدى البعيد، فيسعى المنتج إلى الوصول إلى الأسواق المحلية والعالمية كمكمل غذائي طبيعي داعم للدماغ، ينسجم مع توجهات الطب التكاملي والصحة الوقائية، ويشجع على تبني أنماط علاجية أكثر أمانًا واستدامة.

- تقديم جوهر الاختراع

الاختراع يتمثل في تطوير مكمل غذائي مبتكر مضاد لمرض الزهايمر، يعتمد على مستخلص نباتي طبيعي غني بالمركبات البيولوجية فعالة مثل الفلافونويدات، الكيرسيتين، والمركبات الفينولية، التي أثبتت الدراسات الحديثة فعاليتها في تقليل الإجهاد التأكسدي، والتهابات الأعصاب، وتحسين الوظائف الإدراكية.

هذا المكمل موجه إلى:

- كبار السن المعرضين لخطر الإصابة بالزهايمر.
- الأفراد في المراحل المبكرة من التدهور المعرفي.
- المهتمين بالوقاية ودعم صحة الدماغ بطرق طبيعية وآمنة.

ويهدف الى :

- الوقاية من التدهور المعرفي المرتبط بالعمر.
- تقليل شدة أعراض الزهايمر عبر آليات طبيعية.
- توفير بديل علاجي تكميلي آمن، دون الآثار الجانبية للأدوية الكيميائية.
- دعم الأبحاث المستندة إلى الطب التكاملي والنباتي.

و يتميز بأنه :

- طبيعي و يعتمد على مستخلص نباتي موثوق.
- خالي من المواد الكيميائية أو الصناعية.
- فعّال وآمن للاستخدام طويل الأمد.
- قابل للتصنيع بأشكال مختلفة (كبسولات، بودرة، مشروب)
- مدعوم بتجارب أولية تثبت خصائصه المضادة للأكسدة والالتهاب

النموذج الأولي التجريبي

- عندما يتعلق الأمر بمنتوج (مركب، مزيج، تشكيل....)

صورة للنموذج الأولي للمكمل الغذائي المضاد للزهايمر.

طريقة إنجاز الاختراع:

الخطوة الأولى : تحضير المستخلص:

1. جمع النبات الطبي من مصادر محلية موثوقة.
2. تحضير المستخلص باستخدام تقنية الاستخلاص الإيثانولي.
3. استخراج المذيب بجهاز البخار الدوار.

الخطوة الثانية : اجراء الاختبارات :

4. تحليل المركبات النشطة باستخدام أدوات مثل HPLC و LC/MS.
5. اختبار النشاط البيولوجي BSA /DPPH وغيرها للتأكد من الفعالية.
6. التجريب على النموذج الحيواني للتأكد من الفعالية و عدم وجود نتائج سلبية جانبية.

الخطوة الثالثة : التركيبة النهائية:

7. تطوير التركيبة النهائية بناءً على نتائج الفعالية والتركيز الأمثل.
8. تحويل التركيبة إلى منتج صيدلاني (كبسولات) بأشكال مناسبة للاستخدام البشري.

2. شرح الأشكال و الرسومات: (دون وضعها في الوصف)

رقم 01 : رسم تخطيطي يوضح خطوات تحضير المستخلص النباتي المستخدم في المكمل الغذائي

1- أوراق نبات *Origanum majorana*
2- عملية الغسل والتجفيف
3- الطحن الميكانيكي
4- النقع في الميثانول

رقم 02 رسم توضيحي لطريقة استخراج المذيب :

1- قارورة دوارة – تحمل العينة .
2- حمام الماء – يسخن العينة لتسريع التبخر.
3- المكثف – يقوم بتبريد وتكثيف المذيب المتبخر.
4- قارورة الاستقبال – تجمع المذيب المكثف.
5- مضخة التفريغ – تعمل على خفض الضغط لتقليل نقطة غليان المذيب

رقم03 : نموذج توضيحي لتأثير المكمل الغذائي على الأعصاب والدماغ

1- خلية عصبية سليمة
2- خلية عصبية تحت تأثير الإجهاد التأكسدي
3- المكمل الغذائي
4- دور المكمل الغذائي في علاج الخلايا المصابة

7.طريقة والية عمل الجهاز المخترع او المادة المخترعة

طريقة تطبيق الاختراع:

- الاستخدام اليومي كمكمل غذائي (كبسولة) ضمن الجرعة المحددة.
- يمكن دمجه ضمن برامج التغذية الوقائية لكبار السن.
- يمكن استعماله في مراكز الرعاية والوقاية كجزء من خطط الدعم العصبي.
- يمكن تسويقه عبر الصيدليات، المتاجر الصحية، والمنصات الإلكترونية.

المحور الرابع

المطالب

المطالب

المطلب الرئيسي

يوفر المنتج بديلاً آمنًا ومنخفض التكلفة مقارنة بالأدوية الكيميائية، ويُعد أول مكمل محلي موجه لمرضى الزهايمر مبني على نتائج بحث مخبري موثوق.

يمثل بذلك قيمة مضافة حقيقية في السوق من حيث الفعالية، الأمان، والاعتماد على موارد محلية.

المطالب المستنبطة من المطلب الرئيسي والتي تميز اختراعنا

-وفقا للمطلب الأول هذا الاختراع يتميز بكونه طبيعي مستخلص من نبات Origanum majorana و هو فعال و غير مستخدم في التركيبات العلاجية السابقة مما يمنحه طابعًا ابتكاريًا جديدًا في مجال المكملات العصبية.

-وفقا للمطلب الأول هذا الاختراع يتميز بوجود دعم تجريبي أولي عبر اختبارات مخبرية ونماذج حيوانية تثبت فعاليته في تقليل أعراض التدهور المعرفي المرتبط بمرض الزهايمر

-وفقا للمطلب الأول هذا الاختراع يتميز بإمكانية تحويله إلى صيغ صيدلانية متعددة (مثل الكبسولات أو المساحيق) مناسبة للاستخدام اليومي والآمن دون الحاجة لوصفة طبية.

-وفقا للمطلب الأول هذا الاختراع يتميز بتصميم تركيبة مستخلصة بدقة باستخدام تقنيات استخلاص حراري معتدلة، تضمن الحفاظ على الفعالية البيولوجية للمركبات النباتية المضادة للأكسدة والالتهاب.

قائمة الملاحق

الاشكال والرسومات والجداول..... 10

الشكل رقم 01:

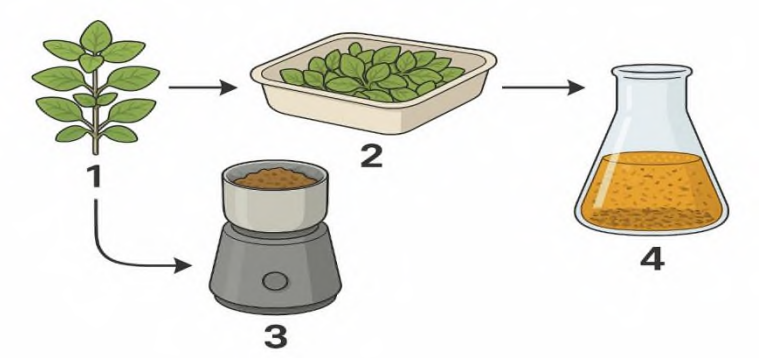

الشكل رقم 02:

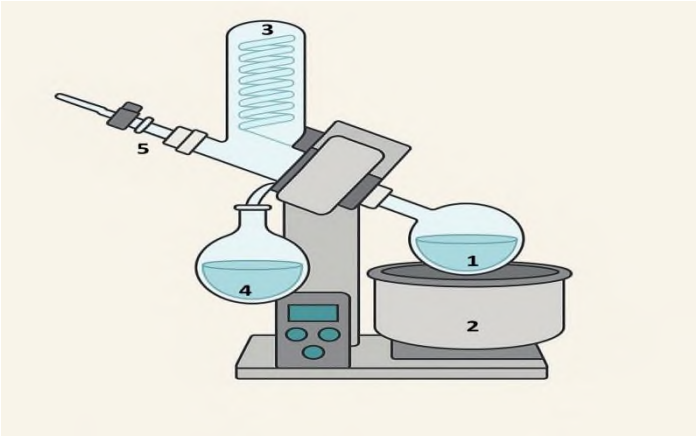

الشكل رقم03:

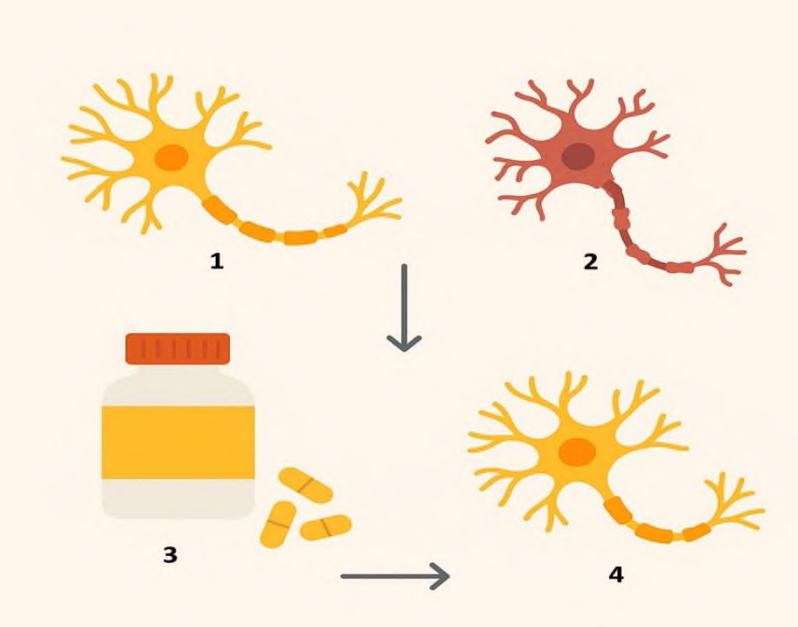

دليل مشروع

للحصول على شهادة مؤسسة ناشئة
في إطار القرار الوزاري 1275

ديسمبر
2022

CNCSIIU — MHESR — ALGERIA